Integrated Spasticity Assessment and Treatment using Disentangled Joint Resistance

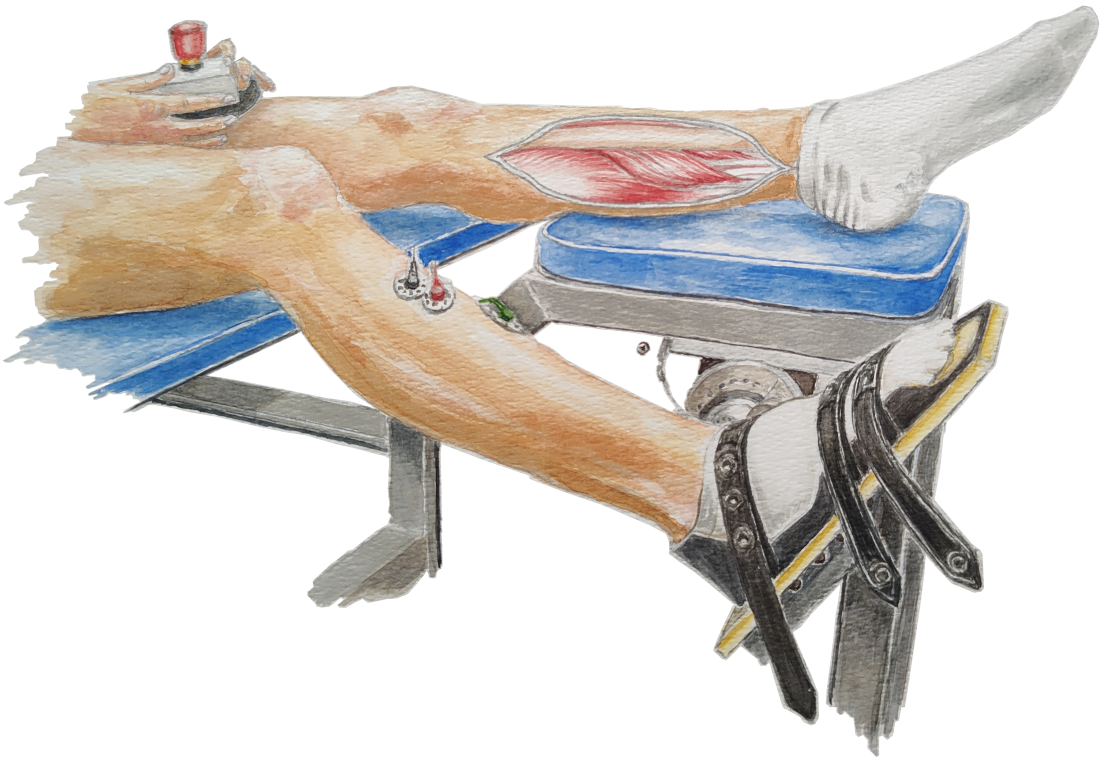

Ronald van 't Veld

Integrated Spasticity Assessment and Treatment using Disentangled Joint Resistance

Ronald Corstiaan van 't Veld

INTEGRATED SPASTICITY ASSESSMENT AND TREATMENT USING DISENTANGLED JOINT RESISTANCE

PROEFSCHRIFT

ter verkrijging van
de graad van doctor aan de Universiteit Twente,
op gezag van de rector magnificus,
prof. dr. ir. A. Veldkamp,
volgens besluit van het College voor Promoties
in het openbaar te verdedigen
op woensdag 25 mei 2022 om 16.45 uur

door

Ronald Corstiaan van 't Veld
geboren op 6 juni 1994
te Rijnsburg

Dit proefshcrift is goedgekeurd door:

Promotor:
prof. dr. ir. H. van der Kooij

Co-promotoren:
dr. E.H.F. van Asseldonk
dr. ir. A.C. Schouten

Omslagontwerp: Marjo van 't Veld-Jonker
Geprint door: Ipskamp printing
ISBN: 978-90-365-5391-9
DOI: 10.3990/1.9789036553919

Promotiecommissie

Voorzitter/Secretaris

prof. dr. ir. H.F.J.M. Koopman	Universiteit Twente

Promotor

prof. dr. ir. H. van der Kooij	Universiteit Twente

Co-promotoren

dr. E.H.F. van Asseldonk	Universiteit Twente
dr. ir. A.C. Schouten	Technische Universiteit Delft

Leden

prof. dr. ir. P.H. Veltink	Universiteit Twente
prof. dr. J.H. Buurke	Universiteit Twente
prof. dr. C.G.M. Meskers	Amsterdam UMC
prof. dr. F.C.T. van der Helm	Technische Universiteit Delft
dr. E.J. Rouse	University of Michigan

Dit werk maakte deel uit van het onderzoeksprogramma NeuroCIMT: Reflexioning met projectnummer 14903 dat (mede)gefinancierd is door de Nederlandse Organisatie voor Wetenschappelijk Onderzoek (NWO). Het Reflexioning project was een samenwerking tussen de Universiteit Twente, het Amsterdam UMC, Vrije Universiteit Amsterdam, de Sint Maartenskliniek en industriële partners Motek Medical en TMSi.

Contents

Summary

Spasticity is a common symptom after various brain and neural injuries, such as spinal cord injury (SCI) or stroke. Spasticity refers to an exaggerated stretch reflex, i.e. stretch hyperreflexia. At the joint level, spasticity is perceived as an increased resistance to movement, i.e. joint hyper-resistance. Patients with spasticity are limited in functional independence and mobility, and often experience substantial pain. The costly and time-intensive treatment of spasticity places a burden on both patients and the healthcare system. Therefore, improvement and personalization of spasticity treatment are desired. At present, many spasticity treatments, even those used within standard care, lack evidence of efficacy and cost-effectiveness. In addition, more objective and reliable quantification of spasticity is essential to enable a correct diagnosis and treatment plan. The core challenge regarding spasticity quantification is the mixed origin of joint hyper-resistance observed clinically. Spasticity increases joint resistance, similar to other symptoms like involuntary background activity, shortened tissue, contractures and fibrosis. The various origins of joint hyper-resistance require different treatment plans. Therefore, disentangling joint hyper-resistance, and as such separating spasticity from other symptoms, is important to select the best available treatment plan.

This thesis developed and evaluated non-invasive spasticity assessment and treatment in an experimental environment with stationary posture. The parallel-cascade (PC) system identification technique, which disentangles overall joint resistance in an intrinsic and reflexive contribution, was selected as analysis methodology. The PC technique extracts measures of intrinsic and reflexive resistance using a data-driven modelling strategy. First, an offline, time-invariant PC algorithm was used for post-trial evaluation of ankle joint resistance in a neuromechanical and clinical setting. Second, an online, adaptive PC algorithm was used for live estimation during measurements to enable biofeedback on either intrinsic or reflexive resistance. Towards spasticity assessment, we evaluated the estimated reflexive joint resistance in terms of validity, reliability and responsiveness. Towards spasticity treatment, we pursued a biofeedback-based, non-invasive approach as alternative for current clinical treatment, using the estimated reflexive joint resistance for biofeedback.

For spasticity assessment, we aimed to advance knowledge on the validity, reliability and responsiveness of PC algorithms, specifically from a neurophysiological perspective. The PC system identification technique and accompanying small amplitude joint perturbations substantially differ from current clinical practice. To assess spasticity, clinicians manually assess joint resistance over the full range of motion (ROM) and score the perceived resistance on a subjective, ordinal scale. The differences between the PC technique and clinical practice raise questions on the validity of the PC technique towards clinical application. Our results using a systematic motorized assessment combined with simulation study showed that both short- and medium-latency stretch reflexes depend on acceleration, velocity and duration of the applied perturbation. These observed dependencies indicate that the short duration, high acceleration joint

perturbations used for the PC technique will only capture the short-latency (M1) stretch reflex in the estimated reflexive joint resistance. Thus, the PC technique only captures the monosynaptic stretch reflex pathway and mainly the initial burst response of the muscle spindle. These perturbation dependencies stress the importance that stretch reflex or spasticity assessments using ramp-and-hold perturbations be executed and reported systematically.

Our studies also showed the potential of the PC technique to disentangle intrinsic and reflexive joint resistance in simulation and experiment. Simulation results showed good responsiveness, accuracy and reliability to study either able-bodied participants or people with spasticity. Experimental results showed moderate to strong correlations between the PC technique and electromyography (EMG)-based outcome measures on a group-level. The PC technique also showed strong correlations with the instrumented spasticity test (SPAT) on a group-level. The instrumented SPAT fundamentally differed from the PC technique as experimental data was collected over the full ROM instead of a limited ROM. Moreover, the instrumented SPAT used elementary data processing methods to extract measures of intrinsic and reflexive resistance instead of data-driven modelling. In support of the clinical application of the PC technique, the experimental results combined showed the group-level neurophysiological validity of the PC technique through the agreement with the neurophysiological basis on which the PC algorithms are built.

To further explore the PC technique potential, a clinical evaluation of the effect of botulinum neurotoxin-A (BoNT-A) injections on spasticity was performed. We hypothesized that BoNT-A would reduce the overall joint resistance and its reflexive contribution. However, the hypothesized joint resistance reduction was only observed in the clinical modified Ashworth Scale (MAS) measure, which assessed overall joint resistance. Using the PC technique and instrumented SPAT, this overall resistance reduction due to BoNT-A could not be attributed to an unambiguous reduction of the reflexive or intrinsic resistance contribution. Therefore, characterization of the diagnostic properties of the PC technique on an individual level is essential for clinical research and application, e.g. to understand the observed heterogeneous response to BoNT-A injections.

For spasticity treatment, we aimed to consolidate the use of PC technique-based biofeedback to achieve a long-term sustained spasticity reduction. A small-sample study has previously shown promising results for the PC technique as biofeedback method to gain voluntary control over reflex magnitude. To consolidate these findings, we explored PC technique-based biofeedback within the patient-proven operant conditioning framework for reflex reduction. Our results first replicated feasibility of the operant conditioning protocol using EMG-based biofeedback and showed at least -15% within-session reflex reduction after 4 to 6 conditioning sessions. In addition, we showed feasibility of using gamification within operant conditioning protocols to increase motivation during these time-intensive protocols. However, an operant conditioning protocol providing feedback on reflexive joint resistance estimated with the online PC algorithm did not achieve a reflex reduction. Therefore, application of the PC technique for spasticity treatment as well as the time-intensiveness and slow improvement rates for the operant conditioning protocol remain an open challenge.

In conclusion, our results showed the neurophysiological validity of the PC technique to assess intrinsic and reflexive joint resistance contributions. In clinical practice,

1-2 min measurements of time-invariant segments provide sufficient data for the PC technique to disentangle the intrinsic and reflexive contributions. Towards spasticity assessment and treatment, a reliable longitudinal quantification of spasticity and a cost-effective non-invasive spasticity treatment remain an open challenge. In absence of a golden standard, concurrent development and assessment of fundamentally different spasticity assessment methodologies is essential to eventually obtain a valid, responsive and reliable spasticity diagnosis approach. Besides experimental methods in stationary posture, complementary simulation studies as well as functional evaluations should be investigated to bridge gaps in our detailed and functional understanding of reflexes and spasticity. To benefit and learn from all future studies, standardization of protocols, unification of theoretical frameworks and definitions, and FAIR published research are essential. Otherwise, known nonlinear dependencies of spasticity and varying definitions will result in misinterpretation and confounding effects between studies and research communities.

Samenvatting

Spasticiteit is een veelvoorkomend symptoom als gevolg van hersen- en zenuwletsel, zoals een dwarslaesie of beroerte. Spasticiteit duidt op een overgevoelige rekreflex, d.w.z. hyperreflexie. Op gewrichtsniveau wordt spasticiteit waargenomen als een verhoogde weerstand tegen een opgelegde beweging, d.w.z. hyperweerstand in het gewricht. Patiënten met spasticiteit zijn beperkt in hun functionele onafhankelijkheid en mobiliteit, en ervaren vaak aanzienlijke pijn. De kostbare en tijdrovende behandeling van spasticiteit vormt een last voor zowel de patiënt als de gezondheidszorg. Daarom is verbetering en personalisatie van spasticiteitsbehandelingen gewenst. Momenteel ontbreekt het bewijs betreft werkzaamheid en kosteneffectiviteit voor veel spasticiteitsbehandelingen, zelfs als deze behandelingen onderdeel zijn van de standaardzorg. Bovendien is een objectievere en betrouwbaardere kwantificering van spasticiteit essentieel om een juiste diagnose en behandelplan mogelijk te maken. De belangrijkste uitdaging bij het kwantificeren van spasticiteit is het mengbeeld van symptomen die invloed hebben op de gewrichtsweerstand. Naast spasticiteit verhogen ook andere symptomen de gewrichtsweerstand, zoals een verhoogde spiertonus, verkort weefsel, contracturen en fibrose. De verschillende oorzaken van hyperweerstand in het gewricht vereisen verschillende behandelplannen. Daarom is het ontwarren van hyperweerstand in het gewricht, en daarmee het scheiden van spasticiteit van andere symptomen, belangrijk voor het kiezen van het best beschikbare behandelplan.

Het doel van dit proefschrift was het ontwikkelen en evalueren van niet-invasieve spasticiteit beoordeling en behandeling in een experimentele omgeving met constant postuur. De parallel-cascade (PC) systeemidentificatie techniek, die de totale gewrichtsweerstand ontwart in een intrinsieke en reflexieve bijdrage, werd gekozen als analysemethode. De PC-techniek bepaalt de intrinsieke en reflexieve weerstand door middel van een data-gedreven modelleer methode. Ten eerste werd een offline, tijdsinvariant PC-algoritme gebruikt voor de post-test evaluatie van de enkelgewrichtsweerstand in een neuromechanische en klinische context. Ten tweede werd een online, adaptief PC-algoritme gebruikt voor directe schattingen tijdens metingen om biofeedback op intrinsieke of reflexieve weerstand mogelijk te maken. Voor de beoordeling van spasticiteit hebben wij de geschatte reflexieve gewrichtsweerstand geëvalueerd op validiteit, betrouwbaarheid en responsiviteit. Voor de behandeling van spasticiteit hebben wij een niet-invasieve benadering op basis van biofeedback nagestreefd als alternatief voor de huidige klinische behandeling, gebruikmakend van de geschatte reflexieve gewrichtsweerstand voor biofeedback.

Betreft de beoordeling van spasticiteit wilden wij de kennis vergroten over de validiteit, betrouwbaarheid en responsiviteit van PC-algoritmes, specifiek vanuit een neurofysiologisch perspectief. De PC systeemidentificatie techniek en bijbehorende opgelegde verstoring met kleine amplitudes verschillen aanzienlijk van de huidige klinische praktijk. Om spasticiteit te beoordelen, evalueren artsen handmatig de gewrichtsweerstand over het volledige bewegingsbereik en scoren de waargenomen weerstand

op een subjectieve, ordinale schaal. De verschillen tussen de PC-techniek en de klinische praktijk roepen vragen op over de validiteit van de PC-techniek richting klinische toepassing. Onze resultaten, gebruikmakend van een systematische, gemotoriseerde beoordeling in combinatie met een simulatiestudie, toonden aan dat zowel de korte- als middellange-latentie rekreflexen afhankelijk zijn van de versnelling, snelheid en duur van de opgelegde verstoring. Deze waargenomen afhankelijkheden impliceren dat de korte duur en hoge versnelling van de verstoringen gebruikt voor de PC-techniek zorgen dat de geschatte reflexieve weerstand enkel de korte-latentie (M1) rekreflex omvat. De PC-techniek beoordeelt dus alleen de monosynaptische reflexboog en voornamelijk de initiële piek reactie van de spierspoeltjes. De afhankelijkheid van de opgelegde verstoring benadrukt het belang van het systematisch uitvoeren en rapporteren van de beoordeling van rekreflexen of spasticiteit.

Onze studies toonden ook de potentie van de PC-techniek om intrinsieke en reflexieve gewrichtsweerstand te ontwarren in zowel simulatie als experiment. Simulatieresultaten lieten een goede responsiviteit, nauwkeurigheid en betrouwbaarheid zien om zowel gezonde deelnemers als mensen met spasticiteit te onderzoeken. Experimentele resultaten toonden matig tot sterke correlaties tussen de PC-techniek en elektromyografie (EMG)-gebaseerde uitkomstmaten op groepsniveau. De PC-techniek vertoonde ook sterke correlaties met de geïnstrumenteerde spasticiteitstest (SPAT) op groepsniveau. De geïnstrumenteerde SPAT verschilde fundamenteel van de PC-techniek, omdat experimentele gegevens werden verzameld over het volledige bewegingsbereik in plaats van een beperkt bewegingsbereik. Bovendien gebruikte de geïnstrumenteerde SPAT elementaire verwerkingsmethoden om de intrinsieke en reflexieve weerstand te berekenen, in plaats van een data-gedreven methode. Ter ondersteuning van de klinische toepassing van de PC-techniek, toonden alle experimentele resultaten samen de neurofysiologische validiteit op groepsniveau aan van de PC-techniek, door de overeenstemming met de neurofysiologische basis waarop de PC-algoritmes gebaseerd zijn.

Om de potentie van de PC-techniek verder te onderzoeken, is een klinische evaluatie van het effect van botulinum neurotoxine-A (BoNT-A) injecties op spasticiteit uitgevoerd. Wij veronderstelden dat BoNT-A de totale gewrichtsweerstand alsook de reflexieve bijdrage zou verminderen. De veronderstelde vermindering van de gewrichtsweerstand werd echter alleen waargenomen met de klinische modified Ashworth scale (MAS), die de totale gewrichtsweerstand beoordeelde. Met behulp van de PC-techniek en geïnstrumenteerde SPAT, kon deze vermindering van de totale weerstand als gevolg van BoNT-A niet worden toegeschreven aan een eenduidige vermindering van de reflexieve of intrinsieke weerstand. Het karakteriseren van de diagnostische eigenschappen van de PC-techniek op individueel niveau is daarom essentieel voor klinisch onderzoek en toepassing, bijv. om de waargenomen heterogene reactie op BoNT-A injecties te kunnen begrijpen.

Betreft de behandeling van spasticiteit wilden we het gebruik van PC-techniek biofeedback ten behoeve van een lange termijn spasticiteit vermindering consolideren. Een eerder exploratief onderzoek heeft veelbelovende resultaten laten zien voor gebruik van PC-techniek biofeedback om vrijwillige controle te krijgen over de omvang van de rekreflex. Om deze bevindingen te consolideren hebben wij PC-techniek biofeedback onderzocht binnen het kader van operant conditioneren, dat binnen patiënt studies succesvolle resultaten heeft laten zien voor reflex vermindering. Onze resulta-

ten konden de haalbaarheid van het operant conditioneringsprotocol met behulp van EMG-gebaseerde biofeedback repliceren met een -15% reflex vermindering binnen 4 tot 6 conditioneringssessies. Daarnaast toonden we de haalbaarheid van het gebruik van gamificatie binnen operant conditioneringsprotocollen aan, met als doel de motivatie tijdens deze tijdsintensieve protocollen te verhogen. Daarentegen werd geen reflex vermindering bereikt met een operant conditioneringsprotocol op basis van feedback op reflexieve gewrichtsweerstand geschat met het online PC-algoritme. Daarom blijven de toepassing van de PC-techniek voor spasticiteitbehandeling, en de tijdsintensieve en hoge hoeveelheid benodigde sessies voor de operant conditioneringsprotocollen een uitdaging.

Concluderend, onze resultaten toonden de neurofysiologische validiteit van de PC-techniek om intrinsieke en reflexieve gewrichtsweerstand te kwantificeren. In de klinische praktijk leveren metingen van 1-2 min tijdinvariante segmenten voldoende gegevens op om met de PC-techniek de intrinsieke en reflexieve weerstanden te kunnen ontwarren. Voor de beoordeling en behandeling van spasticiteit blijven een betrouwbare longitudinale kwantificering van spasticiteit en een kosteneffectieve niet-invasieve behandeling van spasticiteit een uitdaging. Door een gebrek aan een gouden standaard is de gelijktijdige ontwikkeling en evaluatie van fundamenteel verschillende methoden voor spasticiteitsbeoordeling essentieel om uiteindelijk een valide, responsieve en betrouwbare methode voor spasticiteitsdiagnose te verkrijgen. Naast experimentele methoden met constant postuur moeten aanvullende simulatiestudies en functionele evaluaties worden onderzocht om ons gedetailleerde en functionele begrip van reflexen en spasticiteit te verbeteren. Standaardisatie van protocollen, unificeren van theoretische kaders en definities, en FAIR publicatie van onderzoek zijn van essentieel belang om volledig te profiteren en leren van alle toekomstige studies. Anders zullen de niet-lineaire afhankelijkheden van spasticiteit en de uiteenlopende definities leiden tot verkeerde interpretaties en confounders tussen verschillende studies en onderzoekersgroepen.

Chapter 1

General Introduction

1.1 Need for Spasticity Assessment and Treatment

Brain and neural injuries, such as spinal cord injury (SCI), cerebral palsy (CP) and stroke, deregulate the processing of sensory information, which affects joint biomechanics and the muscle stretch reflex, see Box 1.1 [1]. Specifically, an increased joint resistance, i.e. 'hyper-resistance', is observed after brain and neural injuries, which can severely impair walking ability and functional independence. The origin of this hyper-resistance can vary and arises from one or multiple of the following categories [2]:

- a tissue-related non-neural origin, e.g. shortened tissue or fibrosis;
- a tonic neural origin, i.e. involuntary background muscle activation;
- a phasic neural origin, i.e. exaggerated stretch reflex ('spasticity'/'hyperreflexia').

Spasticity, a regularly observed clinical symptom, refers to an exaggerated stretch reflex, i.e. 'hyperreflexia' [2]. Besides, people with spasticity may also experience a limited or lack of reflex modulation [1, 3]. In able-bodied subjects, reflex modulation is observed across the various phases of gait and between different functional tasks [1, 4]. Reflexes are modulated to comply with the functional requirements of a task and the environment. As such, a lack of reflex modulation can further limit the functional independence of people with brain and neural injuries.

Spasticity places a substantial burden on many patients as well as the healthcare system. Approximately 70% of SCI (incidence: ~25 per million per year) [5, 6], 78% of CP (incidence: ~3 per 1000 births) [7] and 33% of stroke (incidence: ~2200 per million per year) [8–10] patients are affected by spasticity in one or more joints. In addition, current treatment options are costly. For example, half of CP treatment costs, estimated at 62 k$ per year for a single patient, are spent on spasticity treatment [11].

The substantial burden of spasticity shows the clinical need for improved spasticity treatment, preferably at lower cost. First, within the broader context of joint hyper-resistance, objective and precise quantification of spasticity is essential to enable a correct diagnosis and treatment plan [2]. The mixed origin of joint hyper-resistance creates a core challenge in the assessment and quantification of spasticity [1–3]. These various origins require different treatments plans, e.g. Botulinum toxin (BoNT-A) and selective dorsal rhizotomy (SDR) aim to reduce spasticity, whereas casting and splinting aim to treat tissue-related impairments [12, 13]. Therefore, disentangling the three contributions to joint hyper-resistance, and as such separating spasticity from other symptoms, is important for the selection of the best available treatment for each patient [2]. In short, objective and precise spasticity quantification can improve treatment

Box 1.1: Stretch Reflex Arc

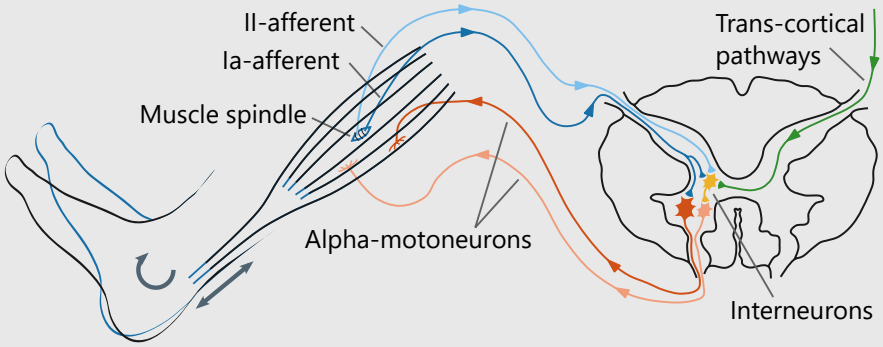

Figure 1.1: Schematic representation of the stretch reflex arc. The calf muscles can be stretched through a rotation of the ankle joint towards dorsiflexion, i.e. toes up. The rapid monosynaptic stretch reflex pathway consists of only the Ia-afferents and alpha-motoneurons. In addition, the slower polysynaptic stretch reflex pathways consist of both Ia- and II-afferents, trans-cortical contributions, interneurons and alpha-motoneurons.

The muscle stretch reflex or 'myotatic reflex' is a widely known feature of human movement control. A classic example is the knee-jerk reflex, where striking the patellar tendon below the knee causes the lower leg to kick forward. The stretch reflex is a form of sensory feedback control, which involuntarily modulates muscle force and activation in response to an unexpected muscle lengthening. The stretch reflex mechanism has a substantial delay, at least 50 ms around the ankle, due to neural transport and electromechanical delay. The stretch reflex is an important mechanism in support of functions like balance and walking. [14, 15]

In the calf, a dorsiflexion rotation of the ankle joint stretches the muscle-tendon units (MTUs), see Fig. 1.1. Through MTU and muscle cross-bridge dynamics, the joint rotation results in a stretch of the muscle fibers. The muscle spindles, consisting of intrafusal muscle fibers, sense the muscle fiber stretch and modulate the group Ia-afferent neuron firing rates. For the rapid monosynaptic pathway, the afferent neuron transmits the neural firing rate via a single synapse in the spinal cord to the efferent alpha-motoneurons, which results in a contraction of the agonist muscle. [14, 15]

In addition, the slower polysynaptic pathway is also part of the reflex arc. The polysynaptic pathway receives additional inputs through the group II-afferent, which also originate from the muscle spindle, and trans-cortical contributions. Moreover, polysynaptic pathways can elicit both a contraction of the agonist as well as inhibition of the antagonist muscle. [14, 15]

For both reflexive pathways the central nervous system (CNS) can modulate muscle spindle operating points and sensitivity, through gamma-motoneurons, as well as presynaptic inhibition/facilitation. Reflex modulation is important to support different requirements across and within the execution of functional tasks. [14–16]

effectiveness through correct clinical decision making. Second, effectiveness of spasticity treatment can be increased through improvement of current methodologies and investigation of new, promising methodologies.

1.2 Spasticity Assessment: Objective and Precise Quantification

Objective and precise quantification of spasticity is instrumental for correct clinical decision making [2, 17]. Moreover, proper spasticity quantification can support development and evaluation of new or improved spasticity treatment methodologies. A core challenge for spasticity quantification is disentangling spasticity from other contributions to joint hyper-resistance, like hypertonia or fibrosis [1–3]. Thus, the reflexive contribution to joint resistance has to be quantified in the presence of variations in the joint viscoelastic properties or tonic muscle activity [18]. A broad range of potential spasticity assessment methods is available.

Current clinical hyper-resistance and spasticity assessment is based on subjective evaluation of the manually sensed joint resistance over the full passive ROM [2, 19, 20]. Clinicians apply manual passive moments to the joint at either a single velocity, e.g. (modified) Ashworth Scale (MAS) [21, 22], or multiple velocities, e.g. Tardieu scale [23, 24] or the spasticity test (SPAT) [2]. Sensing joint resistance at multiple velocities can be used by examiners to unravel hyper-resistance contributions, as these contributions respond differently to changes in velocity. For instance, increased joint resistance at high velocity is associated with an increased reflexive contribution. Current assessments fall short in terms of objectivity, reliability, validity and standardization. Moreover, differentiation between hyper-resistance contributions, even when administering multiple velocities, is difficult [2, 17, 25–27].

Instrumentation and motorization of clinical spasticity tests have been implemented to resolve shortcomings of the current assessments [27–31]. Instrumented and motorized clinical tests focus on objective evaluation of the measured joint resistance over the full passive ROM. The measurements include biomechanical, i.e. kinematics and torque, as well as neurophysiological signals, i.e. electromyography (EMG). Instrumentation improves precision, consistency and objectivity of the registered response. Motorization standardizes the administered movements using a robotic device, improving precision and consistency of the applied movement, including out-of-plane movements [31–33]. However, disentangling hyper-resistance contributions directly from raw biomechanical and neurophysiological responses remains difficult [27, 31].

Disentangling hyper-resistance contributions requires model-based processing of the measured biomechanical and neurophysiological responses. Several physics-based neuromechanical modelling approaches focus on unravelling joint resistance contributions measured over the full passive ROM [27, 32–36]. On the one hand, detailed neuromechanical models are available which include several building blocks, like muscle-tendon, muscle spindle and activation dynamics. Insight into joint resistance contributions is created by estimating subject specific parameters, like slack length or stiffness coefficients of individual muscles [32, 34, 35]. On the other hand, neuromechanical models with a reduced model complexity are also available. For this group of models, insight into joint resistance contributions is created through digital signal processing to compute outcome parameters, e.g. the neural component of torque [27,

33, 36]. The model simplifications do potentially result in a worse performance in terms of disentangling the different joint resistance contributions [37].

For model-based processing, joint resistance estimation uses various sources of information: experimental measurements (data), a priori physiological knowledge, and assumptions [38]. Current physics-based neuromechanical modelling approaches based on full ROM primarily rely on a priori knowledge and assumptions [27, 32–35]. Besides, these approaches are supported by small experimental datasets, which include few repetitions of the joint response to passive movement through the full ROM at up to four different velocities. The resulting datasets do not provide enough information to directly estimate and unravel the joint resistance contributions, especially given the nonlinearity of joint resistance across the ROM [39–41]. Therefore, a priori physiological knowledge and assumptions are used within these approaches to complement the experiment datasets. As a result, these modelling approaches are sensitive to incomplete model definitions and imperfect a priori knowledge [32–35].

System identification methods, another type of model-based processing, use a data-driven approach to unravel joint resistance contributions, see Box 1.2 [38, 42, 43]. System identification primarily relies on experimental data supported by limited a priori knowledge and assumptions. To enable parameter estimation, several methods limit data collection to a small, restricted portion of the ROM with time-invariant task instructions [18, 44–47]. Within these conditions, time-invariant biomechanical responses are elicited using small amplitude perturbations defined as angular, i.e. position, perturbations ('open-loop' identification) [18, 44, 47] or as force perturbations ('closed-loop' identification) [45, 46]. Contrary to the neuromechanical modelling approaches, current methods generate no insight at a scale smaller than joint level, e.g. individual muscle or tendon contributions [38]. Furthermore, multiple experimental datasets are required to characterize the joint properties across the full ROM [39, 48, 49]. Spasticity assessment executed at a single point within the ROM, hence assumes that the estimated joint resistance contributions at this point are characteristic for the full ROM.

System identification methods are not necessarily limited to a small, restricted portion of the ROM or time-invariant conditions. Recently developed system identification methods estimate joint resistance across the full ROM or within functional tasks [50–56]. Main challenge for these methods is the introduction of time-varying joint resistance in the experimental data, hence requiring time-varying identification methods. At this moment, time-varying identification methods are still restricted in terms of applicability to spasticity assessment due to their novelty. First, several methods focus on lumped joint resistance estimation without disentangling the different contributions [50, 53, 55, 56]. Second, several methods focus on joint resistance estimation during imposed movement instead of functional tasks [51–56]. Time-varying identification methods do have a promising clinical application, as joint resistance estimation in functional tasks is most relevant for movement affecting symptoms like spasticity [1, 2].

In conclusion, novel scientific compared with current clinical spasticity assessment methods show promising improvements for objective and precise quantification. First, instrumentation and motorization improve precision, consistency and objectivity of the applied movements and measurements. Second, model-based processing of the biomechanical and neurophysiological responses can be used to unravel different joint resistance contributions. Most methods unravel the reflexive contribution, i.e.

Box 1.2: System Identification Methodology

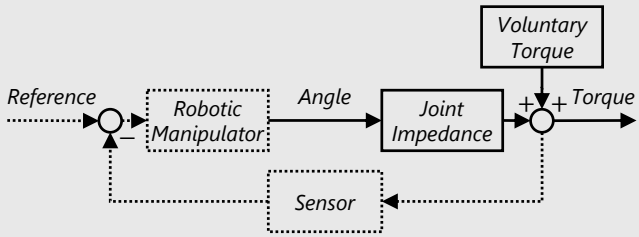

Figure 1.2: Schematic representation of a joint impedance system identification approach. Joint impedance describes the joint's resistance to imposed motion. The *solid* schematic shows an 'open-loop' joint impedance identification scheme. A robotic manipulator controls the angular input exciting the joint impedance system, which allows for isometric or imposed movement experiments. The full *solid & dashed* schematic shows a 'closed-loop' identification scheme. A reference torque is controlled for by the manipulator exciting the joint impedance system as a result, which allows for dynamic, functional experiments. For both schematics, the measured system output is a mix of the elicited torque response and an optional voluntary torque contribution.

System identification methods obtain a mathematical model of dynamic systems from experimental data. Experimental data is gathered by measuring the system response elicited using dedicated perturbation signals, see Fig. 1.2. A mathematical model is estimated by solving for the relation between the applied perturbations *(reference/input)* and subsequent biomechanical response *(output)*. The application of perturbations is instrumental to system identification approaches, because control over the system reference or input allows for unravelling causality, even in closed-loop feedback systems. Moreover, well-defined perturbations can specifically excite relevant system dynamics and improve signal-to-noise ratios. As system identification is a data-driven approach, generally only a limited amount of a priori knowledge and assumptions are required. Instead, extensive datasets with rapidly repeated or continuous perturbations are used to gather sufficient information to acquire good model fits. [38, 42, 43]

spasticity, from the combination of other joint resistance contributions, like hypertonia and fibrosis. Some methods unravel all three joint resistance contributions from each other [34]. For this thesis, we selected system identification methods evaluated within a restricted ROM to perform spasticity assessment. First, these methods have a solid experimental basis including clinical application [39, 48, 49, 57, 58], whereas system identification during functional tasks still requires additional laboratory and simulation studies given its novelty. Second, compared with neuromechanical modelling, the data-driven approach with limited a priori knowledge and assumptions is well suited to the clinical practise with a large heterogeneous population of spastic patients. In addition, the system identification methods do not necessarily use EMG measurements, which eases clinical applicability.

1.3 Spasticity Treatment: Non-Invasive Alternatives

The substantial burden which spasticity places on both patients and the healthcare system calls for improvement and personalization of spasticity treatment. Effectiveness of spasticity treatment can be increased through improvement of current methodologies and investigation of new, promising methodologies. Patient heterogeneity and mixed origin of joint resistance is a core challenge in development and evaluation of spasticity treatments [1–3]. At present, many spasticity treatments, even those used within standard care, lack evidence of efficacy and cost-effectiveness [12, 13, 59].

Spasticity treatment consists of a mix of physical therapy, oral medication, pharmacological interventions and surgical interventions [12, 13]. Physical therapy and oral medication, like Baclofen or Tizanidine, can reduce spasticity, however offer only symptomatic treatment without actual restoration of the deregulated reflexive pathways. Moreover, oral medication may also cause negative side effects like muscle weakness, sedation or respiratory issues [12, 20]. Pharmacological interventions, like BoNT-A and Phenol injections, can also reduce spasticity, again without actual restoration of the deregulated pathways. Pharmacological interventions do allow for increased control with reduced side effects compared with oral medication as well as potential pain alleviation [12, 13]. Potential negative side effects include bowel and bladder dysfunction, promotion of muscle fibrosis and immunoresistance [12, 60–62]. Surgical intervention, specifically SDR, has shown promising sustained results in reducing spasticity through interruption of neural signal transduction, however SDR is mainly performed in children only [12, 63]. Overall, spasticity treatments are invasive, non-specific or temporary with several potential negative side effects. Therefore, a non-invasive spasticity treatment with long-term sustained effect is desired [12, 64].

Over several decades, operant conditioning has been developed towards a non-invasive spasticity treatment alternative based on biofeedback [64, 65]. Operant conditioning aims to reduce spasticity by targeting CNS plasticity to counteract deregulation of the reflexive pathways. A reflexive response is repeatedly elicited in participants using either electrical (H-reflex) [66, 67] or mechanical (stretch reflex) stimuli [68–71]. The reflex response magnitude is visualized as biofeedback to the participant with the instruction to decrease (down-condition) this magnitude. Importantly, participants may not adapt muscle background activation to achieve reflex down-conditioning through alpha-motoneuron excitability [72]. Currently, conditioning protocols quantify reflex magnitude using EMG measurements. The acquisition of reflex down-conditioning has been shown to consist of two stages: a short-term (within-session) and long-term (across-session) change [66, 67, 73]. On average, a short-term effect of -15% reflex reduction was obtained after 4-6 conditioning sessions. Similarly, a long-term sustained effect of -20% reflex reduction was obtained after at least 12-16 conditioning sessions. Follow-up measurements after conditioning sessions finished showed that these long-term effects were retained until at least 1-3 months after the experiment [66, 67]. About 66% of patients and 94% of able-bodied participants were able to successfully execute the conditioning protocol in order to obtain a significant reflex reduction [66, 67, 73].

Clinical application of operant conditioning is promising as functional improvements were reported after reflex reduction [67]. Patients showed a 59% increase in gait speed, improved step-cycle symmetry and patients themselves also experienced func-

tional improvements, such as easier stepping. For clinical application, the target patient population should have a functioning corticospinal tract, as no other descending pathways are required [65]. Before clinical application of the conditioning paradigm, several elements of the conditioning protocol still require improvements. First, fundamentally the protocol is time-intensive (3 session per week) and has a slow improvement rate (at least 16 sessions) [67, 73]. Second, due to the EMG biofeedback used, accurate and consistent across-session electrode placement is required. Although this accurate electrode placement can be checked using electrical stimulation [66], removing the need for accurate, professional electrode placement would be beneficial.

Similar to operant conditioning, an exploratory study showed that participants can voluntarily modulate reflex magnitude using system identification-based biofeedback [74]. For biofeedback, a time-varying system identification method within a restricted ROM was used to capture reflex response magnitude. Specifically, Ludvig *et al.* [74] used mechanical stimuli and an online algorithm processing the biomechanical responses to enable continuous biofeedback on reflex magnitude [75]. As a result, participants showed voluntary variation of reflex magnitude up to a factor 4, already after 2 training sessions. Thus, although only shown in a small 4 subject sample, voluntary modulation of reflex modulation using system identification did show promising results.

In conclusion, improved effectiveness of spasticity treatment is desired, because many current treatment methods lack evidence of efficacy and cost-effectiveness. Besides, spasticity treatments are invasive, non-specific or temporary with several potential negative sides effects. Training patients to reduce reflex magnitude and hence spasticity using biofeedback has shown promising results towards a non-invasive alternative treatment. Operant conditioning protocols have shown long-term sustained reflex reduction with functional improvements as result. Similarly, an exploratory study using system identification-based biofeedback showed the potential to voluntarily modulate reflexive magnitude. Therefore, in this thesis we will pursue a biofeedback-based non-invasive spasticity treatment as alternative for current clinical treatment.

1.4 Joint Impedance-based Integrated Assessment and Treatment

Given the importance of both assessment and treatment, a non-invasive integrated spasticity assessment and treatment approach can substantially improve medical care. We selected system identification within a restricted ROM as assessment method. In addition, we pursued a biofeedback-based non-invasive treatment approach for spasticity reduction. The parallel-cascade (PC) system identification technique provides a solution in line with both choices and has shown promising results in support of both spasticity assessment and treatment [39, 48, 49, 74, 76, 77]. The PC technique is an open-loop identification scheme based on two parallel pathways: an intrinsic and reflexive pathway [18]. The intrinsic pathway combines the tissue-related non-neural and tonic neural contributions to joint resistance [18, 39]. The PC technique exploits the 40 ms neural delay in the stretch reflex arc to disentangle the intrinsic and reflexive pathways. The PC algorithms are executed using mechanical pseudo-random binary sequence (PRBS) stimuli, a perturbation signal which continuously switches between two angles within the ROM. As a result, an added benefit of using the PC technique is that the reflex response is directly discernible within both the EMG and torque signals.

Box 1.3: Attributes of Clinical Methodological Review

Development of novel clinical assessment approach requires thorough evaluation of several attributes. During the development phase, care should be placed on the rationale for the conceptual and measurement approach, the interpretability of envisioned outcome parameters as well as the burden and cost placed on patient and health care system. Evaluation of experimental and clinical results should focus on three important attributes: the validity, reliability and responsiveness of the methodology. [80]
Validity: *The degree to which an instrument measures what it is supposed to measure.* Thus, evidence that the outcome measures match with the intended purpose. Assessments include correlation analysis with other measures or known effects.
Reliability: *The degree to which an instrument can produce consistent results, i.e. free of random error.* Thus, methodologies should be able to produce consistent results, when no change is expected. Assessments include test-retest (within- and between-session) and inter-rater reliability.
Responsiveness: *The degree to which an instrument can detect change over time.* Thus, methodologies should be able to detect differences, when change is expected. Assessments include the minimal detectable difference.

For spasticity assessment, the time-invariant PC system identification technique has shown feasibility across various patient group experiments and for relevant attributes, see Box 1.3. PC technique validity has been established through extensive evaluation of human joint dynamics in response to small amplitude PRBS perturbations [18, 78]. Reliability was shown with a strong intra-subject reliability [79]. Responsiveness of the PC technique is supported as outcome measures logically discriminate both SCI and stroke patients from control groups as well as paretic and non-paretic joints [39, 49]. Note, all clinical evaluations were executed using multiple measurements at several points across the full ROM. In addition, the PC technique showed good responsiveness when employed to quantify the effects of 18 months of functional electrical stimulation-assisted walking [48], Tizanidine [76] and robot-assisted gait training [77].

Nevertheless, an improved neurophysiological understanding of the PC technique is required to support validity and further clinical application. In terms of validity, the PC technique did unexpectedly show a weak correlation with EMG-based outcome measures for the reflexive pathway [81]. Besides, proper neurophysiological understanding on the effect of small amplitude perturbations compared to full ROM assessment methods is required. Specifically, understanding the effect of changing perturbation velocity, acceleration and duration, which all differ between the restricted and full ROM assessment methods [41, 82, 83]. The validity of assessing spasticity at a single point of the ROM instead of the full ROM also requires further investigation [34, 39, 49]. Overall, the PC technique has been well-established within the system identification community, however the technique has not yet transitioned towards clinical practise, while clinicians urgently require objective spasticity quantification [2, 17, 38].

For spasticity treatment, biofeedback using the online, time-varying PC system identification technique has shown promising reflex reduction potential in an exploratory study [74]. Compared with operant conditioning protocols, another biofeedback technique, participants already voluntarily modulated their reflex response after 2 instead of

4-6 sessions [66, 73, 74]. Additionally, the PC system identification technique does not require any electrodes or electrical stimulation. However, these results are only based on a small 4 subject sample. Moreover, the operant conditioning protocol offers a more robust framework used for down-conditioning instead of voluntary modulation and including checks on steadiness of background activation. Therefore, in this thesis we propose to execute the operant conditioning framework using system identification-based biofeedback. This combination is used to further explore system identification-based biofeedback for spasticity treatment with a potentially faster improvement rate and improved practical execution for the operant conditioning protocol.

1.5 Research Questions and Thesis Outline

This thesis develops and evaluates a non-invasive integrated spasticity assessment and treatment approach with a stationary posture. The PC system identification technique is selected for this purpose, specifically using both the available time-invariant [18, 39] and online, time-varying algorithms [75].

1. What is the neurophysiological validity of the PC system identification technique and accompanying joint perturbations for spasticity assessment?
The PC system identification technique and accompanying small amplitude joint perturbations substantially differ from current clinical practice. Therefore, clinical application of the technique raises many questions on the effects of these differences and hence the validity of the technique. We aimed to advance knowledge on the validity of PC algorithms, specifically from a neurophysiological perspective. **Chapter 2** reports on the stretch reflex sensitivity to changes in perturbation velocity, acceleration and duration, which all differ between the PC technique and current clinical practise. A simulation model is used to corroborate experimental results and gain understanding of the underlying neurophysiology causing the observed dependencies. In support of experimental studies, **Chapter 3** revises the PC system identification algorithms for our specific experimental environment and tests the responsiveness, accuracy and reliability in simulation. **Chapter 4** reports on the within-subject neurophysiological validation of the PC system identification technique using EMG-based outcome measures. Before, the PC technique unexpectedly only showed a weak between-subject correlation with EMG-based outcome measures for the reflexive pathway before [81]. However, EMG outcome measures are difficult to compare between subjects, especially non-normalized results (in Volt) as in Xia *et al.* [81], due to subject-dependent characteristics. Therefore, additional insight in neurophysiological validity is gained through our study based on within-subject measurements and a standardized EMG outcome measure.

2. How feasible is the PC system identification technique for use as integrated spasticity assessment and treatment approach?
The online, adaptive PC algorithm has shown promising results as biofeedback method to gain voluntary control over reflex magnitude in a small-sample study. **Chapter 5** aims to consolidate these findings by exploring use of PC technique-based biofeedback within the operant conditioning framework. Combination of the operant conditioning protocol with impedance-based biofeedback may result in faster improvement rates and improved practical execution. In addition, feasibility of biofeedback gamification is also tested to improve participant motivation and engagement during these time-

intensive protocols. As a first step towards spasticity treatment, this exploratory study is executed using able-bodied participants.

3. What is the effect of BoNT-A injections on the intrinsic and reflexive contributions to ankle joint resistance for patients with spasticity?
The PC algorithms have been used successfully for pre-post test assessment, providing insight into the effects of functional electrical stimulation, Tizanidine and robot-assisted gait training. **Chapter 6** expands on these reports by evaluating the longitudinal effect of BoNT-A injections on the intrinsic and reflexive pathways in spastic patients. Clinical effect of spasticity treatment using BoNT-A is not well understood, while BoNT-A injections are commonly used as clinical intervention. We aimed to increase insight into the responsiveness, beneficial and adverse effects of BoNT-A injections using the PC system identification technique.

References

[1] V. Dietz and T. Sinkjær, "Spastic Movement Disorder: Impaired Reflex Function and Altered Muscle Mechanics," *Lancet Neurology*, 6(8), pp. 725–733, 2007. doi: 10.1016/S1474-4422(07)70193-X.

[2] J. C. van den Noort, L. Bar-On, E. Aertbeliën, M. Bonikowski, *et al.*, "European Consensus on the Concepts and Measurement of the Pathophysiological Neuromuscular Responses to Passive Muscle Stretch," *European Journal of Neurology*, 24(7), pp. 981–991, 2017. doi: 10.1111/ene.13322.

[3] J. A. Burne, V. L. Carleton, and N. J. O'Dwyer, "The Spasticity Paradox: Movement Disorder or Disorder of Resting Limbs?" *Journal of Neurology, Neurosurgery and Psychiatry*, 76(1), pp. 47–54, 2005. doi: 10.1136/jnnp.2003.034785.

[4] R. B. Stein and C. Capaday, "The Modulation of Human Reflexes during Functional Motor Tasks," *Trends in Neurosciences*, 11(7), pp. 328–332, 1988. doi: 10.1016/0166-2236(88)90097-5.

[5] J. A. Haisma, L. H. van der Woude, H. J. Stam, M. P. Bergen, *et al.*, "Complications following Spinal Cord Injury: Occurrence and Risk Factors in a Longitudinal Study during and after Inpatient Rehabilitation," *Journal of Rehabilitation Medicine*, 39(5), pp. 393–398, 2007. doi: 10.2340/16501977-0067.

[6] M. M. Post, C. F. Nooijen, K. Postma, J. Dekkers, *et al.*, "People with Spinal Cord Injury in the Netherlands," *American Journal of Physical Medicine and Rehabilitation*, 96(2), S93–S95, 2017. doi: 10.1097/PHM.0000000000000619.

[7] D. Christensen, K. van Naarden Braun, N. S. Doernberg, M. J. Maenner, *et al.*, "Prevalence of Cerebral Palsy, Co-occurring Autism Spectrum Disorders, and Motor Functioning - Autism and Developmental Disabilities Monitoring Network, USA, 2008," *Developmental Medicine and Child Neurology*, 56(1), pp. 59–65, 2014. doi: 10.1111/dmcn.12268.

[8] I. Vaartjes, J. B. Reitsma, A. De Bruin, M. Berger-van Sijl, *et al.*, "Nationwide Incidence of First Stroke and TIA in the Netherlands," *European Journal of Neurology*, 15(12), pp. 1315–1323, 2008. doi: 10.1111/j.1468-1331.2008.02309.x.

[9] Royal College of Physicians, *Spasticity in Adults: Management using Botulinum Toxin*, London, UK, 2018.

[10] H. A. Wafa, C. D. A. Wolfe, E. Emmett, G. A. Roth, *et al.*, "Burden of Stroke in Europe: Thirty-Year Projections of Incidence, Prevalence, Deaths, and Disability-Adjusted Life Years," *Stroke*, 51(8), pp. 2418–2427, 2020. doi: 10.1161/STROKEAHA.120.029606.

[11] M. Saulino, S. Guillemette, J. Leier, and J. Hinnenthal, "Medical cost impact of intrathecal baclofen therapy for severe spasticity," *Neuromodulation*, 18(2), pp. 141–149, 2015. doi: 10.1111/ner.12220.

[12] E. Chang, N. Ghosh, D. Yanni, S. Lee, *et al.*, "A Review of Spasticity Treatments: Pharmacological and Interventional Approaches," *Critical Reviews in Physical and Rehabilitation Medicine*, 25(1-2), pp. 11–22, 2013. doi: 10.1615/CritRevPhysRehabilMed.2013007945.

[13] I. Novak, S. McIntyre, C. Morgan, L. Campbell, *et al.*, "A Systematic Review of Interventions for Children with Cerebral Palsy: State of the Evidence," *Developmental Medicine & Child Neurology*, 55(10), pp. 885–910, 2013. doi: 10.1111/dmcn.12246.

[14] E. R. Kandel, J. H. Schwartz, T. M. Jessell, S. A. Siegelbaum, *et al.*, "Spinal Reflexes," in *Principles of Neural Science*, 5th ed., New York City, NY, USA: McGraw-Hill, 2013, ch. 35.

[15] E. Burdet, D. W. Franklin, and T. E. Milner, *Human Robotics: Neuromechanics and Motor Control*, 1st. Cambridge, MA, USA: MIT Press, 2013.

[16] J. A. Pruszynski and S. H. Scott, "Optimal Feedback Control and the Long-Latency Stretch Response," *Experimental Brain Research*, 218(3), pp. 341–359, 2012. doi: 10.1007/s00221-012-3041-8.

[17] J. F. M. Fleuren, G. E. Voerman, C. V. Erren-Wolters, G. J. Snoek, *et al.*, "Stop using the Ashworth Scale for the assessment of Spasticity," *Journal of Neurology, Neurosurgery and Psychiatry*, 81, pp. 46–52, 2010. doi: 10.1136/jnnp.2009.177071.

[18] R. E. Kearney, R. B. Stein, and L. Parameswaran, "Identification of Intrinsic and Reflex Contributions to Human Ankle Stiffness Dynamics," *IEEE Transactions on Biomedical Engineering*, 44(6), pp. 493–504, 1997. doi: 10.1109/10.581944.

[19] T. Platz, C. Eickhof, G. Nuyens, and P. Vuadens, "Clinical Scales for the Assessment of Spasticity Associated Phenomena, and Function: A Systematic Review of the Literature," *Disability and Rehabilitation*, 27(1-2), pp. 7–18, 2005. doi: 10.1080/09638280400014634.

[20] T. Rekand, "Clinical Assessment and Management of Spasticity: A Review," *Acta Neurologica Scandinavica*, 122(Suppl. 190), pp. 62–66, 2010. doi: 10.1111/j.1600-0404.2010.01378.x.

[21] B. Ashworth, "Preliminary Trial of Carisoprodol in Multiple Sclerosis," *Practitioner*, 192, pp. 540–542, 1964.

[22] R. W. Bohannon and M. B. Smith, "Interrater Reliability of a Modified Ashworth Scale of Muscle Spasticity," *Physical Therapy*, 67(2), pp. 206–207, 1987. doi: 10.1093/ptj/67.2.206.

[23] C. Tardieu, E. Huet de la Tour, M. D. Bret, and G. Tardieu, "Muscle Hypoextensibility in Children with Cerebral Palsy: I. Clinical and Experimental Observations," *Archives of Physical Medicine and Rehabilitation*, 63, pp. 97–102, 1982.

[24] J.-M. Gracies, J. E. Marosszeky, R. Renton, J. Sandanam, *et al.*, "Short-Term Effects of Dynamic Lycra Splints on Upper Limb in Hemiplegic Patients," *Archives of Physical Medicine and Rehabilitation*, 81(12), pp. 1547–1555, 2000. doi: 10.1053/apmr.2000.16346.

[25] A. D. Pandyan, G. R. Johnson, C. I. M. Price, R. H. Curless, *et al.*, "A Review of the Properties and Limitations of the Ashworth and Modified Ashworth Scales as Measures of Spasticity," *Clinical Rehabilitation*, 13(5), pp. 373–383, 1999. doi: 10.1191/026921599677595404.

[26] J. Lorentzen, M. J. Grey, C. Crone, D. Mazevet, *et al.*, "Distinguishing Active from Passive Components of Ankle Plantar Flexor Stiffness in Stroke, Spinal Cord Injury and Multiple Sclerosis," *Clinical Neurophysiology*, 121(11), pp. 1939–1951, 2010. doi: 10.1016/j.clinph.2010.02.167.

[27] L. Bar-On, K. Desloovere, G. Molenaers, J. Harlaar, *et al.*, "Identification of the Neural Component of Torque during Manually-applied Spasticity Assessments in Children with Cerebral Palsy," 40(3), pp. 346–351, 2014. doi: 10.1016/j.gaitpost.2014.04.207.

[28] G. E. Voerman, J. H. Burridge, R. A. Hitchcock, and H. J. Hermens, "Clinometric Properties of a Clinical Spasticity Measurement Tool," *Disability and Rehabilitation*, 29(24), pp. 1870–1880, 2007. doi: 10.1080/09638280601143752.

[29] Y.-N. Wu, Y. Ren, A. Goldsmith, D. Gaebler, *et al.*, "Charachterization of Spasticity in Cerebral Palsy: Dependence of Catch Angle on Velocity," *Developmental Medicine and Child Neurology*, 52(6), pp. 563–569, 2010. doi: 10.1111/j.1469-8749.2009.03602.x.

[30] L. Bar-On, E. Aertbeliën, H. Wambacq, D. Severijns, *et al.*, "A Clinical Measurement to Quantify Spasticity in Children with Cerebral Palsy by Integration of Multidimensional Signals," *Gait and Posture*, 38(1), pp. 141–147, 2013. doi: 10.1016/j.gaitpost.2012.11.003.

[31] L. H. Sloot, L. Bar-On, M. M. van der Krogt, E. Aertbeliën, *et al.*, "Motorized versus Manual Instrumented Spasticity Assessment in Children with Cerebral Palsy," *Developmental Medicine and Child Neurology*, 59(2), pp. 145–151, 2017. doi: 10.1111/dmcn.13194.

[32] E. de Vlugt, J. H. de Groot, K. E. Schenkeveld, J. H. Arendzen, *et al.*, "The Relation between Neuromechanical Parameters and Ashworth Score in Stroke Patients," *Journal of Neuroengineering and Rehabilitation*, 7:35, 2010. doi: 10.1186/1743-0003-7-35.

[33] P. G. Lindberg, J. Gäverth, M. Islam, A. Fagergren, *et al.*, "Validation of a New Biomechanical Model to Measure Muscle Tone in Spastic Muscles," *Neurorehabilitation and Neural Repair*, 25(7), pp. 617–625, 2011. doi: 10.1177/1545968311403494.

[34] L. H. Sloot, M. M. van der Krogt, K. L. de Gooijer-van de Groep, S. van Eesbeek, *et al.*, "The Validity and Reliability of Modelled Neural and Tissue Properties of the Ankle Muscles in Children with Cerebral Palsy," *Gait and Posture*, 42(1), pp. 7–15, 2015. doi: 10.1016/j.gaitpost.2015.04.006.

[35] R. Wang, P. A. Herman, Ö. Ekeberg, J. Gäverth, *et al.*, "Neural and non-neural related properties in the spastic wrist flexors: An optimization study," *Medical Engineering and Physics*, 47, pp. 198–209, 2017. doi: 10.1016/j.medengphy.2017.06.023.

[36] A. Andringa, E. van Wegen, I. van de Port, and G. Kwakkel, "Measurement Properties of the NeuroFlexor Device for Quantifying Neural and Non-neural Components of Wrist Hyper-Resistance in Chronic Stroke," *Frontiers in Neurology*, 10:730, 2019. doi: 10.3389/fneur.2019.00730.

[37] A. Andringa, C. G. M. Meskers, I. van de Port, S. Zandvliet, *et al.*, "Quantifying Neural and Non-neural Componenets of Wrist Hyper-resistance after Stroke: Comparing Two Instrumented Assessment Methods," *Medical Engineering & Physics*, 98, pp. 57–64, 2021. doi: 10.1016/j.medengphy.2021.10.009.

[38] C. P. Cop, G. Cavallo, R. C. van 't Veld, B. F. J. M. Koopman, *et al.*, "Unifying System Identification and Biomechanical Formulations for the Estimation of Muscle, Tendon, and Joint Stiffness during Human Movement," *Progress in Biomedical Engineering*, 3(3), 2021. doi: 10.1088/2516-1091/ac12c4.

[39] M. M. Mirbagheri, H. Barbeau, M. Ladouceur, and R. E. Kearney, "Intrinsic and Reflex Stiffness in Normal and Spastic, Spinal Cord Injured Subjects," *Experimental Brain Research*, 141(4), pp. 446–459, 2001. doi: 10.1007/s00221-001-0901-z.

[40] G. N. Lewis, E. J. Perreault, and C. D. MacKinnon, "The Influence of Perturbation Duration and Velocity on the Long-Latency Response to Stretch in the Biceps Muscle," *Experimental Brain Research*, 163(3), pp. 361–369, 2005. doi: 10.1007/s00221-004-2182-9.

[41] J. Schuurmans, E. de Vlugt, A. C. Schouten, C. G. M. Meskers, *et al.*, "The Monosynaptic Ia Afferent Pathway Can Largely Explain the Stretch Duration Effect of the Long Latency M2 Response," *Experimental Brain Research*, 193(4), pp. 491–500, 2009. doi: 10.1007/s00221-008-1647-7.

[42] D. T. Westwick and R. E. Kearney, "Identification of Linear Systems," in *Identification of Nonlinear Physiological Systems*, Hoboken, NJ, USA: John Wiley & Sons, Inc., 2003, ch. 5, pp. 103–123. doi: 10.1002/0471722960.ch5.

[43] R. Pintelon and J. Schoukens, *System Identification: A Frequency Domain Approach*, 2nd ed. Hoboken, New Jersey: John Wiley & Sons, Inc., 2012.

[44] L.-Q. Zhang and W. Z. Rymer, "Simultaneous and Nonlinear Identification of Mechanical and Reflex Properties of Human Elbow Joint Muscles," *IEEE Transactions on Biomedical Engineering*, 44(12), pp. 1192–1207, 1997. doi: 10.1109/10.649991.

[45] F. C. T. van der Helm, A. C. Schouten, E. de Vlugt, and G. G. Brouwn, "Identification of Intrinsic and Reflexive Components of Human Arm Dynamics during Postural Control," *Journal of Neuroscience Methods*, 119(1), pp. 1–14, 2002. doi: 10.1016/S0165-0270(02)00147-4.

[46] A. C. Schouten, E. de Vlugt, J. J. van Hilten, and F. C. T. van der Helm, "Quantifying Proprioceptive Reflexes during Position Control of the Human Arm," *IEEE Transactions on Biomedical Engineering*, 55(1), pp. 311–321, 2008. doi: 10.1109/TBME.2007.899298.

[47] Y. Zhao, D. T. Westwick, and R. E. Kearney, "Subspace Methods for Identification of Human Ankle Joint Stiffness," *IEEE Transactions on Biomedical Engineering*, 58(11), pp. 3039–3048, 2011. doi: 10.1109/TBME.2010.2092430.

[48] M. M. Mirbagheri, M. Ladouceur, H. Barbeau, and R. E. Kearney, "The Effects of Long Term FES-Assisted Walking on Intrinsic and Reflex Dynamic Stiffness in Spinal Cord Injured Patients," *IEEE Transactions on Neural Systems and Rehabilitation Engineering*, 10(4), pp. 280–289, 2002. doi: 10.1109/TNSRE.2002.806838.

[49] M. M. Mirbagheri, L. Alibiglou, M. Thajchayapong, and W. Z. Rymer, "Muscle and Reflex Changes with Varying Joint Angle in Hemiparetic Stroke," *Journal of NeuroEngineering and Rehabilitation*, 5:6, 2008. doi: 10.1186/1743-0003-5-6.

[50] D. Ludvig and E. J. Perreault, "System Identification of Physiological Systems using Short Data Segments," *IEEE Transactions on Biomedical Engineering*, 59(12), pp. 3541–3549, 2012. doi: 10.1109/TBME.2012.2220767.

[51] K. Jalaleddini, E. Sobhani Tehrani, and R. E. Kearney, "A Subspace Approach to the Structural Decomposition and Identification of Ankle Joint Dynamic Stiffness," *IEEE Transactions on Biomedical Engineering*, 64(6), pp. 1357–1368, 2017. doi: 10.1109/TBME.2016.2604293.

[52] D. L. Guarín and R. E. Kearney, "Estimation of Time-Varying, Intrinsic and Reflex Dynamic Joint Stiffness during Movement. Application to the Ankle Joint," *Frontiers in Computational Neuroscience*, 11:51, 2017. doi: 10.3389/fncom.2017.00051.

[53] D. L. Guarín and R. E. Kearney, "Identification of a Time-Varying, Box-Jenkins Model of Intrinsic Joint Compliance," *IEEE Transactions on Neural Systems and Rehabilitation Engineering*, 25(8), pp. 1211–1220, 2017. doi: 10.1109/TNSRE.2016.2619162.

[54] M. A. Golkar, E. Sobhani Tehrani, and R. E. Kearney, "Linear Parameter Varying Identification of Dynamic Joint Stiffness during Time-Varying Voluntary Contractions," *Frontiers in Computational Neuroscience*, 11:15, 2017. doi: 10.3389/fncom.2017.00035.

[55] D. L. Guarín and R. E. Kearney, "Unbiased Estimation of Human Joint Intrinsic Mechanical Properties during Movement," *IEEE Transactions on Neural Systems and Rehabilitation Engineering*, 26(10), pp. 1975–1984, 2018. doi: 10.1109/TNSRE.2018.2870330.

[56] G. Cavallo, A. C. Schouten, and J. Lataire, "Locally Periodic Kernel-Based Regression to Identify Time-Varying Ankle Impedance During Locomotion: A Simulation Study," in *42nd Annual International Conference of the IEEE Engineering in Medicine and Biology Society*, Montreal, Canada: IEEE, 2020, pp. 4835–4838. doi: 10.1109/EMBC44109.2020.9175835.

[57] A. C. Schouten, W. J. T. van de Beek, J. J. van Hilten, and F. C. T. van der Helm, "Proprioceptive Reflexes in Patients with Reflex Sympathetic Dystrophy," *Experimental Brain Research*, 151, pp. 1–8, 2003. doi: 10.1007/s00221-003-1420-x.

[58] C. G. M. Meskers, A. C. Schouten, J. H. de Groot, E. de Vlugt, *et al.*, "Muscle Weakness and Lack of Reflex Gain Adaptation Predominate during Post-Stroke Posture Control of the Wrist," 6:29, 2009. doi: 10.1186/1743-0003-6-29.

[59] L. Shaw, H. Rodgers, C. Price, F. van Wijck, *et al.*, "BoTULS. A Multicentre Randomised Controlled Trial to Evaluate the Clinical Effectiveness and Cost-effectiveness of Treating Upper Limb Spasticity due to Stroke with Botulinum Toxin Type A," *Health Technology Assessment*, 14(26), 2010. doi: 10.3310/hta14260.

[60] V. Stevenson and D. Playford, "Neurological Rehabilitation and the Management of Spasticity," *Medicine*, 40(9), pp. 513–517, 2012. doi: 10.1016/j.mpmed.2012.06.008.

[61] M. Gough and A. P. Shortland, "Could Muscle Deformity in Children with Spastic Cerebral Palsy be Related to an Impairment of Muscle Growth and Altered Adaptation?" *Developmental Medicine and Child Neurology*, 54(6), pp. 495–499, 2012. doi: 10.1111/j.1469-8749.2012.04229.x.

[62] J. Valentine, K. Stannage, V. Fabian, K. Ellis, *et al.*, "Muscle Histopathology in Children with Spastic Cerebral Palsy Receiving Botulinum Toxin Type A," *Muscle and Nerve*, 53(3), pp. 407–414, 2016. doi: 10.1002/mus.24763.

[63] E. A. Hurvitz, C. M. Marciniak, A. K. Daunter, H. J. Haapala, *et al.*, "Functional Outcomes of Childhood Dorsal Rhizotomy in Adults and Adolescents with Cerebral Palsy," *Journal of Neurosurgery: Pediatrics*, 11(4), pp. 380–388, 2013. doi: 10.3171/2013.1.PEDS12311.

[64] A. K. Thompson and J. R. Wolpaw, "Operant Conditioning of Spinal Reflexes: From Basic Science to Clinical Therapy," *Frontiers in Integrative Neuroscience*, 8:25, 2014. doi: 10.3389/fnint.2014.00025.

[65] J. R. Wolpaw, "Spinal Cord Plasticity in Acquisition and Maintenance of Motor Skills," *Acta Physiologica*, 189(2), pp. 155–169, 2007. doi: 10.1111/j.1748-1716.2006.01656.x.

[66] A. K. Thompson, X. Y. Chen, and J. R. Wolpaw, "Acquisition of a Simple Motor Skill: Task-Dependent Adaptation Plus Long-Term Change in the Human Soleus H-Reflex," *Journal of Neuroscience*, 29(18), pp. 5784–5792, 2009. doi: 10.1523/JNEUROSCI.4326-08.2009.

[67] A. K. Thompson, F. R. Pomerantz, and J. R. Wolpaw, "Operant Conditioning of a Spinal Reflex Can Improve Locomotion after Spinal Cord Injury in Humans," *Journal of Neuroscience*, 33(6), pp. 2365–2375, 2013. doi: 10.1523/JNEUROSCI.3968-12.2013.

[68] M. L. Evatt, S. L. Wolf, and R. L. Segal, "Modification of Human Spinal Stretch Reflexes: Preliminary Studies," *Neuroscience Letters*, 105(3), pp. 350–355, 1989. doi: 10.1016/0304-3940(89)90646-0.

[69] S. L. Wolf and R. L. Segal, "Conditioning of the Spinal Stretch Reflex: Implications for Rehabilitation," 70(10), pp. 652–656, 1990. doi: 10.1093/ptj/70.10.652.

[70] R. L. Segal and S. L. Wolf, "Operant Conditioning of Spinal Stretch Reflexes in Patients with Spinal Cord Injuries," 130(2), pp. 202–213, 1994. doi: 10.1006/exnr.1994.1199.

[71] S. L. Wolf and R. L. Segal, "Reducing Human Biceps Brachii Spinal Stretch Reflex Magnitude," *Journal of Neurophysiology*, 75(4), pp. 1637–1646, 1996. doi: 10.1152/jn.1996.75.4.1637.

[72] P. B. C. Matthews, "Observations on the Automatic Compensation of Reflex Gain on Varying the Pre-Existing Level of Motor Discharge in Man," *The Journal of Physiology*, 374(1), pp. 73–90, 1986. doi: 10.1113/jphysiol.1986.sp016066.

[73] N. Mrachacz-Kersting, U. G. Kersting, P. de Brito Silva, Y. Makihara, *et al.*, "Acquisition of a Simple Motor Skill: Task-dependent Adaptation and Long-term Changes in the Human Soleus Stretch Reflex," *Journal of Neurophysiology*, 122(1), pp. 435–446, 2019. doi: 10.1152/jn.00211.2019.

[74] D. Ludvig, I. Cathers, and R. E. Kearney, "Voluntary Modulation of Human Stretch Reflexes," *Experimental Brain Research*, 183(2), pp. 201–213, 2007. doi: 10.1007/s00221-007-1030-0.

[75] D. Ludvig and R. E. Kearney, "Real-time Estimation of Intrinsic and Reflex Stiffness," *IEEE Transactions on Biomedical Engineering*, 54(10), pp. 1875–1884, 2007. doi: 10.1109/TBME.2007.894737.

[76] M. M. Mirbagheri, D. Chen, and W. Z. Rymer, "Quantification of the Effects of an Alpha-2 Adrenergic Agonist on Reflex Properties in Spinal Cord Injury using a System Identification Technique," *Journal of NeuroEngineering and Rehabilitation*, 7:29, 2010. doi: 10.1186/1743-0003-7-29.

[77] M. M. Mirbagheri, M. W. Kindig, and X. Niu, "Effects of Robotic-Locomotor Training on Stretch Reflex Function and Muscular Properties in Individuals with Spinal Cord Injury," *Clinical Neurophysiology*, 126(5), pp. 997–1006, 2015. doi: 10.1016/j.clinph.2014.09.010.

[78] R. E. Kearney and I. W. Hunter, "System Identification of Human Joint Dynamics," *Critical Reviews in Biomedical Engineering*, 18(1), pp. 55–87, 1990.

[79] M. M. Mirbagheri, R. E. Kearney, and H. Barbeau, "Quantitative, Objective Measurement of Ankle Dynamic Stiffness: Intrasubject Reliability and Intersubject Variability," in *18th Annual International Conference of the IEEE Engineering in Medicine and Biology Society*, Amsterdam, Netherlands: IEEE, 1996, pp. 585–586. doi: 10.1109/IEMBS.1996.651876.

[80] Scientific Advisory Committe of the Medical Outcomes Trust, "Assessing Health Status and Quality-of-Life Instruments: Attributes and Review Criteria," *Quality of Life Research*, 11(3), pp. 193–205, 2002. doi: 10.1023/A:1015291021312.

[81] R. Xia, A. Muthumani, Z.-H. Mao, and D. W. Powell, "Quantification of Neural Reflex and Muscular Intrinsic Contributions to Parkinsonian Rigidity," *Experimental Brain Research*, 234(12), pp. 3587–3595, 2016. doi: 10.1007/s00221-016-4755-9.

[82] J. M. Finley, Y. Y. Dhaher, and E. J. Perreault, "Acceleration Dependence and Task-specific Modulation of Short- and Medium-Latency Reflexes in the Ankle Extensors," *Physiological Reports*, 1(3):e00051, 2013. doi: 10.1002/phy2.51.

[83] K. P. Blum, B. L. D'Incamps, D. Zytnicki, and L. H. Ting, "Force Encoding in Muscle Spindles during Stretch of Passive Muscle," *PLoS Computational Biology*, 13(9):e1005767, 2017. doi: 10.1371/journal.pcbi.1005767.

Chapter 2

Disentangling Acceleration-, Velocity- and Duration-Dependency of the Short- and Medium-Latency Stretch Reflexes in the Ankle Plantarflexors

R. C. van 't Veld, E. H. F. van Asseldonk, H. van der Kooij, A. C. Schouten

Abstract — Motorized assessment of the stretch reflex is instrumental to gain understanding of the stretch reflex, its physiological origin and to differentiate effects of neurological disorders, like spasticity. Both short-latency (M1) and medium-latency (M2) stretch reflexes have been reported to depend on the velocity and acceleration of an applied ramp-and-hold perturbation. In the upper limb, M2 has also been reported to depend on stretch duration. However, wrong conclusions might have been drawn in previous studies as the interdependence of perturbation parameters (amplitude, duration, velocity, acceleration) possibly created uncontrolled, confounding effects. We disentangled the duration-, velocity- and acceleration-dependence and their interactions of the M1 and M2 stretch reflex in the ankle plantarflexors. To disentangle the parameter interdependence, 49 unique ramp-and-hold joint perturbations elicited reflexes in ten healthy volunteers during a torque control task. Linear mixed model analysis showed M1 depended on acceleration, not velocity or duration, whereas M2 depended on acceleration, velocity and duration. Simulations of the muscle spindle Ia afferents coupled to a motoneuron pool corroborated these experimental findings. In addition, this simulation model did show a nonlinear M1 velocity- and duration-dependence for perturbation parameters outside the experimental scope. In conclusion, motorized assessment of the stretch reflex or spasticity using ramp-and-hold perturbations should be systematically executed and reported. Our systematic motorized and simulation assessments showed that M1 and M2 depend on acceleration, velocity and duration of the applied perturbation. The simulation model suggested that these dependencies emerge from: muscle-tendon unit and muscle cross-bridge dynamics, Ia sensitivity to force and yank, and motoneuron synchronization.

This chapter was published in the *Journal of Neurophysiology*, 126(4):1015-1029, 2021. The code and data underlying this publication are available via 4TU.ResearchData. doi: 10.4121/c.5571333

2.1 Introduction

Reflexes are an important mechanism within human movement control to cope with external perturbations during daily living. Specifically, the stretch reflex is the rapid motor response to counteract an unexpected lengthening of a muscle. Unfortunately, an exaggerated stretch reflex, i.e. hyperreflexia or spasticity, is often present in people with brain or neural injuries, such as cerebral palsy or spinal cord injury [1, 2]. Hyperreflexia contributes to the movement disorder observed in these people, limiting their functional independence.

Motorized assessment of the stretch reflex involves imposing a joint movement and measuring the subsequent response in muscle activity. The advantage of motorized above manual assessment is that the stretch perturbations can be precisely controlled and standardized [3]. After a sudden muscle stretch, three consecutive responses can be observed in the electromyography (EMG) in the lower limb: the short-latency (M1), medium-latency (M2) and long-latency (M3) response [4]. Motorized assessment is important to gain understanding of the stretch reflex, its physiological origin and to differentiate effects of neurological disorders.

Previous studies concluded that stretch reflex responses depend on several factors: task [5], predictability [6] and background muscle activation [7]. Moreover, ramp-and-hold perturbation characteristics influence the M1 and M2 responses. Both M1 and M2 are reported to depend on maximum velocity [8–15] and maximum acceleration [16, 17], whereas stretch amplitude does not affect either M1 or M2 [9, 15]. Stretch duration is reported to only affect M2 and not M1 [9, 14, 15, 18]. However, the amplitude, duration, velocity and acceleration parameters of a ramp-and-hold perturbation are related, which warrants further investigation of these observed dependencies.

The interdependence of the amplitude, duration, velocity and acceleration parameters is important to consider when investigating the effect of perturbation characteristics. Regarding these four parameters, perturbation signals can only be designed based on three independent parameters. For example, Dietz *et al.* [11] investigated the velocity-dependence, but scaling of perturbation velocity was achieved by scaling acceleration, creating a potential confounder. All other studies that investigated velocity-dependence also potentially had acceleration as confounder, as none reported the acceleration profile used [8–10, 12–15]. Similarly, studies on muscle spindle firing dynamics are subject to the same interdependence. For example, Blum *et al.* [19] observed a relationship of the Ia afferent response's dynamic index with stretch velocity and initial burst with stretch acceleration. However, the simulated stretch velocity and acceleration were varied with a perfect correlation, thus the observed relations cannot conclusively be linked to either velocity or acceleration. In general, wrong conclusions might have been drawn in previous studies regarding the amplitude, duration, velocity and acceleration dependence of muscle spindle dynamics and subsequent M1 and M2 response.

The goal of this chapter is to disentangle the duration-, velocity- and acceleration-dependence and their interactions of the M1 and M2 stretch reflex in the ankle plantarflexors. Ramp-and-hold perturbations with the amplitude parameter as dependent variable are used to investigate M1 and M2. Therefore, the amplitude dependency is not investigated. Based on the previously reported dependencies, we hypothesize that the M1 response depends on velocity and acceleration. Moreover, we hypothe-

size that the M2 response depends on duration, velocity and acceleration. The M2 duration-dependence has only been reported in the upper limb [17]. To disentangle the perturbation parameters under investigation, 49 unique perturbation profiles are used. In addition, a biophysical simulation model of the muscle spindle Ia afferents [19] coupled to a motoneuron pool [20] was implemented. This simulation model was used to corroborate the experimental findings, investigate stretch reflex dependencies across an extended set of perturbation parameters and gain a physiological understanding of the observed dependencies. The outcome of this study aims to help understanding of the stretch reflex and to stress the importance of a sound perturbation profile design in future stretch reflex studies.

2.2 Materials and Methods

2.2.1 Participants

Ten volunteers with no history of neuromuscular disorders participated in the study: age 26.4±1.9 yr, 2 women. The EEMCS/ET ethics committee of the University of Twente approved the study (RP 2018-58) and all participants provided written informed consent.

2.2.2 Apparatus

Participants were seated on an adjustable chair with the right foot connected to a robotic manipulator fixed onto the chair frame, see Fig. 2.1. The foot connection to the manipulator used a rigid footplate and Velcro straps. The posture was controlled for by supporting the upper body and leg using the adjustable chair. The chair ensured that knee and hip angles were fixed at 150° and 120°, respectively. Both knee and hip were defined at 180° for a perfectly straight posture. The starting manipulator angle was set at a 90° ankle angle, defined as the angle between shank and foot determined using a goniometer. The ankle and manipulator axes of rotation were visually aligned at the start of the experiment, minimizing knee translation due to the applied ankle rotations.

A one degree-of-freedom (DOF) manipulator (Moog, Nieuw-Vennep, the Netherlands) applied ramp-and-hold perturbations stretching the ankle plantarflexors in the sagittal plane. Ankle angle and angular velocity were represented by the angular position and velocity of the footplate measured using the actuator's encoder. Ankle torque was measured with a torque sensor placed between the actuator and footplate. Angle, velocity and torque were recorded at 2048 Hz, all defined positive in dorsiflexion direction. The muscle activity of Soleus (SOL), Tibialis Anterior (TA), Gastrocnemius Medialis and Lateralis (GM and GL, respectively) were recorded at 2048 Hz using a Porti electromyography (EMG) device (TMSi, Oldenzaal, the Netherlands). EMG electrodes were placed according to the SENIAM guidelines [21].

2.2.3 Experimental Protocol

Participants were instructed to keep background torque constant throughout the experiment using a feedback screen, see Fig. 2.1. The feedback screen provided biofeedback of a 6 s history of the smoothed (moving average, 200 ms window) measured torque and a -3±0.1 Nm torque target, i.e. the participant exerted a plantarflexion torque. The torque

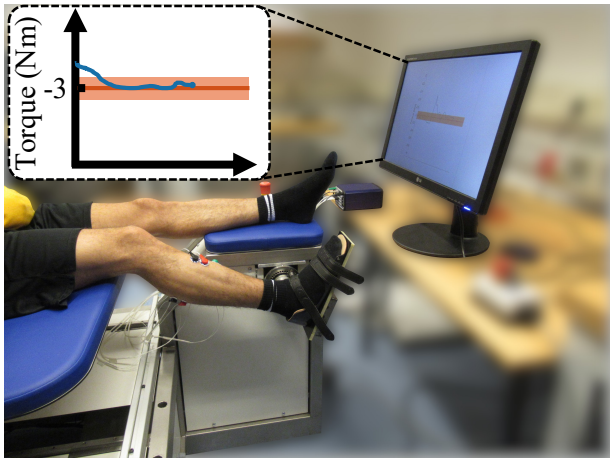

Figure 2.1: Overview experimental setup. Participants were seated on an adjustable chair. An manipulator applied dorsiflexion, ramp-and-hold perturbations around the right ankle joint, while measuring the response in muscle activity. Participants were instructed to keep a constant background torque using a feedback screen. The feedback screen showed a (*red*) plantarflexion torque target around -3±0.1 Nm and a (*blue*) smoothed history of the torque exerted by the participant.

task was used to ensure a constant background muscle activation, uncorrelated to changes in perturbation parameters. As task instruction can influence the stretch reflex response, participants were instructed to not respond to the perturbations, similar to Finley *et al.* [17]. Moreover, participants were instructed to generate background torque as if rotating the ankle without using the upper leg. To support these instructions, the influence of the ramp-and-hold perturbations on the torque feedback was attenuated. A constant value was shown during each perturbation, equal to the torque value shown just before perturbation onset.

Stretch reflexes were elicited using 49 unique perturbation profiles. These 49 perturbation profiles were the combination of 2 acceleration levels (140 and 175 rad/s^2), 3 velocity levels (2.0, 2.5 and 3.0 rad/s) and 10 duration levels (30 to 75 ms with 5 ms steps), see Fig. 2.2. As a result, stretch amplitudes ranged from 0.031 rad (1.76°) to 0.165 rad (9.45°). The experimental scope was limited to avoid excessive muscle fatigue and participant loss of attention. As existing data sets already focused on acceleration and velocity [12, 13, 16, 17], we opted to include a broad range of duration levels. Combining all levels would give 60 unique perturbations, however 11 of these perturbations had an infeasible combination of parameters. Specifically, for short duration stretches, high velocities cannot be reached given the chosen acceleration levels.

Perturbation profiles were designed to disentangle the duration, velocity and acceleration parameters, see Fig. 2.2. The acceleration levels (140 and 175 rad/s^2) were taken directly from Finley *et al.* [17], as a clear M2 response was present in the ankle plantarflexors at these levels. The acceleration profile consisted of four smooth transition shapes (6 samples, sinusoidal) with a constant level in-between. The profile was scaled linearly to achieve the chosen acceleration levels. Moreover, changing the length of constant acceleration periods allowed to set velocity levels. The velocity levels (2.0,

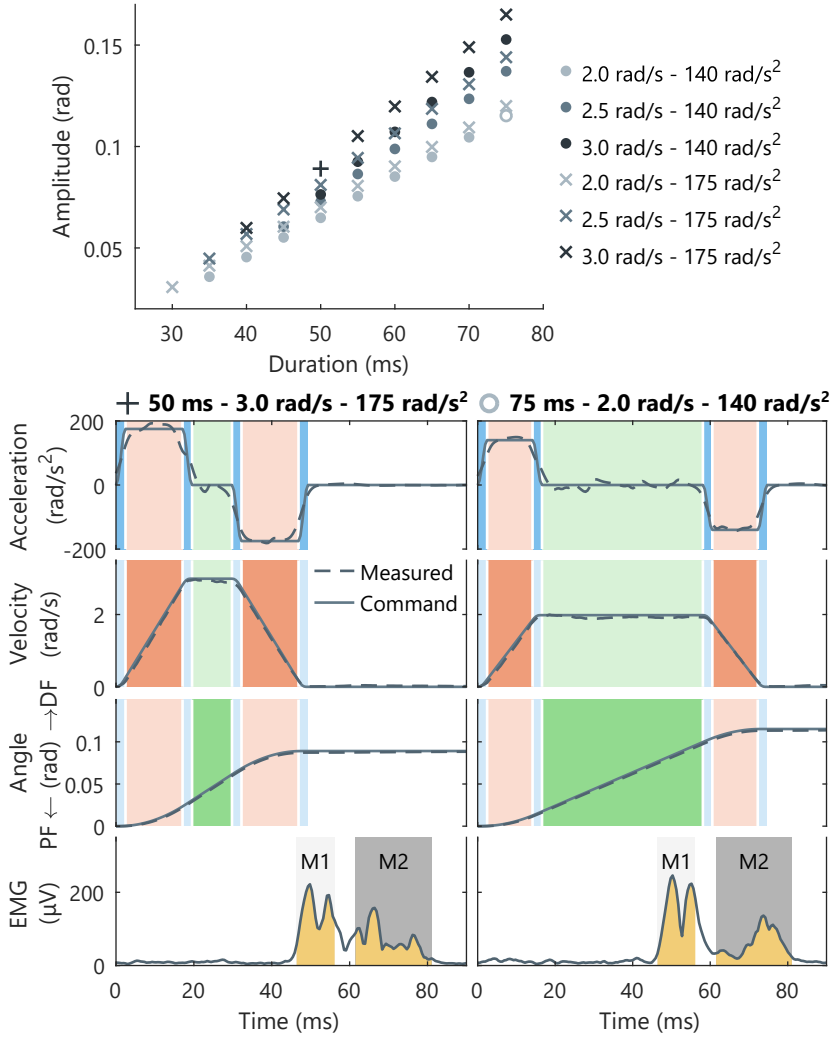

Figure 2.2: Stretch reflex perturbation design. *(Left)* Overview of all 49 perturbation profile parameters executed during the experiment. For each profile the duration, maximum velocity and maximum acceleration parameters were fixed with the amplitude as dependent parameter. Detailed time series are shown for the two highlighted perturbation profiles *(plus & circle)*.
(Right) Commanded and measured angle, velocity and acceleration for the two highlighted perturbation profiles. The corresponding ensemble-averaged stretch reflex EMG response of a single representative participant are also shown. The maximum acceleration parameter was set by scaling the *(blue shaded)* sinusoidal shape transitions. The maximum velocity parameter was set by elongating the *(red shaded)* period with maximum acceleration. The perturbation duration was set by elongating the *(green shaded)* period with maximum velocity. The stretch reflex EMG response shows the *(yellow shaded)* 10 ms M1 window and 20 ms M2 window used to quantify reflex activity.

2.5 and 3.0 rad/s) were chosen in a similar range to previous experiments reporting velocity-dependency of the ankle stretch reflex [10, 12, 13]. Changing the length of constant velocity periods allowed to set duration levels. The range of duration levels (30 to 75 ms) was defined based on the duration-dependency shown in the wrist [14, 15]. A small resolution of 5 ms was chosen as the duration effect for M2 has not been explored in the ankle before and nonlinear effects may exist [14, 15].

The experiment consisted of 12 blocks with all 49 perturbation profiles elicited exactly once per block. The order of the perturbations was randomized for each block. The stretch reflexes were elicited with a random 3-5 s interval between each perturbation. The blocks were executed with a 2 min. break between each block and a larger 5 min. break between Blocks 4-5 and Blocks 8-9 to prevent fatigue.

2.2.4 Data Analysis

The correct execution of the torque task was checked for each stretch reflex during data analysis. This check was necessary as stretch reflexes were applied continuously, even when participants did not maintain the desired torque. The background torque was computed as the average torque over the 200 ms period before perturbation onset. All stretches with a background torque deviating more than ±0.2 Nm from the -3 Nm instructed were rejected from further analysis.

EMG signals were high-pass filtered (2nd-order, 5 Hz, Butterworth) and rectified. For each muscle of every participant, the M1 and M2 analysis windows were determined via visual inspection. The M1 and M2 windows were set using the ensemble average of all stretch reflex responses of a participant, aligned at perturbation onset. The M1 analysis window was set centered around peak M1 activity with a 10 ms window width. A narrow window width was used as M1 timing was quite consistent across reflexes and to avoid contamination with M2 activity [17]. Across subjects, the SOL and GM/GL M1 windows were placed starting at 39-53 ms (49 ms median) and 39-49 ms (47 ms median) after perturbation onset, respectively. The M2 analysis window was centered around peak M2 activity with a 20 ms window width. Contrary to M1, a wider 20 ms window was used for M2 to reflect the larger variability in timing observed compared with M1. The SOL and GM/GL M2 windows started at 54-70 ms (64 ms median) and 52-67 ms (62 ms median) after perturbation onset, respectively. Fig. 2.2 depicts this difference between M1 and M2 timing for a representative participant.

For each stretch reflex of every participant, background EMG activity as well as M1 and M2 response magnitude were quantified. Background EMG should reflect an average activity over the period before perturbation onset. As a result, the background EMG was computed as the mean EMG activity over the 100 ms period before perturbation onset. M1 and M2 response measures should reflect the true reflexive magnitude, typically appearing as a double-peak shape due to rectification. To compensate for background activity, background EMG was subtracted from the reflexive response and the resulting signal was half-wave rectified. M1 and M2 magnitudes were defined as the root mean square (RMS) value of this half-wave rectified signal within the M1 and M2 analysis windows, respectively. Finally, for each perturbation profile the background EMG, M1 magnitude and M2 magnitude measures were averaged across all repetitions of that profile within a participant.

2.2.5 Statistical Analysis

The statistical analysis was performed using linear models (LMs) and linear mixed-effect models (LMMs) in R3.6.2 (R Foundation for Statistical Computing, Vienna, Austria). An LM was used to check the constancy of the background activity of all muscles and the torque to exclude potential confounding effects on any of the 49 perturbation profiles. All background scores were standardized within-subject using the Z-score. This standardization was required to avoid heteroscedasticity due to different µV levels of background EMG activity introducing unequal variances across-subjects. An LM with perturbation identifier as fixed effect, i.e. using 49 nominal levels, was fit for each background activity separately and the potential effect was evaluated using an ANOVA F-test.

LMMs, fitted for each ankle plantarflexor muscle (SOL, GM, GL) separately, were used to evaluate the dependence of the M1 and M2 stretch reflex. All M1 and M2 responses were normalized within-subject by dividing them with the subject mean across all responses, thus expressing M1 and M2 in %EMGmean. This normalization avoided convergence issues due to across-subject differences in response magnitude and variance. A consistent model building strategy was employed across all LMMs to minimize bias within the presented results. First, the fixed effects models were built, which always included an acceleration, velocity and duration predictor to test the main hypotheses. For the M2 response models a two-piece linear predictor for duration was used to fit any nonlinear effects, as observed previously [14, 15]. The two-piece linear predictor adds a discontinuity to allow the predictor to have a different slope at both sides of this breakpoint [22, 23]. The breakpoint was placed by minimizing the model residual error using a 5 ms resolution. Such a breakpoint was not added to the M1 model, as we hypothesized that no M1 duration-dependence would appear. In addition, to avoid overfitting, interaction effects were added in full sets per order. Thus, initially all first order interactions, then all second order interactions, etc., as long as model improvements were significant at α=0.05 using an ANOVA F-test. Second, maximum random effects structures were added to the LMMs to allow for between-subject variation of all fixed effects [24]. Note, no random effect for intercept was added, because the intercept for each subject was exactly equal to 100 %EMGmean due to the applied normalization. The addition of a random effect for every fixed effect induced convergence issues in all models. To achieve convergence, the step-by-step recommendations of Brauer and Curtin [25] were used, selectively removing covariances between random effects as well as any random effect parameters equal to zero. As a result, exact random effect models varied per LMM, e.g. SOL M1 model included an acceleration, duration and acceleration by duration random effect, whereas SOL M2 included an acceleration, velocity and nonlinear duration random effect.

The main hypotheses about acceleration-, velocity- and duration-dependence of the M1 and M2 responses were evaluated by testing the respective main effects. Conditional main effects, i.e. those influenced by interaction effects, were tested across a wide range of conditions to provide insight into the stretch reflex dependencies. For M1, conditional main effects were evaluated at all three velocity and both acceleration levels, as well as the shortest (35 ms) and longest (75 ms) duration. For M2, conditional main effects were evaluated at all three velocity and both acceleration levels as well as the

shortest (35 ms), middle (55 ms) and longest (75 ms) duration. The 55 ms duration was added for M2, as the breakpoint for all LMMs was located at this point. The conditional main effects were tested using a Wald t-test with Kenward-Roger correction for DOF and a Bonferroni correction, applied to the p-value, for multiple comparison per fixed effect. Unconditional main effects and the interaction effects were tested using a type-II ANOVA F-test with Kenward-Roger correction for DOF. Random effects were not used for any statistical inferences and were solely included to improve the DOF and standard error estimates of the fixed effects model.

2.2.6 Simulation Model

A simulation model was implemented (Matlab 2017b, Mathworks, Natick, MA, USA) to qualitatively support the experimental results, in a similar fashion to a study by Schuurmans *et al.* [15]. In short, the experimental perturbation profiles were applied to a muscle spindle model to obtain the Ia afferent firing rate. Together with a constant tonic alpha drive, the Ia firing rate was used as input for a motoneuron pool to simulate neural activity. M1 and M2 response measures were extracted from the motoneuron pool output as in the experimental protocol. The muscle spindle model used within Schuurmans *et al.* [15] by design lacked an initial burst response after perturbation onset [26]. Due to the rapid timing of the stretch reflex response, this initial Ia burst response has been considered as an important contributor to the stretch reflex and especially the M1 response, see supplementary Fig. B.1 [16, 17]. Therefore, the muscle spindle model [26] was replaced with a multiscale muscle mechanics model in which this burst does emerge [19].

Equal to the experimental protocol, ramp-and-hold perturbations with decoupled acceleration, velocity and duration parameters, as in Fig. 2.2, were used within the simulation environment. The velocity of the entire muscle-tendon unit (MTU), required as model input, was assumed to scale linearly with perturbation velocity [15]. The used scaling factor $r_{muscle}/L_{muscle} \cdot L_0$ consisted of the muscle moment arm r_{muscle} (52 mm) and muscle length L_{muscle} (367 mm), based on the Soleus muscle [27, 28], and initial half-sarcomere length L_0 (1300 nm) [19]. An extended set of 167 perturbation profiles was used within simulation to also gain insight on dependencies outside of the experimental scope. These 167 perturbation profiles were the combination of 6 acceleration levels (87, 105, 140, 175, 240 and 300 rad/s^2), 6 velocity levels (0.5, 1.0, 2.0, 3.0, 4.0 and 5.0 rad/s) and 10 duration levels (13, 18, 23, 30, 35, 41, 44, 49, 52 and 64 ms).

A multiscale muscle mechanics model was used to obtain Ia afferent firing rate based on applied MTU velocity, and alpha and fusimotor drive inputs [19]. The multiscale element refers to the muscle spindle and muscle-tendon mechanics included within the model. The model has been validated qualitatively, not quantitatively, against well-known muscle spindle firing characteristics in isometric conditions and after ramp-and-hold and triangular stretches [19]. The validated model implementation and parameterization was adopted without any changes. The alpha and fusimotor drives were set to 15% and 70%, respectively, to allow for the initial burst to appear within the Ia afferent response [19].

An integrate-and-fire motoneuron pool model, consisting of 300 neurons, was used to obtain neural output based on Ia firing rate, alpha drive (42.5 sp/s) and the

transport delay (40 ms) [15]. To obtain a suitable model response, the normalized Ia firing rate was scaled (arbitrarily) with a gain of 400 and alpha drive was set to achieve an approximate background activity of 10 sp/s [15, 20, 29]. To serve as input to each fiber of the motoneuron pool, both Ia firing rate and alpha drive were converted into spike trains via a Poisson process. The model implementation and parameterization was taken directly from studies by Schuurmans *et al.* [15] and Stienen *et al.* [30] with only a single parameter adaptation. A refractory time constant τ_r of 5 ms instead of 20 ms was used to better reflect the relative timing of M1 and M2 observed experimentally.

Twelve repetitions of the perturbation profiles were simulated at a 2048 Hz discrete time frequency to match the experimental protocol. Motoneuron pool output was low-pass filtered (2nd-order, 200 Hz, Butterworth) to smooth the results. M1 and M2 magnitudes were computed using the same data analysis methods as in the experiment. The M1 and M2 analysis windows were placed at 42-57 ms and 57.5-76 ms, respectively, to best accommodate the motoneuron pool output.

2.3 Results

We investigated the M1 and M2 stretch reflex response to disentangle previously reported acceleration-, velocity- and duration-dependence. A total of 49 perturbation profiles were used to elicit stretch reflexes, across 2 acceleration levels, 3 velocity levels and 10 duration levels. To study our hypotheses, LMMs were fit for M1 and M2 response of the SOL, GM and GL muscles to these perturbations averaged across 12 repetitions per participant. In addition, we studied an extended set of 167 perturbation profiles within a qualitative simulation environment in support of the experimental findings.

2.3.1 Ensemble Reflexive Responses

Participants were able to keep background torque constant at -3 Nm (plantarflexion) throughout the experiment as instructed. Across participants, 4.3% of all stretches was rejected from further analysis, as background torque deviated more than ±0.2 Nm. Per participant, rejection rates varied between 0.5 and 12.1%, similar to rates reported by Schuurmans *et al.* [15], with a minimum of 7 (of 12) reflex responses used to average across repetitions. For all muscles and the torque, variations in background activity did not consistently differ for any of the 49 perturbation profiles within the LMs (SOL: $F_{(48,441)} = 0.874$, $p = 0.71$; GM: $F_{(48,441)} = 1.05$, $p = 0.39$; GL: $F_{(48,441)} = 0.982$, $p = 0.51$; TA: $F_{(48,441)} = 0.779$, $p = 0.86$; Torque: $F_{(48,441)} = 0.663$, $p = 0.96$).

Visual inspection of the time series of the ensemble-averaged SOL reflexive response showed clear effects due to acceleration and duration, see Fig. 2.3. The time series showed that M1 magnitude increased with acceleration and, contrarily, that M2 magnitude decreased with acceleration. Furthermore, M2 increased with duration for short durations up to around 50 ms. Visual inspection did not show an M1 or M2 velocity-dependence, or M1 duration-dependence. LMMs were used to confirm these observations across all participants, muscles and the entire set of perturbation parameters.

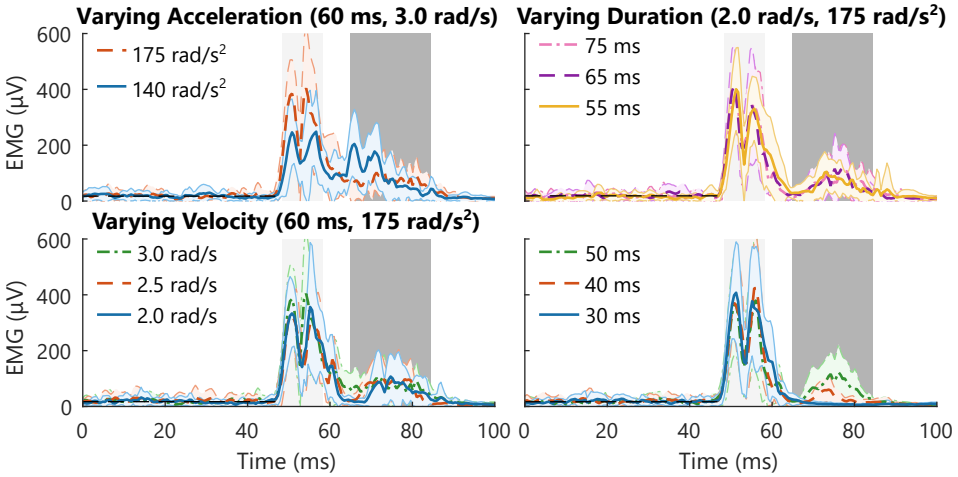

Figure 2.3: Ensemble averages (± SD, 7-12 repetitions) of Soleus stretch reflex responses for several perturbation parameters for a single representative participant. Ensemble averages of stretch reflex responses were aligned at perturbation onset. The participant-specific *(light-grey shaded)* M1 and *(dark-grey shaded)* M2 window were placed between 48-58 ms and 65-85 ms, respectively. Mean baseline activity is indicated until the M1 area *(black, dashed line)*. The reflexive responses are shown across: *(Left, Top)* 2 maximum acceleration levels for constant duration (60 ms) and maximum velocity (3 rad/s), and *(Left, Bottom)* 3 maximum velocity levels for constant duration (60 ms) and maximum acceleration (175 rad/s^2), *(Right)* 6 (of 10) durations levels for constant maximum velocity (2 rad/s) and acceleration (175 rad/s^2).

2.3.2 Simulated Reflexive Responses

The stretch reflex arc model allowed for a double burst of activity for both Ia firing rate and motoneuron pool output, see Fig. 2.4. High acceleration (64 ms - 4 rad/s - 240 rad/s^2) showed two Ia firing rate peaks, at 18 ms and 45 ms, also visible within the bag1 ("dynamic") intrafusal yank profile. A lower acceleration (140 rad/s^2) only showed a single peak at 26 ms. The motoneuron pool output showed a double peak output for both accelerations with an M1 response around 49-52 ms and an M2 response around 62.5-69 ms, similar to the experimental results.

Visual inspection of the model time series showed effects of acceleration, velocity and duration on the Ia firing rate and both M1 and M2 magnitude, see Fig. 2.5. With increased acceleration, the Ia firing rate slope steepened and both peak and steady-state firing rate were reached earlier (Fig. 2.5A). Moreover, M1 increased with acceleration, whereas M2 showed a nonlinear acceleration dependence (Fig. 2.5D). With increased velocity, the ascending slope of the Ia firing rate continued to rise longer and towards a higher magnitude, because the perturbation had a longer period of maximum acceleration (Fig. 2.5B). Both M1 and M2 increased with velocity, although M1 plateaued above 2 rad/s (Fig. 2.5E). Stretch duration only affected the final period of the Ia firing rate with magnitude dropping and reaching steady-state at the set stretch duration (Fig. 2.5C). Both M1 and M2 increased with duration and reached a plateau value above 23 and 41 ms, respectively (Fig. 2.5F).

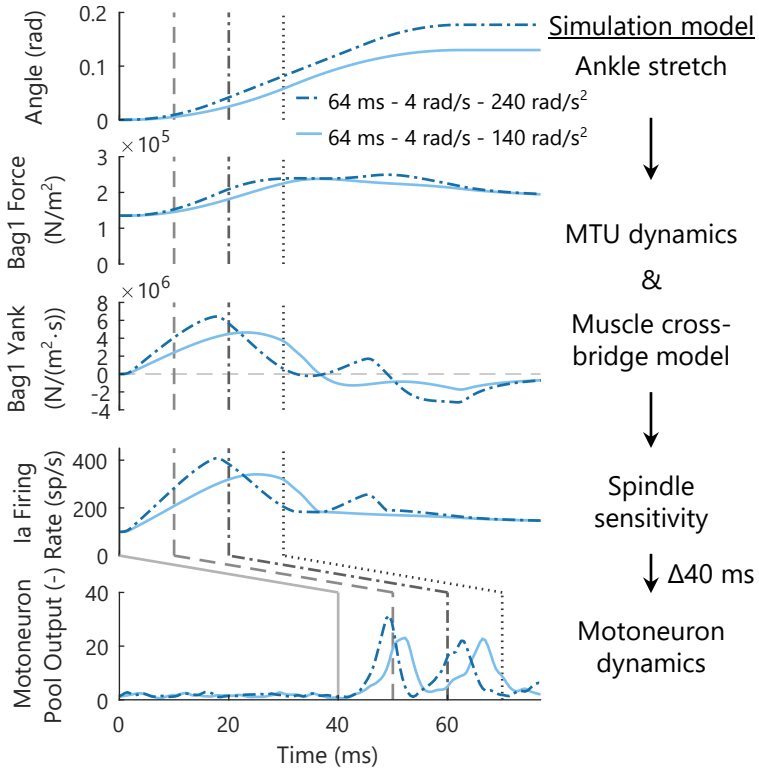

Figure 2.4: Model simulation of stretch reflex arc for two typical perturbation profiles with varying acceleration at 64 ms duration and 4 rad/s velocity. *(1st row)* Simulated joint angle. *(2nd/3rd row)* Bag1 or dynamic intrafusal muscle fiber force and yank. Intrafusal force and yank profiles emerge from the muscle-tendon unit (MTU) and muscle cross-bridge dynamics in response to the applied joint perturbation. *(4th row)* Muscle spindle Ia afferent instantaneous firing rate. Ia firing rate emerges directly from the spindle sensitivity to the intrafusal force and yank profiles. *(5th row)* Motoneuron pool neural output. Motoneuron output emerges from the neural integrate-and-fire dynamics stimulated by the Ia firing rate and a tonic supraspinal input. For all rows, the grey vertical lines show the relative timing of all events, with the lines shifted by the 40 ms transport delay within the motoneuron pool towards the bottom row.

The simulations revealed that the relative timing of the applied perturbation, Ia firing rate and motoneuron output, as well as motoneuron synchronization were instrumental for the observed dependencies. M1 and M2 were simulated with a 40 ms transport delay and quantified using windows between 42-57 ms and 57.5-76 ms. Therefore, M1 and M2 could only be causally influenced by the perturbation and Ia firing rate between 0-17 ms (M1) and 0-36 ms (M2), see M1/M2 brackets Fig. 2.5A-C. For example, the Ia firing rate burst around 45 ms observed for high acceleration could not influence either M1 or M2, see Fig. 2.4 and Fig. 2.5A/D. Besides, the plateau observed for the M1 velocity-dependence above 2.0 rad/s could not be explained based on timing (Fig. 2.5E). The 2.0 rad/s and 4.0 rad/s perturbations had a different Ia firing rate within the 0-17 ms window, see M1 bracket Fig. 2.5B. Yet, both M1 magnitudes were equal due to

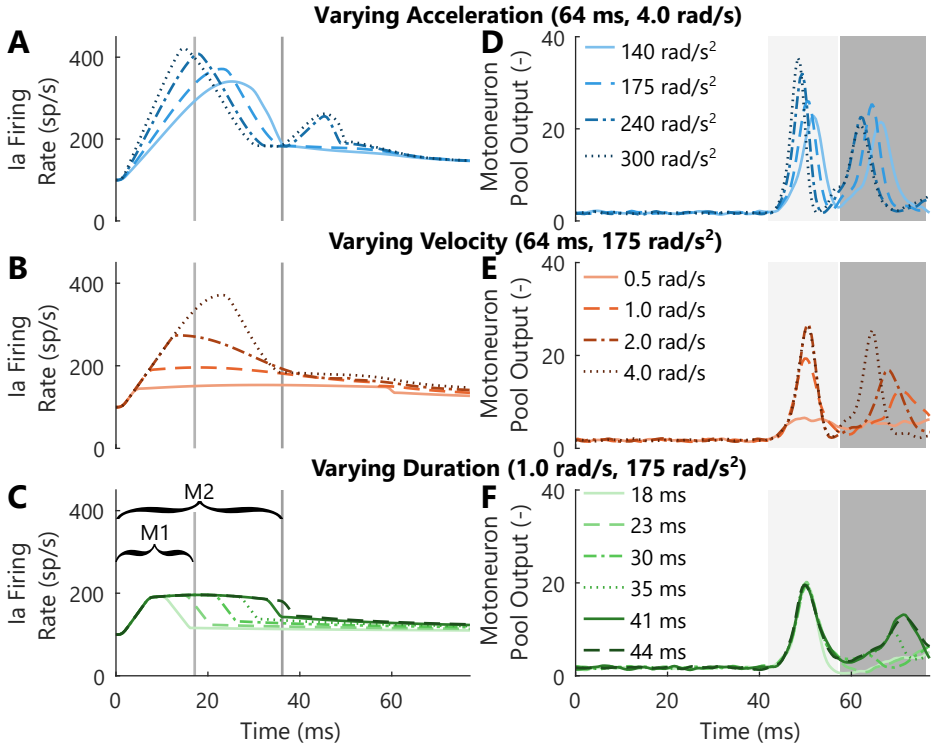

Figure 2.5: Simulated stretch reflex responses for several perturbation parameters. Both Ia firing rate *(A-C)* and ensemble-averaged motoneuron pool output *(D-F)* were aligned at perturbation onset. The *(light-grey shaded)* M1 and *(dark-grey shaded)* M2 windows *(D-F)* were placed between 42-57 ms and 57.5-76 ms, respectively. As a result, the Ia firing rate *(A-C)* can only causally influence M1 *(bracket until light-grey vertical)* and M2 *(bracket until dark-grey vertical)* between 0-17 and 0-36 ms after perturbation onset given the 40 ms neural transport delay. The reflexive responses are shown across: *(A/D)* 4 maximum acceleration levels for constant duration (64 ms) and maximum velocity (4 rad/s); *(B/E)* 4 maximum velocity levels for constant duration (64 ms) and maximum acceleration (175 rad/s^2); and *(C/F)* 6 durations levels for constant maximum velocity (1 rad/s) and acceleration (175 rad/s^2). Note, several lines partially overlap due to the lack of sources with large variability within the simulation environment.

synchronization of firing and refractory periods of all available neurons within the motoneuron pool. Afterwards, the increased Ia firing rate within the 0-36 ms M2 bracket for the 4.0 rad/s perturbation causes an earlier second synchronized burst (M2) of motoneuron activity with increased magnitude (Fig. 2.5E).

2.3.3 Short-Latency M1 Dependencies

Experimentally, the LMM consistently showed the increase of SOL M1 magnitude with acceleration was consistently present across participants and perturbations profiles, see Fig. 2.6A and Table 2.1. The effect size of increasing acceleration ranged from [0.53,0.81] %EMG$_{mean}$/rad/s^2 (p always <0.001). These differences in effects size were

Table 2.1: Linear mixed model results for Soleus M1 stretch reflex response with perturbation parameter predictors. Model parameters are expressed as $\%EMG_{mean}$ per fixed effect unit (± SE). Conditional main effects were tested using a Wald t-test with Kenward-Roger correction for DOF and a Bonferroni correction, applied to the p-value, for multiple comparison per fixed effect. Interactions were tested using a type-II ANOVA F-test with Kenward-Roger correction for DOF.

Fixed Effect	**Condition**	**Model Param.**	**Statistical Parameters**	
Acceleration	35 ms, 2.0 r/s	0.73 ± 0.069	$t(108) = 10.7$	$p < 0.001$
	35 ms, 2.5 r/s	0.81 ± 0.068	$t(106) = 11.8$	$p < 0.001$
	75 ms, 2.0 r/s	0.53 ± 0.071	$t(122) = 7.42$	$p < 0.001$
	75 ms, 2.5 r/s	0.60 ± 0.059	$t(61.2) = 10.3$	$p < 0.001$
	75 ms, 3.0 r/s	0.68 ± 0.066	$t(91.7) = 10.4$	$p < 0.001$
Velocity	140 r/s^2, 35 ms	-3.1 ± 3.1	$t(465) = -0.994$	$p = 1$
	140 r/s^2, 75 ms	-4.0 ± 2.4	$t(465) = -1.69$	$p = 0.37$
	175 r/s^2, 35 ms	2.1 ± 2.6	$t(465) = 0.795$	$p = 1$
	175 r/s^2, 75 ms	1.2 ± 2.6	$t(465) = 0.462$	$p = 1$
Duration	140 r/s^2, 2.0 r/s	0.073 ± 0.091	$t(29.4) = 0.799$	$p = 1$
	140 r/s^2, 2.5 r/s	0.062 ± 0.089	$t(26.3) = 0.694$	$p = 1$
	140 r/s^2, 3.0 r/s	0.050 ± 0.11	$t(63.4) = 0.450$	$p = 1$
	175 r/s^2, 2.0 r/s	-0.11 ± 0.085	$t(21.8) = -1.23$	$p = 1$
	175 r/s^2, 2.5 r/s	-0.12 ± 0.076	$t(14.1) = -1.53$	$p = 0.89$
	175 r/s^2, 3.0 r/s	-0.13 ± 0.097	$t(37.0) = -1.31$	$p = 1$
Acceleration by Velocity		0.15 ± 0.071	$F_{(1,465)} = 4.34$	$p = 0.04$
Acceleration by Duration		-0.0051 ± 0.002	$F_{(1,465)} = 4.57$	$p = 0.03$
Velocity by Duration		-0.023 ± 0.10	$F_{(1,465)} = 0.0506$	$p = 0.82$
Random Effect		**Standard Deviation or Correlation**		
Subject Acceleration		0.097		
Subject Duration		0.18		
Subject Acceleration by Duration		-0.85		
Model Fit: R^2-Marginal: 0.54; R^2-Conditional: 0.58; $N = 490$				

due to the interactions of acceleration with both velocity ($F_{(1,465)} = 4.34$, $p = 0.04$) and duration ($F_{(1,465)} = 4.57$, $p = 0.03$). The acceleration effect size translated to a modeled difference of 25 $\%EMG_{mean}$ between the 140 and 175 rad/s^2 levels at 2.5 rad/s and 55 ms. The GM and GL showed similar results, see supplementary Tables B.1 to B.4, and only results different from the SOL will be highlighted here.

Contrarily, no consistent effects of both velocity (p = [0.37,1]) or duration (p = [0.89,1]) on experimental SOL M1 magnitude were present in the LMM, see Fig. 2.6B-C and Table 2.1. The GL M1 response showed a deviation from the SOL results with an unconditional main effect for duration of 0.10±0.046 $\%EMG_{mean}$/ms ($F_{(1,10.0)} = 5.09$, p = 0.05). This duration effect size translated to a modeled difference of only 4.2 $\%EMG_{mean}$ between the 35 and 75 ms levels.

For the simulation model, M1 dependence showed a split between perturbations below or above the plateau values of 2.0 rad/s and 23 ms, see Fig. 2.6D-F and Fig. 2.8A-C.

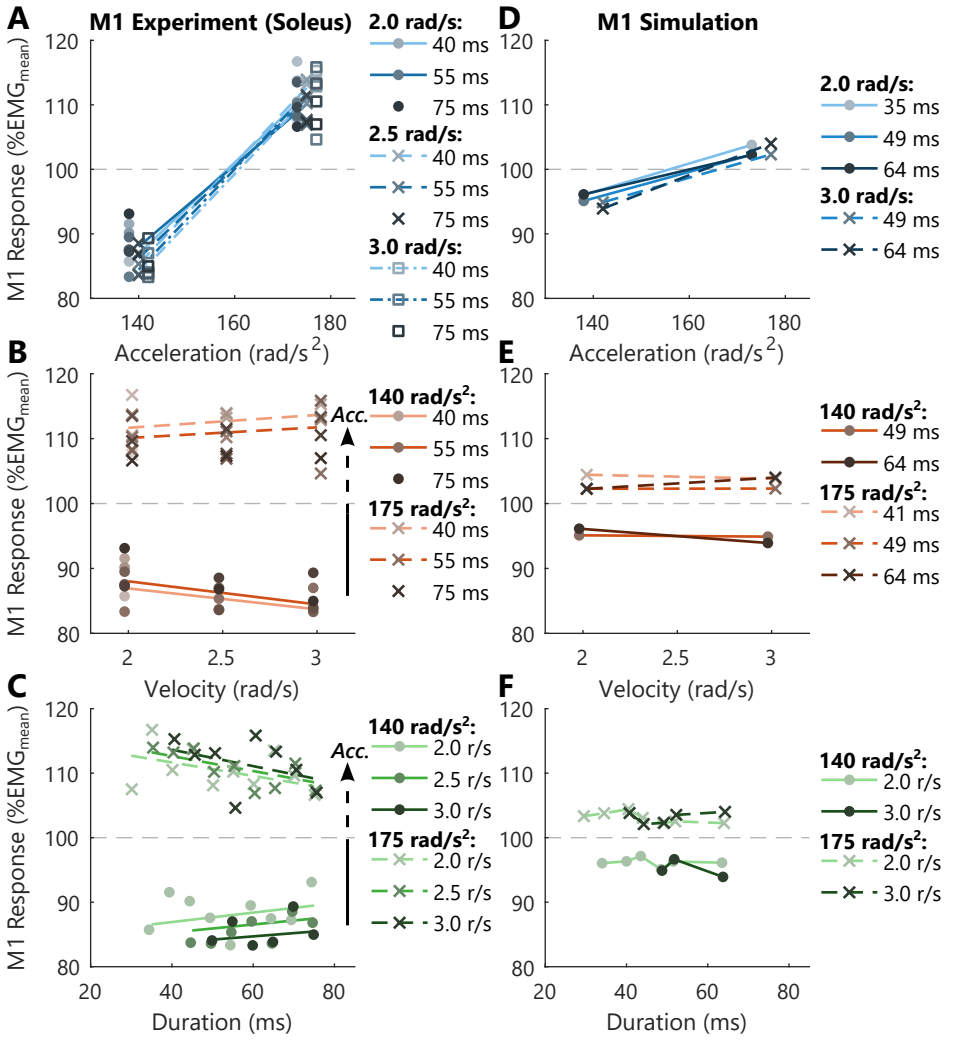

Figure 2.6: Experimental Soleus and simulated M1 stretch reflex response dependency on stretch acceleration, velocity and duration. *(A-C)* Mean experimental results across all 10 participants *(markers)* and LMM fits *(lines)*. The LMM fits were generated using the full fixed effects model, including the acceleration, velocity and duration predictors and all interactions. Statistically significant main effects, as analyzed with the LMM, are highlighted *(arrows)*, when not displayed on the x-axis. *(D-F)* Mean simulated results across all 12 repetitions *(markers/lines)* for a set of perturbation parameters matching the experimental parameters. To enhance visualization, small offsets along the x-axis were used for the individual data points in all subplots.
(A/D) M1 acceleration-dependence, split across multiple levels of duration *(color lightness)* and maximum velocity *(lines/marker style)*. *(B/E)* M1 velocity-dependence, split across multiple levels of duration *(color lightness)* and maximum acceleration *(lines/marker style)*. *(C/F)* M1 duration-dependence, split across multiple levels of maximum velocity *(color lightness)* and maximum acceleration *(lines/marker style)*. Note, for *(A/B)* only the minimum, median and maximum duration levels *(color lightness)* are included in the legend, all durations are included in the plot.

Above these 2.0 rad/s and 23 ms threshold values, M1 was unaffected by stretch velocity (Fig. 2.6E/Fig. 2.8B) and duration (Fig. 2.6F/Fig. 2.8C) and M1 increased with acceleration (Fig. 2.6D/Fig. 2.8A). The model results matched the experimental dependencies, assuming that the velocity and duration plateau threshold translated to the experimental setting, see Fig. 2.6D-F. In addition, M1 showed a velocity- and duration-dependence below these threshold values. M1 increased with velocity for velocities below 2.0 rad/s (Fig. 2.8B) and M1 increased with duration for durations below 23 ms (Fig. 2.8C). Below these threshold values, the acceleration-dependence was limited especially for perturbations with low velocity (Fig. 2.8A).

2.3.4 Short-Latency M2 Dependencies

Experimentally, the decrease of SOL M2 with acceleration varied depending on the velocity and duration levels, see Fig. 2.7A and Table 2.2. The effect size of increasing acceleration ranged from [-0.72,0.32] $\%EMG_{mean}/rad/s^2$ (p ranged from [<0.001,1]). As for M1, the variation was the result of the interactions of acceleration with both velocity ($F_{(1,448)} = 10.6$, $p = 0.001$) and duration (>55 ms: $F_{(1,448)} = 3.24$, $p = 0.07$). Specifically, for long durations (>55 ms) and high velocities (3.0 rad/s) SOL M2 decreased with acceleration. Contrarily, for short durations and low velocities no effects of acceleration were present. The acceleration effect size translated to a maximum modeled difference of -25 $\%EMG_{mean}$ between the 140 and 175 rad/s^2 levels at 3.0 rad/s and 75 ms.

The effect of increasing velocity on experimental SOL M2 magnitude depended on acceleration and duration levels, see Fig. 2.7B and Table 2.2. The effect size of increasing velocity ranged from [3.1,69] $\%EMG_{mean}/rad/s$ (p ranged from [<0.001,1]). The variation was the result of the interactions with both acceleration, and short and long durations (≤55 ms: $F_{(1,448)} = 13.0$, $p < 0.001$; >55 ms: $F_{(1,448)} = 6.00$, $p = 0.01$). Specifically, for long durations (>55 ms) SOL M2 increased with velocity, whereas no effects of velocity were present for short durations. The interaction with acceleration did not influence these dependencies. The velocity effect size translated to a maximum modeled difference of 35 $\%EMG_{mean}$ between the 2.0, 2.5 and 3.0 rad/s levels at 140 rad/s^2 and 75 ms.

To investigate the effect of duration on experimental SOL M2 magnitude a two-piece linear predictor was required, as expected based on results of the upper limb [14, 15]. The effect size of increasing duration varied due to this nonlinearity and the reported interactions with velocity and acceleration. In general, an increase in SOL M2 with duration was present for short durations (≤55 ms), which leveled off for long durations, see Fig. 2.7C and Table 2.2. The positive effect for short durations ranged from [3.0,5.2] $\%EMG_{mean}/ms$ (p always <0.001), whereas no effect for long duration was present (p = [0.16,1]). This translated to a modeled difference of 77 $\%EMG_{mean}$ between the 35 and 55 ms levels at 2.5 rad/s and 175 rad/s^2.

The experimental M2 duration-dependence was clearly confirmed within the simulation model, see Fig. 2.7F and Fig. 2.8F. The simulated M2 response showed a monotonic increase with duration across all acceleration and velocity levels. Simulated M2 was minimal for the shortest durations, given that most of the Ia afferent response fell within the 0-17 ms M1 bracket, see Fig. 2.5C. Like the experimental results, M2 leveled off for longer durations (41-49 ms) with the exact duration interacting with acceleration and velocity.

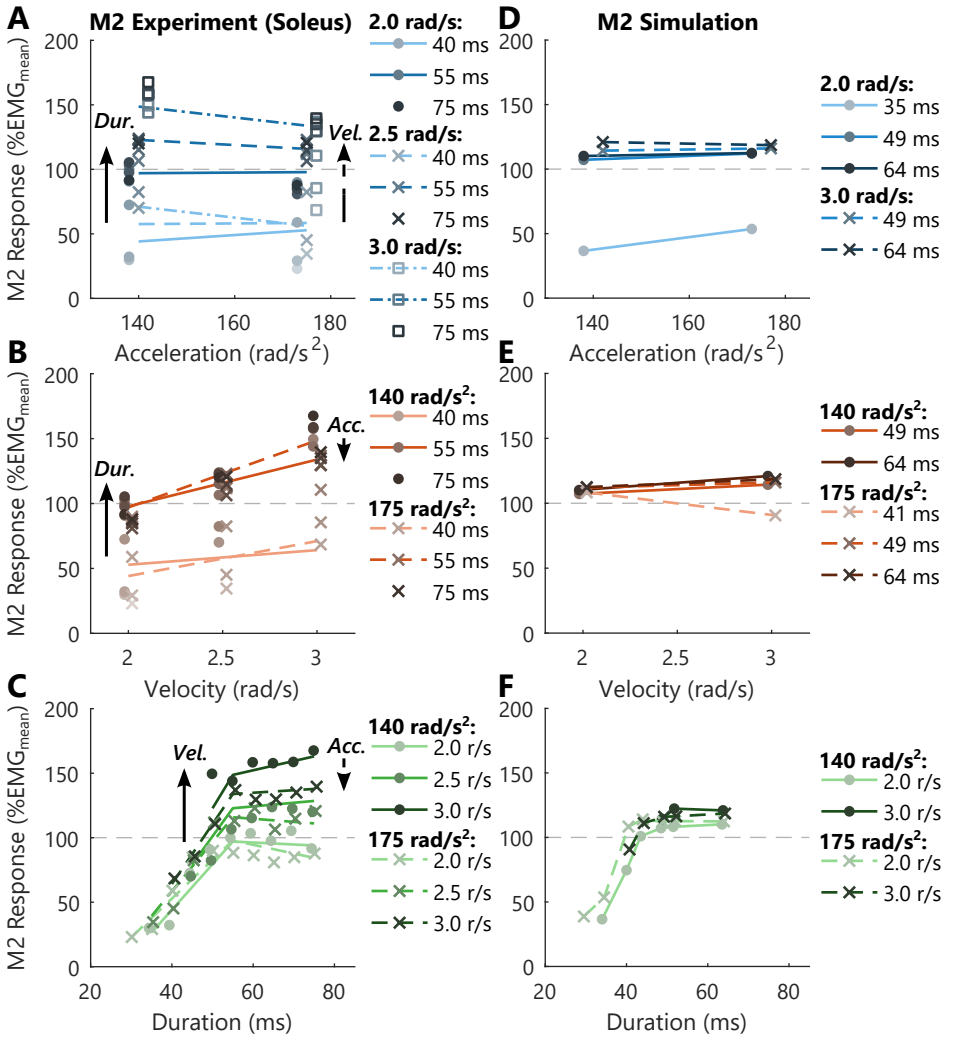

Figure 2.7: Experimental Soleus and simulated M2 stretch reflex response dependency on stretch acceleration, velocity and duration. *(A-C)* Mean experimental results across all 10 participants *(markers)* and LMM fits *(lines)*. The LMM fits were generated using the full fixed effects model, including the acceleration, velocity and duration predictors and all interactions. Statistically significant main effects, as analyzed with the LMM, are highlighted *(arrows)*, when not displayed on the x-axis. *(D-F)* Mean simulated results across all 12 repetitions *(markers/lines)* for a set of perturbation parameters matching the experimental parameters. To enhance visualization, small offsets along the x-axis were used for the individual data points in all subplots.
(A/D) M2 acceleration-dependence, split across multiple levels of duration *(color lightness)* and maximum velocity *(lines/marker style)*. *(B/E)* M2 velocity-dependence, split across multiple levels of duration *(color lightness)* and maximum acceleration *(lines/marker style)*. *(C/F)* M2 duration-dependence, split across multiple levels of maximum velocity *(color lightness)* and maximum acceleration *(lines/marker style)*. Note, for *(A/B)* only the minimum, median and maximum duration levels *(color lightness)* are included in the legend, all durations are included in the plot.

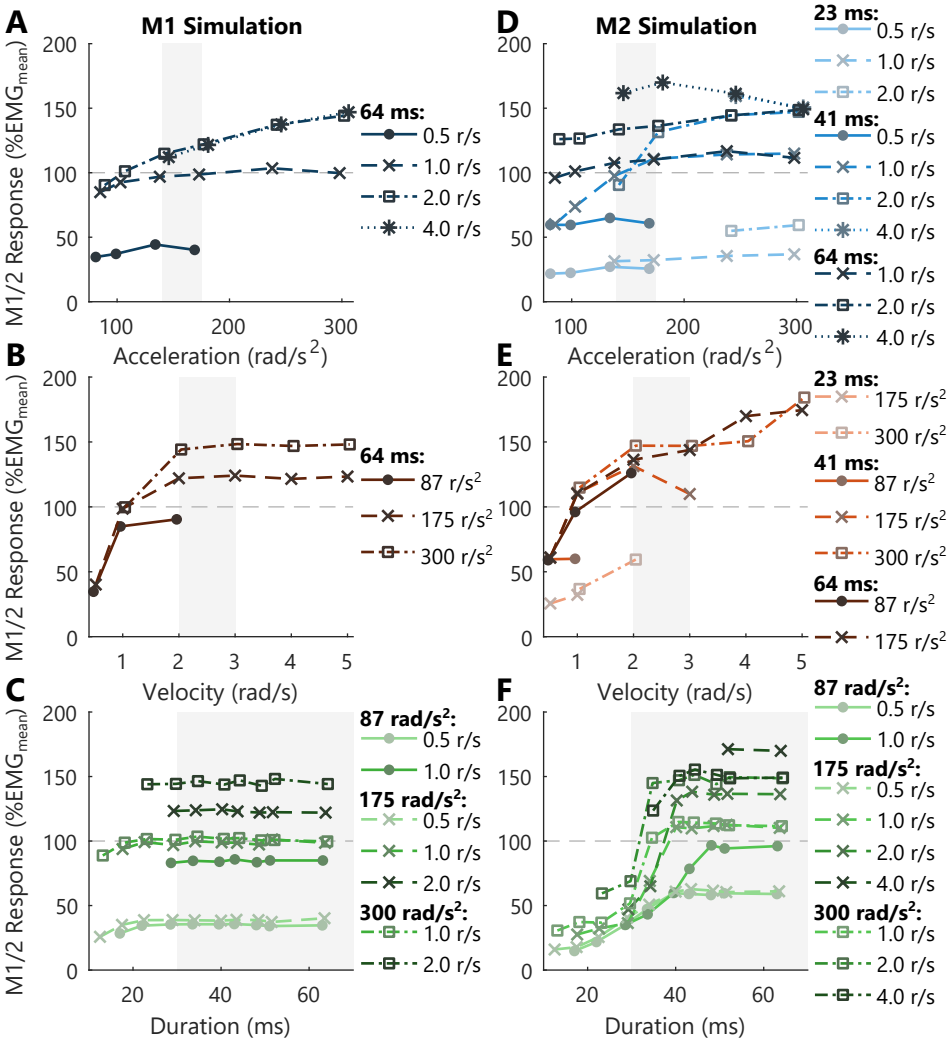

Figure 2.8: Simulated M1 and M2 stretch reflex response dependency on stretch acceleration, velocity and duration. Mean simulated results for M1 *(A-C)* and M2 *(D-F)* across all 12 repetitions *(markers/lines)* for an extended set of perturbation parameters. For reference, the limited set of experimental parameters depicted in Fig. 2.6 and Fig. 2.7 is highlighted *(grey-shaded area)*. To enhance visualization, small offsets along the x-axis were used for the individual data points in all subplots.
(A/D) M1/M2 acceleration-dependence, split across multiple levels of duration *(color lightness)* and maximum velocity *(lines/marker style)*. *(B/E)* M1/M2 velocity-dependence, split across multiple levels of duration *(color lightness)* and maximum acceleration *(lines/marker style)*. *(C/F)* M1/M2 duration-dependence, split across multiple levels of maximum velocity *(color lightness)* and maximum acceleration *(lines/marker style)*.

Table 2.2: Linear mixed model results for Soleus M2 stretch reflex response with perturbation parameter predictors. Model parameters are expressed as $\%EMG_{mean}$ per fixed effect unit (± SE). Conditional main effects were tested using a Wald t-test with Kenward-Roger correction for DOF and a Bonferroni correction, applied to the p-value, for multiple comparison per fixed effect. Interactions were tested using a type-II ANOVA F-test with Kenward-Roger correction for DOF.

Fixed Effect	**Condition**	**Model Param.**	**Statistical Parameters**	
Acceleration	35 ms, 2.0 r/s	0.32 ± 0.15	$t(367) = 2.14$	$p = 0.26$
	35 ms, 2.5 r/s	0.10 ± 0.16	$t(390) = 0.612$	$p = 1$
	55 ms, 2.0 r/s	0.024 ± 0.12	$t(279) = 0.196$	$p = 1$
	55 ms, 2.5 r/s	-0.20 ± 0.10	$t(170) = -2.04$	$p = 0.35$
	55 ms, 3.0 r/s	-0.42 ± 0.12	$t(256) = -3.62$	$p = 0.003$
	75 ms, 2.0 r/s	-0.27 ± 0.13	$t(310) = -2.10$	$p = 0.30$
	75 ms, 2.5 r/s	-0.50 ± 0.11	$t(237) = -4.43$	$p < 0.001$
	75 ms, 3.0 r/s	-0.72 ± 0.13	$t(316) = -5.44$	$p < 0.001$
Velocity	140 r/s^2, 35 ms	19 ± 12	$t(30.0) = 1.58$	$p = 0.74$
	140 r/s^2, 55 ms	52 ± 9.6	$t(13.5) = 5.36$	$p < 0.001$
	140 r/s^2, 75 ms	69 ± 10	$t(15.4) = 6.93$	$p < 0.001$
	175 r/s^2, 35 ms	3.1 ± 11	$t(21.5) = 0.281$	$p = 1$
	175 r/s^2, 55 ms	36 ± 9.7	$t(13.8) = 3.71$	$p = 0.01$
	175 r/s^2, 75 ms	53 ± 9.9	$t(15.3) = 5.37$	$p < 0.001$
Short (≤55 ms) Duration	140 r/s^2, 2.0 r/s	3.5 ± 0.47	$t(23.5) = 7.54$	$p < 0.001$
	140 r/s^2, 2.5 r/s	4.4 ± 0.49	$t(27.9) = 8.90$	$p < 0.001$
	140 r/s^2, 3.0 r/s	5.2 ± 0.60	$t(61.7) = 8.58$	$p < 0.001$
	175 r/s^2, 2.0 r/s	3.0 ± 0.42	$t(15.8) = 7.10$	$p < 0.001$
	175 r/s^2, 2.5 r/s	3.8 ± 0.41	$t(13.9) = 9.34$	$p < 0.001$
	175 r/s^2, 3.0 r/s	4.7 ± 0.51	$t(33.3) = 9.09$	$p < 0.001$
Long (>55ms) Duration	140 r/s^2, 2.0 r/s	-0.15 ± 0.31	$t(72.8) = -0.489$	$p = 1$
	140 r/s^2, 2.5 r/s	0.28 ± 0.26	$t(37.0) = 1.09$	$p = 1$
	140 r/s^2, 3.0 r/s	0.72 ± 0.32	$t(77.9) = 2.26$	$p = 0.16$
	175 r/s^2, 2.0 r/s	-0.67 ± 0.31	$t(68.5) = -2.20$	$p = 0.19$
	175 r/s^2, 2.5 r/s	-0.24 ± 0.26	$t(34.7) = -0.936$	$p = 1$
	175 r/s^2, 3.0 r/s	0.20 ± 0.32	$t(76.2) = 0.621$	$p = 1$
Acceleration by Velocity		-0.45 ± 0.14	$F_{(1,448)} = 10.6$	$p = 0.001$
Acceleration by Short-Duration		-0.015 ± 0.010	$F_{(1,448)} = 2.08$	$p = 0.15$
Velocity by Short-Duration		1.6 ± 0.46	$F_{(1,448)} = 13.0$	$p < 0.001$
Acceleration by Long-Duration		-0.015 ± 0.008	$F_{(1,448)} = 3.24$	$p = 0.07$
Velocity by Long-Duration		0.87 ± 0.36	$F_{(1,448)} = 6.00$	$p = 0.01$
Random Effect		**Standard Deviation or Correlation**		
Subject Acceleration		0.068		
Subject Velocity		27		
Subject Short-Duration		1.1		
Subject Long-Duration		0.49		
Subject Short-Dur. by Long-Dur.		0.97		
Model Fit: R^2-Marginal: 0.66; R^2-Conditional: 0.79; $N = 490$				

The simulated M2 velocity- and acceleration-dependence did not clearly match experimental results, especially within the experimental ranges of 2-3 rad/s and 140-175 rad/s^2, see Fig. 2.7D-E. In general, simulated M2 did show a monotonic increase with velocity across acceleration and duration levels (Fig. 2.8E). Still, in the experimental range the dependence on velocity was limited and sometimes even decreased with velocity. Simulated M2 showed both increasing and decreasing effects with acceleration across the velocity and duration levels (Fig. 2.7D/Fig. 2.8D). However, in the experimental range, simulated M2 mainly increased with acceleration, whereas experimental results showed a steady or decreasing M2. Such a decrease was seen for simulated M2 at higher velocity and accelerations (4.0 rad/s and 175-300 rad/s^2). For both velocity and acceleration, simulated dependencies were mainly observed for medium to long durations, as M2 was minimal at short durations.

2.4 Discussion

The goal of this chapter was to disentangle the duration-, velocity- and acceleration-dependence and their interactions of the M1 and M2 stretch reflex in the ankle plantarflexors. Experimentally, M1 magnitude increased with acceleration, whereas no effect of velocity or duration was present. These experimental findings were qualitatively replicated with a simulation model for moderate to high velocities and durations. For low velocities or short durations, not included in the experimental protocol, the simulated M1 response did show velocity- and duration-dependence with a limited acceleration-dependence. Regarding M2, a nonlinear effect of duration was present experimentally as M2 magnitude increased with duration until 55 ms, above which the effect leveled off. M2 magnitude decreased with acceleration and increased with velocity at long durations (>55 ms), whereas no effect of acceleration or velocity was present at short durations (≤55 ms). A monotonic increase in M2 response with duration was replicated with a simulation model. Moreover, the simulation model also showed M2 dependence on acceleration and velocity, although the effect of these dependencies and interaction effects did not clearly match between experiment and simulation.

2.4.1 Short-Latency M1 Dependencies

The M1 response was measured between 49-59 ms experimentally (SOL, median across-participants) and between 42-57 ms in simulation, in line with previously reported latencies [17, 31]. As such, the stretch perturbation and resulting Ia afferent response could only causally influence the M1 response until 19 ms (experiment) or 17 ms (simulation) after perturbation onset, assuming a 40 ms transport delay [29]. The simulation model showed that within this window acceleration, velocity and the shortest durations (≤23 ms) influenced the Ia afferent and M1 responses. Given the previous qualitative validation of the simulation model elements, we expect these results to translate to the experimental setting, although exact results and timings would require detailed parameter optimization [15, 19, 20]. Given the minimum 35 ms duration used experimentally, no M1 duration-dependence was expected to be measured. The SOL and GM muscles did indeed not show an experimental duration-dependence, whereas the GL unexpectedly did show a small effect. Overall, causality and timing support the lack of

M1 duration-dependence generally observed in experiments, also in previous studies [9, 14, 15, 18].

The observed acceleration-dependence of the M1 response, both experimentally and in simulation, is in line with previous results in the ankle [16, 17]. The simulation model showed that, through complex biomechanics, increased acceleration caused a steeper slope and higher magnitude of the initial burst in the Ia afferent response. Thus, the M1 acceleration-dependence is linked directly to this initial burst response and resulting motoneuron synchronization as previously simulated and hypothesized [16, 17, 19].

The observed lack of an M1 velocity-dependence for medium to high velocities, both experimentally and in simulation, contradicts previously published results [8–15]. Importantly, M1 velocity-dependence in the ankle plantarflexors was previously investigated at a larger, mainly higher, range of velocities: 1.5-7.5 rad/s [12] and 1.5-5.0 rad/s [13]. Notably, all studies that reported this velocity-dependence did not explicitly keep stretch acceleration constant. Specifically, a scaling of velocity was likely achieved by scaling acceleration, as shown by Dietz *et al.* [11]. This supposed co-variation combined with the observed acceleration-dependence in our results suggests that the observed velocity-dependence at medium to high velocities in literature could be explained as actual acceleration effects.

The nonlinear M1 velocity-dependence observed in simulation can be explained through the Ia afferent initial burst response and motoneuron synchronization. The simulation model suggested that, due to timing of all events, M1 velocity-dependence at low velocity was linked to the Ia afferent initial burst with the ascending slope continuing to rise longer towards a higher magnitude. This extends previous results that mainly linked stretch velocity to the Ia afferent dynamic index [19] and shows the importance of simulation models in which this initial burst emerges [15, 19, 26]. Moreover, our simulation results suggested that the M1 velocity-dependence plateau at medium to high velocities was caused through synchronization of motoneuron firing and refractory period [15]. As such, the additional excitation due to a higher velocity, at constant acceleration, did not increase M1 magnitude as it fell within a synchronized refractory period of the simulated motoneurons.

2.4.2 Medium-Latency M2 Dependencies

The M2 response was measured between 64-84 ms (SOL, median across-participants) experimentally and between 57.5-76 ms in simulation in line with previously reported latencies [17, 31]. As such, the stretch perturbation and resulting Ia afferent response could only causally influence the M2 response until 44 ms (experiment) or 36 ms (simulation) after perturbation onset, assuming a 40 ms transport delay [29]. Both experiment and simulation model showed that within this window acceleration, velocity and duration shape the Ia afferent and M2 responses. The M2 duration-dependence leveled-off at 55 ms (experiment) and 49 ms (simulation). The observed M2 duration-dependence is in line with previous results in the upper limb [9, 14, 15] and can be explained based on timing and causality, similar to M1. In other words, the M2 response will follow M1 when the stretch duration is applied long enough for a second synchronous burst of activity (M2) to be elicited after the first synchronous burst (M1) [15].

The M2 acceleration- and velocity-dependence observed in experiment and simulation roughly matched, albeit at different quantitative values. For both experiment and simulation, the acceleration and velocity dependencies appeared at medium to long durations, as the M2 response was minimal at short durations. The experimental M2 response showed a decrease in magnitude with acceleration at high velocities (3.0 rad/s). This outcome is in line with Finley *et al.* [17], which showed a nonlinear M2 acceleration-dependence with a decrease between 140 and 175 rad/s^2. The simulation model qualitatively also showed this nonlinear dependency, however only at a higher velocity (4.0 rad/s) and across a higher acceleration range (175-300 rad/s^2).

The experimental M2 response increased with velocity and the simulated M2 response in general also showed a monotonic increase with velocity. In previous studies, contradicting observations were reported either observing an M2 velocity-dependence [8, 10, 11, 13, 14] or not [10, 12]. Moreover, as discussed for M1, stretch acceleration was not explicitly kept constant when changing stretch velocity in previous studies, introducing the acceleration as potential confounder. Overall, the simulation model suggested that the M2 acceleration- and velocity-dependence arise through interaction between Ia afferent initial burst response and the motoneuron dynamics. Specifically, the Ia afferent peak response was often observed around the 17 ms M1 cut-off threshold, thus falling within the synchronized refractory period in the motoneuron pool given the 40 ms transport delay. This mechanism may, for example, explain the M2 decreasing with acceleration as the Ia afferent peak falls earlier resulting in less motoneuron input after the refractory period. The quantitative differences between experiment and simulation are also likely to emerge within this complex physiological interaction. As such, a more detailed investigation of M2 acceleration- and velocity-dependence would be valuable after extensive model parameter optimization.

2.4.3 Stretch Reflex Physiology

The stretch reflex arc consists of causally linked elements, in order: applied stretch perturbation, stretch proprioception, neural transport and muscle contraction. The simulation model implemented in our study simplifies the arc by using only the Ia afferent as stretch proprioceptor and a monosynaptic motoneuron pool for neural transport. This basic simulation model was able to qualitatively explain most M1 and M2 perturbation dependencies observed experimentally. Essential physiological elements of the simulation model required to achieve these explanations were: MTU and muscle cross-bridge dynamics, Ia afferent sensitivity to intrafusal force and yank, and motoneuron synchronization.

The stretch perturbation at joint scale was translated to the muscle spindle scale through simulation of MTU and muscle cross-bridge mechanics [19]. In addition, the resulting intrafusal force and yank profiles, not length, velocity or acceleration, were considered to drive the Ia afferent response [19, 32]. Combined, these multiscale mechanics determined the Ia afferent initial burst response, which dictated the resulting M1 and M2 responses based on timing. Changes in stretch acceleration and velocity converted to changes in the Ia afferent initial burst, like modulation of the slope, peak magnitude and timing, consequently changing M1 and M2.

Motoneuron synchronization of both motoneuron firing and refractory periods

translated the single Ia afferent burst into two distinguishable burst within the neural output, M1 and M2 [15]. Due to the synchronization, a long enough stretch duration is required to elicit Ia afferent input to trigger the second burst, i.e. M2 [15]. In addition, the simulation model also suggested that motoneuron synchronization can explain the lack of M1 velocity-dependence for medium to high velocities, as well as observed nonlinearities in M2 acceleration-dependence [17].

Despite general reproduction of experimental results, additional physiological mechanisms could be added to refine the match between experiment and simulation. The monosynaptic Ia afferent pathway alone cannot explain several M2 characteristics [15], like M2 exceeding M1 [33] or separate modulation of M1 and M2 [34]. First, within simulation multiple bursts of Ia afferent activity emerged through the multiscale muscle spindle mechanics, also matching previous experimental observations [35, 36]. Previous simulation studies with the muscle spindle model also showed these multiple bursts at high stretch accelerations before a more steady-state Ia firing rate is obtained [19]. These multiple burst likely emerge due to the cross-bridge cycling kinetics included in the model. Although current timing and causality links M1 and M2 completely to the initial burst, model parameter optimization to experimental results might change relative timing of events [19]. Second, additional proprioceptive pathways can contribute to the stretch reflex response. Specifically, multiple studies have shown that the muscle spindle group II afferents are likely to influence the M2 response [18, 37]. The multiscale muscle spindle model used within this study might offer an interesting framework to also study this type of afferents [19]. Third, the M2 response is also likely to originate from a mix of both spinal and trans-cortical contributions [5, 33]. These trans-cortical contributions were shown through M2 potentially exceeding M1, and M2 dependence on task [5] and predictability [6].

2.4.4 Study Limitations and Application to Physiological and Clinical Research

The interpretation and generalizability of both experimental and simulation model aspects of our study should be done with care. The experimental perturbation parameter space was limited to 49 unique profiles to avoid muscle fatigue and participant loss of attention. As a result, aspects of M1 and M2 perturbation dependencies were not caught in the experimental dataset, as shown through the extended simulation study and other experimental studies, for example including an extended set of acceleration levels [17]. The simulation model was built as a mechanistic model, qualitatively validated with experimental datasets without any additional tuning of the model parameters [15, 19]. Our basic simulation model misses several known physiological elements and the quantitative fit could be improved through extensive parameter optimization. The combined limitations show in the observed M2 acceleration- and velocity-dependence, which did not fully match between experiment and simulation.

Still, the M1 and M2 dependence on acceleration, velocity and duration do raise questions beyond the scope of the experiment. Decoupling of perturbation parameters in physiological and clinical research may lead to new or revised conclusions. Most stretch reflex studies at joint level reported on velocity-dependence [8–15], which was potentially confounded by the underlying acceleration-dependence. Similarly, Finley *et al.* [17] were unaware of any duration-dependency in the ankle plantarflexors, therefore

their study design did not control for duration. Given that the duration parameter varied between 50 and 90 ms, thus including duration shorter than 55 ms, their investigation of the M2 acceleration-dependence might have been confounded. At the muscle spindle level, the Ia afferent initial burst and dynamic index characteristics were linked to acceleration and velocity, respectively [19]. Applying the systematically designed perturbations to the same model showed that both acceleration and velocity influence the initial burst in distinctive manners.

The clinical evaluation and definitions of spasticity, i.e. an exaggerated stretch reflex, have focused on a velocity-dependent resistance to passive muscle stretch [2, 38]. A paradigm shift away from a sole velocity-dependence might improve the current understanding of spasticity and its influence on daily living [1]. This paradigm shift is further supported by the Ia afferent sensitivity to force and yank [19, 32] and successful force-based modeling of spasticity [39]. Towards clinical application, the systematic evaluation shows that standardization of perturbation profiles in motorized assessment prototypes is essential. The M1 acceleration-dependence further confirms the hypothesis of Sloot et al. [3, 40] that variations in acceleration can account for differences in motorized and manual assessments. Without standardized perturbations, clinical assessments would become device- and protocol-specific, while the advantage of adding motorized assessment to clinical practice should lie within its precision and objectivity. This recommendation for standardized tests and consideration of stretch acceleration and duration generalizes to all spasticity evaluation techniques under development, like velocity-dependent stretch reflex thresholds [41] or velocity-based parallel-cascade system identification [42].

2.5 Conclusions

Motorized assessment of the stretch reflex or spasticity using ramp-and-hold perturbations should be performed systematically. Experimental protocols should consider all M1 and M2 duration, velocity and acceleration dependencies, and the interdependence of these perturbation parameters. Using a systematic evaluation, we showed that M1 magnitude depended on stretch acceleration in experiment and simulation. Perturbation parameters outside the experimental scope also showed a nonlinear velocity- and duration-dependence in simulation, explaining the lack of velocity- and duration-dependence observed experimentally. Moreover, we showed that the M2 magnitude in the ankle plantarflexors depended on stretch duration, velocity and acceleration. The simulation model explained these findings using MTU and muscle cross-bridge dynamics, Ia afferent sensitivity to intrafusal force and yank, and motoneuron synchronization. The recommendation for systematic motorized assessment is important for both scientific and clinical applications investigating the physiological origin or effects of neurological disorders on the stretch reflex.

References

[1] V. Dietz and T. Sinkjær, “Spastic Movement Disorder: Impaired Reflex Function and Altered Muscle Mechanics,” *Lancet Neurology*, 6(8), pp. 725–733, 2007. doi: 10.1016/S1474-4422(07)70193-X.

[2] J. C. van den Noort, L. Bar-On, E. Aertbeliën, M. Bonikowski, *et al.*, "European Consensus on the Concepts and Measurement of the Pathophysiological Neuromuscular Responses to Passive Muscle Stretch," *European Journal of Neurology*, 24(7), pp. 981–991, 2017. doi: 10.1111/ene.13322.

[3] L. H. Sloot, L. Bar-On, M. M. van der Krogt, E. Aertbeliën, *et al.*, "Motorized versus Manual Instrumented Spasticity Assessment in Children with Cerebral Palsy," *Developmental Medicine and Child Neurology*, 59(2), pp. 145–151, 2017. doi: 10.1111/dmcn.13194.

[4] E. Toft, T. Sinkjær, and S. Andreassen, "Mechanical and Electromyographic Responses to Stretch of the Human Anterior Tibial Muscle at Different Levels of Contraction," *Experimental Brain Research*, 74(1), pp. 213–219, 1989. doi: 10.1007/BF00248294.

[5] J. A. Pruszynski and S. H. Scott, "Optimal Feedback Control and the Long-Latency Stretch Response," *Experimental Brain Research*, 218(3), pp. 341–359, 2012. doi: 10.1007/s00221-012-3041-8.

[6] C. J. Forgaard, I. M. Franks, D. Maslovat, and R. Chua, "Perturbation Predictability Can Influence the Long-Latency Stretch Response," *PLoS ONE*, 11(10):e0163854, 2016. doi: 10.1371/journal.pone.0163854.

[7] P. B. C. Matthews, "Observations on the Automatic Compensation of Reflex Gain on Varying the Pre-Existing Level of Motor Discharge in Man," *The Journal of Physiology*, 374(1), pp. 73–90, 1986. doi: 10.1113/jphysiol.1986.sp016066.

[8] G. L. Gottlieb and G. C. Agarwal, "Response to Sudden Torques About Ankle in Man: Myotatic Reflex," *Journal of Neurophysiology*, 42(1), pp. 91–106, 1979. doi: 10.1152/jn.1979.42.1.91.

[9] R. G. Lee and W. G. Tatton, "Long Latency Reflexes to Imposed Displacements of the Human Wrist: Dependence on Duration of Movement," *Experimental Brain Research*, 45(1), pp. 207–216, 1982. doi: 10.1007/BF00235780.

[10] A. F. Thilmann, M. Schwarz, R. Töpper, S. J. Fellows, *et al.*, "Different Mechanisms Underlie the Long-Latency Stretch Reflex Response of Active Human Muscle at Different Joints," *Journal of Physiology*, 444(1), pp. 631–643, 1991. doi: 10.1113/jphysiol.1991.sp018898.

[11] V. Dietz, M. Discher, and M. Trippel, "Task-Dependent Moduation of Short- and Long-Latency Electromyographic Responses in Upper Limb Muscles," *Electroencephalography and Clinical Neurophysiology*, 93(1), pp. 49–56, 1994. doi: 10.1016/0168-5597(94)90091-4.

[12] M. J. Grey, B. Larsen, and T. Sinkjær, "A Task Dependent Change in the Medium Latency Component of the Soleus Stretch Reflex," *Experimental Brain Research*, 145(3), pp. 316–322, 2002. doi: 10.1007/s00221-002-1109-6.

[13] N. Kawashima, K. Nakazawa, S. I. Yamamoto, D. Nozaki, *et al.*, "Stretch Reflex Excitability of the Anti-Gravity Ankle Extensor Muscle in Elderly Humans," *Acta Physiologica Scandinavica*, 180(1), pp. 99–105, 2004. doi: 10.1046/j.0001-6772.2003.01230.x.

[14] G. N. Lewis, E. J. Perreault, and C. D. MacKinnon, "The Influence of Perturbation Duration and Velocity on the Long-Latency Response to Stretch in the Biceps Muscle," *Experimental Brain Research*, 163(3), pp. 361–369, 2005. doi: 10.1007/s00221-004-2182-9.

[15] J. Schuurmans, E. de Vlugt, A. C. Schouten, C. G. M. Meskers, *et al.*, "The Monosynaptic Ia Afferent Pathway Can Largely Explain the Stretch Duration Effect of the Long Latency M2 Response," *Experimental Brain Research*, 193(4), pp. 491–500, 2009. doi: 10.1007/s00221-008-1647-7.

[16] A. Berardelli, M. Hallett, C. Kaufman, E. Fine, *et al.*, "Stretch Reflexes of Triceps Surae in Normal Man," *Journal of Neurology Neurosurgery and Psychiatry*, 45(6), pp. 513–525, 1982. doi: 10.1136/jnnp.45.6.513.

[17] J. M. Finley, Y. Y. Dhaher, and E. J. Perreault, "Acceleration Dependence and Task-specific Modulation of Short- and Medium-Latency Reflexes in the Ankle Extensors," *Physiological Reports*, 1(3):e00051, 2013. doi: 10.1002/phy2.51.

[18] C. G. M. Meskers, A. C. Schouten, M. M. L. Rich, J. H. de Groot, *et al.*, "Tizanidine does not Affect the Linear Relation of Stretch Duration to the Long Latency M2 Response of m. Flexor Carpi Radialis," *Experimental Brain Research*, 201(4), pp. 681–688, 2010. doi: 10.1007/s00221-009-2085-x.

[19] K. P. Blum, K. S. Campbell, B. C. Horslen, P. Nardelli, *et al.*, "Diverse and Complex Muscle Spindle Afferent Firing Properties Emerge from Multiscale Muscle Mechanics," *eLife*, 9:e55177, 2020. doi: 10.7554/ELIFE.55177.

[20] R. J. MacGregor and R. M. Oliver, "A Model for Repetitive Firing in Neurons," *Kybernetik*, 16(1), pp. 53–64, 1974. doi: 10.1007/BF00270295.

[21] H. J. Hermens, B. Freriks, C. Disselhorst-Klug, and G. Rau, "Development of Recommendations for SEMG Sensors and Sensor Placement Procedures," *Journal of Electromyography and Kinesiology*, 10(5), pp. 361–374, 2000. doi: 10.1016/S1050-6411(00)00027-4.

[22] F. E. Harrell, *Regression Modeling Strategies*, 2nd ed., ser. Springer Series in Statistics. Switzerland: Springer International Publishing, 2015, p. 582. doi: 10.1007/978-3-319-19425-7.

[23] L. Hoffman, *Longitudinal Analysis: Modeling Within-Person Fluctuation and Change*, 1st ed. New York City, NY, USA: Routledge, 2015, p. 654. doi: 10.4324/9781315744094.

[24] D. J. Barr, R. Levy, C. Scheepers, and H. Tily, "Random Effects Structure for Confirmatory Hypothesis Testing: Keep it Maximal," *Journal of Memory and Language*, 68(3), pp. 255–278, 2013. doi: 10.1016/j.jml.2012.11.001.

[25] M. Brauer and J. J. Curtin, "Linear mixed-effects models and the analysis of nonindependent data: A unified framework to analyze categorical and continuous independent variables that vary within-subjects and/or within-items," *Psychological Methods*, 23(3), pp. 389–411, 2017. doi: 10.1037/met0000159.

[26] M. P. Mileusnic, I. E. Brown, N. Lan, and G. E. Loeb, "Mathematical Models of Proprioceptors. I. Control and Transduction in the Muscle Spindle," *Journal of Neurophysiology*, 96(4), pp. 1772–1788, 2006. doi: 10.1152/jn.00868.2005.

[27] T. W. Davies, "Resting Length of the Human Soleus Muscle," *Journal of Anatomy*, 162, pp. 169–75, 1989.

[28] C. W. Spoor, J. L. van Leeuwen, C. G. M. Meskers, A. F. Titulaer, *et al.*, "Estimation of Instantaneous Moment Arms of Lower-Leg Muscles," *Journal of Biomechanics*, 23(12), pp. 1247–1259, 1990. doi: 10.1016/0021-9290(90)90382-D.

[29] R. E. Kearney, R. B. Stein, and L. Parameswaran, "Identification of Intrinsic and Reflex Contributions to Human Ankle Stiffness Dynamics," *IEEE Transactions on Biomedical Engineering*, 44(6), pp. 493–504, 1997. doi: 10.1109/10.581944.

[30] A. H. A. Stienen, A. C. Schouten, J. Schuurmans, and F. C. T. van der Helm, "Analysis of Reflex Modulation with a Biologically Realistic Neural Network," *Journal of Computational Neuroscience*, 23(3), pp. 333–348, 2007. doi: 10.1007/s10827-007-0037-7.

[31] E. Toft, T. Sinkjær, S. Andreassen, and K. Larsen, "Mechanical and Electromyographic Responses to Stretch of the Human Ankle Extensors," *Journal of Neurophysiology*, 65(6), pp. 1402–1410, 1991. doi: 10.1152/jn.1991.65.6.1402.

[32] K. P. Blum, B. L. D'Incamps, D. Zytnicki, and L. H. Ting, "Force Encoding in Muscle Spindles during Stretch of Passive Muscle," *PLoS Computational Biology*, 13(9):e1005767, 2017. doi: 10.1371/journal.pcbi.1005767.

[33] I. L. Kurtzer, J. A. Pruszynski, and S. H. Scott, "Long-Latency Reflexes of the Human Arm Reflect an Internal Model of Limb Dynamics," *Current Biology*, 18(6), pp. 449–453, 2008. doi: 10.1016/j.cub.2008.02.053.

[34] N. Mrachacz-Kersting, U. G. Kersting, P. de Brito Silva, Y. Makihara, *et al.*, "Acquisition of a Simple Motor Skill: Task-dependent Adaptation and Long-term Changes in the Human Soleus Stretch Reflex," *Journal of Neurophysiology*, 122(1), pp. 435–446, 2019. doi: 10.1152/jn.00211.2019.

[35] K.-E. Hagbarth, R. R. Young, J. V. Hägglund, and E. U. Wallin, "Segmentation of Human Spindle and EMG Responses to Sudden Muscle Stretch," *Neuroscience Letters*, 19(2), pp. 213–217, 1980. doi: 10.1016/0304-3940(80)90197-4.

[36] K.-E. Hagbarth, J. V. Hägglund, E. U. Wallin, and R. R. Young, "Grouped Spindle and Electromyographic Responses to Abrupt Wrist Extension Movements in Man," *Journal of Physiology*, 312(1), pp. 81–96, 1981. doi: 10.1113/jphysiol.1981.sp013617.

[37] M. J. Grey, M. Ladouceur, J. B. Andersen, J. B. Nielsen, *et al.*, "Group II Muscle Afferents Probably Contribute to the Medium Latency Soleus Stretch Reflex during Walking in Humans," *Journal of Physiology*, 534(3), pp. 925–933, 2001. doi: 10.1111/j.1469-7793.2001.00925.x.

[38] J. W. Lance, "Symposium Synopsis," in *Spasticity: Disordered Motor Control*, R. G. Feldman, R. R. Young, and W. P. Koella, Eds., Chicago, IL, USA: Year Book Medical Publishers, 1980, pp. 485–495.

[39] A. Falisse, L. Bar-On, K. Desloovere, I. Jonkers, *et al.*, "A Spasticity Model based on Feedback from Muscle Force Explains Muscle Activity during Passive Stretches and Gait in Children with Cerebral Palsy," *PLoS ONE*, 13(12):e0208811, 2018. doi: 10.1371/journal.pone.0208811.

[40] L. H. Sloot, G. Weide, M. M. van der Krogt, K. Desloovere, *et al.*, "Applying Stretch to Evoke Hyperreflexia in Spasticity Testing: Velocity vs. Acceleration," *Frontiers in Bioengineering and Biotechnology*, 8:e591004, 2021. doi: 10.3389/fbioe.2020.591004.

[41] A. K. Blanchette, A. A. Mullick, K. Moïn-Darbari, and M. F. Levin, "Tonic Stretch Reflex Threshold as a Measure of Ankle Plantar-Flexor Spasticity after Stroke," *Physical Therapy*, 96(5), pp. 687–695, 2016. doi: 10.2522/ptj.20140243.

[42] M. M. Mirbagheri, H. Barbeau, M. Ladouceur, and R. E. Kearney, "Intrinsic and Reflex Stiffness in Normal and Spastic, Spinal Cord Injured Subjects," *Experimental Brain Research*, 141(4), pp. 446–459, 2001. doi: 10.1007/s00221-001-0901-z.

Chapter 3

Offline and Online Estimation of Intrinsic and Reflexive Joint Impedance

R. C. van 't Veld, A. C. Schouten, H. van der Kooij, E. H. F. van Asseldonk

Abstract — Objective and precise quantification of joint impedance is essential to understand human motor control strategies and movement disorders affecting these strategies. The parallel-cascade (PC) system identification technique disentangles the intrinsic and reflexive joint impedance contributions, thus offering a potential neuromechanical and clinical assessment tool. For post-trial evaluation of data recorded with a time-invariant task, an offline time-invariant PC algorithm is available. For live evaluation during a time-invariant or time-variant task, an online adaptive PC algorithm is available. The goal of this chapter was to characterize and improve the responsiveness, accuracy and reliability of both an offline and online PC algorithm for use in our experimental setup. The PC algorithms were evaluated in a simulation emulating our experimental environment. For the offline algorithm, implementing incremental improvements achieve an improved responsiveness (r^2), accuracy (bias) and reliability (mean average deviation, MAD) for both the intrinsic and reflexive pathway. For the online algorithm, an improved estimation accuracy was achieve with similar responsiveness and reliability. Comparing both algorithms, the adapted offline PC algorithm consistently showed best parameter estimation performance. Furthermore, simulation of spastic characteristics within the reflexive pathway did not substantially change the estimation performance of either algorithm. In conclusion, our simulated results showed good responsiveness, accuracy and reliability for both offline and online PC algorithms to study either able-bodied participants or people with spasticity. The offline algorithm should be used for post-trial evaluation, if data is time-invariant. The online algorithm should be used to provide live joint impedance estimates during experiments.

The simulation study of the online algorithm for able-bodied conditions was published in the *7th International Conference on Biomedical Robotics and Biomechatronics*, pp. 13-18, 2018. The code and data underlying this chapter are available via 4TU.ResearchData. doi: 10.4121/c.5986246

3.1 Introduction

Human joint impedance, i.e. the joint's resistance to imposed motion, is a fundamental neuromechanical property characterizing how humans respond and interact with their surrounding environment [1, 2]. Correct control of human joint impedance enables efficient and stable execution of activities of daily living [2, 3]. People with brain or neural injuries, e.g. spinal cord injury, may experience increased joint impedance ('hyper-resistance') and lack of impedance modulation resulting in a loss of functional independence [4–6]. To understand human motor control strategies and movement disorders, objective and precise quantification of joint impedance is essential.

Precise joint impedance quantification calls for a thorough understanding of the neuromechanical origin of joint impedance, which has three contributions [7]:

1. an intrinsic contribution due to limb inertia and viscoelasticity of muscle fibers and tissues in rest;
2. an intrinsic contribution due to viscoelasticity of activated muscle fibers;
3. a reflexive contribution due to neural reflex activity.

Joint hyper-resistance arises from one or multiple of these contributions, which creates a challenge for both diagnosis and treatment [6]. Current clinical practise lacks a valid and reliable procedure to quantify joint impedance and unravel these three contributions.

The parallel-cascade (PC) system identification technique can disentangle the intrinsic and reflexive joint impedance, offering a potential neuromechanical and clinical assessment tool [7–9]. For Chapters 4 to 6, we intended to use the PC system identification technique for two different use cases in our experimental setup. First, to evaluate ankle joint resistance in a neuromechanical and clinical setting, a PC algorithm capable of post-trial evaluation was desired. For post-trial evaluation of data recorded with a time-invariant task, multiple offline time-invariant PC algorithm are available [7, 10–15]. Second, to enable biofeedback on either intrinsic or reflexive impedance, a PC algorithm capable of live estimation during measurements was desired. For live evaluation of a time-invariant or slow time-variant task, an online adaptive PC algorithm is available [16, 17]. From the offline PC algorithms, we selected to use the original Kearney *et al.* [7] algorithm, because this algorithm can process data elicited with the pseudo-random binary sequence (PRBS)-like perturbation of the online algorithm [16]. The other available offline algorithms were discarded as these were either based on different perturbation signals [10, 12] or focused on processing short data-segments and time-variant data [11, 13–15].

The goal of this chapter is to characterise and improve the responsiveness, accuracy and reliability of an offline [7] and online [16] PC algorithm for use in our experimental setup. Both algorithms are adapted to improve characteristics specific to our experimental setup and, if possible, in general. The PC algorithms are evaluated in simulation based on Ludvig *et al.* [16], which evaluated the online algorithm. This evaluation characterizes the ability of the PC algorithms to detect change (responsiveness), amount of structural error, i.e. bias (accuracy) and amount of random error, i.e. variability (reliability). These characteristics have not yet been investigated in simulation for the offline algorithm. In extension to Ludvig *et al.* [16], the simulation environment was adapted to create a better match between simulation and experiment. Adaptations

made to improve the match between simulation and our specific experimental setup included: direct velocity measurements, sampling frequency and signal-to-noise ratios. Adaptations made to improve the match between simulation and experiments in general included: simulation causality and continuity, finite actuator bandwidth, spastic reflexive impedance and added voluntary torque. These adaptation of the simulation environment should ensure translation of these characteristics towards experimental environments. Overall, characterizing and improving the responsiveness, accuracy and reliability of the PC algorithms provides the best possible algorithm understanding and performance in support of the planned experimental studies.

3.2 Joint Impedance Modeling and Identification

The joint impedance simulation consisted of three components: the perturbation signal, the simulation model and the identification algorithm. The signal excited the system, i.e. a joint impedance model in simulation and the participants' joint during experiments. The simulation model generated the data, mimicking an experiment, see Fig. 3.1A. The identification algorithm was subsequently used for data analysis to estimate the joint impedance. Specifically, the PC algorithms identified the impedance parameters using the perturbation signal angle and system response torque.

3.2.1 Joint Impedance Model and Perturbation Signal

The joint impedance simulation environment (Matlab/Simulink 2017b, Mathworks, Natick, MA, USA) was developed to provide a realistic torque response of an ankle joint in response to an angular perturbation, mimicking experimental measurements of Chapters 4 to 6. In short, the experimental setup consisted of a one degree of freedom manipulator (Moog, Nieuw-Vennep, the Netherlands) used to apply angular perturbations in the sagittal plane around the ankle joint, see Fig. 3.1C. Experimental data was gathered in either time-invariant conditions with at least 60 s long segments or slow time-variant conditions.

A 0.035 rad amplitude pulse-step perturbation, used to elicit the intrinsic and reflexive responses, has been purposely designed for the online algorithm, see Fig. 3.1B [16]. To enable a comparison between both algorithms, the pulse-step perturbation required for the online PC algorithm was retained as excitation signal for the offline algorithm, although other excitation signals would also be feasible [7]. This perturbation signal randomly switched between 'pulses', 40 ms long ramp-hold-return perturbations, and 'steps', 460 or 660 ms long ramp-hold-return perturbations. The length of steps was adapted for able-bodied 460 ms and spastic 660 ms participants, because duration of the reflexive response was expected to vary [8, 16, 18]. Rising and falling edges of the perturbation profiles were equal for both pulses and steps and generated by low-pass filtering (2nd-order, 30 Hz, critically-damped) a rate-limited (227.6 rad/s) block pulse. The low-pass filtering and rate-limiting were imposed to avoid oscillations and overshoot in the imposed ankle angle given the setup limited actuator bandwidth, see Appendix A.

The intrinsic pathway was modelled as a second order system with an inertia, damping and stiffness component, i.e. acceleration-, velocity- and angle-dependent respectively, see Fig. 3.1A [16]. The reflexive pathway was modelled based on delayed, half-

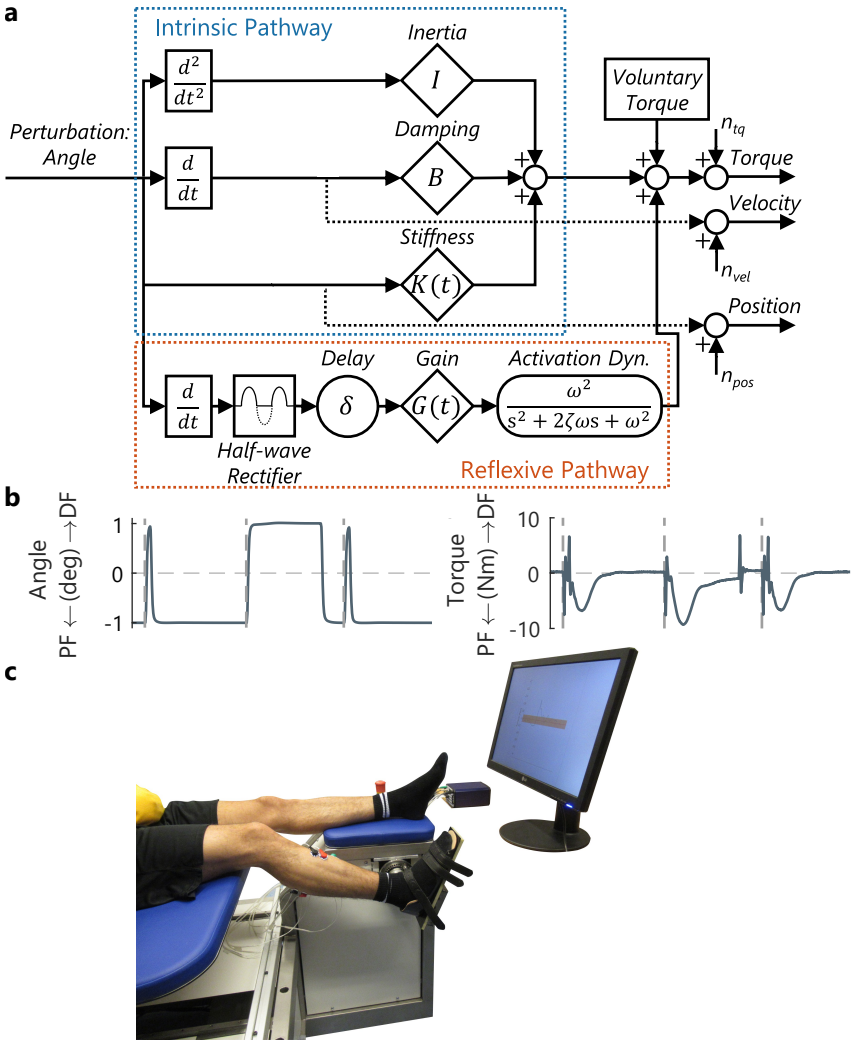

Figure 3.1: Ankle joint impedance experimental environment simulated by the parallel-cascade model. *(A)* Parallel-cascade (PC) model with intrinsic and reflexive pathways used to mimick the experimental environment. The intrinsic impedance contribution was modelled as a 2nd-order mass-spring-damper system with parameters: inertia I, damping B and stiffness K. The reflexive impedance contribution was modelled based on half-wave rectified velocity with a delay δ, reflexive gain G and 2nd-order muscle activation dynamics with damping ζ and natural frequency ω. All parameters were considered time-invariant, except for the time-varying intrinsic stiffness $K(t)$ and reflexive gain $G(t)$. In addition, a time-varying voluntary torque contribution was added to the modelled torque output. The voluntary torque modeled a potential participant deviation from the instructed constant torque task. Random Gaussian noise (n_{pos},n_{vel},n_{tq}) was added to the angle, velocity and torque output signals. The offline algorithm estimates all simulated parameters (*diamond & round* boxes), whereas the online algorithm only estimates I, B, K and G (*diamond* boxes). *(B)* Example of the experimental input, i.e. perturbation angle, and experimental output, i.e. torque response, to be modelled in the simulation environment. *(C)* Overview of our experimental setup.

wave rectified velocity as input for the second order muscle activation dynamics and a reflexive feedback gain. Compared to Ludvig *et al.* [16], the model was extended to include both an able-bodied and spastic reflexive impedance option, as well as a voluntary torque component. The simulated neuromechanical parameters, like stiffness and reflex gain, were based on previously reported experimental values [8, 16, 18]. Both able-bodied and spastic reflexive impedance options were simulated using the same model structure, but using different parameters for the reflexive gain and activation dynamics [8]. During experiments, participants were instructed to keep voluntary torque constant, however most participants were not able to precisely follow this instruction. Therefore, a voluntary torque component was added to model the potential participant deviation from the instructed constant torque task.

Model causality and continuity were adapted using perturbation velocity and acceleration as input signals, instead of using a numerical approximation based on a backwards-difference method [16]. Moreover, a variable-step, instead of a fixed-step, solver was used to simulate the continuous nature of the ankle joint impedance neuromechanics. Before processing the data using the PC algorithms, all signals were sampled after anti-alias filtering at 90% Nyquist frequency to mimick experimental data recording. To match our specific experimental environment, a 2048 Hz sampling frequency was used and 52.7, 37.7, 24.1 dB signal-to-noise ratios were applied for the measured angle, velocity and torque, respectively.

3.2.2 Offline Joint Impedance Estimation

The offline PC algorithm [7] estimated the intrinsic I, B, K and reflexive gain G, delay δ, damping ζ and natural frequency ω parameters, see Fig. 3.2. The offline algorithm was implemented using digital filters with cut-off frequencies optimized through trial-and-error in simulation. The intrinsic impulse response function (IRF) length was selected to prevent contamination by reflex effects, whereas the reflexive IRF length was chosen to have sufficient length to capture the full reflexive dynamics [19]. The adapted offline algorithm was implemented as follows (*adaptations in italics*) [7]:

1. The measured angle, velocity and torque signals were anti-alias filtered (2nd-order, 65.8 Hz, critically-damped) and downsampled to 146.3 Hz to remove high-frequency noise and reduce computational complexity.
2. Measured acceleration was extracted from the state vector of the velocity low-pass filter (implemented using a state-space representation), and also downsampled to 146.3 Hz.
3. Non-parametric estimation of intrinsic, reflexive and voluntary torque contributions via an iterative procedure. Iterations continued until variance accounted for (%VAF) did not improve (<0.005%) or reached max. 10 iterations. *Voluntary torque estimation was added to improve intrinsic and reflexive IRF estimation.*
   (a) (1^{st}-iteration) Reflexive and voluntary torque were set equal to zero, hence the residual intrinsic torque was set equal to net torque.
   (b) The intrinsic IRF, with 35 ms length, was estimated using a correlation-based method between angle and residual intrinsic torque. A pseudo-inverse approach based on minimum description length was used to retain only

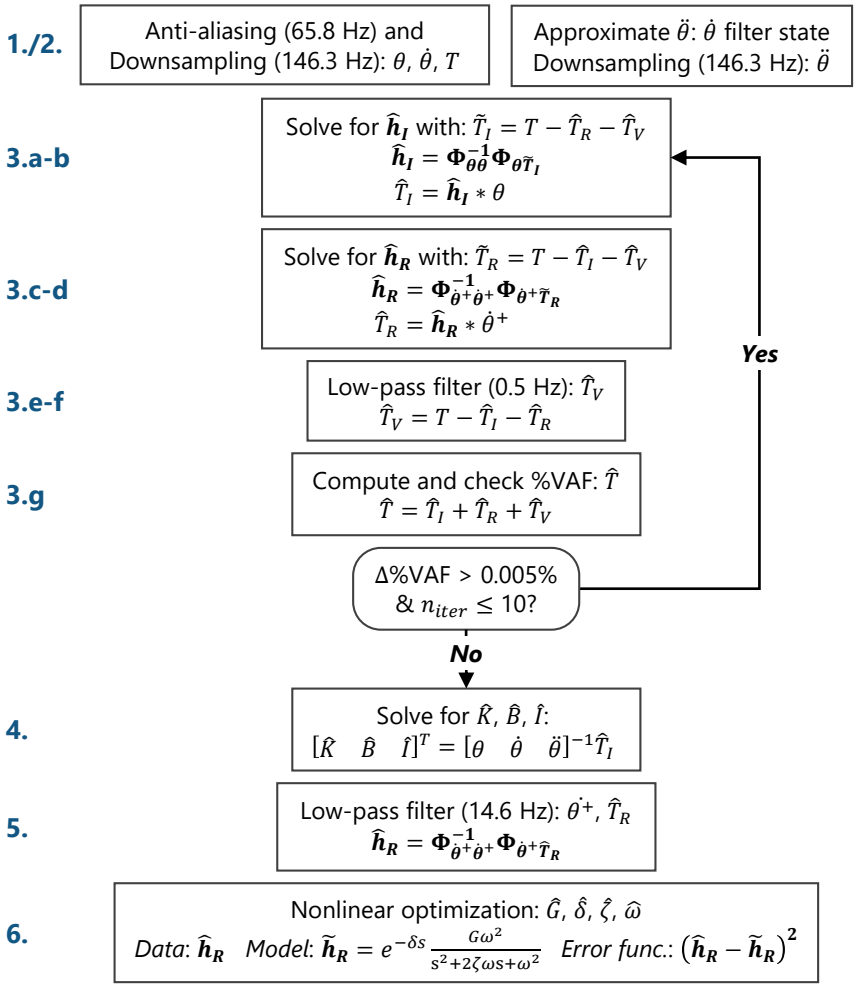

Figure 3.2: Schematic representation of the offline PC algorithm implementation. The 6-step offline algorithm can be split in three stages: input processing (*1-2*), iterative nonparametric identification (*3*) and parametric identification (*4-6*). The input processing stage filters and approximates the signals used in the identification stages: angle θ, velocity $\dot{\theta}$, half-wave rectified velocity $\dot{\theta}^+$, acceleration $\ddot{\theta}$, torque T. The nonparametric identification stage estimates the intrinsic $\hat{h}_I$ and reflexive IRF $\hat{h}_R$ using auto- and cross-correlation functions Φ. In addition, at this stage the intrinsic $\hat{T}_I$, reflexive $\hat{T}_R$ and voluntary torques are estimated. The iterative nonparametric identification stops if the variance accounted for (%VAF) does not improve more than 0.5% or after 10 iterations. The parametric identification stage estimates the parameters of both intrinsic and reflexive pathways. The stiffness $\hat{K}$, damping $\hat{B}$, inertia $\hat{I}$ are estimated using linear least squares and the estimated intrinsic torque. The reflexive gain $\hat{G}$, neural delay $\hat{\delta}$, damping $\hat{\zeta}$ and natural frequency $\hat{\omega}$ are estimated using nonlinear least squares and the estimated reflexive IRF.

1. Low-pass filter (100 Hz): θ, $\dot{\theta}$, T

2./3. Approximate $\ddot{\theta}$: $\dot{\theta}$ 4th-order backwards difference; High-pass filter (0.033 Hz): T

4. Low-pass filter (0.033 Hz): Zero-lag auto- and cross-correlations $\Phi_{\theta\theta}$, $\Phi_{\theta\dot{\theta}}$, $\Phi_{\theta\ddot{\theta}}$, $\Phi_{\dot{\theta}\dot{\theta}}$, $\Phi_{\dot{\theta}\ddot{\theta}}$, $\Phi_{\ddot{\theta}\ddot{\theta}}$, $\Phi_{\theta T}$, $\Phi_{\dot{\theta}T}$, $\Phi_{\ddot{\theta}T}$

5. Solve for $\hat{K}$, $\hat{B}$, $\hat{I}$:

$$\begin{bmatrix}\hat{K}\\ \hat{B}\\ \hat{I}\end{bmatrix} = \begin{bmatrix}\Phi_{\theta\theta} & \Phi_{\theta\dot{\theta}} & \Phi_{\theta\ddot{\theta}}\\ \Phi_{\dot{\theta}\theta} & \Phi_{\dot{\theta}\dot{\theta}} & \Phi_{\dot{\theta}\ddot{\theta}}\\ \Phi_{\ddot{\theta}\theta} & \Phi_{\ddot{\theta}\dot{\theta}} & \Phi_{\ddot{\theta}\ddot{\theta}}\end{bmatrix}^{-1}\begin{bmatrix}\Phi_{\theta T}\\ \Phi_{\dot{\theta}T}\\ \Phi_{\ddot{\theta}T}\end{bmatrix}$$

6. High-pass filter (0.033 Hz): $\hat{T}_I$

$$\hat{T}_I = \hat{K}\theta + \hat{B}\dot{\theta} + \hat{I}\ddot{\theta}$$

7. $\hat{T}_R = T - \hat{T}_I$; High-pass filter (0.033 Hz): $\dot{\theta}^+$

8. Anti-aliasing (81.9 Hz) and Downsampling (204.8 Hz): $\hat{T}_R$, $\dot{\theta}^+$

9. Solve for $\hat{\boldsymbol{h}}_{\boldsymbol{R}}$:

$$\begin{bmatrix}\hat{h}_R(\Delta)\\ \hat{h}_R(\Delta+1)\\ \vdots\\ \hat{h}_R(m)\end{bmatrix} = \begin{bmatrix}\dot{\theta}^+(j-\Delta) & \dot{\theta}^+(j-\Delta-1) & \cdots & \dot{\theta}^+(j-m)\\ \dot{\theta}^+(j-\Delta-1) & \dot{\theta}^+(j-\Delta-2) & \cdots & \dot{\theta}^+(j-1-m)\\ \vdots & \vdots & \ddots & \vdots\\ \dot{\theta}^+(j-\mathrm{n}) & \dot{\theta}^+(j-n-1) & \cdots & \dot{\theta}^+(j-\mathrm{n}-\mathrm{m})\end{bmatrix}^{-1}\begin{bmatrix}\hat{T}_R(j)\\ \hat{T}_R(j-1)\\ \vdots\\ \hat{T}_R(j-n)\end{bmatrix}$$

10. Low-pass filter (0.033 Hz): $\hat{G}$

$$\hat{G} = \sum \hat{\boldsymbol{h}}_{\boldsymbol{R}}$$

Figure 3.3: Schematic representation of the online PC algorithm implementation. The 10-step online algorithm can be split in three stages: input processing (*1-3*), intrinsic pathway identification (*4-6*), reflexive pathway identification (*7-10*). The input processing stage filters and approximates the signals used in the identification stages: angle θ, velocity $\dot{\theta}$, acceleration $\ddot{\theta}$, torque T. The intrinsic pathway identification stage estimates the stiffness $\hat{K}$, damping $\hat{B}$, inertia $\hat{I}$ and intrinsic torque $\hat{T}_I$ using zero-lag auto- and cross-correlations Φ. The reflexive pathway identification stage estimates reflex IRF $\hat{h}_R$ and reflex gain $\hat{G}$ using half-wave rectified velocity $\dot{\theta}^+$ and reflexive torque $\hat{T}_R$.

significant terms [20].

(c) Residual reflexive torque was computed by subtracting voluntary and intrinsic torque,i.e. the convolved intrinsic IRF with angle, from the net torque.

(d) The reflexive IRF, with length fixed at 450 or 650 ms for able-bodied or spastic data, was estimated using the correlation-based method between half-wave rectified velocity and residual reflexive torque. *Half-wave rectified velocity was used to avoid nonlinear identification from a binary perturbation signal.*

(e) Residual voluntary torque was computed by subtracting intrinsic and reflexive torque, i.e. the convolved reflexive IRF with half-wave rectified velocity, from net torque.

(f) Voluntary torque was estimated as low-pass filtered (2nd-order, 0.5 Hz, Butterworth) residual voluntary torque to remove relevant dynamics.

(g) %VAF was computed between net torque and the summation of intrinsic, reflexive and voluntary torque.

4. The intrinsic I, B and K were estimated using linear least squares between acceleration, velocity and angle, and intrinsic torque. *This adapted estimation method avoids the inaccurate inversion of the acausal intrinsic IRF, required to estimate I, B and K from the IRF.*
5. The reflexive IRF was fit between half-wave rectified velocity and reflexive torque with both signals low-pass filtered (2nd-order, 14.6 Hz, critically-damped). *Filters were added to reduce variability without affecting relevant reflexive dynamics.*
6. The reflexive parameters were fit via nonlinear optimization using the reflexive IRF. Delay δ was estimated via a grid search (35 to 65 ms, 1 ms increments), coupled to a nonlinear least squares fit of gain G, damping ζ and natural frequency ω.

3.2.3 Online Joint Impedance Estimation

The online PC algorithm [16] estimated the intrinsic inertia I, damping B and stiffness K parameters, as well as the reflexive gain G, see Fig. 3.2. The essential element within the online PC algorithm was the use of the dedicated pulse-step perturbation to disentangle the intrinsic and reflexive contributions [16]. The random switching between pulses and steps eliminates any reflexive contributions from the cross-correlations between torque and angle, velocity and acceleration in Step 5 used to estimate the intrinsic parameters, see Fig. 3.3.

The algorithm was implemented using digital filters instead of analog (Bessel) filters to improve general applicability, as digital filters do not require solving differential equations. The filter cut-off frequencies were taken directly from Ludvig *et al.* [16], as participants experienced these frequency most comfortable for biofeedback in an experimental setting. The adapted online algorithm was implemented as follows (*adaptations in italics*) [16]:

1. The measured angle, velocity and torque signals were low-pass filtered (2nd-order, 100 Hz, Butterworth). *Both use of measured velocity as direct input and addition of low-pass filters were implemented to reduce influence of high-frequency noise without affecting relevant dynamics.*
2. Measured acceleration was unavailable and was estimated using numerical differentiation of low-pass filtered velocity. *A 4^{th}-order, instead of 1^{st}-order, backwards*

difference method was used to provide a closer match between actual acceleration and the numerical approximation.

3. Low-pass filtered torque was also high-pass filtered (2nd-order, 0.033 Hz, Butterworth) to reduce influence of voluntary torque.
4. The zero-lag auto- and cross-correlation between angle, velocity and acceleration, and cross-correlation between torque and angle, velocity and acceleration were computed and low-pass filtered (2nd-order, 0.033 Hz, Butterworth).
5. The intrinsic inertia I, damping B and stiffness K were estimated by solving an equation relating these 12 auto- and cross-correlations.
6. Intrinsic torque was computed via forward simulation using the estimated I, B and K parameters and high-pass filtered (2nd-order, 0.033 Hz, Butterworth).
7. Reflexive torque was computed as measured minus intrinsic torque. Velocity was half-wave rectified and high-pass filtered (2nd-order, 0.033 Hz, Butterworth).
8. Reflexive torque and half-wave rectified velocity were anti-alias filtered (8th-order, 81.9 Hz, 0.05 dB, Chebyshev) and downsampled to 204.8 Hz. *These filter and sampling parameters were adapted to match the 2048 Hz data sampling frequency.*
9. The reflexive impulse response function (IRF) was estimated at 20.48 Hz using a linear least-squares method based on 1 s data segments of reflexive torque and lagged half-wave rectified velocity (min. 50 ms to max. 400 or 600 ms for able-bodied or spastic data [8, 16]).
10. The reflexive gain G was computed as the sum of the reflexive IRF and low-pass filtered (2nd-order, 0.033 Hz, Butterworth).

3.3 Simulation Study

3.3.1 Methods

The simulation study evaluated the adapted offline and online algorithms for responsiveness, accuracy and reliability of the estimated parameters, in similar fashion to Ludvig *et al.* [16]. Simulations ran for 240 s and the first 30 s of parameter estimations were ignored for the online algorithm to avoid errors due to simulation model and algorithm transients. All simulations were run using the adapted joint impedance model and perturbation signal. The simulations were run using three variants of the identification algorithm: the adapted offline algorithm ("offline") [7], the original online algorithm ("online-original") and the adapted online algorithm ("online-adapted") [16]. Simulations were not run for the original offline algorithm, as either reference results or a fully replicable model description were not available. First, all identification algorithms were evaluated for able-bodied simulation conditions. Second, additional able-bodied simulations were run with minor variations in the adapted offline and online algorithm implementations to provide insight into the effect of these variations. Third, both adapted algorithms were evaluated for spastic simulated conditions.

Parameter identification responsiveness, accuracy and reliability were evaluated across 100 simulated trials for three conditions:

1. a uniform random intrinsic stiffness K, between 0-200 Nm/rad, with a fixed reflexive gain G of 10 Nm·s/rad;

2. a uniform random G, between 0-20 Nm·s/rad, with fixed K of 100 Nm/rad;
3. both a uniform random K, between 0-200 Nm/rad, and uniform random G, between 0-20 Nm·s/rad.

For each simulated trial a voluntary torque profile with 4 Nm peak-to-peak amplitude and randomly picked shape was used, selected from: no torque, linear decreasing torque, a triangular decreasing then increasing torque, sigmoidal decreasing torque or sinusoidal torque (0.005 Hz). Across simulated trials with varying K or G, the algorithm across-trial responsiveness was evaluated using the Pearson's correlation coefficient r between simulated and estimated magnitudes. Accuracy and reliability were assessed based on the difference between simulated and estimated magnitudes, using the across-trial mean and mean average deviation (MAD) respectively. Note, MAD was used instead of standard deviation to assess reliability to mitigate the influence of outliers. Outliers mainly appeared during processing of simulated trials with simulated magnitudes of K/G close to zero.

Besides the K and G parameters, other parameters were all simulated with time-invariant magnitudes fixed across simulation trials [8, 16, 18]. Parameters were set to an intrinsic viscosity B of 0.63 Nm·s/rad and inertia I of 0.0137 Nm·s^2/rad as well as a reflexive delay δ of 40 ms, natural frequency ω of 21 rad/s and damping ζ of 0.8 [16]. For spasticity simulations, all reflexive gains G were multiplied with a factor 2.5 and the ω and ζ were adjusted to 10 rad/s and 0.9, respectively. The reflex damping and frequency were adjusted to simulate the potential increase duration of the reflexive response due to spasticity. Accuracy and reliability of all parameters was assessed using the across-trial mean and MAD respectively.

For the online algorithms, a single simulation run with fixed K of 100 Nm/rad and G of 10 Nm·s/rad was used to assess within-trial reliability based on the time series standard deviation. Another simulation run with a jump in K from 50 to 150 Nm/rad at 100 s and in G from 5 to 15 Nm·s/rad was used to assess the within-trial responsiveness. Responsiveness was assessed using the rise time, defined as the time between 10% to 90% of the modeled jump.

3.3.2 Results

The time series of the estimated joint impedance showed that both adapted algorithms (offline & online) matched the simulated values of intrinsic stiffness and reflexive gain, see Fig. 3.4A. The adapted online algorithm showed strong co-variation with the original online algorithm. The original online algorithm had a negative estimation bias for intrinsic stiffness and a positive estimation bias for the reflexive gain. The adapted online algorithm showed a reduced estimation bias, while estimation variability remained similar. The difference in estimation bias was also confirmed in the %VAF, increasing from 81.4% to 99.1% for the adapted online algorithm, see Fig. 3.4B. The offline PC algorithm estimated the parameters with even less bias and accompanying %VAF of 99.97%. For the online algorithms, the strong co-variation between the algorithms was an indicator for similar transient characteristics among both algorithms. The quantified within-trial reliability and responsiveness confirmed this similarity, as similar values for variability and rise time were found, see Table 3.1. Thus, the adapted online algorithm did not show substantial changes to transient characteristics in the time series and the

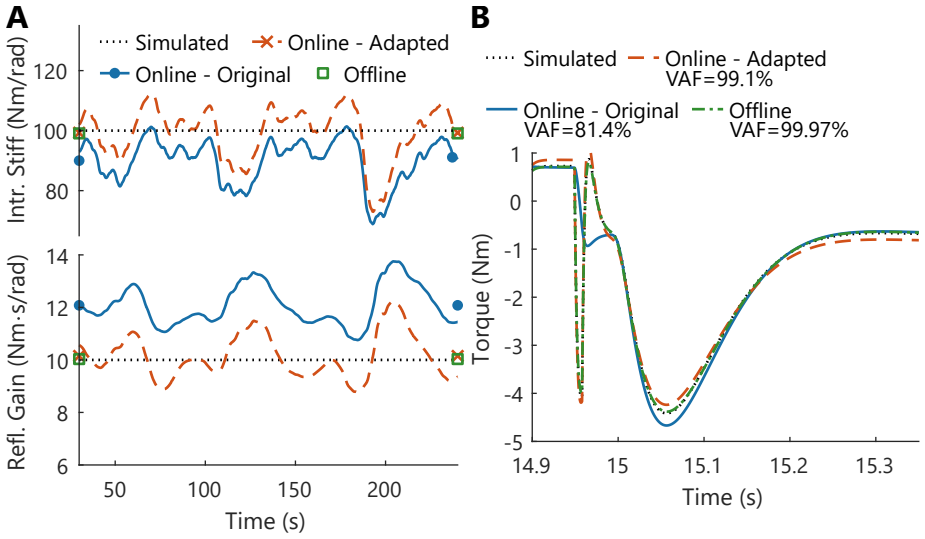

Figure 3.4: Offline and online joint impedance time series for single able-bodied simulation trial.
(A) Intrinsic stiffness and reflexive gain estimates for simulated values of 100 Nm/rad and 10 Nm·s/rad, respectively. For online algorithms the estimation time series *(lines)* are provided and for all algorithms the mean estimated value *(markers left & right)* is shown.
(B) Simulated net torque response from the joint impedance model and forward simulated torques based on algorithm estimated parameters. The variance accounted for quantifying the match between forward simulated torques and net torque response for each algorithm is listed in the legend. Mean estimated parameters were used in forward simulation and for the online algorithms, δ, ω and ζ were set to the true simulated values as parameters are not estimated.

implemented adaptations mainly influenced accuracy of the estimated parameters.

Evaluation of the average estimated parameters across all 100 simulations confirmed the observations shown for the single time series, see Fig. 3.5 and Table 3.1. Regarding the responsiveness, the offline algorithm scored a nearly perfect correlation in both pathways (1.00), see Table 3.1. The online algorithms showed excellent, yet slightly lower, correlation between estimated and simulated magnitudes for both intrinsic stiffness and reflexive gain (0.98-0.99).

Regarding the estimation accuracy, the average estimated parameters across all simulations also confirmed the biases observed for the single time series, see Fig. 3.5 and Table 3.1. The adapted offline algorithm showed a small bias for both intrinsic stiffness (-1.0 Nm/rad) and little bias for reflexive gain (+0.02 Nm·s/rad). The original online algorithm did show a negative bias (-11 Nm/rad) for intrinsic stiffness, especially at high simulated stiffness values, see Fig. 3.5. Moreover, the original online algorithm showed a positive bias for reflexive gain (+2 Nm·s/rad). In comparison, the adapted online algorithm showed a reduced overall bias for both intrinsic stiffness (-2 Nm/rad) and reflexive gain (+0.1 Nm·s/rad). Still, a trend was observed for the adapted online algorithm with positive biases at low simulated values and negative biases at high simulated values, see Fig. 3.5. Both adapted algorithms showed similar characteristics between the able-bodied and spastic trials, although a negative bias did appear for the

Table 3.1: Joint impedance estimation performance in able-bodied and spastic simulation environment. Algorithm responsiveness was quantified using the Pearson's correlation coefficient r^2 between estimated and simulated magnitudes ($N = 100$). Algorithm estimation accuracy and reliability was quantified using the mean (±) mean average deviation (MAD), the MAD was used instead of standard deviation to decrease sensitivity to outliers ($N = 100$). Algorithm estimation accuracy and reliability was quantified for conditions with varying K and G based on the difference between estimated and simulated magnitudes $\Delta\hat{K}$ and $\Delta\hat{G}$. In addition, performance across conditions with constant parameter magnitudes was evaluated $\hat{K}$, $\hat{G}$, $\hat{B}$, $\hat{I}$, $\hat{\omega}$, $\hat{\zeta}$, $\hat{\delta}$. Overall quality of the estimation performance was computed using the %VAF of the measured torque. For the online algorithms, within trial variability (std) and rise time τ were quantified.

	Offline		**Online**		
	Able-bodied	**Spasticity**	**Able-bodied**		**Spasticity**
	Adapted		**Original**	**Adapted**	
r^2 $\hat{K}$ (-)	1.00	1.00	0.986	0.987	0.986
r^2 $\hat{G}$ (-)	1.00	1.00	0.986	0.978	0.984
$\Delta\hat{K}$ (Nm/rad)	-1.0±0.14	-0.9±0.11	-11±5	-2±5	0.3±5
$\Delta\hat{G}$ (Nm·s/rad)	0.02±0.06	-0.4±0.15	2±0.6	0.1±0.7	-0.8±1.5
$\hat{K}$=100 (Nm/rad)	99.1±0.38	99.3±0.46	90±5	99±5	102±6
$\hat{G}$=10/25 (Nm·s/rad)	10.0±0.03	24.7±0.16	12±0.8	10±0.7	25±1.1
$\hat{B}$=0.63 (Nm·s/rad)	0.63±0.01	0.64±0.02	0.52±0.05	0.58±0.05	0.62±0.04
$\hat{I}$=0.0137 (Nm·s^2/rad)	0.0137±2e-4	0.0137±2e-4	5e-5±1e-5	0.0145±8e-4	0.0144±7e-4
$\hat{\omega}$=21/10 (rad/s)	21.0±1.2	10.0±0.3			
$\hat{\zeta}$=0.8/0.9 (rad/s)	0.81±0.08	0.88±0.04			
$\hat{\delta}$=40 (ms)	38.8±1.3	39.3±1.0			
VAF torque (%)	100.0±0.01	100.0±0.01	81.4±15.5	99.5±0.5	99.5±0.4
std $\hat{K}$ (% of mean)			8.4	8.9	8.3
std $\hat{G}$ (% of mean)			6.3	8.4	6.4
τ_K (s)			16.7	16.5	9.7
τ_G (s)			7.3	8.2	7.6

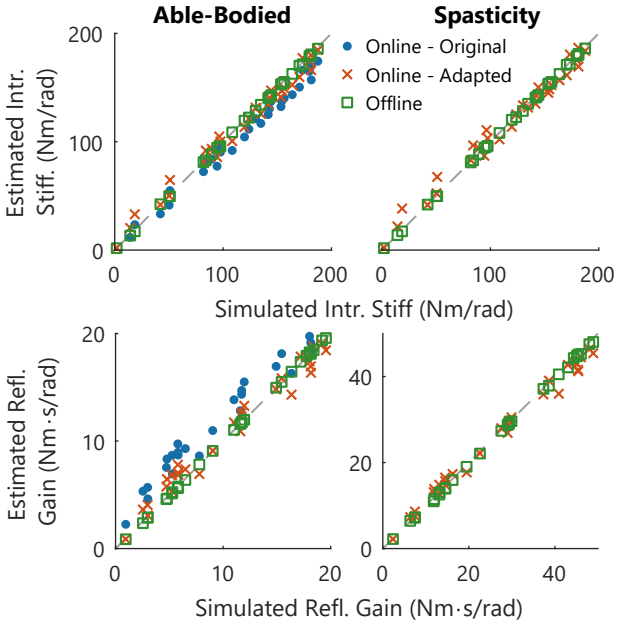

Figure 3.5: Offline and online joint impedance performance in able-bodied and spastic simulation environment. The mean estimated intrinsic stiffness *(Top)* and reflexive gain *(Bottom)* with the respective simulated values are shown across 30 of 100 simulation trials. Algorithms with perfect estimation performance would show all markers on top of the diagonal *(grey line)*.

reflexive gain estimation (online: -0.4 Nm·s/rad; offline: -0.8 Nm·s/rad). Estimation accuracy for the other parameters, simulated with constant magnitudes, showed similar results with largest bias for original online algorithm, reduced bias for the adapted original algorithm and lowest bias for the offline algorithm. For all parameter estimates combined, the differences in estimation accuracy were reflected in the %VAF of the net torque response with average values of 81.4% (online-original), 99.5% (online adapted) and 100.0% (offline-adapted).

Regarding estimation reliability, the adapted offline algorithm in able-bodied conditions showed the lowest MAD for intrinsic stiffness(±0.38 Nm/rad) and reflexive gain (±0.03 Nm·s/rad). The online algorithms showed reduced reliability across trials with a MAD for intrinsic stiffness(±5 Nm/rad) and reflexive gain (±0.7-0.8 Nm·s/rad). Contrary to the estimation accuracy, the adapted online algorithm did not improve in terms of estimation reliability compared to the original online algorithm. The spastic simulated trials showed similar reliability to the able-bodied simulations for both offline and online algorithms. Only a reduced reliability was observed for reflexive gain for both adapted algorithms (online: ±0.16 Nm·s/rad; offline: ±1.1 Nm·s/rad).

For the offline algorithm, the adaptations in the iterative non-parametric estimation procedure (Step 3) were important to improve algorithm performance for both the intrinsic and reflexive pathway, see Table 3.2. Algorithm responsiveness (r^2) and reliability (MAD) were improved for both pathways by assuming the reflexive pathway to depend

Table 3.2: Effect of implemented adaptations on joint estimation performance for the offline PC algorithm in able-bodied simulation environment. Joint impedance estimation performance parameters for the adapted offline algorithm were taken as reference, see Table 3.1. Each adaptation was investigated by changing the reference algorithm to the original algorithm [7] at the indicated step as described in Fig. 3.2 and Section 3.2.2. *(3.d)* Half-wave rectified velocity was not assumed and a static nonlinearity was estimated using a Hammerstein identification procedure; *(3.e-f)* Voluntary torque was not estimated and fixed at zero throughout the identification procedure; *(4.)* Intrinsic I, B and K parameters were estimated through a nonlinear optimization on the intrinsic compliance IRF. The compliance IRF was obtained through inversion of the acausal intrinsic IRF; *(5.)* Half-wave rectified velocity and reflexive torque were not low-pass filtered before fitting the final reflexive IRF.

	Offline, Able-bodied				
	Reference	**Half-wave rect. (3.d)**	**Vol. Torque (3.e-f)**	**Intr. IRF inversion (4.)**	**Refl. IRF filter (5.)**
r^2 $\hat{K}$ (-)	1.00	1.00	0.996	0.995	1.00
r^2 $\hat{G}$ (-)	1.00	0.985	0.988	1.00	1.00
$\Delta\hat{K}$ (Nm/rad)	-1.0±0.14	-0.7±2.3	-2.7±0.65	-6.1±3.3	-1.0±0.14
$\Delta\hat{G}$ (Nm·s/rad)	0.02±0.06	-0.2±0.44	-0.2±0.52	0.02±0.06	0.02±0.06
$\hat{K}$=100 (Nm/rad)	99.1±0.38	97.6±1.3	99.0±2.48	95.4±1.1	99.1±0.38
$\hat{G}$=10/25 (Nm·s/rad)	10.0±0.03	9.95±0.34	9.83±0.44	10.0±0.03	10.0±0.03
$\hat{B}$=0.63 (Nm·s/rad)	0.632±0.012	0.635±0.020	0.648±0.029	0.661±0.039	0.632±0.012
$\hat{I}$=0.0137 (Nm·s^2/rad)	0.0137±2e-4	0.0136±3e-4	0.0138±3e-4	0.0138±5e-4	0.0137±2e-4
$\hat{\omega}$=21/10 (rad/s)	21.0±1.2	27.3±1.5	19.8±0.8	21.0±1.2	20.7±1.2
$\hat{\zeta}$=0.8/0.9 (rad/s)	0.81±0.08	0.73±0.18	0.71±0.10	0.81±0.08	0.80±0.08
$\hat{\delta}$=40 (ms)	38.8±1.3	54.7±5.2	38.0±1.5	38.8±1.3	38.0±1.3
VAF torque (%)	100±0.01	99.8±0.27	99.4±3.9	99.8±0.12	100±0.01

Table 3.3: Effect of implemented adaptations on joint estimation performance for the online PC algorithm in able-bodied simulation environment. Joint impedance estimation performance parameters for the adapted online algorithm were taken as reference, see Table 3.1. Each adaptation was investigated by changing the reference algorithm to the original algorithm [16] at the indicated step as described in Fig. 3.3 and Section 3.2.3. *(1.)* Input signals were not low-pass filtered before further processing; *(2.)* A 1th-order, instead of 4st-order, backwards difference method was used for numerical approximation of acceleration from velocity; *(1./2.)* The velocity input signal was numerically approximated through differentiation of the position signal instead of using direct measurements.

		Online, Able-bodied		
	Reference	**Input filter (1.)**	**Numerical diff. (2.)**	**Velocity meas. (1./2.)**
r^2 $\hat{K}$ (-)	0.987	0.988	0.987	0.987
r^2 $\hat{G}$ (-)	0.978	0.981	0.977	0.979
$\Delta\hat{K}$ (Nm/rad)	-2±5	-8±5	-2±5	-4±5
$\Delta\hat{G}$ (Nm·s/rad)	0.1±0.7	1.0±0.7	0.03±0.7	0.4±0.7
$\hat{K}$=100 (Nm/rad)	99±5	94±5	99±5	98±5
$\hat{G}$=10/25 (Nm·s/rad)	10.3±0.7	11.2±0.7	10.3±0.7	10.6±0.7
$\hat{B}$=0.63 (Nm·s/rad)	0.58±0.05	0.58±0.05	0.53±0.05	0.58±0.05
$\hat{I}$=0.0137 (Nm·s^2/rad)	0.0145±8e-4	0.0047±2e-4	0.0145±8e-4	0.0113±6e-4
VAF torque (%)	99.5±0.5	92.3±6.7	99.4±0.6	98.9±0.8
std $\hat{K}$ (% of mean)	8.9	9.2	8.9	9.0
std $\hat{G}$ (% of mean)	8.4	7.3	8.4	8.1
τ_K (s)	16.5	13.5	16.5	16.3
τ_G (s)	8.2	7.6	8.2	8.0

on half-wave rectified velocity instead of using a nonlinear Hammerstein identification procedure. Inclusion of a voluntary torque estimation in the non-parametric procedure improved responsiveness (r^2), accuracy (mean, bias) and reliability (MAD) across both pathways. For the intrinsic pathway, adaptation of the parametric estimation procedure (Step 4), avoiding inversion of the acausal IRF, improved responsiveness, accuracy and reliability of the estimated intrinsic parameters. For the reflexive pathway addition of a low-pass filter in the parametric estimation procedure (Step 5) had minimal impact, as only the accuracy for the reflexive natural frequency and delay was improved. Overall, the performance improvement was captured in an increase in %VAF (100.0% instead of 99.4-100.0%) due to the isolated implementation of the proposed adaptations.

For the online algorithm, performance analysis of isolated adaptations showed the importance of adding a low-pass filter for the input signals and using directly available velocity measurements, see Table 3.3. As expected, the effect of the isolated adaptations on algorithm performance was smaller than the difference in performance between the original and adapted algorithm, see Table 3.1. In addition, as for the original algorithm the isolated adaptations mainly affected estimation accuracy (increased bias), whereas responsiveness and reliability only showed little to no changes. Adapting the numerical differentiation method used, i.e. adapting the order of the backwards difference method, had little impact and only improved estimation accuracy for intrinsic damping B. Again, the overall performance improvement was captured in an increase in %VAF (99.5% instead of 92.3-99.4%) due to the isolated implementation of the proposed adaptations.

3.4 Discussion and Conclusion

The aim of this study was to characterise and improve an offline [7] and online [16] PC algorithm to obtain intrinsic and reflexive joint impedance estimates in our experimental setup. Adaptations made to the offline algorithm improved responsiveness, accuracy and reliability for both the intrinsic and reflexive pathway. Adaptations made to the online algorithm improved parameter estimation accuracy for both the intrinsic and reflexive pathways. The adapted online algorithm had similar transient characteristics as the original algorithm, shown through the strong co-variation between the joint impedance estimates of both algorithms. As expected based on Ludvig *et al.* [16], the adapted offline PC algorithm consistently showed best parameter estimation performance compared with the adapted online PC algorithm. The adapted offline and online algorithms both showed similar performance between simulation with able-bodied and spastic conditions.

For the offline algorithm, the most important adaptations were implemented in the non-parametric identification step, as performance improvement for both the intrinsic and reflexive pathways were achieved. First, the static nonlinearity in the reflexive pathway was assumed to be a half-wave rectifier, i.e. reflexes are only elicited after dorsiflexion perturbations. Physiologically, this assumption holds if the ankle is positioned towards dorsiflexion creating tension in the calf muscles and slack in the tibialis anterior (TA) [19]. As a result, the dorsiflexion perturbations elicit a stretch reflex in the calf muscles, whereas no reflexive torque response is elicited in the TA after a plantarflexion perturbation. Assuming half-wave rectified velocity is important, as the velocity distribution in the applied binary PRBS-like perturbation signal does not contain enough

information to reliably estimate this nonlinearity [7]. Second, the results showed that any non-constant voluntary torque applied by participants influenced estimation performance of both intrinsic and reflexive pathways. Non-constant voluntary torque can be unravelled non-parametrically from the other contribution assuming that voluntary torque has low-frequency content only. Besides adaptations in the non-parametric identification procedure, avoiding inversion of the acausal intrinsic IRF was important to improve estimation quality of the intrinsic parameters. A theoretical inversion of the acausal IRF to the causal equivalent does not exist and the inversion has to be approximated through simulation. Our results showed that this approximation introduced bias and variability into the intrinsic pathway estimations.

For the online algorithm, the most important adaptations were implemented in the input processing steps through addition of low-pass filters and the direct use of measured velocity. First, low-pass filters were added to remove high frequency noise content, while retaining relevant dynamics. For our experimental setup, we expected a lower signal-to-noise ratio than other devices used to executed experiments for the PC technique [7, 16, 21]. Interestingly, as known from theory and shown in our results, noise on the input signals can actually result in a bias of the outcome parameters [20]. Second, inclusion of velocity measurements, if available, can result in an improved algorithm performance as numerical approximation is avoided.

Simulation of spastic characteristics did not change the performance of either the adapted offline and online algorithm. This was expected as the neurophysiological basis on which PC algorithms are built can be adapted for reflexes with elongated duration [16]. The results did show a reduced reliability for the reflexive gain during spastic conditions. To place this increase in context, the spastic conditions also increased the simulated reflexive gain with a factor 2.5. From a practical perspective, the length of the steps (660 ms instead of 460 ms) of the perturbation was adapted for spastic participants, as duration of the spastic reflexive response measured during experiments could be elongated [8, 16, 18]. Unfortunately, the exact length of the reflexive response will not be known before the experiment execution. Additional simulation should be performed to investigate the effect of reflexive duration and influence on algorithm performance. The results of this simulation study could provide recommendations on which perturbation signal and algorithm settings to use for each experimental design.

Despite all implemented modifications, the simulation model emulating the experimental environment still contained potential discrepancies with reality. First, the intrinsic and reflexive pathways were implemented using simplifications as second-order models. For the intrinsic pathway, the second-order model cannot explain the mechanical interaction between muscle and tendons, as for example seen in a Hill-type muscle model [22]. For the reflexive pathway, the second-order model cannot capture the oscillations regularly observed in the reflexive torque response [8, 23]. Note, this discrepancy for the reflexive pathway appears during active conditions, not the passive conditions as planned in Chapters 5 and 6. Second, the simulation environment was time-invariant, except for a few step responses in the simulated intrinsic stiffness and reflexive gain to test transient characteristics. Even in experimental conditions with constant participant posture and behavior, for which impedance could be assumed to remain constant on average, fully time-invariant conditions do not reflect the observed neurophysiological response. The human stretch reflex response shows a natural varia-

tion across each single dorsiflexion perturbation for both EMG and torque responses, see also Chapters 2 and 4-6 [8, 17]. This natural variation is likely to affect the transient behavior of the online algorithm. Third, experimental data contains additional disturbances besides the Gaussian measurement noise implemented in simulation. Most importantly, the measured angle, velocity and torque do not perfectly reflect the actual response of the foot. For example, in our experimental setup, the actuator encoder measured angle and angular velocity of the foot, whereas a torque sensor between a footplate and actuator measured ankle torque. As such, the structural components between the foot and sensors all affect these measurements, especially if structural eigenfrequencies are excited, see Appendix A.

To summarize, our simulated results showed good responsiveness, accuracy and reliability for both offline and online PC algorithms to study either able-bodied participants or people with spasticity. Despite the implemented modification, discrepancies between the simulated and experimental environments remain. In terms of application, the online algorithm should be used to provide live joint impedance estimates during experiments. The offline algorithm should be used for post-trial evaluation, if data is time-invariant.

References

[1] R. E. Kearney and I. W. Hunter, "System Identification of Human Joint Dynamics," *Critical Reviews in Biomedical Engineering*, 18(1), pp. 55–87, 1990.

[2] E. Burdet, R. Osu, D. W. Franklin, T. E. Milner, *et al.*, "The Central Nervous System Stabalizes Unstable Dynamics by Learning Optimal Impedance," *Nature*, 414(6862), pp. 446–449, 2001. doi: 10.1038/35106566.

[3] D. W. Franklin, E. Burdet, R. Osu, M. Kawato, *et al.*, "Functional Significance of Stiffness in Adaptation of Multijoint Arm Movements to Stable and Unstable Dynamics," *Experimental Brain Research*, 151(2), pp. 145–157, 2003. doi: 10.1007/s00221-003-1443-3.

[4] J. A. Burne, V. L. Carleton, and N. J. O'Dwyer, "The Spasticity Paradox: Movement Disorder or Disorder of Resting Limbs?" *Journal of Neurology, Neurosurgery and Psychiatry*, 76(1), pp. 47–54, 2005. doi: 10.1136/jnnp.2003.034785.

[5] V. Dietz and T. Sinkjær, "Spastic Movement Disorder: Impaired Reflex Function and Altered Muscle Mechanics," *Lancet Neurology*, 6(8), pp. 725–733, 2007. doi: 10.1016/S1474-4422(07)70193-X.

[6] J. C. van den Noort, L. Bar-On, E. Aertbeliën, M. Bonikowski, *et al.*, "European Consensus on the Concepts and Measurement of the Pathophysiological Neuromuscular Responses to Passive Muscle Stretch," *European Journal of Neurology*, 24(7), pp. 981–991, 2017. doi: 10.1111/ene.13322.

[7] R. E. Kearney, R. B. Stein, and L. Parameswaran, "Identification of Intrinsic and Reflex Contributions to Human Ankle Stiffness Dynamics," *IEEE Transactions on Biomedical Engineering*, 44(6), pp. 493–504, 1997. doi: 10.1109/10.581944.

[8] M. M. Mirbagheri, H. Barbeau, M. Ladouceur, and R. E. Kearney, "Intrinsic and Reflex Stiffness in Normal and Spastic, Spinal Cord Injured Subjects," *Experimental Brain Research*, 141(4), pp. 446–459, 2001. doi: 10.1007/s00221-001-0901-z.

[9] M. M. Mirbagheri, M. Ladouceur, H. Barbeau, and R. E. Kearney, "The Effects of Long Term FES-Assisted Walking on Intrinsic and Reflex Dynamic Stiffness in Spinal Cord Injured Patients," *IEEE Transactions on Neural Systems and Rehabilitation Engineering*, 10(4), pp. 280–289, 2002. doi: 10.1109/TNSRE.2002.806838.

[10] Y. Zhao, D. T. Westwick, and R. E. Kearney, "Subspace Methods for Identification of Human Ankle Joint Stiffness," *IEEE Transactions on Biomedical Engineering*, 58(11), pp. 3039–3048, 2011. doi: 10.1109/TBME.2010.2092430.

[11] D. Ludvig, T. S. Visser, H. Giesbrecht, and R. E. Kearney, "Identification of Time-Varying Intrinsic and Reflex Joint Stiffness," *IEEE Transactions on Biomedical Engineering*, 58(6), pp. 1715–1723, 2011. doi: 10.1109/TBME.2011.2113184.

[12] K. Jalaleddini, E. Sobhani Tehrani, and R. E. Kearney, "A Subspace Approach to the Structural Decomposition and Identification of Ankle Joint Dynamic Stiffness," *IEEE Transactions on Biomedical Engineering*, 64(6), pp. 1357–1368, 2017. doi: 10.1109/TBME.2016.2604293.

[13] K. Jalaleddini, M. A. Golkar, and R. E. Kearney, "Measurement of Dynamic Joint Stiffness from Multiple Short Data Segments," *IEEE Transactions on Neural Systems and Rehabilitation Engineering*, 25(7), pp. 925–934, 2017. doi: 10.1109/TNSRE.2017.2659749.

[14] M. A. Golkar, E. Sobhani Tehrani, and R. E. Kearney, "Linear Parameter Varying Identification of Dynamic Joint Stiffness during Time-Varying Voluntary Contractions," *Frontiers in Computational Neuroscience*, 11:15, 2017. doi: 10.3389/fncom.2017.00035.

[15] D. L. Guarín and R. E. Kearney, "Unbiased Estimation of Human Joint Intrinsic Mechanical Properties during Movement," *IEEE Transactions on Neural Systems and Rehabilitation Engineering*, 26(10), pp. 1975–1984, 2018. doi: 10.1109/TNSRE.2018.2870330.

[16] D. Ludvig and R. E. Kearney, "Real-time Estimation of Intrinsic and Reflex Stiffness," *IEEE Transactions on Biomedical Engineering*, 54(10), pp. 1875–1884, 2007. doi: 10.1109/TBME.2007.894737.

[17] D. Ludvig, I. Cathers, and R. E. Kearney, "Voluntary Modulation of Human Stretch Reflexes," *Experimental Brain Research*, 183(2), pp. 201–213, 2007. doi: 10.1007/s00221-007-1030-0.

[18] L. Galiana, J. Fung, and R. E. Kearney, "Identification of Intrinsic and Reflex Ankle Stiffness Components in Stroke Patients," *Experimental Brain Research*, 165(4), pp. 422–434, 2005. doi: 10.1007/s00221-005-2320-z.

[19] M. M. Mirbagheri, H. Barbeau, and R. E. Kearney, "Intrinsic and Reflex Contributions to Human Ankle Stiffness: Variation with Activation Level and Position," *Experimental Brain Research*, 135(4), pp. 423–436, 2000. doi: 10.1007/s002210000534.

[20] D. T. Westwick and R. E. Kearney, "Identification of Linear Systems," in *Identification of Nonlinear Physiological Systems*, Hoboken, NJ, USA: John Wiley & Sons, Inc., 2003, ch. 5, pp. 103–123. doi: 10.1002/0471722960.ch5.

[21] R. C. van 't Veld, A. C. Schouten, H. van der Kooij, and E. H. F. van Asseldonk, "Validation of Online Intrinsic and Reflexive Joint Impedance Estimates using Correlation with EMG Measurements," in *7th International Conference on Biomedical Robotics and Biomechatronics*, Enschede, Netherlands: IEEE, 2018, pp. 13–18. doi: 10.1109/BIOROB.2018.8488123.

[22] E. Sobhani Tehrani, K. Jalaleddini, and R. E. Kearney, "Ankle Joint Intrinsic Dynamics is More Complex than a Mass-Spring-Damper Model," *IEEE Transactions on Neural Systems and Rehabilitation Engineering*, 25(9), pp. 1568–1580, 2017. doi: 10.1109/TNSRE.2017.2679722.

[23] M. M. Mirbagheri, R. E. Kearney, H. Barbeau, and M. Ladouceur, "Parametric Modeling of the Reflex Contribution to Dynamic Ankle Stiffness in Normal and Spinal Cord Injured Spastic Subjects," in *17th Annual International Conference of the IEEE Engineering in Medicine and Biology Society*, Montreal, Canada: IEEE, 1995, pp. 1241–1242. doi: 10.1109/IEMBS.1995.579661.

Chapter 4

Neurophysiological Validation of Simultaneous Intrinsic and Reflexive Joint Impedance Estimates

R. C. van 't Veld, A. C. Schouten, H. van der Kooij, E. H. F. van Asseldonk

Abstract — People with brain or neural injuries, such as cerebral palsy or spinal cord injury, commonly have joint hyper-resistance. Diagnosis and treatment of joint hyper-resistance is challenging due to a mix of tonic and phasic contributions. The parallel-cascade (PC) system identification technique offers a potential solution to disentangle the intrinsic (tonic) and reflexive (phasic) contributions to joint impedance, i.e. resistance. However, a simultaneous neurophysiological validation of both intrinsic and reflexive joint impedances is lacking. This simultaneous validation is important given the mix of tonic and phasic contributions to joint hyper-resistance. Therefore, the main goal of this chapter is to perform a group-level neurophysiological validation of the PC system identification technique using electromyography (EMG) measurements. Ten healthy people participated in the study. Perturbations were applied to the ankle joint to elicit reflexes and allow for system identification. Participants completed 20 hold periods of 60 seconds, assumed to have constant joint impedance, with varying magnitudes of intrinsic and reflexive joint impedances across periods. Each hold period provided a paired data point between the PC-based estimates and neurophysiological measures, i.e. between intrinsic stiffness and background EMG, and between reflexive gain and reflex EMG. The intrinsic paired data points, with all subjects combined, were strongly correlated, with a range of $r = [0.87, 0.91]$ in both ankle plantarflexors and dorsiflexors. The reflexive paired data points were moderately correlated, with $r = [0.64, 0.69]$ in the ankle plantarflexors only. In conclusion, an agreement with the neurophysiological basis on which PC algorithms are built is necessary to support its clinical application in people with joint hyper-resistance. Our results show this agreement for the PC system identification technique on a group-level. Consequently, these results show the validity of the use of the technique for the integrated assessment and training of people with joint hyper-resistance in clinical practice.

This chapter was published in the *Journal of NeuroEngineering and Rehabilitation*, 18:36, 2021. The code and data underlying this publication are available via 4TU.ResearchData. doi: 10.4121/c.5281478

4.1 Introduction

People with brain or neural injuries, such as cerebral palsy or spinal cord injury, commonly have an increased joint resistance (or 'hyper-resistance') [1]. This joint hyper-resistance can severely impair both walking ability and functional independence. The origin of the hyper-resistance can vary and arises from one or multiple of the following categories [2]:

Intrinsic:

1. a tissue-related non-neural origin, e.g. shortened tissue or fibrosis;
2. a tonic neural origin, i.e. involuntary background muscle activation;

Reflexive:

3. a phasic neural origin, i.e. stretch hyperreflexia ('spasticity').

The mixed origin of the joint hyper-resistance creates a challenge in the diagnosis and treatment of hyper-resistance. Ideally, diagnostic methods unravel the three contributions to hyper-resistance [2]. However, current clinical practise lacks a valid and reliable procedure to unravel these contributions. Besides, current treatment includes non-specific interventions with questionable cost-effectiveness. For example, Botulinum neurotoxin injections reduce both involuntary background activation and spasticity, but also the ability to perform voluntary muscle contractions [3, 4].

The parallel-cascade (PC) system identification technique offers a potential solution for the integrated assessment and treatment of joint hyper-resistance [5]. The technique disentangles and simultaneously estimates the intrinsic and reflexive contributions to joint impedance, i.e. the joint's resistance to imposed motion. PC algorithms have been used successfully to assess joint hyper-resistance compared to a control group and to assess the effect of treatments on joint resistance [6, 7]. Moreover, an online PC algorithm is available, which directly estimates joint impedance contributions during data acquisition and can consequently be used to provide biofeedback [8]. Training people using this joint impedance biofeedback was shown to achieve voluntary within-session modulation of both intrinsic and reflexive contributions independently [9]. This ability to train joint impedance modulation enables a novel treatment using the PC algorithm to specifically reduce spasticity. For such a treatment, the within-session modulation of reflexive impedance should be consolidated to an across-session, long-term effect. This transformation from within- to across-session effects are key for an effective intervention and has been shown in electromyography (EMG)-based operant conditioning protocols [10, 11].

The main goal of this chapter is to perform a group-level neurophysiological validation of the PC system identification technique to support its clinical application. The validation is performed using the online PC algorithm, because of the ability to provide biofeedback. Primarily, the neurophysiological validation will be performed by investigating the linear association of the system identification outcome measures [9] with equivalent EMG-based outcome measures [10, 11]. We expect the following parameters to be correlated (also see pilot experiment [12]):

1. estimated intrinsic joint stiffness is correlated with background EMG activity in both ankle plantarflexors and dorsiflexors [13];

2. estimated reflexive gain is correlated with reflex EMG activity in the ankle plantarflexors only [9].

Secondarily, the effect of varying voluntary torque on these linear associations is investigated, as the various assessment and treatment methodologies use a mix of relaxed and tonically activated plantarflexors [6, 11]. The change between the relaxed and activated conditions is known to influence both the intrinsic joint stiffness and reflexive gain [14].

This study investigates the agreement between the PC system identification technique and the neurophysiological basis on which it is built [5]. The association between PC algorithms and EMG-based outcome measures has been investigated for reflexive contributions only [9, 15, 16]. However, validating both intrinsic and reflexive pathways simultaneously is important, given the mixed intrinsic and reflexive origins of joint hyper-resistance. Besides, all previous results investigating this linear association were restricted by limited or no variation in voluntary muscle activation. A successful validation would increase clinical confidence in the PC technology when used for people with joint hyper-resistance.

4.2 Methods

4.2.1 Participants

Ten volunteers with no history of neuromuscular disorders participated in the study: age 27.8±1.7 yr, 4 women. The EEMCS/ET ethics committee of the University of Twente approved the study (RP 2018-71) and all participants provided written informed consent.

4.2.2 Apparatus

The experiment was executed using an adjustable chair, robotic manipulator, EMG device and feedback screen, see Fig. 4.1. Participants were seated on the adjustable chair, which supported the upper leg and upper body, while controlling for hip (120°) and knee (150°) angles. Both knee and hip were defined at 180° for a perfectly straight posture. The right foot was connected to the manipulator, integrated into the frame of the chair, using a rigid footplate and Velcro straps. The ankle and manipulator axes of rotation were visually aligned before the start of the experiment, minimizing knee translation due to the applied ankle rotations.

A one degree of freedom manipulator (Moog, Nieuw-Vennep, the Netherlands) was used to apply the perturbations required for the PC algorithm. These angular, i.e. position, perturbations were applied in the sagittal plane around the ankle joint. The manipulator's encoder measured the angle and velocity of the footplate representing imposed ankle angle and angular velocity. Similarly, a torque sensor was placed between the footplate and actuator to measure of ankle torque. Angle, velocity and torque were recorded at 2048 Hz, all defined positive in dorsiflexion direction.

A Porti EMG device (TMSi, Oldenzaal, the Netherlands) recorded activity of the Soleus (SOL), Tibialis Anterior (TA), Gastrocnemius Medialis and Lateralis (GM and GL, respectively) muscles at 2048 Hz. EMG electrodes were placed according to the SENIAM guidelines [17].

A feedback screen provided biofeedback at a rate around 25 Hz using Matlab 2017b (Mathworks, Natick, MA, USA). The 2D feedback screen, see Fig. 4.1, visualized a 6 s

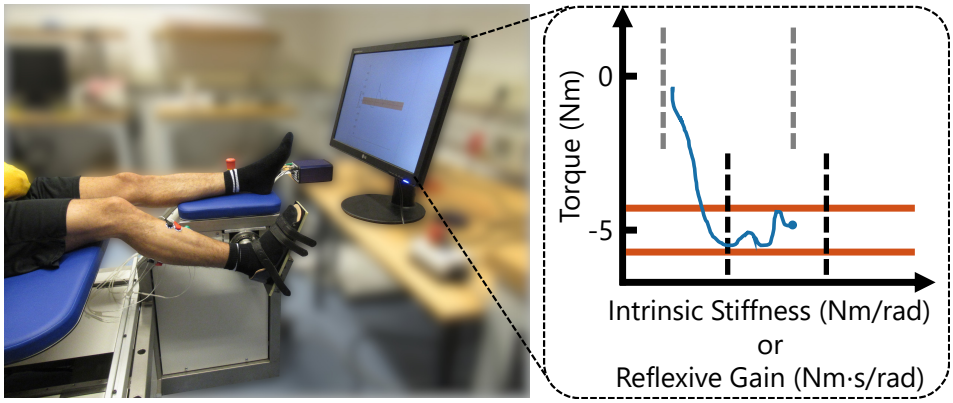

Figure 4.1: Experimental setup overview. Participants were seated on an adjustable chair with their right foot connected to a manipulator, applying perturbations around the ankle joint. Feedback was given using a (*blue*) 2D trace on both torque (*y-axis*) and an impedance parameter (*x-axis*). On the y-axis, a (*red*) torque target was shown around either 0 or -5 Nm. On the x-axis, (*black-dashed*) reference lines were shown with the average magnitude of the impedance parameter from previously completed 60 s hold periods at each torque level. In the specific example situation depicted, a participant would have had the following two tasks: 1. (*y-axis*) keep voluntary torque stable within the target boundaries around -5 Nm; and 2. (*x-axis*) keep the impedance parameter stable and away from the black-dashed reference lines shown.

historic trace of the low-pass filtered torque (2nd-order, 0.1 Hz, critically-damped) in combination with the intrinsic stiffness or reflexive gain parameter from the online PC algorithm. Using the online PC algorithm estimates was challenging, as these estimates had a long transient period of about 15 s before becoming reliable [8, 9]. Therefore, each data collection period only started when both researcher and participant mutually agreed that the participant could keep the feedback constant.

4.2.3 Experimental Protocol

First, an appropriate joint angle to elicit reflexes was determined for each participant, as reflexes depend on joint angle [14]. An initial trial was run at a 90° ankle angle, i.e. the angle between shank and foot determined using a goniometer. This initial trial also familiarized participants with the robotic setup, applied perturbations, feedback screen and task instructions. If participants had an estimated reflexive gain below 3 Nm·s/rad at 0 Nm torque, the ankle angle was increased in 5° steps. This more dorsiflexed ankle angle was used to increase the minimum reflex magnitudes and avoid multiple measurements close to zero distorting data analysis. Eventually, 5 participants performed the experiment at a 90° ankle angle and another 5 at 95°.

The experiment was split in 4 blocks of max. 15 minutes with continuous perturbations and biofeedback. A 3-5 minute break was included between blocks to avoid fatigue and loss of concentration. Participants were instructed to keep their voluntary torque between the two torque target boundaries. Moreover, participants were instructed to generate this torque by focusing on ankle rotation without using the upper leg. The

torque target switched in randomised order between the 0 and -5 Nm levels, i.e. the participant exerted a zero or plantarflexion torque, also within blocks. The difference in torque levels was selected to be large enough to impact both intrinsic and reflexive pathways [14], while limiting fatigue. Moreover, in each block, the participant was motivated to find 5 different combinations of torque and depicted intrinsic stiffness (Block 1 & 3) or reflexive gain (Block 2 & 4). The participant was requested to hold each combination of torque and the impedance parameter (stiffness or reflexive gain) constant for 60 seconds, referred to as a 'hold period'. Between hold periods, participants searched for a new impedance parameter value different from the averages in previous hold periods.

The protocol was intended to measure a large range of intrinsic and reflexive impedances within each participant. This large range of variation is desired to properly investigate the association between the PC algorithm and EMG-based outcome measures. Participants could use the provided biofeedback to guide their modulation strategy across hold periods and to keep the parameters constant during the hold periods, see Fig. 4.1. No specific instruction on modulation strategies were given and co-contraction was permitted. Participants were instructed to keep away from the average impedance parameter magnitudes measured in previous hold periods. These average magnitudes were shown on screen as black-dashed vertical lines, see Fig. 4.1. Participants started the experiment with a screen without any black-dashed lines in Blocks 1 & 2 and placed an additional line with each completed hold period. The lines from Blocks 1 & 2 were used as starting point in Blocks 3 & 4 respectively.

4.2.4 Online Joint Impedance Estimation

The online algorithm of the PC system identification technique was used to simultaneously estimate intrinsic and reflexive impedances based on the model of Fig. 4.2. The PC model consisted of an intrinsic and reflexive pathway to relate the angular perturbation as input with the measured torque response as output. The online PC algorithm required a 2° amplitude pulse-step angular perturbation to be applied to the joint. Moreover, the PC model assumed a constant voluntary torque, therefore the initial impedance estimates after a change in torque target were unreliable for about 15 s [8, 9].

Algorithm

The implemented algorithm was based on the original algorithm combined with some specific improvements to decrease the bias on the identified parameters [8, 12]. The algorithm consists of the following 10 steps:

1. The measured angle (with neutral angle subtracted), velocity and torque signals were low-pass filtered (2nd-order, 100 Hz, Butterworth) to remove high-frequency noise.
2. The acceleration was estimated via numerical differentiation (4th order, backwards difference) of the low-pass filtered velocity.
3. The torque was high-pass filtered (2nd-order, 0.033 Hz, Butterworth) to remove any constant voluntary torque.

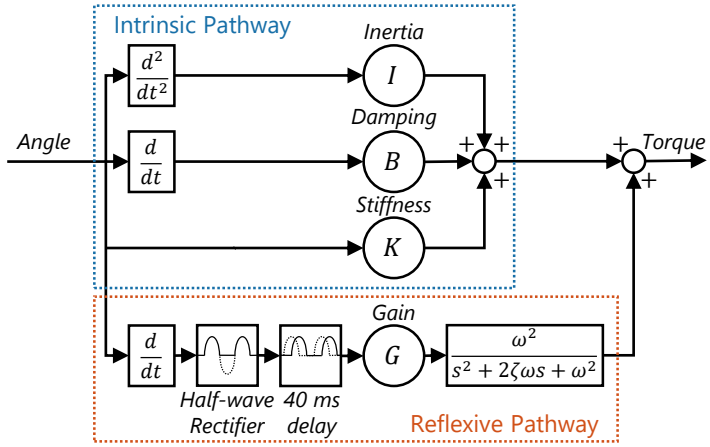

Figure 4.2: Parallel-cascade joint impedance model with intrinsic and reflexive pathway. The intrinsic pathway was modelled as a 2nd-order mass-spring-damper system with parameters: inertia I, damping B and stiffness K. The reflexive pathway was modelled based on the 40 ms delayed, half-wave rectified velocity using 2nd-order muscle activation dynamics and a parameter for reflexive gain G.

4. The 9 zero-lag auto- and cross-correlations between angle, velocity and acceleration, as well as the 3 zero-lag cross-correlations between torque and angle, velocity and acceleration were computed via a low-pass filter (2nd-order, 0.033 Hz, Butterworth).
5. The intrinsic inertia I, damping B and stiffness K parameters were estimated by solving an equation relating the 12 auto- and cross-correlations.
6. The intrinsic torque contribution was computed as defined in Fig. 4.2 using the estimated I, B and K parameters and high-pass filtered (2nd-order, 0.033 Hz, Butterworth) to remove the mean.
7. The reflexive torque was taken as measured torque minus intrinsic torque, see Fig. 4.2. The velocity was half-wave rectified and high-pass filtered (2nd-order, 0.033 Hz, Butterworth).
8. An anti-aliasing filter was applied to both reflexive torque and half-wave rectified velocity (8th-order, 81.9 Hz, 0.05 dB, Chebyshev) and both were downsampled with a factor 10, to 204.8 Hz.
9. The reflexive IRF was estimated every 48.8 ms using a linear least-squares method, based on the reflexive torque and lagged half-wave rectified velocity (ranging from min. 50 ms to max. 400 ms lag) both with a data length of 1 s, see [8].
10. The reflexive gain G was computed as the sum of the reflexive IRF. The time series of reflexive gains G was then low-pass filtered (2nd-order, 0.033 Hz, Butterworth).

Pulse-Step Perturbation

The online PC algorithm required a purposely designed pulse-step angular perturbation [8]. Intrinsic parameters estimation (Step 5) was based on the assumption that the cross-

correlation between torque and angle, velocity and acceleration are not affected by any reflexive contributions. The dedicated pulse-step perturbation signal was required to comply with this assumption and to avoid biased intrinsic parameter estimates. The signal randomly switched between 'pulses', ramp-hold-return perturbations with a 40 ms width, and 'steps', ramp-hold-return perturbations with a 460 ms width. The rising and falling edge angular profiles were equal for pulses and steps and were generated by low-pass filtering (2nd-order, 30 Hz, critically-damped) a rate-limited (227.6 rad/s) block pulse. The perturbation was low-pass filtered and rate-limited to avoid excessive oscillations and overshoot in the imposed ankle angle, see Appendix A.

4.2.5 Data Analysis

The study outcome measures were based on the K and G parameters of the PC algorithm and the EMG measurements. For each hold period, an average of the intrinsic stiffness (K) and reflexive gain (G) was obtained. The model fit quality for each hold period was investigated by checking the amount of variance accounted for (VAF) of the measured torque ensemble. The torque ensemble was obtained by aligning all data at dorsiflexion perturbation onset and removing average background torque measured over the 40 ms period before onset. The online PC algorithm does not estimate all parameters of the PC model required to calculate model torque output, which is used to compute the VAF, see Fig. 4.2. Therefore, the unidentified activation dynamics parameters ω and ζ had to be estimated afterwards during data analysis. A nonlinear least squares optimization procedure was used per data point to find the ω and ζ maximizing VAF.

Average background and reflex EMG measures were calculated based on [10, 11], see Fig. 4.3A. Before analysis, the EMG measurements were high-pass filtered (2nd-order, 5 Hz, Butterworth) and rectified. The background EMG measure should reflect an average activity over the short, unperturbed period before perturbation onset. Therefore, background EMG activity was computed as the mean EMG activity over the 40 ms period before each dorsiflexion perturbation onset. The reflex EMG measure should reflect the true reflexive magnitude, observed as characteristic double-peak shape after rectification. To compensate for background activity, background EMG was subtracted from the reflexive response and the resulting signal was half-wave rectified. Reflex EMG activity was defined as the root mean square (RMS) of this half-wave rectified signal within a subject-specific 20 ms window centered around the M1 response. For the SOL, GM and GL reflex measures, dorsiflexion perturbation onset was used as timing reference. For the TA reflex measure, plantarflexion perturbation onsets of all steps were used as reference. Pulses were excluded for the TA, as the TA muscle stretch during a pulse follows only 40 ms after shortening.

Each hold period provided a paired data point between intrinsic stiffness and background EMG, and between reflexive gain and reflex EMG. A total of 200 hold periods (20 hold periods for 10 participants) were executed, equally split between the 0 and -5 Nm torque levels. Some data points were removed due to EMG measurement artifacts. Additionally, one data point was removed as the participant indicated that she had executed the task instructions incorrectly. She modulated the impedance parameter by deliberately varying voluntary torque. Therefore, 94 to 100 paired data points remained to investigate the linear associations.

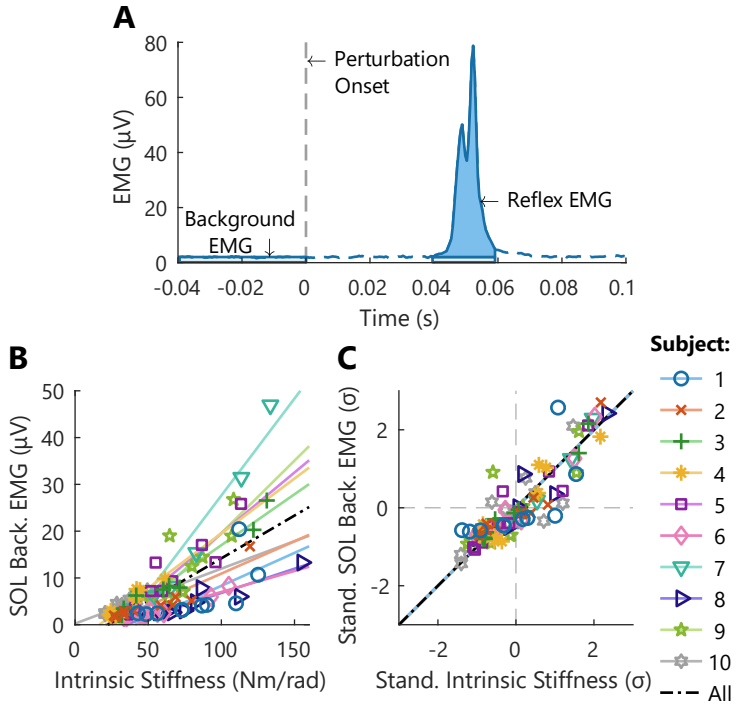

Figure 4.3: Data analysis methodology. *(A)* Background and reflexive EMG activity were calculated using the perturbation onset as reference. Background activity was based on the 40 ms period before perturbation onset, while reflexive activity was based on a 20 ms period about 40 ms after perturbation onset. *(B)* Absolute and *(C)* standardized correlation analysis. Both plots show a representative example using the intrinsic stiffness and SOL background EMG outcome measures collected at a 0 Nm torque target. A total least squares (TLS) fit shows the slope and intercept of the datasets of each individual participant.

Linear associations for both intrinsic and reflexive pathways were calculated on a group-level using Pearson's correlation coefficient, r. The correlation coefficient cannot be computed directly across the dataset, because the absolute values showed a subject-specific slope and intercept, see Fig. 4.3B. Therefore, all investigated datasets were standardized using the Z-score per participant. The Z-score standardization avoids any influence of subject-specific slopes and intercepts on the correlation coefficient, see Fig. 4.3C. The robustness of r was investigated using the 95% confidence interval (CI) constructed via a non-parametric bootstrap procedure using the bias corrected and accelerated method [18]. The data analysis was performed using Matlab 2017b (Mathworks, Natick, MA, USA) with the statistical analysis executed in R3.6.2 (R Foundation for Statistical Computing, Vienna, Austria).

4.3 Results

We investigated the neurophysiological validity of an online PC algorithm, which disentangles the intrinsic and reflexive contribution to joint impedance. Participants

completed 20 hold periods of 60 s with varying magnitudes of intrinsic and reflexive joint impedances across 2 voluntary torque levels, 0 and -5 Nm (plantarflexion). Each hold period provided a paired data point between estimated intrinsic stiffness and background EMG, and between estimated reflexive gain and reflex EMG. These paired data points were used to study the linear association by analyzing the correlation coefficient.

4.3.1 Experiment Time Series

The measured time series signals show the stretch reflex elicitation and causality within the reflex loop in response to an angular perturbation, see Fig. 4.4. The dorsiflexion perturbations stretch the ankle plantarflexors (SOL, GM and GL) and first show a reflexive EMG response after roughly 40 ms. This EMG response is followed by a contraction of the plantarflexors resulting in a reflexive plantarflexion torque with a peak roughly 150-200 ms after perturbation onset. Note, the antagonist TA muscle also appears to show reflexive EMG activity 40 ms after dorsiflexion perturbations, however this is considered to be cross-talk from the plantarflexors [9].

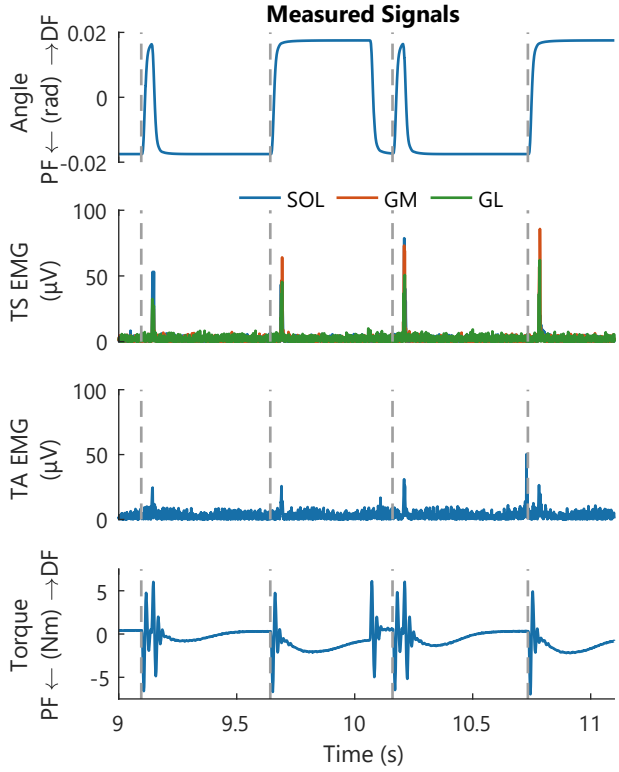

Figure 4.4: Time series of measured signals, typical example for a single representative participant. Four consecutive dorsiflexion perturbations with perturbation onset *(grey-dashed vertical lines)*. The response to the angular perturbations are shown for the high-pass filtered, rectified EMG of Triceps Surae (TS) and TA as well as measured ankle joint torque.

The processed time series show the simultaneous increase of the joint impedance parameters and EMG activity for both intrinsic and reflexive pathways across hold periods, see Fig. 4.5. The transition period between the hold periods lasted a minute, to have the participant familiarize themselves with the new task execution. Furthermore, the transition period is required to avoid violation of the online PC algorithm's constant voluntary torque assumption.

4.3.2 Hold Period Ensemble Averages

The simultaneous variation in joint impedance parameters and EMG activity was further investigated using the ensemble averages of each hold period, see Fig. 4.6. The model fitted the torque ensembles with a VAF of $76.2 \pm 7.2\%$ with a range of [56.9,88.6]% across all hold periods and participants. The activation dynamics parameters found via nonlinear optimization to compute the VAF were: $\omega = 11.4 \pm 2.0$ rad/s and $\zeta = 0.76 \pm 0.12$.

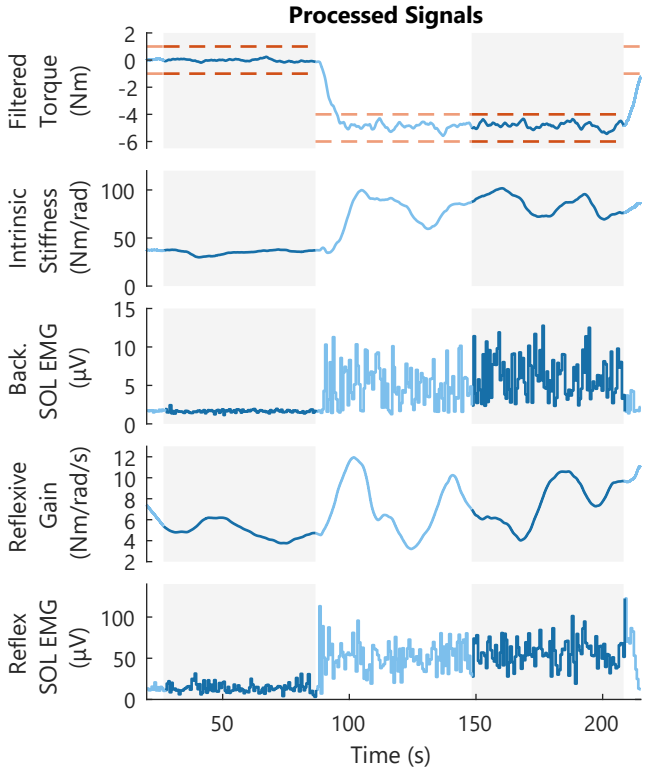

Figure 4.5: Time series of processed signals, typical example for a single representative participant. Two consecutive 60 s hold periods *(grey background)* with transition period. 2D feedback was provided on torque and intrinsic stiffness. The time series show the voluntary modulation of the low-pass filtered torque and active torque target (*red*), intrinsic stiffness K, background SOL EMG activity, reflexive gain G and reflexive SOL EMG activity. The PC algorithm parameters K and G were computed continuously, while the EMG activity computations were performed around every perturbation onset.

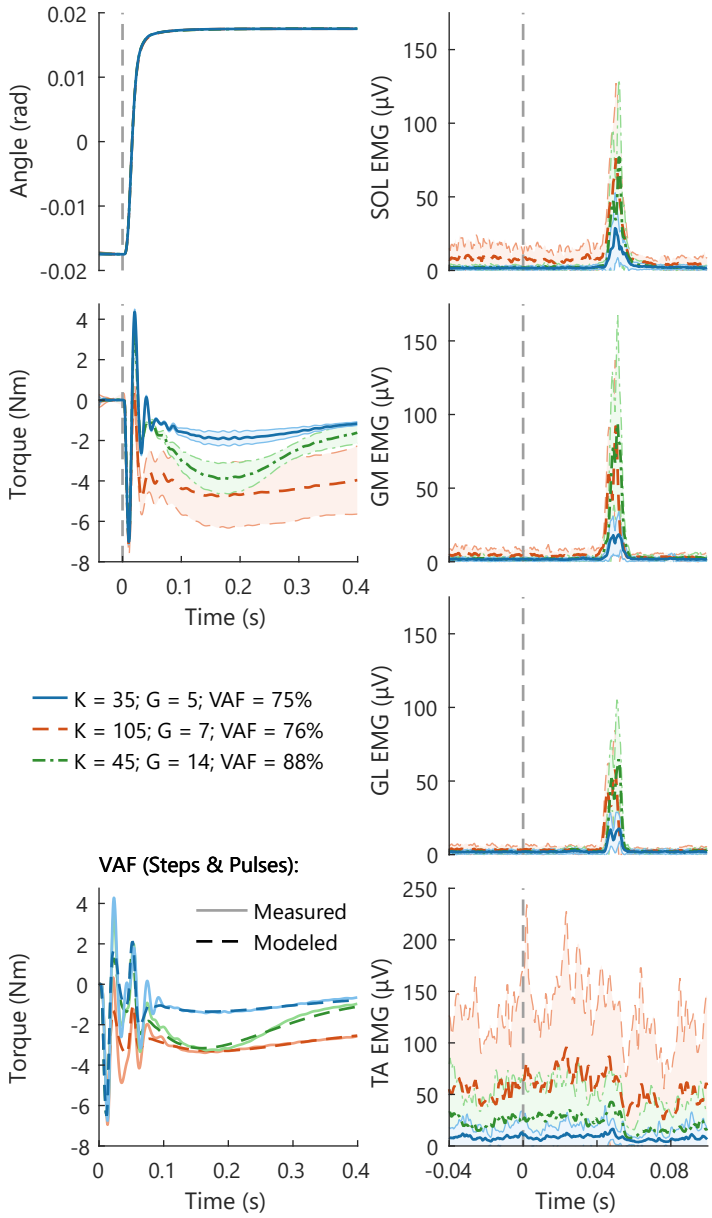

Figure 4.6: Ensemble averages (±SD) of hold periods with modulated impedance, typical examples for a single representative participant. Ensemble averages of the measured signals, created by aligning all step perturbations at perturbation onset *(grey-dashed vertical lines)*. %VAF was computed using the measured and modeled torque ensemble of both step and pulse perturbations. The K (Nm/rad) and G (Nm/rad/s) parameter values provided represent the mean value across each hold period. All torque ensembles were normalized by subtracting the average background torque to enhance visualization of intrinsic and reflexive torque effects. All three hold periods were executed at a 0 Nm torque target.

To check the constant voluntary torque assumption, the variance of the measured torque at all dorsiflexion perturbation onsets within a 60 s hold period was investigated. Across all participants, the hold periods showed a significantly lower torque average standard deviation at the 0 Nm target ($\sigma = 0.78 \pm 0.26$ Nm) than at -5 Nm ($\sigma = 1.32 \pm 0.27$ Nm) with $t(9) = -7.93$, $p = < 0.001$ (paired t-test).

An increased intrinsic stiffness was reflected in a larger plantarflexion torque across the 400 ms period after perturbation onset. Moreover, the increased stiffness was also reflected in increased background activity in both plantarflexors and dorsiflexors. This torque response matched with the concept of intrinsic stiffness, because the 2° dorsiflexion step perturbation lengthened the plantarflexor muscle-tendon unit over this entire 400 ms period. The EMG response showed the neural, non-velocity dependent contribution to joint impedance, with a large intrinsic stiffness matching high levels of co-contraction.

An increased reflexive gain was reflected in a larger reflexive plantarflexion torque with peak around 150-200 ms after perturbation onset. Moreover, the increased reflexive gain was also reflected in a larger EMG burst activity. The delayed timing with respect to perturbation onset and limited duration of both torque and EMG responses matches with the concept of a stretch reflex. The reflexive torque response is further delayed and smeared out compared with the EMG response due to the muscle activation dynamics, as included in the PC model Fig. 4.2. Note, EMG burst activity in the TA was observed in all participants after perturbations towards plantarflexion, stretching the TA, not the dorsiflexion perturbations shown in Fig. 4.6.

4.3.3 Correlation Analysis

The consistency of the simultaneous variation of the joint impedance parameters and EMG activity across all participants and torque levels was investigated using Pearson's correlation coefficient, see Fig. 4.7 and Table 4.1. For the intrinsic pathway, a positive correlation at both torque levels was observed for all muscles. For the reflexive pathway, a positive correlation at both torque levels was only observed for the plantarflexors.

The intrinsic pathway (top row of Fig. 4.7) showed fairly similar linear trends in the plantarflexors for the two torque levels, whereas the linear trend of the dorsiflexor differed between both torque levels. Furthermore, the correlation analysis at the -5 Nm

Table 4.1: Pearson's correlation coefficients (r) and their 95% confidence intervals across all hold periods *(N = 94-100)*. Correlations between identified intrinsic stiffness and background EMG activity (intrinsic pathway) and identified reflexive gain and reflex EMG activity (reflexive pathway). The 95% confidence intervals were constructed using a non-parametric bootstrap procedure.

	Intrinsic		Reflexive	
Torque	**0 Nm**	**-5 Nm**	**0 Nm**	**-5 Nm**
SOL	0.89 [0.82, 0.93]	0.68 [0.53, 0.78]	0.64 [0.46, 0.75]	0.54 [0.34, 0.69]
GM	0.89 [0.82, 0.93]	0.54 [0.33, 0.67]	0.69 [0.57, 0.78]	0.31 [0.13, 0.50]
GL	0.87 [0.80, 0.92]	0.52 [0.35, 0.66]	0.68 [0.48, 0.78]	0.54 [0.38, 0.65]
TA	0.91 [0.84, 0.95]	0.84 [0.78, 0.89]	0.37 [0.13, 0.56]	−0.02 [−0.24, 0.20]

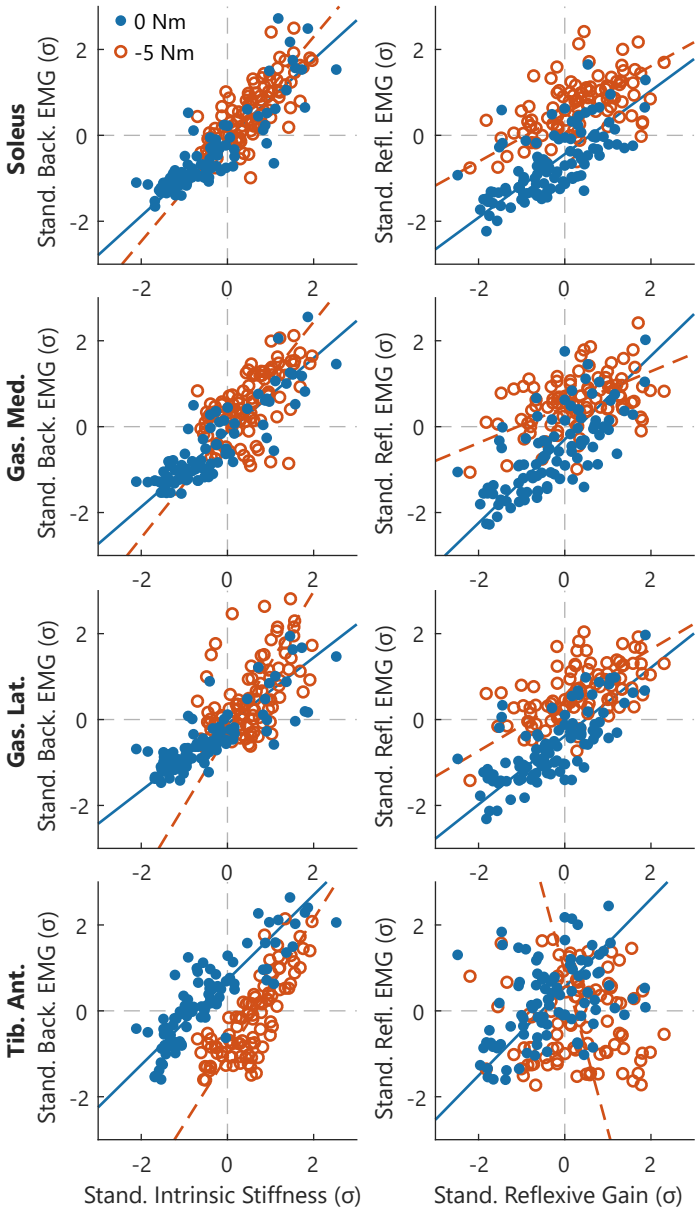

Figure 4.7: Linear associations between Z-score standardized joint impedance parameters and EMG activity across all participants. All datasets are shown for all hold periods across both torque levels. The TLS fit is shown for both torque levels to help visualize and interpret the linear associations.

level was restricted to smaller intervals for all muscles. All observations for the intrinsic pathway were caused by the additional plantarflexion activation required to reach a -5 Nm plantarflexion torque. On the other hand, the range of dorsiflexor muscle activity was not influenced by the -5 Nm level. These changes in muscle activation limit the range of plantarflexor activity and intrinsic stiffness. In contrast, maximum values for background EMG as well as intrinsic stiffness reached similar magnitudes at both torque levels.

The intrinsic pathway had a moderate to strong correlation with a range of r = [0.52,0.91]. If the two torque levels are considered separately, the degree of correlation was different between both levels for the three plantarflexors, based on the 95% CIs. The 0 Nm level showed a strong correlation (r = [0.87,0.91]) compared with a moderate correlation at -5 Nm (r = [0.52,0.68]). For the dorsiflexor, both torque levels showed a strong correlation (r = 0.91 and 0.84).

The reflexive pathway (bottom row of Fig. 4.7) also showed fairly similar linear trends in the plantarflexors for the two torque levels, while the TA muscle trends differed. Again, low values of EMG activity were sporadically reached at the -5 Nm torque level, while maximum EMG values were more similar, especially for GM and GL. Contrary to the intrinsic pathway, the range of reflexive gain values did not seem restricted due to the -5 Nm torque level. Moreover, a relative shift appeared in the relation between EMG and reflexive gain in the lower range values (i.e. left hand side). The same level of reflex EMG corresponded to a lower level of reflexive gain in the -5 Nm task compared with the 0 Nm task.

The reflexive pathway had a weak to moderate correlation in the plantarflexors (r = [0.31,0.69]). The 0 Nm level showed a moderate correlation (r = [0.64,0.69]) compared with a weak to moderate correlation at -5 Nm (r = [0.32,0.55]). Contrary to the intrinsic pathway, the 95% CIs did overlap, except for the GM. The dorsiflexor had a weak correlation r = 0.38 at 0 Nm and no correlation r = -0.02 at the -5 Nm level.

4.4 Discussion

The main goal of this chapter was to support the clinical application of the PC system identification technique through a neurophysiological validation on a group-level. For the intrinsic pathway, a strong positive correlation between estimated intrinsic stiffness and background EMG was observed for plantarflexors and dorsiflexors at a 0 Nm voluntary torque level. For the reflexive pathway, a moderate positive correlation between estimated reflexive gain and reflex EMG was only observed for the plantarflexors at the 0 Nm torque level. For both intrinsic and reflexive pathways, a lower degree of correlation was found for the -5 Nm plantarflexion torque condition compared with a 0 Nm torque level.

4.4.1 Linear Association Parallel-Cascade System Identification and EMG

The linear association between PC system identification technique and EMG outcome measures was previously only investigated for the reflexive pathway [9, 15, 16]. The multitude of outcome parameters used and the use of both between within- and between-subject measurements make it difficult to compare the previous results. Two studies

investigated between-subject measurements. The first study investigated the intrinsic and reflexive ankle impedance components in stroke survivors using an offline PC algorithm [15]. The relative between-subject contribution of both intrinsic and reflexive impedance on the total response torque measured was investigated using the VAF. They found an unquantified positive association between the VAF by the reflexive contribution and reflexive EMG gain of GM or GL. The second study used an offline PC algorithm to investigate the intrinsic and reflexive contributions to wrist impedance in people with Parkinson's disease [16]. The effect of medication on the neural, phasic component was studied by comparing the correlation between reflexive torque and reflexive EMG. For both on- and off-medication conditions moderate correlations of $r = 0.45$ and 0.46 were found. Finally, one study investigated the within-subject voluntary modulation of reflexive impedance and stretch reflexes using the online PC algorithm [9]. For a single representative participant a correlation of $r \approx 0.98$ between reflexive gain and GL reflexive EMG was found to confirm that both measures modulated simultaneously.

The linear association between joint impedance and EMG is best investigated using within-subject measurements. Multiple subject-dependent characteristics influence both EMG amplitude, e.g. varying amounts of fat tissue, and joint impedance amplitudes, e.g. passive muscle slack length. These underlying subject-dependent characteristics would directly influence the linear association when between-subject measures are used. We applied a Z-score standardization to the data of each participant separately to compute a combined within-subject correlation coefficient. If all participants contribute the same number of samples, the combined correlation coefficient would equal the mean correlation of all ten participants. Therefore, our within-subject results can be compared directly with the within-subject results of Ludvig *et al.* [9].

Our results showed a lower correlation between reflexive gain and reflexive EMG of the GL than Ludvig *et al.* [9] at a 0 Nm torque target ($r = 0.68$ vs. 0.98). These results can potentially be explained by the differences in protocol and data analysis. First, the results of Ludvig *et al.* [9] were based on a single participant instead of ten. When calculating correlation coefficient for each individual a range of correlation values of $r = [0.04,0.94]$ was found compared with $r = 0.68$ at group-level. However, as the individual results were based on only 10 paired data points per participant, a dedicated study design is recommended for validation on an individual level. Second, Ludvig *et al.* [9] did not allow co-contraction to reduce variation in intrinsic stiffness. This reduced variation could improve reflexive gain estimates, as simulation results showed that the online reflexive gain estimate is influenced by changes in intrinsic stiffness [8]. Third, the result of Ludvig *et al.* [9] was obtained in a second session, thus the participant was more familiar with the experiment and task. This familiarity could improve control over both reflexive impedance and torque and as a result improve the quality of the parameter estimations.

The higher degree of correlation for the intrinsic compared with the reflexive pathway potentially reveals a better neurophysiological basis for the intrinsic pathway. However, the correlation sensitivity to both within-subject modulation range and amount of variation around the true value has to be taken as reservation. First, participants perceived modulating intrinsic impedance easier than reflexive impedance, as participants were used to conscious intrinsic stiffness modulation through co-contraction in daily living. This familiarity could have increased relative modulation range, thus

resulting in larger correlations. Second, the reflexive gain parameter showed higher levels of variation during hold periods, see Fig. 4.5, which could result in a lower correlation. Note, the results of the dorsiflexor TA muscle was not taken into account when comparing correlations between the intrinsic and reflexive pathway. The dorsiflexor was excluded, because the input of the reflexive pathway in the PC model only uses the dorsiflexion perturbations, which stretch the plantarflexors, and not the plantarflexion perturbations, which stretch the dorsiflexors.

Despite the strong and moderate correlations found for the intrinsic and reflexive contributions to joint impedance, the neurophysiological basis of both pathways can be extended upon. Recent studies have shown that additional model parameters and elements are required to build complete models. The maximum VAF of 88.6% found in our results does indicate that there are unmodeled system dynamics in the experimental data. For the intrinsic pathway, a third-order model can better capture the agonist-antagonist musculoskeletal structure of the human ankle than the second-order IBK model used [19]. Fortunately, the estimated intrinsic stiffness component only shows a small bias for the 90-95° ankle angles used. For angles smaller than 90° the IBK model overestimates the stiffness, whereas for angles larger than 95° the IBK model underestimates the stiffness [19]. For the reflexive pathway, several studies on muscle spindles and spasticity have shown that the reflexive response is not only velocity dependent. Complete models would also potentially require elements based on acceleration, force and force derivative [20–22]. Note, all pulse and step perturbations applied during our experiment stretched the plantarflexors with exactly the same velocity, acceleration and force profile. Therefore, all observed modulations of joint impedance are attributed to task-driven changes made by the participants, which justifies the use of the PC model.

The 0 Nm torque target is recommended for future neurophysiological validation of joint impedance estimation algorithm, as it showed better characteristics for correlation analysis. Again, the sensitivity of the correlation analysis could explain the decrease in correlation at the -5 Nm target. First, Fig. 4.7 shows a smaller modulation range at -5 Nm on a group-level, decreasing correlation. Second, correlation could have decreased due to increased variability as participants perceived it more difficult to keep torque constant at the -5 Nm level (σ = 1.32 Nm vs. 0.78 Nm at 0 Nm). The algorithm assumes this voluntary torque to be constant, thus torque variability can increase joint impedance estimation errors [8]. Third, small EMG magnitudes were occasionally measured from a specific muscle within a participant. As a result, the amount of modulation observed also remained small. The small EMG magnitudes occurred most frequently within the GM or GL muscle in combination with the -5 Nm torque condition. These occurrences for the GM and GL are reflected in the lower group-level correlations compared to the SOL.

4.4.2 Clinical Application Parallel-Cascade System Identification

The successful neurophysiological validation on a group-level should support the clinical application of the PC model. This neurophysiological validation for the group of system identification methods is supported by the large degree of association between online and offline PC algorithms [8, 9]. A specific example of valid clinical applications would be within rehabilitation, utilizing the PC algorithms to unravel intrinsic

and reflexive contributions. For example, this information could help in clinical decision making process to evaluate the current neurological impact of brain or neural injuries [6] or the effects of other treatments [7]. A strict limitation of the PC model is that isometric experimental conditions are required. Thus, self-generated movements cannot be analyzed using the PC model and other system identification techniques are required, e.g. [23]. Compared to our experimental conditions, recent advances did show that isometric conditions with faster variations in voluntary torques can be studied using the PC model [24]. As a result, application of the PC model to evaluate functional tasks within a clinical setting, such as walking or balance, is difficult, because self-generated movement is a critical element of these tasks. Nevertheless, there is a relevant clinical need to unravel the contributions to joint hyper-resistance, even within an isometric context [2]. Still, the results do not show a perfect correlation between the joint impedance estimates and EMG measurements, which does raise a question which methodology is more suitable for use in clinical practise.

The lack of gold standard for reliably unravelling intrinsic and reflexive joint resistance contributions [2], makes it difficult to select the best method, EMG-based or PC-based, to quantify hyper-resistance in a clinical setting. Both methods could have their potential strengths and weaknesses depending on the hypothesized origin of a patients functional impairment and user aim. First, the joint impedance estimates and EMG measurements act at a joint and muscle level respectively. Second, the PC-based methods outcome measures are in mechanical units (K in Nm/rad and G in Nm·s/rad), whereas EMG-based methods have electrical units of V. As a result, the PC-based measures can be more directly related to the concept of resistance as felt by clinicians. Moreover, these outcome measures remove the need for normalization as required for the EMG-based methods to compare between-subject or across-session within-subject results. Third, the online PC algorithm showed slow variations, whereas online EMG measurements show fast variations, see Fig. 4.5. The online PC algorithm was purposely designed for these slow variations, as implementation of a 0.033 Hz low-pass filter improved participant control over the biofeedback [8]. Consequently, the online PC algorithm requires a transient period of about 15 s before estimates become reliable [8, 9]. On the other hand, due to the fast variations EMG-based methods are generally based on ensemble averages and hence require multiple perturbations to obtain a reliable measure as well. Fourth, PC-based methods require an experimental setup similar to Fig. 4.1 with a powerful manipulator to apply the stretch perturbations. However, the need for EMG and sometimes even electrical stimulation [10, 11] equipment would be avoided. Contrarily, EMG-based methods can be used for motorized assessment, requiring less powerful manipulators, and can even be executed without manipulator via manual assessment [25].

4.4.3 Study Limitations

The study protocol design limits our results and conclusions to a group-level, as discussed above, and data periods of 60 s, assumed to have constant joint impedance. Moreover, the correlation coefficient used is sensitive to the ratio of within-subject modulation range and amount of variation around the true value. This effect influenced both the difference between the 0 and -5 Nm torque levels and the intrinsic and reflexive

pathways. Furthermore, a limited amount of EMG activity in the GM and GL muscles in some participants also influenced the study outcome in a similar manner. To mitigate issues due to correlation sensitivity, biofeedback was provided on both torque and joint impedance with instruction to minimize variations within hold periods. Additionally, the joint impedance biofeedback helped to increase modulation range. Unfortunately, the large modulation range did in turn increase variability again for high intrinsic and reflexive impedance values, see Figs. 4.5 and 4.6. Moreover, the inclusion of several 60 s hold periods at high muscle activation levels also induce fatigue and hence again additional variability in the measurements. In short, participant instruction and protocol design were aimed to balance these multiple sources of variation to reduce their effect on the correlation coefficients.

4.5 Conclusions

We have shown the neurophysiological validity of the PC system identification technique on a group-level through the evaluation of an online PC algorithm. As hypothesized, for the intrinsic pathway, a strong positive correlation between estimated intrinsic stiffness and background EMG was found for both plantarflexors and dorsiflexors. For the reflexive pathway, a moderate positive correlation between estimated reflexive gain and reflex EMG was found for the plantarflexors only. For both intrinsic and reflexive pathways, a higher degree of correlation was found for the 0 Nm voluntary torque condition compared with a constant -5 Nm plantarflexion torque.

The successful neurophysiological validation shows the validity of the PC model and system identification techniques to study the human physiological system. The simultaneous validation of both intrinsic and reflexive pathways performed is important given the mix of physiological origins of joint hyper-resistance. As a result, it is valid to use the PC system identification technique for the integrated assessment and training of participants with joint hyper-resistance in clinical practise.

References

[1] V. Dietz and T. Sinkjær, "Spastic Movement Disorder: Impaired Reflex Function and Altered Muscle Mechanics," *Lancet Neurology*, 6(8), pp. 725–733, 2007. doi: 10.1016/S1474-4422(07)70193-X.

[2] J. C. van den Noort, L. Bar-On, E. Aertbeliën, M. Bonikowski, *et al.*, "European Consensus on the Concepts and Measurement of the Pathophysiological Neuromuscular Responses to Passive Muscle Stretch," *European Journal of Neurology*, 24(7), pp. 981–991, 2017. doi: 10.1111/ene.13322.

[3] E. C. Davis and M. P. Barnes, "Botulinum Toxin and Spasticity," *Journal of Neurology Neurosurgery and Psychiatry*, 69(2), pp. 143–147, 2000. doi: 10.1136/jnnp.69.2.143.

[4] L. Shaw, H. Rodgers, C. Price, F. van Wijck, *et al.*, "BoTULS. A Multicentre Randomised Controlled Trial to Evaluate the Clinical Effectiveness and Cost-effectiveness of Treating Upper Limb Spasticity due to Stroke with Botulinum Toxin Type A," *Health Technology Assessment*, 14(26), 2010. doi: 10.3310/hta14260.

[5] R. E. Kearney, R. B. Stein, and L. Parameswaran, "Identification of Intrinsic and Reflex Contributions to Human Ankle Stiffness Dynamics," *IEEE Transactions on Biomedical Engineering*, 44(6), pp. 493–504, 1997. doi: 10.1109/10.581944.

[6] M. M. Mirbagheri, H. Barbeau, M. Ladouceur, and R. E. Kearney, "Intrinsic and Reflex Stiffness in Normal and Spastic, Spinal Cord Injured Subjects," *Experimental Brain Research*, 141(4), pp. 446–459, 2001. doi: 10.1007/s00221-001-0901-z.

[7] M. M. Mirbagheri, M. Ladouceur, H. Barbeau, and R. E. Kearney, "The Effects of Long Term FES-Assisted Walking on Intrinsic and Reflex Dynamic Stiffness in Spinal Cord Injured Patients," *IEEE Transactions on Neural Systems and Rehabilitation Engineering*, 10(4), pp. 280–289, 2002. doi: 10.1109/TNSRE.2002.806838.

[8] D. Ludvig and R. E. Kearney, "Real-time Estimation of Intrinsic and Reflex Stiffness," *IEEE Transactions on Biomedical Engineering*, 54(10), pp. 1875–1884, 2007. doi: 10.1109/TBME.2007.894737.

[9] D. Ludvig, I. Cathers, and R. E. Kearney, "Voluntary Modulation of Human Stretch Reflexes," *Experimental Brain Research*, 183(2), pp. 201–213, 2007. doi: 10.1007/s00221-007-1030-0.

[10] A. K. Thompson, F. R. Pomerantz, and J. R. Wolpaw, "Operant Conditioning of a Spinal Reflex Can Improve Locomotion after Spinal Cord Injury in Humans," *Journal of Neuroscience*, 33(6), pp. 2365–2375, 2013. doi: 10.1523/JNEUROSCI.3968-12.2013.

[11] N. Mrachacz-Kersting, U. G. Kersting, P. de Brito Silva, Y. Makihara, *et al.*, "Acquisition of a Simple Motor Skill: Task-dependent Adaptation and Long-term Changes in the Human Soleus Stretch Reflex," *Journal of Neurophysiology*, 122(1), pp. 435–446, 2019. doi: 10.1152/jn.00211.2019.

[12] R. C. van 't Veld, A. C. Schouten, H. van der Kooij, and E. H. F. van Asseldonk, "Validation of Online Intrinsic and Reflexive Joint Impedance Estimates using Correlation with EMG Measurements," in *7th International Conference on Biomedical Robotics and Biomechatronics*, Enschede, Netherlands: IEEE, 2018, pp. 13–18. doi: 10.1109/BIOROB.2018.8488123.

[13] N. Hogan, "Adaptive Control of Mechanical Impedance by Coactivation of Antagonist Muscles," *IEEE Transactions on Automatic Control*, 29(8), pp. 681–690, 1984. doi: 10.1109/TAC.1984.1103644.

[14] M. M. Mirbagheri, H. Barbeau, and R. E. Kearney, "Intrinsic and Reflex Contributions to Human Ankle Stiffness: Variation with Activation Level and Position," *Experimental Brain Research*, 135(4), pp. 423–436, 2000. doi: 10.1007/s002210000534.

[15] L. Galiana, J. Fung, and R. E. Kearney, "Identification of Intrinsic and Reflex Ankle Stiffness Components in Stroke Patients," *Experimental Brain Research*, 165(4), pp. 422–434, 2005. doi: 10.1007/s00221-005-2320-z.

[16] R. Xia, A. Muthumani, Z.-H. Mao, and D. W. Powell, "Quantification of Neural Reflex and Muscular Intrinsic Contributions to Parkinsonian Rigidity," *Experimental Brain Research*, 234(12), pp. 3587–3595, 2016. doi: 10.1007/s00221-016-4755-9.

[17] H. J. Hermens, B. Freriks, C. Disselhorst-Klug, and G. Rau, "Development of Recommendations for SEMG Sensors and Sensor Placement Procedures," *Journal of Electromyography and Kinesiology*, 10(5), pp. 361–374, 2000. doi: 10.1016/S1050-6411(00)00027-4.

[18] J. Carpenter and J. Bithell, "Bootstrap Confidence Intervals: When, Which, What? A Practical Guide for Medical Statisticians," *Statistics in Medicine*, 19(9), pp. 1141–1164, 2000. doi: 10.1002/(SICI)1097-0258(20000515)19:9<1141::AID-SIM479>3.0.CO;2-F.

[19] E. Sobhani Tehrani, K. Jalaleddini, and R. E. Kearney, "Ankle Joint Intrinsic Dynamics is More Complex than a Mass-Spring-Damper Model," *IEEE Transactions on Neural Systems and Rehabilitation Engineering*, 25(9), pp. 1568–1580, 2017. doi: 10.1109/TNSRE.2017.2679722.

[20] K. P. Blum, B. L. D'Incamps, D. Zytnicki, and L. H. Ting, "Force Encoding in Muscle Spindles during Stretch of Passive Muscle," *PLoS Computational Biology*, 13(9):e1005767, 2017. doi: 10.1371/journal.pcbi.1005767.

[21] A. Falisse, L. Bar-On, K. Desloovere, I. Jonkers, *et al.*, "A Spasticity Model based on Feedback from Muscle Force Explains Muscle Activity during Passive Stretches and Gait in Children with Cerebral Palsy," *PLoS ONE*, 13(12):e0208811, 2018. doi: 10.1371/journal.pone.0208811.

[22] D. C. Lin, C. P. McGowan, K. P. Blum, and L. H. Ting, "Yank: The Time Derivative of Force is an Important Biomechanical Variable in Sensorimotor Systems," *Journal of Experimental Biology*, 222(18):e180414, 2019. doi: 10.1242/jeb.180414.

[23] D. Ludvig, M. Plocharski, P. Plocharski, and E. J. Perreault, "Mechanisms Contributing to Reduced Knee Stiffness during Movement," *Experimental Brain Research*, 235(10), pp. 2959–2970, 2017. doi: 10.1007/s00221-017-5032-2.

[24] M. A. Golkar, E. Sobhani Tehrani, and R. E. Kearney, "Linear Parameter Varying Identification of Dynamic Joint Stiffness during Time-Varying Voluntary Contractions," *Frontiers in Computational Neuroscience*, 11:15, 2017. doi: 10.3389/fncom.2017.00035.

[25] L. H. Sloot, L. Bar-On, M. M. van der Krogt, E. Aertbeliën, *et al.*, "Motorized versus Manual Instrumented Spasticity Assessment in Children with Cerebral Palsy," *Developmental Medicine and Child Neurology*, 59(2), pp. 145–151, 2017. doi: 10.1111/dmcn.13194.

Chapter 5

Reducing the Soleus Stretch Reflex with Conditioning: Exploring Game- and Impedance-based Biofeedback

R. C. van 't Veld, E. Flux, A. C. Schouten, M. M. van der Krogt, H. van der Kooij, E. H. F. van Asseldonk

Abstract — People with spasticity, i.e. stretch hyperreflexia, have a limited functional independence and mobility. While a broad range of spasticity treatments is available, many treatments are invasive, non-specific or temporary and might have negative side effects. Operant conditioning of the stretch reflex is a promising non-invasive paradigm with potential long-term sustained effects. Within this conditioning paradigm, seated participants have to reduce the mechanically elicited reflex response using electromyography (EMG) biofeedback of reflex magnitude. Before clinical application of the conditioning paradigm, improvements are needed regarding the time-intensiveness and slow learning curve. Previous research has shown that gamification of biofeedback can improve participant motivation and long-term engagement. Moreover, reflexive biofeedback quantified using reflexive joint impedance may obtain similar effectiveness within fewer sessions. Nine healthy volunteers participated in the study, split in three groups. First, as a reference the *'Conventional'* group received EMG-, bar-based biofeedback similar to previous research. Second, we explored feasibility of game-based biofeedback with the *'Gaming'* group receiving EMG-, game-based biofeedback. Third, we explored the feasibility of game- and impedance-based biofeedback with the *'Impedance'* group receiving impedance-, game-based biofeedback. Participants completed 5 baseline sessions (without reflex biofeedback) and 6 conditioning sessions (with reflex biofeedback). Participants were instructed to reduce reflex magnitude without modulating background activity. The Conventional and Gaming groups showed feasibility of the protocol in 2 and 3 out of 3 participants, respectively. These participants achieved a significant Soleus short-latency (M1) within-session reduction of at least -15% in the 4th to 6th conditioning session. Impedance group participants did not show any within-session decrease in Soleus reflex magnitude. The feasibility of the EMG-, game-based biofeedback calls for further research on gamification of the conditioning paradigm to obtain improved participant motivation and engagement, while achieving long-term conditioning effects. Before clinical application, the time-intensiveness and slow learning curve of the conditioning paradigm remain an open challenge.

This chapter was published in the *Frontiers in Rehabilitation Sciences*, 2:742030, 2021. The code and data underlying this publication are available via 4TU.ResearchData. doi: 10.4121/c.5605085

5.1 Introduction

Spasticity is a common symptom after brain and neural injuries, like spinal cord injury, stroke and cerebral palsy [1]. Spasticity is defined as the exaggerated stretch reflex response, i.e. stretch hyperreflexia [2]. Patients with spasticity are limited in functional independence and mobility, and often experience substantial pain. A broad range of spasticity treatments is available, including physical therapy, oral medication, interventional procedures and surgical treatments [3]. Unfortunately, current treatments are invasive, non-specific or temporary and might have negative side effects [3]. Therefore, there is a clinical need for a non-invasive spasticity treatment with long-term sustained effect.

Operant conditioning of the reflex response is a promising, non-invasive paradigm to obtain a long-term spasticity reduction [4, 5]. Within the conditioning paradigm, participants are trained to either increase ('up-condition') or reduce ('down-condition') the reflex response using biofeedback of reflex magnitude. Currently, paradigm feasibility has been shown for both electrical stimulation, i.e. H-reflex conditioning, and mechanical stimulation, i.e. stretch reflex conditioning, using electromyography (EMG) biofeedback of the calf muscles [6, 7]. Both forms of stimulation have shown equal effectiveness during conditioning with static posture in able-bodied participants: an average -15% short-term (within-session) and -20% long-term (across-session) down-conditioning effect was obtained after 4-6 and 12-16 conditioning sessions, respectively [6, 7]. From a practical, clinical perspective, the mechanical stimulation is advantageous as it yields higher participant comfort and applicability to other joints. Besides, protocols with EMG biofeedback require accurate electrode placement, checked using electrical stimulation, to ensure that conditioning effects are not due to across-session changes in electrode placement. Removing the need for accurate electrode placement checked via electrical stimulation would be beneficial considering home applications. Overall, before clinical application of the conditioning paradigm, improvements are needed regarding the time-intensiveness (3 session per week) and slow learning curve (at least 16 sessions).

As potential improvements for stretch reflex conditioning, we propose the use of gamification and reflexive joint impedance biofeedback. First, gamification entails the introduction of a gaming element into non-gaming situations, like rehabilitation, to make activities more pleasurable and increase long-term engagement [8, 9]. Gamification can improve participant motivation in view of the possibly demotivating conditioning paradigm [10], given the long baseline measurements and slow learning curves [6, 7]. Numerous studies have shown these improvements in motivation and engagement in patients with neurological conditions, such as cerebral palsy, stroke and Parkinson's disease [11, 12]. Alongside improved motivation, most game-based interventions ensure equal or even increased treatment effectiveness [10–12]. However, negative effects of gamification were also reported, e.g. high levels of motivation due to gamification can distract from the primary motor learning goal and encourage undesirable compensation strategies [13]. Therefore, it is important to assess whether gamification interferes with potential treatment outcomes.

Second, reflexive joint impedance biofeedback entails quantification of reflex magnitude using a mechanical-based methodology instead of the muscle-based EMG biofeed-

back to accelerate learning curves [14, 15]. The impedance-based biofeedback disentangles the reflexive joint resistance due to the mechanical stimuli from other non-reflexive joint resistance contributions using joint torques and kinematics [16]. As such, an impedance-based conditioning treatment would not require any electrodes or electrical stimulation. Previous research suggests a faster learning curve for impedance-based biofeedback, as participants were able to already modulate their reflex response after 2 sessions [15]. Ludvig *et al.* [15] used a specific online algorithm to provide biofeedback on reflex magnitude [14]. Thus, use of impedance- instead of EMG-based biofeedback can potentially improve the learning curve and practical execution.

The goal of this chapter is to explore the feasibility of two forms of biofeedback within the stretch reflex down-conditioning paradigm: 1) gamification of the biofeedback; and 2) impedance-based biofeedback. To explore feasibility, the within-session conditioning effect is investigated across 6 conditioning sessions. The investigation is split across three participant groups, executed in three separate phases: 1) *'Conventional'* receiving EMG-, bar-based biofeedback as in Mrachacz-Kersting *et al.* [7]; 2) *'Gaming'* receiving EMG-, game-based biofeedback; and 3) *'Impedance'* receiving impedance-, game-based biofeedback. The use of a specific biofeedback method is considered feasible when the reference -15% within-session effect reported in previous studies can be achieved across the 4th to 6th conditioning session [6, 7]. Each experimental phase was only started once the previous experimental phase was evaluated as being feasible. Our study aims to open the way for stretch reflex conditioning as non-invasive spasticity treatment by introducing new biofeedback methods to make improvements regarding the time-intensiveness and slow learning curve.

5.2 Materials and Methods

5.2.1 Participants and Study Schedule

Nine volunteers with no history of neuromuscular disorders participated in the study: age 26.0±5.0 yr, 7 women. The EEMCS/ET ethics committee of the University of Twente approved the study (RP2019-87) and all participants provided written informed consent. The participants were split in the three biofeedback groups in order of inclusion, see Fig. 5.1A: 1) EMG-, bar-based biofeedback (*'Conventional'*); 2) EMG-, game-based biofeedback (*'Gaming'*); and 3) Impedance-, game-based biofeedback (*'Impedance'*).

All groups completed the same study schedule, designed in similar fashion to studies by Thompson *et al.* [6] and Mrachacz-Kersting *et al.* [7], see Fig. 5.1A. The study consisted of: one preparation (PRE), one acclimatization (A1), five baseline (B1-5) and six conditioning (C1-6) sessions. The preparation session was aimed at defining all personalized hard- and software settings using a protocol distinct from all other sessions. The acclimation followed the baseline session protocol and aimed to familiarize participants with this protocol [4, 6]. The baseline sessions (without reflex biofeedback) and conditioning sessions (with reflex biofeedback) formed the core data collection sessions of the paradigm, see Fig. 5.1A. Three sessions were scheduled per week (Monday, Wednesday, Friday) with baseline and conditioning sessions typically lasting 1h with a 1.5h maximum. Any diurnal variation in reflexive response was minimized by scheduling all sessions at the same time of day, i.e. within the same 3h period.

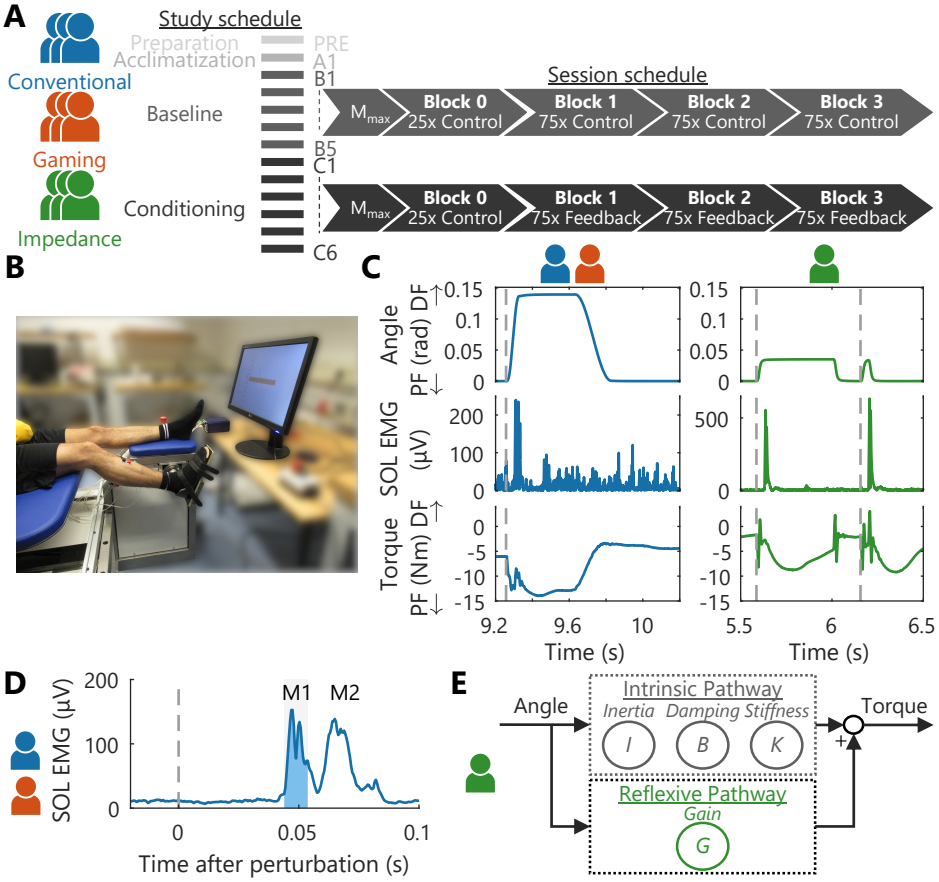

Figure 5.1: Overview experimental methodology. *(A)* Nine participants were split in three groups, all following the same 13 session study schedule (3 times per week). Per session, M_{max} was obtained using electrical stimulation, followed by 4 blocks with stretch reflexes containing either 25 or 75 feedback instances [7]. *(B)* Stretch reflexes were elicited around the right ankle joint using a robotic manipulator. Participants were seated on an adjustable chair to support a static posture. *(C)* Dorsiflexion perturbations around the ankle joint elicited a stretch reflex response as visualized in the SOL muscle and torque. For the EMG-based groups a discrete ramp-and-hold stretch profile was used [7], whereas a continuous pulse-step perturbation profile was applied for the Impedance group [14]. *(D)* EMG-based groups received biofeedback on the SOL EMG, specifically background EMG activity and the short-latency (M1) reflex response *(shaded area)* [7]. *(E)* The Impedance group received biofeedback on background torque and the estimated reflexive joint impedance gain (G). A mechanical-based methodology using recorded torques and kinematics was used to disentangle this reflexive contribution from the intrinsic contribution with parameters: inertia I, damping B and stiffness K [14].

5.2.2 Experimental Setup

Ankle Manipulator and Stretch Reflex Perturbations

Stretch reflexes were elicited around the ankle joint using a one degree-of-freedom (DOF) manipulator (Moog, Nieuw-Vennep, the Netherlands) in the sagittal plane, see Fig. 5.1B. The manipulator applied dorsiflexion, ramp-and-hold perturbations to the right foot via a rigid footplate interface and Velcro straps. The encoder of the manipulator's actuator measured foot plate angular position and velocity representing ankle angle and angular velocity. A torque sensor, located between the actuator and footplate, measured the ankle torque. Angle, velocity and torque were recorded at 2048 Hz, all defined positive in dorsiflexion direction. To compensate for gravitational effects on the ankle and footplate, the net torque with no voluntary participant activity was measured at the start of each block and subtracted from the torque measurements. Matlab 2017b (Mathworks, Natick, MA, USA) was used for the data collection and biofeedback during the experiment.

Participants were seated on an adjustable chair to support and control the posture during all stretch reflexes, see Fig. 5.1B. The chair supported the upper body and upper leg to control the hip and knee angles at 120° and 150°, respectively. Both knee and hip were defined at 180° for a perfectly straight posture and angles were measured using a goniometer. All stretch perturbations started at a 90° ankle angle, defined as the angle between shank and foot. The ankle axis of rotation was visually aligned with the actuator axis, minimizing hip and knee translations due to the applied perturbations. Participants were instructed to attain background activation by pressing into the position-controlled footplate as if rotating the ankle without use of the upper leg. Session-to-session variability of the seated posture was minimized by reusing the same personalized chair settings for each participant.

For the EMG-based groups, discrete dorsiflexion perturbations were used to elicit a stretch reflex [7]. These ramp-and-hold perturbations had an 8° amplitude, 190 °/s max. velocity, 8000 °/s^2 max. acceleration and 66 ms duration, see Fig. 5.1C. Max. amplitude was held for 300 ms before the manipulator slowly returned to the 90° starting angle.

For the Impedance group, continuous dorsiflexion perturbations were used to elicit a stretch reflex, see Chapters 3 and 4. These ramp-and-hold perturbations had an 2° amplitude, 125 °/s max. velocity, 15800 °/s^2 max. acceleration and 40 ms duration, see Fig. 5.1C. The perturbations randomly switched between 'pulses', i.e. no hold period at max. amplitude, and 'steps', i.e. a 380 ms hold period at max. amplitude. Return towards the starting angle was with an equal and opposite profile to the dorsiflexion perturbation. The perturbation profile changes compared with the EMG-based groups were made to comply with impedance estimation procedure requirements [14].

Reflexive joint impedance was estimated using a parallel-cascade identification algorithm outlined in Chapter 3, see Fig. 5.1E. In short, using the recorded torques and kinematics the algorithm first estimates the intrinsic impedance parameters: inertia I, damping B and stiffness K. These parameters capture the joint resistance in response to the mechanical perturbations from the tissue-related, non-neural origin and tonic neural origin. The predicted intrinsic torque resulting from these parameters is subtracted from the total torque measured to estimate the reflexive torque. The gain G of the reflexive pathway is then estimated by relating this reflexive torque to

the 40 ms-delayed, half-wave rectified velocity. The gain G reflects the joint resistance magnitude in response to the mechanical perturbations from a phasic neural origin. The parameters estimated within the initial 30 s of each block were discarded as the algorithm parameter estimation is unreliable within this transient period [14].

Electromyography Measurements and Processing

Muscle activity was measured using the Porti EMG device (TMSi, Oldenzaal, the Netherlands). Bipolar electrodes (Kendall H124SG, 24 mm diameter; Covidien, Dublin, Ireland) were placed on the Soleus (SOL) and Tibialis Anterior (TA) according to the SENIAM guidelines [17]. Session-to-session variability in electrode placement was minimized by marking each electrode on the skin (4 dots on each side, re-marked every session). Moreover, a drawing of the electrode placement with respect to anatomical and skin landmarks (e.g. bones, moles, scars, vessels) was used in case the electrode markings had faded [6, 7].

EMG was recorded at 2048 Hz, high-pass filtered (2nd-order, 5 Hz, Butterworth) and rectified. SOL and TA background activity was defined as the smoothed (moving average, 100 ms window) rectified EMG [6, 7]. During trials with continuous perturbations, background torque was used instead of SOL EMG, this background activity was computed using low-pass filters (2nd-order, 0.1 Hz, Butterworth {TA}; critically-damped {torque}) to reduce the influence of these perturbations, see Chapter 3.

EMG reflex magnitude was obtain using the SOL short-latency (M1) reflex response. To obtain M1 magnitude, background activity at perturbation onset was subtracted from the reflex response and the result was half-wave rectified. M1 magnitude was then defined as the root mean square (RMS) of the activity within a 10 ms window, see Fig. 5.1D [7]. This participant-specific window was manually set centered around the first peak response, typically 44-54 ms after perturbation onset, after the last baseline sessions (B5).

Electrical Stimulation of M_{max}

To confirm correct placement of EMG electrodes across-sessions, the direct motor response (M-wave) of the Soleus (SOL) muscle was elicited using a constant current electrical stimulator (DS7A; Digitimer, Hertfordshire, UK). The cathode (Disk electrode, 20 mm diameter; Technomed, Beek, the Netherlands) was placed in the popliteal fossa, whereas the anode (Square electrode, 41 mm height/width; Medimax Maxpatch, UK) was placed proximal to the patella. Participants were standing with a natural, upright posture for the M-wave measurements.

The simulator delivered a 1 ms width square stimulus pulse to the tibial nerve of the right leg. The M-wave magnitude was defined after each electrical stimulus as the peak-to-peak value of the unrectified SOL EMG within a 22 ms processing window [6, 7]. This participant-specific window was manually placed during the preparation session, typically 4-26 ms after stimulation. To check electrode placement, the maximum M-wave M_{max} is of interest, as a steady M_{max} indicates correct electrode placement [6, 7]. To obtain M_{max}, stimulation intensity was gradually increased with 5 mA increments to find the intensity at which the M-wave magnitude plateaued. For data collection, 3 stimulation intensities above the plateau value were selected to obtain M_{max} and con-

firm that the intensities were within the range at which M-wave magnitude plateaued. These participant-specific intensities were set during the preparation session, e.g. at 20, 25, 30 mA or 60, 65, 70 mA.

Intrinsic Motivation Inventory (IMI)

To assess motivation and engagement, all participants completed the intrinsic motivation inventory (IMI) questionnaire after the last conditioning session (C6) [18]. The questionnaire was used to assess the participant experience with the stretch reflex perturbations only, i.e. participants were instructed to ignore the electrical stimulation element for this questionnaire.

5.2.3 Experimental Protocol

Preparation Session

All participants attended a preparation session to define all personalized hard- and software settings, retained through all other sessions [6, 7]. A couple of trial electrical stimuli were applied to check whether participants felt comfortable with electrical stimulation. Two participants opted out of the study due to discomfort (lightheaded, nauseous) after these trial stimuli. New volunteers were included in the study to retain the total number of participants at nine.

To normalize EMG background activity, SOL maximum voluntary contraction (MVC) was determined [6, 7]. Participants were seated (hip, knee, ankle angle all 90°) on a stool with their upper leg locked beneath a rigid structure. Participants were instructed to produce maximum SOL activity by pressing against the rigid structure, while retaining their toes on the ground, to generate a plantarflexion torque. The SOL MVC was defined as the maximum value of the smoothed (moving average, 100 ms window) rectified SOL EMG. Each participant performed three MVC trials and the participant-specific MVC value was set as the maximum MVC across all three trials.

To match the SOL and torque background activity target levels used throughout data collection, a tonic EMG-torque mapping was obtained. Participants executed a torque tracking task using the ankle manipulator by holding isometric torque for 3 s at 0 to 10 Nm in increments of 2 Nm. To obtain the EMG-torque mapping, mean SOL activity at each torque level was computed. The SOL background target was defined as a 5% MVC range matching the 4 Nm level of the EMG-torque mapping, typical ranges were 2.5-7.5% MVC and 5-10% MVC [6, 7]. The torque background target was defined as a 1 Nm range set at 3.5-4.5 Nm. The TA background activity target was set at resting level, i.e. 0-7.5 μV [6, 7]. Participants completed several trials with the stretch reflex perturbations and electrical stimulation, while instructed to maintain background activity within the set targets. These trials were used to check whether participants could comfortably execute these task, given all personalized settings.

Acclimatization, Baseline and Conditioning Sessions

The acclimatization, baseline and conditioning sessions all followed the same schedule for each participant, see Fig. 5.1A [6, 7]. For all groups, 12 electrical stimuli, i.e. 4 repetitions at 3 intensities, were applied with increasing stimulation intensity to determine

M_{max}. Participants were instructed to maintain steady SOL and TA background activity using bar-based biofeedback, see Fig. 5.2 [6, 7]. Stimuli were applied at 5-7 s intervals and only if participants complied with the background targets for the last 2 s.

In Block 0, the Control magnitude was measured, i.e. reflex magnitude before within-session conditioning [6, 7]. Participants only received background biofeedback: SOL/TA biofeedback for EMG-based groups [6, 7] and torque/TA biofeedback for the Impedance group [15]. For EMG-based groups, 25 discrete stretch perturbations were elicited at a 5-7 s interval and only if participants complied with the background activity targets for the last 2 s. For the Impedance group, these 25 discrete instances coupled to steady background activity were retained to create similar block duration across groups. Consequently, these instances were decoupled from the continuously applied pulse-step perturbation, resulting in roughly 250 stretch perturbations at a 0.5-0.7 s interval.

In Block 1-3 the Conditioned magnitude was measured, i.e. stretch reflex magnitude during within-session conditioning [6, 7]. For baseline sessions, the protocol remained equal to Block 0 with only background biofeedback provided. For conditioning sessions, reflex biofeedback was added to the background biofeedback with the instruction to reduce reflex magnitude. Despite the use of continuous biofeedback by Ludvig *et al.* [15], the Impedance group received discrete reflex biofeedback to avoid any difficulty interpreting a biofeedback parameter with large variability, see Chapter 3. In each block 75 discrete perturbations for EMG-based groups and roughly 750 continuous perturbations for the Impedance group were applied [6, 7].

5.2.4 Biofeedback

Visualization and Timing

The Conventional group received bar-based biofeedback on background activity (all trials), and on reflex magnitude, average baseline (B1-5) reflex magnitude, number of trials completed and success rate (conditioning trials only), see Fig. 5.2. Biofeedback was provided via bar size and color, based on whether the set target was met or not. The background bar color also changed whenever TA background activity was off-target, although current TA activity was not directly visualized. Background biofeedback was continuously updated at 10 Hz, whereas the reflex biofeedback update was directly coupled to a stretch perturbation.

For game-based groups, the bar-based visualization was substituted with a third-person game about a banana delivery truck, which provided biofeedback on background activity (all trials) and reflex reduction success (conditioning trials only), see Fig. 5.2. Reflex reduction success was represented by the number of bananas in the trunk: starting at 150 bananas every block, two bananas would fall out after each failure to meet the reflex target at a feedback instance. An increased 30 Hz background update frequency was used for the game-based biofeedback to create a smooth gaming experience.

To obtain a pleasant gaming experience, the amount of biofeedback was reduced during gamification. As a result, participants did not receive information on: 1) background target success/failure; 2) quantified reflex magnitude; and 3) average baseline (B1-5) reflex magnitude, number of trials completed and success rate. The experiment leaders could access this missing information during each block and communicate it to participants, e.g. success rates were regularly announced to the participants.

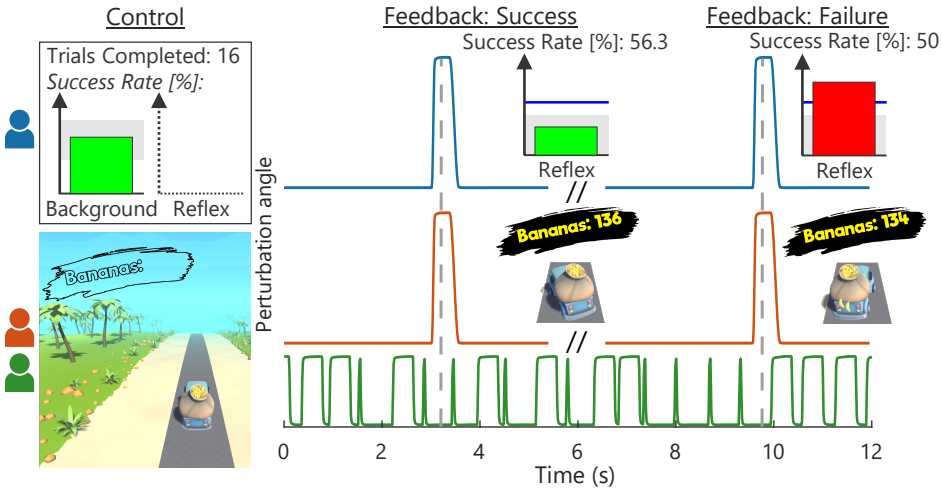

Figure 5.2: Biofeedback Visualization and Timing. For the (*blue*) Conventional group, a background (all trials) and a reflex (conditioning trials only) bar-graph directly represented current magnitudes. Moreover, a (*grey*) target area was displayed with the bar color visualizing whether this target was met (*green*) or not (*red*) [7]. The reflex graph also showed a blue reference line based on average baseline (B1-5) reflex magnitude. The reflex biofeedback (*grey-dashed vertical)* was coupled to a stretch perturbation, displayed after a short data processing delay. Additionally, the completed number of trials and success rate were displayed.
The game-based Gaming (*red*) and Impedance (*green*) groups, had truck left-right position represent current background magnitude with the (*grey*) road as target area. Reflex activity controlled the number of bananas in the trunk after each feedback instance, visualized as wobble of the truck. After the wobble, all bananas were retained when the (non-visual) reflex target was met and two bananas would fall out on failure. As a result, the continuous perturbations of the Impedance group were decoupled from the feedback instances.

Reward criterion

The reflexive target range was adaptive throughout all conditioning sessions to keep the reflex reduction target equally challenging. The upper bound of the target range was set as the 66th percentile of the previous block reflex magnitude, i.e. Block 1 based on Block 0, etc. [6, 7]. Participants earned a modest monetary reward if a block was completed with a success rate larger than 50%. Given the 66th percentile upper bound, a larger than 50% success rate was expected when reflex magnitude did not change between blocks [6, 7]. Participants were verbally motivated to always maximize success rate, also beyond the 50% monetary threshold. Participants were not given any specific instructions or indications reflex reduction strategies and were motivated to find their own strategy for success. Besides, participants were motivated to not purposely search for the edges of the background target ranges in order to modulate the reflex response. For additional motivation and engagement, the game-based groups also earned in-game currency per banana delivered, which could buy in-game visual upgrades for the truck and environment.

5.2.5 Data Analysis

Per session, the M-wave magnitudes were averaged across repetitions at each stimulation intensity with M_{max} defined as the maximum value across all intensities. Per stretch perturbation, background activity was computed over the 100 ms period before dorsiflexion perturbation onset for EMG-based groups [6, 7] and a shorter 40 ms period for the Impedance group to avoid movement artifacts [14]. SOL and TA background were computed as mean rectified EMG and torque background as mean unfiltered torque.

The SOL M1 magnitudes, as defined in experiment setup, of both control (Block 0) and conditioned (Block 1-3) reflexes were normalized as % baseline, using baseline (B1-5) mean of the control and conditioned reflexes respectively [6, 7]. Per session, a within-session conditioning effect was defined as the mean normalized conditioned reflex minus mean normalized control reflex.

Besides, to support the use of reflexive gain G as biofeedback variable, the correlation between the EMG-based and impedance-based reflex magnitude was investigated. First, a set of across-block paired data points was created using the mean SOL M1 and gain G for each block per participant. Second, a set of within-block paired data points was created using the mean SOL M1 and gain G for each feedback instance per block per participant. Thus, for Block 0 (25×) and Block 1-3 (75×) all data leading up to a feedback instance was averaged for both reflexive magnitudes.

For all groups, the IMI questionnaire, taken in Session C6, consisted of 4 questions across 4 dimensions: interest-enjoyment, perceived competence, effort-importance and tension-pressure. For each participant all answers within a single dimension were averaged to obtain an overall score for this dimension.

5.2.6 Statistical Analysis

The feasibility of each biofeedback method was investigated by evaluating the within-session conditioning effect, with a -15% reference in Session C4-6 defined as success [6, 7]. For each participant a linear model (LM) was built using normalized SOL M1 (% baseline) as outcome measure ($N = 2750$ for Coventional & Gaming; $N \approx 27500$ for Impedance). Both session (B1 to C6), block (Blocks 0-3) and their interaction were used as predictor to investigate the within-session conditioning effect. Due to EMG measurement artifacts (high amplitude noise across broad frequency range), Session B1 for participant 7 and Session B5 for participant 8 were discarded. A planned contrast was used to evaluate the conditioning effect, contrasting the within-session outcome of Session C4-6 to B1-5 computed as the average of Blocks 1-3 ('Conditioned' reflex) minus Block 0 ('Control' reflex). To avoid confounding effects of the background activity, the SOL, TA and torque background outcomes were all added to the LM as predictors to function as covariates. Per participant, the contrast was tested twice, once with and once without these covariates. Ideally, M_{max} would also be included in the LM as covariate. However, as only a single M_{max} outcome is available per session, adding M_{max} as covariate is impossible as this predictor would be collinear with the session predictor.

To support the need for an acclimatization session before starting the actual baseline, the SOL M1 was investigated further. An LM was built with data from Sessions A1 and

B1-5 using only the mean control reflex (Block 0), using session as predictor. A planned reverse-Helmert like contrast was used to evaluate the difference in reflex magnitude between A1 vs. B1-5 and B1 vs. B2-5 for all participants combined.

The use of reflexive gain G as biofeedback variable was investigated using the correlation with SOL M1 magnitudes of the Impedance group (Sessions B1-C6 and Blocks 1-3). First, within-block correlation was investigated via a within-block Z-score standardization of all 75 data pairs for all 99 blocks (33 blocks per participants). The Z-score standardization allows to combine all data across-blocks and -subjects before computing the correlation, see Chapter 4. Second, the across-block correlation was investigated by using the mean of 75 data pairs per block and using a within-subject Z-score standardization to combine data across-subjects.

5.3 Results

We explored the feasibility of three different biofeedback methods to achieve a within-session reduction of SOL M1 magnitude with a Conventional, Gaming and Impedance group. All participants completed 12 data collection sessions: 6 acclimatization/baseline sessions (A1, B1-5) and 6 conditioning sessions (C1-6). All sessions first contained a short control block (Block 0) with 25 feedback instances followed by three blocks of 75 feedback instances without (A1 to B5) or with reflex biofeedback (C1 to C6). Key prerequisite on SOL M1 reduction was lack of modulation in several parameters throughout data collection to avoid confounding effects: SOL M_{max}, and SOL, TA and torque background activity.

5.3.1 Steadiness of M_{max} and Background Activity

Based on session averages, all M_{max} and background activity parameters were visually considered steady throughout data collection, see Fig. 5.3. Subsequently, steadiness of M_{max} was interpreted as consistent electrode placement throughout data collection. Similarly, steady background activity was used to avoid influences on reflex magnitude via voluntary increase or decrease of tonic activation. TA background also remained below resting levels indicating that co-contraction was not present. The session averages do clearly show that the EMG-based groups (Conventional and Gaming) were provided with SOL background biofeedback to keep activity steady, whereas the Impedance group used background torque biofeedback. Although no clear trends are visible, both groups show larger across-session variability for the variables on which no biofeedback was received. Thus, it was still important to evaluate the within-session effects with an LM including background variables as covariates.

5.3.2 Soleus Stretch Reflex Reduction

Both EMG-based groups (Conventional and Gaming) had several successful within-session conditioning results, reaching the reference -15% target, see bottom row Fig. 5.4 [6, 7]. Thus, within these sessions the difference between the normalized Conditioned and Control reflex measures was at least 15%, see top rows Fig. 5.4. Contrarily, no successful within-session conditioning effect was observed for the Impedance group.

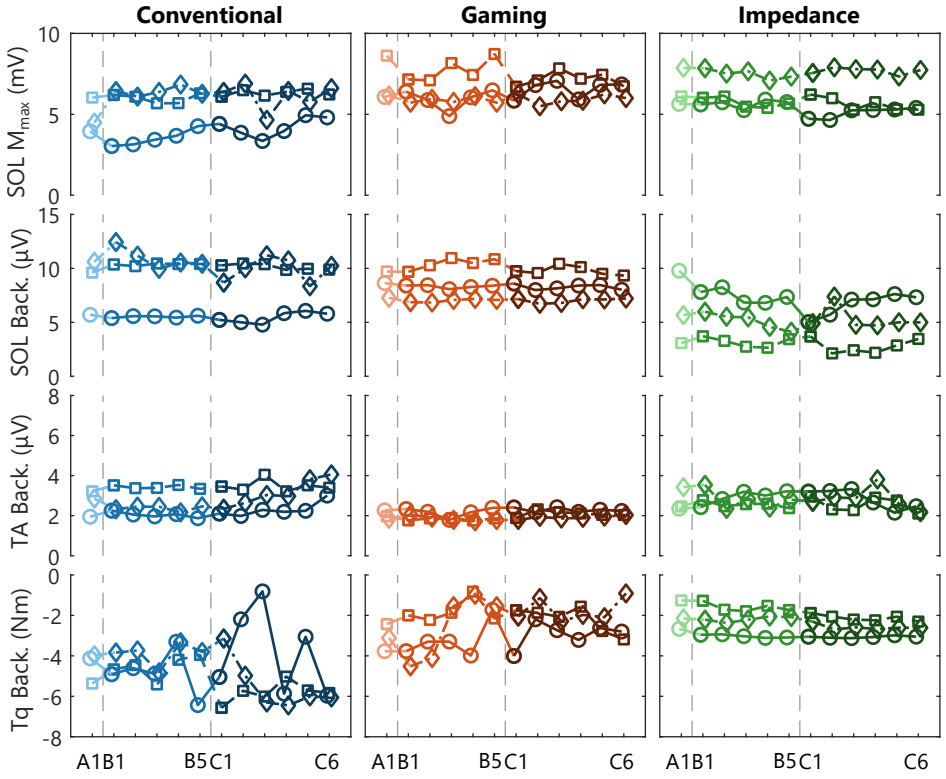

Figure 5.3: Steadiness M_{max} and background activity. Individual participant traces of SOL M_{max}, and SOL, TA and torque background activity for acclimatization (A1), baseline (B1-5) and conditioning (C1-6) sessions. All variables were required to remain steady throughout data collection. Each data point reflects the average of all blocks (Block 0-3) within a single session. Conventional and Gaming groups received biofeedback on SOL activity, whereas the Impedance group received biofeedback on torque activity. For all groups TA activity was required to remain at a resting level (<7.5 μV). Each icon (circle, square, diamond) per group is linked to an individual participant and consistently used across figures.

Across the full experiment, feasibility of the conditioning paradigm was confirmed in 2 (Conventional group) and 3 (Gaming group) out of 3 participants, see Table 5.1. In the Conventional group, the background-corrected results showed a -24% ($p < 0.001$) and -17% ($p < 0.001$) within-session effect for participants 1 and 3, whereas participant 2 showed a weaker SOL M1 reduction at -8.7% ($p = 0.22$). The Gaming group showed a -33% ($p < 0.001$), -22% ($p < 0.001$) and -16% ($p = 0.007$) effect for the participants. Thus, gamification of the conditioning paradigm seemed feasible without interfering with conditioning outcomes.

Feasibility was not shown for the Impedance group as all three participants showed an increase in within-session SOL M1 effect (3.4, 6.3 and 0.3%), see Table 5.1. Furthermore, also the impedance-based reflex magnitude showed no reflex reduction, see supplementary Fig. C.1. Therefore, substituting EMG- with impedance-based reflex biofeedback did not seem feasible within the conditioning paradigm.

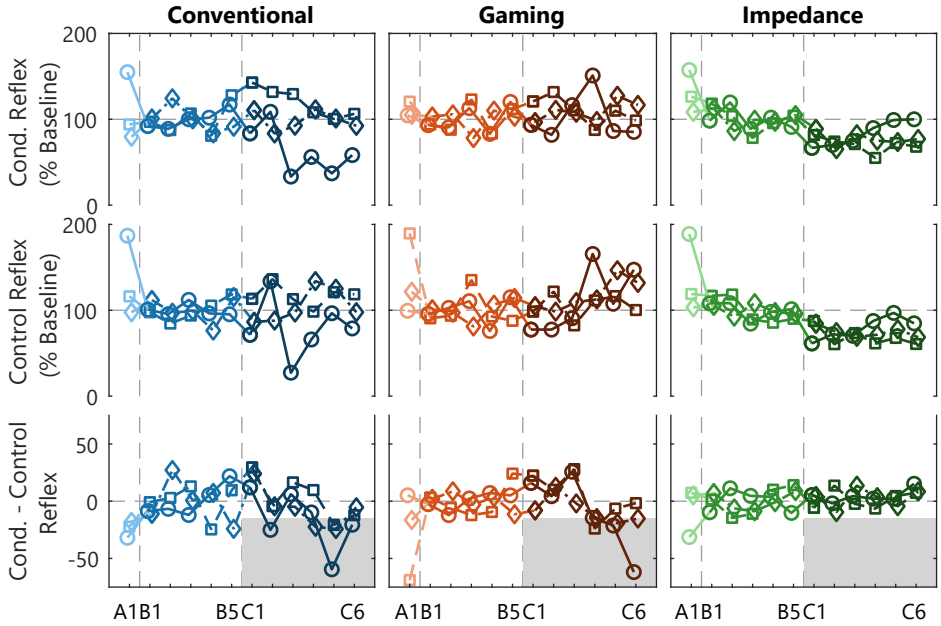

Figure 5.4: SOL M1 reflex results and within-session effect. Individual participant traces of the average conditioned reflex (mean Blocks 1-3) and control reflex (Block 0) per session for acclimatization (A1), baseline (B1-5) and conditioning (C1-6) sessions. The within-session effect is derived from the difference between the conditioned and control reflex within a session. Conventional and Gaming groups received biofeedback on SOL M1 activity, whereas the Impedance group received biofeedback on reflexive impedance gain G. A -15% within-session effect in session C4-6 was defined as success criteria to determine feasibility of the biofeedback method for each participant, see (*grey*) shaded target area. Each icon (circle, square, diamond) per group is linked to an individual participant and consistently used across figures.

5.3.3 Necessity Acclimatization Session

The addition of an acclimatization session before the baseline sessions was observed to potentially be beneficial for the steadiness of the reflex magnitude during baseline for all groups, see Fig. 5.4. The results of the first depicted session (A1) could be added to the baseline session (B1-5), as the protocol executed is exactly equal. However, the reflex variables generally showed an increased control and conditioned reflexive magnitude and variability across-participants in combination with a negative within-session effect for A1 compared with B1-5. To confirm these observations, an LM of the control SOL M1 magnitude (Block 0, Session A1 to B5) for all participants did indeed show a significant effect of adding the session predictor ($F_{(5,48)} = 5.27$, $p < 0.001$). A contrast further showed that the reflex magnitude for session A1 was significantly larger than sessions B1-5 35.8 ± 7.2 %baseline ($t(48) = 4.95$, $p < 0.001$). This effect faded away when contrasting Session B1 versus the other baseline sessions (B2-5) ($t(48) = 0.53$, $p = 0.60$). Note, no clear discrepancies between Sessions A1 and B1-5 were observed for M_{max} and all background variables, see Fig. 5.3.

Table 5.1: Contrasts between B1-5 and C4-C6 for the within-session SOL M1 effect without and with covariates. Within-session effect contrasts are expressed in % baseline, thus mean within-session effect for B1-5 equal zero within all participants. All contrasts were tested using a t-test for both the models without and with covariates.

		LM:~Session×Block			LM:~Session×Block Covariates:~SOL_{back}+TA_{back}+$Torque_{back}$		
Group		**Contrasts**	**Statistical Parameters**		**Contrasts**	**Statistical Parameters**	
Conventional	#1	-30 ± 4.3	$t(2706)$ = -6.93	$p < 0.001$	-24 ± 4.5	$t(2703)$ = -5.39	$p < 0.001$
	#2	-7.7 ± 7.0	$t(2706)$ = -1.10	$p = 0.27$	-8.7 ± 7.1	$t(2703)$ = -1.24	$p = 0.22$
	#3	-17 ± 4.2	$t(2706)$ = -4.08	$p < 0.001$	-17 ± 4.3	$t(2703)$ = -4.03	$p < 0.001$
Gaming	#4	-33 ± 7.5	$t(2706)$ = -4.36	$p < 0.001$	-33 ± 7.5	$t(2703)$ = -4.36	$p < 0.001$
	#5	-11 ± 6.5	$t(2706)$ = -1.64	$p = 0.10$	-22 ± 6.6	$t(2703)$ = -3.30	$p < 0.001$
	#6	-16 ± 6.0	$t(2706)$ = -2.72	$p = 0.007$	-16 ± 6.0	$t(2703)$ = -2.70	$p = 0.007$
Impedance	#7	4.2 ± 2.5	$t(24427) = 1.65$	$p = 0.10$	3.4 ± 2.5	$t(24424) = 1.37$	$p = 0.172$
	#8	5.3 ± 1.2	$t(25284) = 4.48$	$p < 0.001$	6.3 ± 1.2	$t(25281) = 5.31$	$p < 0.001$
	#9	2.5 ± 1.9	$t(27363) = 1.36$	$p = 0.17$	0.29 ± 1.8	$t(27360) = 0.163$	$p = 0.87$

5.3.4 Correlation EMG and Impedance-based Biofeedback

The observed commonality between the EMG-based and impedance-based reflex magnitudes depended on the time frame of the evaluation, see Fig. 5.5. A moderate correlation (r = 0.68) was found for the across-block correlation, whereas a weak correlation (r = 0.31) was found for the within-block correlation for data of all Blocks 1-3 of the Impedance groups. The moderate across-block correlation was further corroborated given the similarity between block-averaged conditioned, control and within-session reflex outcomes, see Fig. 5.4 and supplementary Fig. C.1. Thus, the observed correlation was larger when data was averaged over a full block (ca. 750 stretches, 7.5 minutes) compared with averaged per feedback instance (ca. 10 stretches, 6 seconds).

5.3.5 Intrinsic Motivation Inventory

The IMI questionnaire showed a positive reception of the game-based conditioning paradigms, ignoring the electrical stimulation element, in terms of motivation and engagement, see Table 5.2. Participants in both game-based groups reported good scores for interest-enjoyment (8.5 and 8.0 out of 10) score as well as perceived competence (8.5 and 7.2). Note, these psychological results should be interpreted and compared with care, e.g. a large variation across the effort-importance scale was observed over the three groups, whereas no difference was expected.

5.4 Discussion

The goal of this study was to explore the feasibility of two forms of biofeedback to obtain a within-session reduction of the Soleus stretch reflex with conditioning. First, we explored the feasibility of gamification and second, the feasibility of combined game-

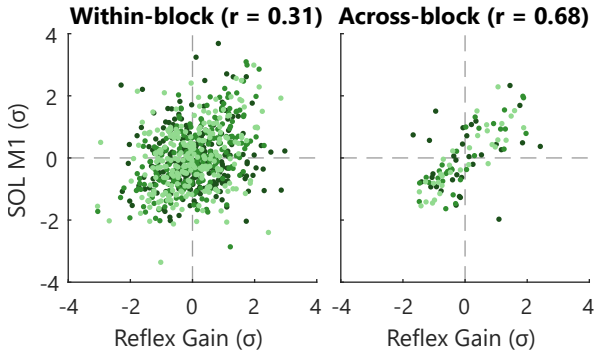

Figure 5.5: Within- and across-block correlation of reflexive biofeedback variables. Individual participants are visualized with a different color. Correlation analysis for the Impedance group for Session B1 to C6 and Blocks 1-3. The within-block correlations were computed using the averaged measures per feedback instance. The across-block correlations were computed using the averaged measures per blocks. Data was Z-score standardized within-block and within-subject respectively to allow combination of data over sessions and participants. To improve visualization only 10% of all within-block data points are shown.

Table 5.2: Intrinsic Motivation Inventory (IMI) scores completed after Session C6. Scores are the across-subject averages within each group and are based on 4 questions per category. Scales used were between 1 (not at all true) and 10 (very true).

	Conventional	Gaming	Impedance
Interest-Enjoyment	6.6	8.5	8.0
Competence	6.2	8.5	7.2
Effort-Importance	6.8	7.0	8.6
Tension-Pressure	4.5	3.3	2.1

and impedance-based biofeedback. For the EMG-based groups, using either bar-based or game-based biofeedback, feasibility of the conditioning paradigm was shown in 2 and 3 out of 3 participants, respectively. Contrarily, feasibility was not shown for any participant using impedance-, game-based biofeedback. Thus, whereas the combined game- and impedance-based biofeedback was not considered feasible, the gamification of EMG-based biofeedback used to improve motivation and long-term engagement was considered feasible.

5.4.1 Feasibility Game-based Biofeedback

Exploring the use of EMG-, game-based biofeedback within the conditioning paradigm confirmed the feasibility of the proposed biofeedback gamification. First, the switch from bar-based to game-based biofeedback did not interfere with conditioning outcomes. Our results showed feasibility of the proposed method in all participants of the Gaming group after correcting for potentially confounding background effects. Previous studies did not report on individual within-session effects and only reported a group-average -15% effect across the 16 (out of 17) successful participants, which achieved a long-term down-conditioning effect [6, 7]. Comparing this result to the observed -24% Gaming group-average within-session effect should be done with caution due to the exploratory nature and small population size of our study. Moreover, the Conditioned and Control reflex were not interpreted separately, as previous studies showed no clear expected trends and large variability [6, 7]. Second, feasibility of the gamification was also shown from a psychological perspective as the IMI scores of the Gaming group showed a positive evaluation for participant motivation and engagement. Given these results, improving motivation and long-term engagement of the conditioning paradigm to mitigate time-intensiveness and a slow learning curve is considered feasible.

Towards future use of gamification, the methodological differences between the game- (Gaming group) and bar-based (Conventional group) biofeedback were solely made to the biofeedback visualization. The main challenge towards a suitable gaming experience was the high information density of the bar-based biofeedback [6, 7]. After gamification, participants most importantly did not receive information on: 1) background target success/failure; and 2) quantified reflex magnitude. Whereas the background biofeedback implementation has varied across previous studies on human stretch reflex reduction, all studies provided quantified reflex biofeedback [7, 19, 20]. A previous study on primate stretch reflex reduction did obtain successful conditioning results without quantified reflex magnitude using food to convey success or failure [21].

Our results show that such a binary (success/failure) biofeedback can also be considered feasible for human stretch reflex reduction paradigms.

5.4.2 Feasibility Combined Game- and Impedance-based Biofeedback

Conditioning based on combined game- and impedance-based biofeedback did not yield a feasible paradigm. No participants showed a within-session reduction of reflex magnitude after impedance-based conditioning, despite positive findings in previous studies using impedance-based biofeedback outside of the conditioning paradigm [15]. Any influences of potential confounders were not observed, as no trends in M_{max} or background activity were recorded and the psychometric scores for the Impedance group showed a positive evaluation. As such, accelerating the learning curve and improving practical execution of the conditioning paradigm remains an open challenge.

To find plausible explanations for the lack of within-session reflex reduction of the Impedance group, all methodological differences between Impedance and EMG-based groups were considered: 1) stretch reflex perturbations; 2) biofeedback gamification; 3) biofeedback processing and 4) biofeedback visualization. First, compared with the EMG-based groups the stretch reflex required for the impedance-based biofeedback had a decreased amplitude, duration and velocity, whereas the acceleration and number of perturbations was increased. As expected from literature, the adapted perturbation parameters affected the reflex response as only M1 was observed, instead of both M1 and M2 [22]. Yet, all previous stretch reflex studies focused on M1 conditioning [7, 19, 20], M2 does not co-condition with the M1 reflex [7] and H-reflex conditioning also just elicits a single reflexive response, most equivalent to M1 [4, 6]. Therefore, the lack of M2 is not considered a plausible explanation for the lack of reflex reduction. Contrarily, the increased acceleration of the perturbation might saturate the M1 response due to the M1 acceleration-dependence [22], which could plausibly explain the difficulty of reducing the reflex response. Besides, despite an increased number of perturbations, each stretch perturbation did elicit a stretch response as seen in similar impedance-based studies [14, 23]. Consequently, while receiving an equal amount of feedback, participants in the Impedance group experienced an increased number of elicited reflexes, which might have influenced conditioning outcomes. Although previous studies do not provide an indication whether increased perturbation occurrence would either improve or interfere with treatment outcome. Second, the gamified biofeedback visualization is not considered as likely explanation, as the exact same game was used for both Gaming and Impedance groups.

Third, an important difference between the biofeedback processing of the EMG- and impedance-based biofeedback was revealed through correlation analysis. A weak within-block correlation ($r = 0.31$) of the EMG- and impedance-based reflexive biofeedback was found based on 6 s data segments. Oppositely, for longer segments a moderate across-block correlation was found ($r = 0.68$; 7.5 min segments) and reported previously ($r = 0.69$; 60 s segments) in Chapter 4. This difference between the correlation of short and long segments is likely related to the inherent 15 s risetime of the impedance estimation algorithm [14]. Practically, this 15 s risetime causes a slow and delayed impedance estimation compared with the direct instance-based M1 EMG processing. Consequently, the direct coupling between a feedback instance and stretch perturbation

as in the EMG-based biofeedback lacks for the impedance-based biofeedback. Fourth, the biofeedback visualization used was a mix of a continuous impedance-based [15] and discrete EMG-based paradigm [7]. Ludvig *et al.* [15] provided continuous line-based biofeedback on magnitude, which was converted to a discrete, binary biofeedback on reflex reduction success over the last 5-7 s interval. This conversion ensured a match with the EMG-based conditioning paradigm. However, the converted impedance-based visualization did not result in a feasible paradigm, while this visualization was inspired by two previously successful studies [7, 15]. This result may show the importance of quantitative or continuous impedance-based biofeedback, given the slow and delayed impedance-based biofeedback characteristics. For example, due to the variability of the reflex response, the delayed biofeedback might show reflex reduction success, while the last couple reflexes were actually too large and vice versa. Moreover, the lack of quantitative or continuous biofeedback will hide this processing effect from the participant. Overall, the lack of reflex reduction observed can potentially be explained by the delayed and decoupled biofeedback processing as well as its combination with the lack of a quantitative or continuous visualization.

5.4.3 Study Limitations and Future Outlook

The current study can solely be interpreted as exploration of the feasibility of several biofeedback methods, given the limited number of participants. Furthermore, the protocol was limited to studying short-term (within-session) effects as long-term effects have been shown to arise after 12-16 sessions [6, 7]. Within these restrictions, we recommend game-based biofeedback be implemented and tested in longer study schedules, with more participants and in a neurological population. Experimental execution should include a sufficient number of preliminary trials (at least a preparation and an acclimatization session) to ensure steadiness of baseline measurements. The goal of further exploring feasibility of the gamified conditioning paradigm is to increase participant motivation and long-term engagement during this time-intensive paradigm with a slow learning curve. Furthermore, feasibility should be explored in a neurological population before clinical implementation.

Before applying the conditioning paradigm clinically, improving the time-intensiveness and slow learning curves remains an open challenge. The implementation of impedance-based biofeedback, previously used to voluntarily modulate the reflex response, within the conditioning paradigm did not result in a feasible protocol. The impedance-based biofeedback was explored combined with the game-based biofeedback, whereas an impedance-, bar-based biofeedback group was not included. Therefore, exploring impedance-, bar-based biofeedback would be useful to provide a more direct comparison between impedance- and EMG-based biofeedback. Besides, potential improvements of the impedance-based biofeedback may lie within an improved algorithm without a 15 s risetime to avoid delayed biofeedback and directly couple the biofeedback with the participant's current actions. Moreover, an improved impedance-based algorithm may solve the reduced correlation with EMG-based reflex magnitude for short data segments. Besides impedance-based biofeedback, other paradigm changes like conditioning during locomotion have also shown promising improvements of the slow learning curves [24].

5.5 Conclusions

We have shown the feasibility of EMG-, game-based biofeedback within the operant conditioning paradigm to obtain a within-session reduction of the SOL stretch reflex. Contrarily, we did not observe feasibility for the impedance-, game-based biofeedback. Stretch reflex conditioning should be applied clinically to potentially obtain a non-invasive spasticity treatment with long-term sustained effect. Before clinical application, the time-intensiveness and slow learning curve of the conditioning paradigm remain an open challenge. These results call for further research on gamification of conditioning paradigms to obtain improved participant motivation and engagement, while achieving long-term conditioning effects.

References

[1] V. Dietz and T. Sinkjær, "Spastic Movement Disorder: Impaired Reflex Function and Altered Muscle Mechanics," *Lancet Neurology*, 6(8), pp. 725–733, 2007. doi: 10.1016/S1474-4422(07)70193-X.

[2] J. C. van den Noort, L. Bar-On, E. Aertbeliën, M. Bonikowski, *et al.*, "European Consensus on the Concepts and Measurement of the Pathophysiological Neuromuscular Responses to Passive Muscle Stretch," *European Journal of Neurology*, 24(7), pp. 981–991, 2017. doi: 10.1111/ene.13322.

[3] E. Chang, N. Ghosh, D. Yanni, S. Lee, *et al.*, "A Review of Spasticity Treatments: Pharmacological and Interventional Approaches," *Critical Reviews in Physical and Rehabilitation Medicine*, 25(1-2), pp. 11–22, 2013. doi: 10.1615/CritRevPhysRehabilMed.2013007945.

[4] A. K. Thompson, F. R. Pomerantz, and J. R. Wolpaw, "Operant Conditioning of a Spinal Reflex Can Improve Locomotion after Spinal Cord Injury in Humans," *Journal of Neuroscience*, 33(6), pp. 2365–2375, 2013. doi: 10.1523/JNEUROSCI.3968-12.2013.

[5] A. K. Thompson and J. R. Wolpaw, "Operant Conditioning of Spinal Reflexes: From Basic Science to Clinical Therapy," *Frontiers in Integrative Neuroscience*, 8:25, 2014. doi: 10.3389/fnint.2014.00025.

[6] A. K. Thompson, X. Y. Chen, and J. R. Wolpaw, "Acquisition of a Simple Motor Skill: Task-Dependent Adaptation Plus Long-Term Change in the Human Soleus H-Reflex," *Journal of Neuroscience*, 29(18), pp. 5784–5792, 2009. doi: 10.1523/JNEUROSCI.4326-08.2009.

[7] N. Mrachacz-Kersting, U. G. Kersting, P. de Brito Silva, Y. Makihara, *et al.*, "Acquisition of a Simple Motor Skill: Task-dependent Adaptation and Long-term Changes in the Human Soleus Stretch Reflex," *Journal of Neurophysiology*, 122(1), pp. 435–446, 2019. doi: 10.1152/jn.00211.2019.

[8] S. Deterding, M. Sicart, L. Nacke, K. O'Hara, *et al.*, "Gamification: Using Game Design Elements in Non-Gaming Contexts," in *CHI '11 Extended Abstracts on Human Factors in Computing Systems*, Vancouver, Canada: Association for Computing Machinery, 2011, pp. 2425–2428. doi: 10.1145/1979742.1979575.

[9] Z. Turan, Z. Avinc, K. Kara, and Y. Goktas, "Gamification and Education: Achievements, Cognitive Loads, and Views of Students," *International Journal of Emerging Technologies in Learning*, 11(7), pp. 64–69, 2016. doi: 10.3991/ijet.v11i07.5455.

[10] J. P. Proença, C. Quaresma, and P. Vieira, "Serious Games for Upper Limb Rehabilitation: A Systematic Review," *Disability and Rehabilitation: Assistive Technology*, 13(1), pp. 95–100, 2018. doi: 10.1080/17483107.2017.1290702.

[11] B. Bonnechère, B. Jansen, L. Omelina, and S. van Sint Jan, "The Use of Commercial Video Games in Rehabilitation: A Systematic Review," *International Journal of Rehabilitation Research*, 39(4), pp. 277–290, 2016. doi: 10.1097/MRR.0000000000000190.

[12] S. Lopes, P. Magalhães, A. Pereira, J. Martins, *et al.*, "Games Used with Serious Purposes: A Systematic Review of Interventions in Patients with Cerebral Palsy," *Frontiers in Psychology*, 9:1712, 2018. doi: 10.3389/fpsyg.2018.01712.

[13] J. Howcroft, D. Fehlings, V. Wright, K. Zabjek, *et al.*, "A Comparison of Solo and Multiplayer Active Videogame Play in Children with Unilateral Cerebral Palsy," *Games for Health Journal*, 1(4), pp. 287–293, 2012. doi: 10.1089/g4h.2012.0015.

[14] D. Ludvig and R. E. Kearney, "Real-time Estimation of Intrinsic and Reflex Stiffness," *IEEE Transactions on Biomedical Engineering*, 54(10), pp. 1875–1884, 2007. doi: 10.1109/TBME.2007.894737.

[15] D. Ludvig, I. Cathers, and R. E. Kearney, "Voluntary Modulation of Human Stretch Reflexes," *Experimental Brain Research*, 183(2), pp. 201–213, 2007. doi: 10.1007/s00221-007-1030-0.

[16] R. E. Kearney, R. B. Stein, and L. Parameswaran, "Identification of Intrinsic and Reflex Contributions to Human Ankle Stiffness Dynamics," *IEEE Transactions on Biomedical Engineering*, 44(6), pp. 493–504, 1997. doi: 10.1109/10.581944.

[17] H. J. Hermens, B. Freriks, C. Disselhorst-Klug, and G. Rau, "Development of Recommendations for SEMG Sensors and Sensor Placement Procedures," *Journal of Electromyography and Kinesiology*, 10(5), pp. 361–374, 2000. doi: 10.1016/S1050-6411(00)00027-4.

[18] E. D. McAuley, T. Duncan, and V. V. Tammen, "Psychometric Properties of the Intrinsic Motivation Inventoiy in a Competitive Sport Setting: A Confirmatory Factor Analysis," *Research Quarterly for Exercise and Sport*, 60(1), pp. 48–58, 1989. doi: 10.1080/02701367.1989.10607413.

[19] M. L. Evatt, S. L. Wolf, and R. L. Segal, "Modification of Human Spinal Stretch Reflexes: Preliminary Studies," *Neuroscience Letters*, 105(3), pp. 350–355, 1989. doi: 10.1016/0304-3940(89)90646-0.

[20] S. L. Wolf and R. L. Segal, "Reducing Human Biceps Brachii Spinal Stretch Reflex Magnitude," *Journal of Neurophysiology*, 75(4), pp. 1637–1646, 1996. doi: 10.1152/jn.1996.75.4.1637.

[21] J. R. Wolpaw and J. A. O'Keefe, "Adaptive Plasticity in the Primate Spinal Stretch Reflex: Evidence for a Two-Phase Process," *Journal of Neuroscience*, 11(4), pp. 2718–2724, 1984. doi: 10.1523/JNEUROSCI.04-11-02718.1984.

[22] J. M. Finley, Y. Y. Dhaher, and E. J. Perreault, "Acceleration Dependence and Task-specific Modulation of Short- and Medium-Latency Reflexes in the Ankle Extensors," *Physiological Reports*, 1(3):e00051, 2013. doi: 10.1002/phy2.51.

[23] R. B. Stein and R. E. Kearney, "Nonlinear Behavior of Muscle Reflexes at the Human Ankle Joint," *Journal of Neurophysiology*, 73(1), pp. 65–72, 1995. doi: 10.1152/jn.1995.73.1.65.

[24] A. K. Thompson and J. R. Wolpaw, "H-Reflex Conditioning during Locomotion in People with Spinal Cord Injury," *Journal of Physiology*, 599(9), pp. 2453–2469, 2019. doi: 10.1113/JP278173.

Chapter 6

Disentangling the Intrinsic and Reflexive Contributions to Ankle Joint Hyper-Resistance Treated with Botulinum Toxin-A

R. C. van 't Veld, E. Flux, W. van Oorschot, A. C. Schouten, M. M. van der Krogt, H. van der Kooij, M. Vos-van der Hulst, N. L. W. Keijsers, E. H. F. van Asseldonk

Abstract — Spasticity, i.e. stretch hyperreflexia, increases joint resistance similar to symptoms like hypertonia and contractures. Botulinum neurotoxin-A (BoNT-A) injections are a widely used intervention to reduce spasticity. BoNT-A effects on spasticity are poorly understood, because clinical measures, e.g. modified Ashworth scale (MAS), cannot differentiate between the symptoms affecting joint resistance. This paper disentangles ankle joint resistance into reflexive and intrinsic contributions for participants treated with BoNT-A injections. We hypothesized that the overall joint resistance and reflexive contribution decrease 6 weeks after injection, while returning close to baseline after 12 weeks. Nine participants with spasticity after spinal cord injury or after stroke were evaluated across three sessions: 0, 6 and 12 weeks after BoNT-A injection in the calf muscles. Evaluation included clinical measures (MAS, Tardieu Scale) and motorized instrumented assessment using the instrumented spasticity test (SPAT) and parallel-cascade (PC) system identification. Assessments included measures for: 1) overall resistance from MAS and fast velocity SPAT; 2) reflexive resistance contribution from Tardieu Scale, difference between fast and slow velocity SPAT and PC reflexive gain; and 3) intrinsic resistance contribution from slow velocity SPAT and PC intrinsic stiffness/damping. Individually, the hypothesized BoNT-A effect, the combination of a reduced resistance (week 6) and return towards baseline (week 12), was observed in the MAS (5 participants), fast velocity SPAT (2 participants), Tardieu Scale (2 participants), SPAT (1 participant) and reflexive gain (4 participants). On a group-level, the hypothesis was only confirmed for the MAS, which showed a significant resistance reduction at week 6. All instrumented measures were strongly correlated when quantifying the same resistance contribution. At group-level, the expected joint resistance reduction due to BoNT-A injections was only observed in the MAS (overall resistance). This observed reduction could not be attributed to an unambiguous group-level reduction of the reflexive resistance contribution, as no instrumented measure confirmed the hypothesis. Validity of the instrumented measures was supported through a strong association between different assessment methods. Therefore, further quantification of the individual contributions to joint resistance changes using instrumented measures across a large sample size are essential to understand the heterogeneous response to BoNT-A injections.

This chapter has been submitted in April 2022. The code and data underlying this chapter are available via 4TU.ResearchData. doi: 10.4121/c.5986267

6.1 Introduction

Botulinum neurotoxin-A (BoNT-A) injections are currently the most frequently used clinical intervention for focal spasticity [1–3]. Spasticity is a common symptom after various brain and neural injuries, such as spinal cord injury (SCI) or stroke, referring to an exaggerated stretch reflex, i.e. stretch hyperreflexia [4, 5]. Spasticity is perceived as an increased joint resistance to movement, i.e. joint hyper-resistance. BoNT-A injections are used clinically to reduce muscle activity and hence spasticity [1]. BoNT-A injections reduce muscle activity by inhibiting the release of acetylcholine at the neuromuscular junction, which chemically denervates the exposed muscle fibers. BoNT-A effects reduce after 2 to 4 months due to nerve sprouting and muscle re-innervation [1].

Clinical evaluation of BoNT-A injections has shown a significant reduction in joint resistance after 2-8 weeks using the modified Ashworth scale (MAS) [6–8]. With the MAS, clinicians evaluate overall joint resistance, which can physiologically include tissue characteristics, and tonic and reflexive muscle activity [5, 9–11]. For the MAS, a slow passive movement is repeatedly applied, whereas movements with varying characteristic, e.g. slow and fast velocities, are required to unravel joint resistance contributions. Therefore, the MAS can clinically only evaluate spasticity indirectly and concurrent with other symptoms as involuntary background activity, shortened tissue, contractures and fibrosis [4, 12, 13]. Furthermore, the MAS has a questionable reliability, especially when applied at the lower limb [11, 14]. Hence, the clinical effect of BoNT-A injections on spasticity is poorly understood, while BoNT-A injections are a frequently used clinical intervention for spasticity.

Quantification of the intrinsic and reflexive contributions to joint hyper-resistance is essential to understand the beneficial and adverse effects of BoNT-A injections. The intrinsic resistance represents the combination of tissue-related non-neural and tonic neural contributions to joint resistance [10]. The reflexive resistance, representing the phasic neural contributions, can be used as measure for spasticity. Model-based processing of neuromechanical responses can be used to unravel and quantify these intrinsic and reflexive contributions [10, 15–19]. Furthermore, instrumentation and motorization using robotic devices can improve precision, consistency and objectivity of the applied movements and measurements [20–22].

Model-based evaluation of BoNT-A effects on joint hyper-resistance contributions have been applied using neuromechanical models [23–26]. These studies showed conflicting results on BoNT-A effects with either no change or a significant reduction of the reflexive resistance observed after injection. The neuromechanical modelling approaches used limited experimental datasets measured over the full range of motion (ROM), similar to current clinical measures. The subsequent joint resistance estimation primarily relies on a priori knowledge and simplifying assumptions. As a result, these methodologies are sensitive to incomplete model definitions and imperfect a priori knowledge [16, 17, 19]. Furthermore, the lack of a gold standard complicates interpretation of the reported conflicting results [5, 27, 28]. Given the conflicting results and lack of a gold standard, investigating fundamentally different approaches to assess joint hyper-resistance is of interest to improve understanding of BoNT-A effects.

An alternative approach to assess BoNT-A effects on joint hyper-resistance contributions is data-driven modelling. Data-driven modelling evaluation of BoNT-A effects

on joint hyper-resistance contributions could be executed using system identification [10, 15, 29, 30]. For example, the parallel-cascade (PC) system identification technique has shown the ability to discriminate spastic participants from controls and paretic from non-paretic joints [29, 31]. The PC technique has also shown good group-level responsiveness during the evaluation of several clinical treatments, like functional electrical stimulation-assisted walking, Tizanidine and robot-assisted gait training [32–34]. Currently, no system identification results have been reported on BoNT-A effects. Contrary to neuromechanical modelling, the system identification techniques previously tested in a clinical setting used rich experimental datasets measured over only a limited portion of the ROM [29–34]. As intrinsic and reflexive joint resistance depend on joint angle, the obtained joint resistance estimates do not characterize the full ROM [35].

The goal of this paper was to disentangle intrinsic and reflexive ankle joint resistance for participants treated with BoNT-A injections to reduce spasticity. We hypothesized that reflexive joint resistance decreases 6 weeks after injection, while returning close to baseline after 12 weeks [23, 24]. Due to the reduced reflexive joint resistance, we also expected the overall joint resistance to decrease 6 weeks after injection, while returning close to baseline after 12 weeks [6–8]. In absence of a gold standard, the joint resistance contributions were assessed using multiple joint resistance measures with different characteristics and limitations. Joint resistance contributions were estimated using clinical measures (MAS/Tardieu Scale) [9, 36], an instrumented spasticity test (SPAT) [21, 22] and a parallel-cascade (PC) system identification technique [10, 29]. To support validity of the measures used, the linear association between the various outcome measures was investigated.

6.2 Methods

6.2.1 Participants and Study Schedule

Six people with SCI and three stroke survivors participated in the study: age 54.4±11.1 yr, 2 women, see Table 6.1. The local medical ethics committe of the VU University Medical Center Amsterdam approved the study (Protocol ID: NL71757.029.19) and all participants provided written informed consent. Patients treated at the Sint Maartenskliniek, Nijmegen were assessed for eligibility by their rehabilitation physician. Inclusion criteria were: 1) adult, older than 18 yr; 2) stable neurological condition in chronic phase, minimum 6 months post-lesion/-stroke; 3) a MAS or Tardieu score ≥1 for any of the m. triceps surae; 4) treatment of any of the m. triceps surae with BoNT-A injections aimed at spasticity reduction; and 5) ROM of the affected ankle joint in the sagittal plane ≥20°. Participants were excluded if BoNT-A injections were combined with other treatments aimed at reducing spasticity. Note, included participants did typically receive the BoNT-A injections in combination with home stretching exercises in line with usual care. Participants gave written informed consent before definitive inclusion.

In this exploratory longitudinal study, ankle joint resistance was evaluated across three sessions: a baseline (week 0) measurement on the same day as BoNT-A injection and two post-intervention measurements at 6 and 12 weeks after BoNT-A injection. The week 12 evaluation was usually measured on the same day as a new BoNT-A injection, as BoNT-A injections were repeated every three months. In each session the clinical

Table 6.1: Participant demographic, clinical and BoNT-A injection characteristics (*N = 9*). The (most) affected side with a range of motion (ROM) $\geq 20^{\circ}$ was selected as measured side during experiments. Abbreviations: AIS: American Spinal Injury Association (ASIA) Impairment Scale; BoNT-A: Botulinum Neurotoxin type-A; GM: Gastrocnemius Medialis; GL: Gastrocnemius Lateralis; SCI: Spinal Cord Injury; SOL: Soleus; TP: Tibialis Posterior

Age	Gender	Diagnosis	Meas. side	Months post stroke/SCI	AIS (SCI)	BoNT-A injection	BoNT-A brand	BoNT-A dose per muscle (units)
54	M	Stroke (Ischaemic)	R	12		4^{th}	Dysport	GM (300); GL (300)
58	M	Stroke (Ischaemic)	L	69		5^{th}	Allergan	SOL (50); GM (50); GL (50)
49	M	Stroke (Hemorrhagic)	L	64		1^{st}	Dysport	SOL (400); GM (200); GL (200)
67	M	SCI (C5-C7)	L	30	D	8^{th}	Dysport	SOL (300)
62	F	SCI (T7-T12)	L	54	B	13^{th}	Dysport	SOL (400); GM (200) GL (200); TP (200)
29	M	SCI (T7-T12)	R	25	A	4^{th}	Dysport	SOL (200); GM (200); GL (100)
51	M	SCI (T7-T12)	R	183	C	3^{rd}	Dysport	SOL (300); GM (200); GL (200)
59	M	SCI (L1)	L	144	C	7^{th}	Dysport	SOL (150); GM (160); GL (160)
61	F	Cauda equina syndrome (L4-L5)	R	17		1^{st}	Dysport	SOL (300); GM (200) GL (200); TP (300)

Figure 6.1: Experimental Setup. Participants were seated on an adjustable chair for the instrumented evaluations. The manipulator connected to the adjustable chair applied dorsiflexion, ramp-and-hold perturbations around the ankle joint, while measuring the biomechanical response. If the left foot was measured, the right leg was supported with a right lower leg support inserted into the chair frame (not shown).

evaluation was executed by the same trained physiotherapist (non-blinded), whereas the instrumented evaluation was executed by a researcher using a robotic manipulator, see Fig. 6.1.

6.2.2 Instrumented Experimental Setup

The instrumented evaluations (SPAT and PC technique) were performed with participants seated on an adjustable chair, see Fig. 6.1. The (most) affected side in compliance with the inclusion/exclusion criteria was measured. The measured foot was placed on a rigid footplate and secured using Velcro straps. The rigid footplate was part of the robotic manipulator fixed onto the frame of the adjustable chair. The chair supported the participant's back and upper leg to achieve a fixed posture with 70° hip and 30° knee flexion. For each participant, the chair was adjusted to these hip and knee angles in the first session. For subsequent sessions, the chair was re-adjusted to the position of the first session to ensure constant posture across sessions. The ankle and manipulator axes of rotation were visually aligned by minimizing knee translation in the sagittal plane while rotating the footplate.

The robotic manipulator used a one degree-of-freedom actuator (MOOG, Nieuw-Vennep, the Netherlands) to apply the desired joint perturbations in the sagittal plane. Ankle angle and angular velocity were measured using an encoder situated at the actuator axis. Ankle torque was measured using a torque sensor placed between the actuator and footplate. The ankle angle, velocity and torque were recorded at 2048 Hz with the dorsiflexion direction defined as positive. For ankle angle, the neutral (0°) angle was determined using a goniometer at 0° dorsiflexion/plantarflexion. For safety, manipulator movement was restricted to the maximal ankle ROM, which was re-evaluated every

session, using adjustable hardware endstops. Measurements over full ROM (SPAT) were executed with a 2° margin at both endstops. Measurements over a limited ROM (PC technique) started 10° below the dorsiflexion endstop to avoid slack of the calf muscles. As ROM was re-evaluated every session, anatomical angles for both instrumented measurements could vary across sessions. At the start of each measurement, mean torque was measured over a 1 s period to determine the neutral (0 Nm) torque for that measurement.

6.2.3 Experimental Protocol

The same protocol was executed in all three sessions. A clinical evaluation was executed with participants lying supine on an examination table to obtain scores for the MAS (overall joint resistance) [9] and Tardieu Scale (reflexive joint resistance) [36]. During clinical evaluation, the knee was supported by a cushion to achieve 30° knee flexion, similar to the instrumented setup. For the MAS, the ankle joint was rotated three times over the full ROM in 1 s [9]. The MAS was scored on an ordinal six-point scale from 0, no increase in muscle tone, to 4, affected part(s) rigid in flexion or extension. For the Tardieu Scale, the ankle joint was rotated over the full ROM at three different velocities: V1, as slow as possible; V2, velocity approximately equal to limb falling under gravity; and V3, as fast as possible [36]. The quality (TS_Q) of the joint response was scored for all velocities on an ordinal five-point scale from 0, no resistance throughout the movement, to 4, infatigable clonus at a precise angle [36].

The instrumented SPAT evaluation consisted of two measurements at different velocities emulating V1 and V3 of the Tardieu Scale, see Fig. 6.2A [21, 22]. First, three slow (10°/s) dorsiflexion perturbations over the full ROM were applied. Second, three fast (150°/s) dorsiflexion perturbations over the full ROM were applied. At both velocities, repetitions were separated by 20 s of rest. The maximum dorsiflexion angle was held for 1 s before returning towards plantarflexion with an opposite profile to the dorsiflexion perturbation. Participants were instructed to relax and not respond to the perturbations.

The PC technique evaluation consisted of two measurement blocks (2 min) with 1 min rest in between. In each block, a series of small (2° amplitude) ramp-hold-return perturbations were continuously applied, see Fig. 6.2B [37]. These ramp-and-hold perturbations had a 125 °/s max. velocity, 15800 °/s^2 max. acceleration and 40 ms duration. Perturbations randomly switched between 'steps', i.e. the maximum dorsiflexion angle was held for 580 ms, and 'pulses', i.e. no hold period at the maximum dorsiflexion angle [38]. The manipulator returned towards plantarflexion with an opposite profile to the dorsiflexion perturbation. Participants were again instructed to relax and not respond to the perturbations.

6.2.4 Data Analysis

All data was analyzed using Matlab 2017b (Mathworks, Natick, MA, USA). For the instrumented SPAT, the work, i.e. product of force and displacement, around the ankle was used to quantify joint resistance [21, 22]. Work was computed as area under the torque-angle curve, ranging from 10% to 90% ROM. The torque-angle curve was corrected for gravitational effects of the footplate and foot. Work was computed as measure of: 1) intrinsic joint resistance from the slow velocity trials W_{slow}; 2) overall joint resistance

from the fast velocity trials W_{fast}; and 3) reflexive joint resistance from the difference between the fast and slow trials ΔW. All values of work were normalized for body weight (kg) and ROM. Due to a calibration issue, instrumented SPAT outcomes for the session at week 12 of one participant were removed.

For the PC technique, intrinsic and reflexive joint resistance parameters were estimated using a time-invariant algorithm modified from the original algorithm by Kearney *et al.* [10]. The algorithm consisted of the following steps:

1. The measured angle, velocity and torque signals were anti-alias filtered (2nd-order, 65.8 Hz, critically-damped) and downsampled to 146.3 Hz.
2. Measured acceleration was extracted from the state vector of the velocity low-pass filter and also downsampled to 146.3 Hz.
3. Non-parametric estimation of intrinsic, reflexive and voluntary torque contributions were obtained via an iterative procedure. Iterations continued until variance accounted for (%VAF) did not improve (<0.005%) or reached max. 10 iterations.
   (a) Residual intrinsic torque was computed by subtracting reflexive and voluntary torque from the net torque. (*1st-iteration*) Reflexive and voluntary torque were set to zero.
   (b) A 35 ms intrinsic impulse response function (IRF) was estimated using a correlation-based method between angle and residual intrinsic torque. A pseudo-inverse approach based on minimum description length was used to retain only significant terms [39].
   (c) Residual reflexive torque was computed by subtracting voluntary and intrinsic torque, i.e. the convolved intrinsic IRF with angle, from the net torque.
   (d) A 650 ms reflexive IRF was estimated between half-wave rectified velocity and residual reflexive torque using the same correlation-based method.
   (e) Residual voluntary torque was computed by subtracting intrinsic and reflexive torque, i.e. the convolved reflexive IRF with half-wave rectified velocity, from net torque.
   (f) Voluntary torque was estimated as the low-pass filtered (2nd-order, 0.5 Hz, Butterworth) residual voluntary torque.
4. The intrinsic inertia I (acceleration-component), damping B (velocity-component) and stiffness K (angle-component) were estimated using linear least squares between acceleration, velocity and angle, and intrinsic torque.
5. The reflexive IRF was fit between half-wave rectified velocity and reflexive torque with both signals low-pass filtered (2nd-order, 14.6 Hz, critically-damped).
6. The reflexive delay δ was estimated via a grid search (35 to 65 ms, 1 ms increments), coupled to a nonlinear least squares fit on the reflexive IRF of reflexive gain G, damping ζ and frequency ω.

6.2.5 Statistical Analysis

The statistical analysis was performed using Matlab 2017b and R3.6.2 (R Foundation for Statistical Computing, Vienna, Austria). The outcome measures included two clinical measures (MAS, TS_Q), three instrumented SPAT measures (W_{fast}, ΔW, W_{slow}) and three PC technique measures (G, K, B). TS_Q was evaluated based on the highest

velocity (V3) assessment of the Tardieu Scale only, as this velocity was closest to the instrumented evaluations.

On an individual level, the hypothesized longitudinal BoNT-A effects were evaluated by comparing the measured resistance between baseline and week 6, as well as between week 6 and week 12. For each outcome measure, we considered the hypothesized BoNT-A effect observed, if a reduced resistance compared to baseline was measured at week 6 in combination with a return towards baseline at week 12. On a group-level, the hypotheses on the longitudinal BoNT-A effects were evaluated using the Friedman non-parametric one-way repeated measures analysis for all outcome measures [26]. Post-hoc multiple comparison tests between sessions were executed for significant Friedman test results. For each multiple comparison, p-values were adjusted using the Bonferonni correction. Significance level was set at α=0.05.

To support reliability of the longitudinal BoNT-A evaluation, repeatability of the instrumented measures was assessed using the intraclass correlation coefficient (ICC) [40]. ICCs were computed with a two-way mixed effects model, assessing absolute agreement between single repetitions. ICC robustness was investigated using the 95% confidence interval (CI) constructed via a non-parametric bootstrap procedure using the bias corrected and accelerated (BCa) method [41].

Validity of the outcome measures was assessed based on linear associations. We expected strong ($r > 0.7$) linear associations between outcome measures estimating the same contribution, i.e. between the overall measures (MAS, W_{fast}), the reflexive measures (TS_Q, ΔW, G) and the intrinsic measures (W_{slow}, K, B). Furthermore, we expected no or weak linear associations between outcome measures estimating different contributions. The non-parametric Spearman's rank correlation coefficient ρ was used for associations involving the ordinal clinical measures. Pearson's correlation coefficient r was used for associations involving only instrumented measures. Robustness of ρ and r were investigated using the 95% CI based on a BCa bootstrap procedure.

6.3 Results

We investigated BoNT-A effects on the intrinsic and reflexive contributions to ankle joint hyper-resistance in nine participants at three sessions: week 0 (T0), 6 (T1) and 12 (T2) after BoNT-A injection. Joint resistance was assessed using common clinical measures, i.e. MAS, Tardieu Scale (TS_Q), an instrumented SPAT (W_{fast}, ΔW, W_{slow}) and PC system identification technique (G, K, B).

6.3.1 Qualitative Analysis of Instrumented Measures

The reflexive response elicited during the instrumented evaluation strongly varied between participants. For example, some participants showed a clear reflexive response in both instrumented measures, whereas other participants showed a small or no reflexive response, see Fig. 6.2A/C. This heterogeneity in the reflexive response was observed both before and after BoNT-A injection, see Fig. 6.2D/E. For the instrumented SPAT, the reflexive response was mainly present in the part of the ROM close to maximum dorsiflexion, see dark-shaded area Fig. 6.2A. For the PC technique, the reflexive response was observed 100-300 ms after each dorsiflexion perturbation, see Fig. 6.2C/E.

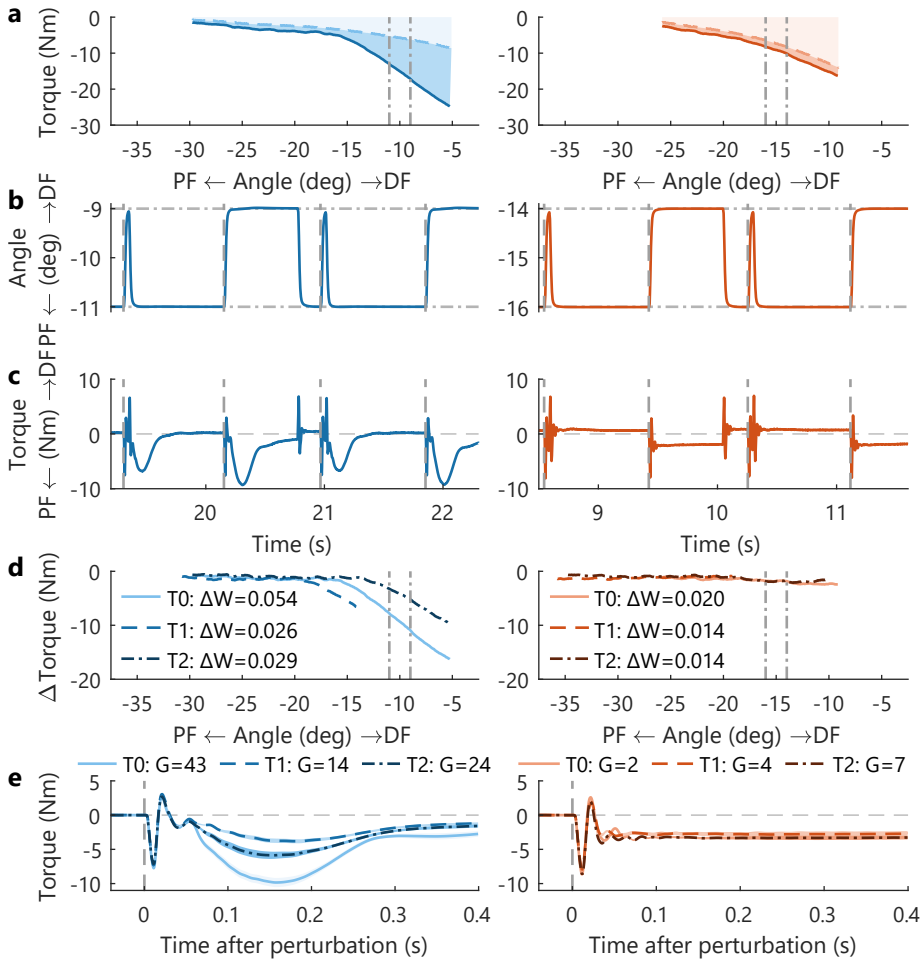

Figure 6.2: Instrumented assessment for two representative participants with a clear (*left*) and little (*right*) reflexive response. *(A)* Ensemble averaged (3 repetitions) torque-angle curves for the instrumented SPAT at both slow *(dashed line)* and fast *(solid line)* velocity at week 0 (T0). The work delivered by the ankle joint is highlighted for the slow velocity trial *(light-shaded area)* and difference between fast and slow velocity trials *(dark-shaded area)*. The instrumented SPAT was analyzed from 10-90% ROM with the limited ROM used for the PC technique demarcated *(dash-dotted verticals)*. *(B)* Four consecutive dorsiflexion perturbations *(onset at dashed verticals)* used for the PC technique at week 0 (T0). Perturbation signals were randomly generated, hence the different time-axes used to visualize a similar sequence of pulse and step perturbations. *(C)* The subsequent ankle joint response, measured as torque, elicited through each dorsiflexion perturbation. *(D)* Ensemble averaged difference in torque between the fast and slow velocity SPAT at each session: week 0 (T0), 6 (T1) and 12 (T2) after BoNT-A injection. Torque differences were computed by interpolating the slow velocity torque data onto the exact angles measured in the fast velocity dataset. *(E)* Ensemble averaged (±SD, single measurement block) torque response at each session. The torque ensemble averages were created by aligning all step perturbations at the perturbation onset *(dashed verticals)*. The reflexive gain G (Nm·s/rad) shows the quantified reflexive contribution at each session. To enhance visualization, torque ensembles were normalized to zero torque at perturbation onset.

The observed intrinsic response also varied between participants. For the instrumented SPAT, variation of the intrinsic response was seen over the full ROM, see light-shaded area Fig. 6.2A. For the PC technique, variation of the intrinsic response was visible in the sustained plantarflexion torque response after step perturbations (i.e. a 580 ms hold period at maximum dorsiflexion), see Fig. 6.2C. This spring-like behavior around the joint, especially visible in the absence of a reflexive response, was interpreted as the elastic intrinsic resistance, i.e. intrinsic stiffness.

6.3.2 Longitudinal Evaluation of BoNT-A Injections

The longitudinal evaluation of the BoNT-A effect on joint resistance showed a heterogeneous response across all participants, see Fig. 6.3 and Table 6.2. For overall joint resistance, the MAS showed a reduced resistance in 6 of 9 participants at T1 with 5 out of these 6 participants returning to baseline value at T2. The instrumented SPAT overall resistance measure (W_{fast}) only showed reduced resistance in 4 participants at T1 with 2 out of these 4 participants returning towards baseline value at T2. On average, both MAS and W_{fast} showed a reduced resistance at T1 with MAS returning close to baseline at T2, whereas W_{fast} showed a further reduction. Only the MAS showed the hypothesized longitudinal BoNT-A effect on a group-level ($\chi^2[2] = 6.91$, $p = 0.03$), with post-hoc comparisons showing a significant reduction between T0 and T1 (t = 2.41, $p = 0.05$). The ROM over which the instrumented assessments were measured changed across sessions in 5 participants. For 2 participants the dorsiflexion ROM was reduced (10°) at T1, whereas for 3 participants the full ROM shifted (10°) either towards dorsiflexion (2 participants) or plantarflexion (1 participant). The changes in ROM remained at T2 for 3 participants, whereas 2 participants had a ROM in T2 equal to T0.

For reflexive joint resistance, the Tardieu Scale (TS_Q) showed a reduced resistance in 4 participants with 2 of 4 out of these participants returning to baseline value at T2, see Fig. 6.3 and Table 6.2. Regarding the instrumented measures a reduction in reflexive resistance at T1 was observed in: 5 participants for ΔW, 6 participants for G, and 3 participants for both G and ΔW. Out of these participants with reduced resistance at T1, an increase towards baseline value at T2 was observed in: 1 of 5 participants for ΔW, 4 of 6 participants for G, and 1 of 3 participants for both G and ΔW. The participants that did not show a reduction in G at T1 had the lowest values for G at baseline, see Fig. 6.3. Combined with the MAS, 4 participants showed reduced resistance at T1 for both MAS and ΔW and 3 participants showed a reduction for both MAS and G. On average, all reflexive resistance measures showed a reduction at T1 with both TS_Q and G returning towards baseline at T2, whereas ΔW showed a further reduction. A significant longitudinal BoNT-A effect on reflexive resistance was only found for the ΔW ($\chi^2[2] = 11.9$, $p = 0.003$), although post-hoc comparisons did not find any significant differences between sessions.

For intrinsic joint resistance, a reduced resistance at T1 was observed in: 3 participants for W_{slow}, 5 participants for K, and 3 participants for both K and W_{slow}, see Fig. 6.3 and Table 6.2. Out of these participants with reduced resistance at T1, an increase towards baseline value at T2 was observed in: 2 of 3 participants for W_{slow}, 3 of 5 participants for K, and 2 of 3 participants for both K and W_{slow}. On average, both intrinsic resistance measures showed a reduction at T1 with W_{slow} returning towards

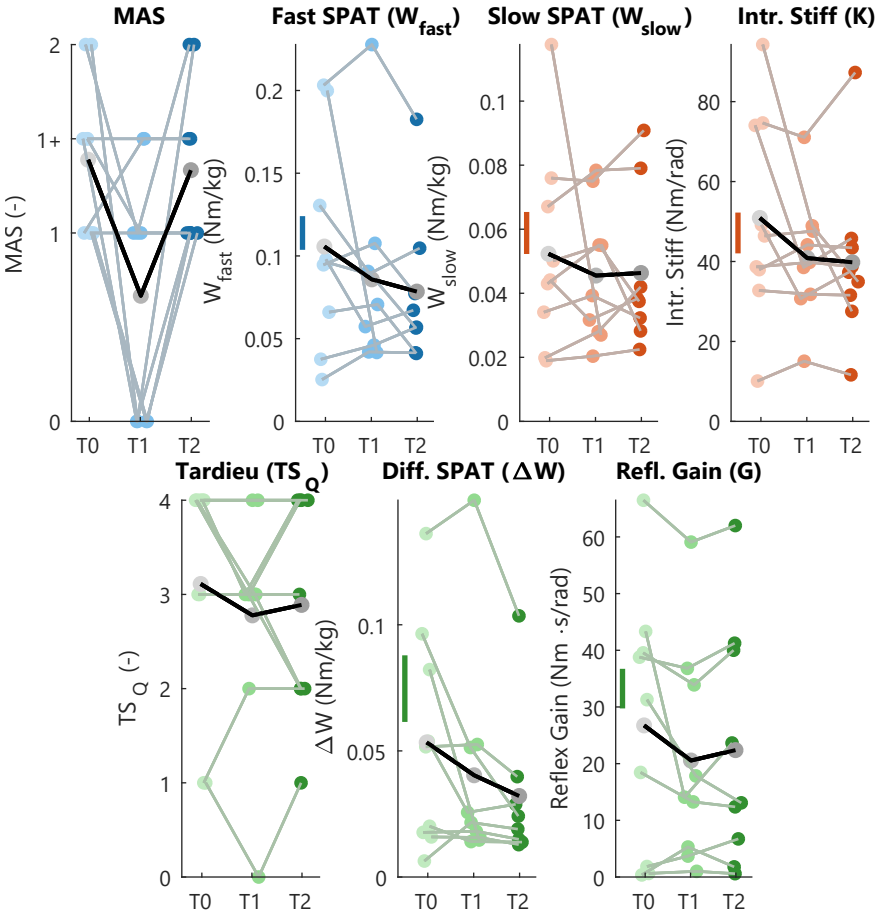

Figure 6.3: Longitudinal BoNT-A effect on joint resistance contributions for all participants. The quantified joint resistance contributions are shown for each participant *(lines)* at each session *(dots)*: week 0 *(T0, light)*, week 6 *(T1,medium)* and week 12 *(T2, dark)*. The mean values across all participants is shown at each session *(grey dots, bold black lines)*. The BoNT-A effect on overall joint resistance is shown for the MAS (clinical) and W_{fast} (SPAT) *(blue)*. The BoNT-A effect on intrinsic resistance is shown for *(red)*: W_{slow} (SPAT) and intrinsic stiffness (K, PC). Finally, the BoNT-A effect on reflexive resistance is shown for *(green)*: the Tardieu Scale (TS_Q, clinical), ΔWork (SPAT) and reflexive gain (G, PC). The best-case minimal detectable difference (MDD) *(vertical line)* is depicted for reference, see Supplementary Table D.1.

baseline at T2 and K showing a further reduction. No significant longitudinal BoNT-A effect on intrinsic resistance was found.

6.3.3 Linear Associations and Repeatability of Joint Resistance Measures

Excellent ICC values were observed for both the instrumented SPAT ($r = [0.98, 0.94, 0.97]$) and PC technique ($r = [0.98, 0.97, 0.99]$) measures, see Table 6.4. The 95% CIs lower bounds did show relatively high uncertainty for ΔW (0.88), W_{slow} (0.89) and K (0.87).

Table 6.2: Pre- and post-BoNT-A injection outcome measures for the intrinsic and reflexive contributions to ankle joint resistance *(N = 9)* The median [25th,75th percentile] across participants are reported. Longitudinal differences across all sessions were evaluated using the Friedman test. Significant Friedman tests (ΔW, MAS) were investigated using a multiple comparisons test adjusted with the Bonferonni correction. Sessions with a significant difference compared with week 0 are indicated (*).

	T0 (Week 0)	**T1 (Week 6)**	**T2 (Week 12)**	**Friedman test**
MAS (-)	1.5 [1,1.6]	1 [0,1.1]*	1 [1,1.6]	p = **0.03**
Fast SPAT W_{fast} (Nm/kg)	0.096 [0.059,0.148]	0.071 [0.045,0.095]	0.062 [0.049,0.091]	p = 0.48
Tardieu TS_Q (-)	4 [2.5 4]	3 [2.75,3.25]	3 [2,4]	p = 0.52
Diff. SPAT ΔW (Nm/kg)	0.052 [0.017,0.086]	0.022 [0.015,0.052]	0.022 [0.014,0.034]	p = **0.003**
Refl. Gain G (Nm·s/rad)	31 [1.5,40]	14 [4.9,35]	13 [5.5,40]	p = 0.31
Slow SPAT W_{slow} (Nm/kg)	0.044 [0.031,0.069]	0.039 [0.028,0.060]	0.038 [0.030,0.061]	p = 0.26
Intr. Stiffness K (Nm/rad)	46 [37,74]	40 [32,48]	37 [31,44]	p = 0.67

Table 6.3: Spearman's/Pearson's correlation coefficients and their 95% confidence intervals *(N = 26-27)* Correlations between the clinical measures (MAS, TS_Q), instrumented SPAT (W_{fast}, ΔW, W_{slow}) and PC technique measures (reflexive gain G, intrinsic stiffness K and intrinsic damping B). Spearman's rank correlation coefficient ρ was used for all correlations involving the ordinal clinical measures, whereas Pearson's correlation coefficient r was used otherwise. The 95% CIs were constructed using a non-parametric BCa bootstrap procedure.

	MAS	**Tardieu TS_Q**	**Refl. Gain G**	**Intr. Stiffness K**	**Intr. Damping B**
Fast SPAT W_{fast}	0.05 [-0.38,0.40]	0.24 [-0.22,0.61]	0.73 [0.48,0.87]	0.46 [0.16,0.78]	0.83 [0.73,0.90]
Diff. SPAT ΔW	-0.01 [-0.42,0.41]	0.60 [0.23,0.81]	0.86 [0.71,0.93]	0.17 [-0.15,0.51]	0.72 [0.43,0.86]
Refl. Gain G	-0.08 [-0.48,0.33]	0.57 [0.21,0.80]			
Slow SPAT W_{slow}	-0.03 [-0.44,0.40]	-0.09 [-0.50,0.31]	0.27 [-0.12,0.59]	0.74 [0.39,0.90]	0.71 [0.41,0.83]
Intr. Stiffness K	-0.20 [-0.62,0.27]	-0.07 [-0.44,0.40]			
Intr. Damping B	-0.04 [-0.46,0.36]	0.38 [-0.07,0.67]			

Table 6.4: Intraclass correlation coefficient (ICC) and their 95% confidence intervals *(N = 54/78)* ICCs for the instrumented assessment based on three repetitions per session for the instrumented SPAT and two repetitions per session for the PC technique. The 95% CIs were constructed using a non-parametric bootstrap procedure.

Outcome Measure	ICC
Fast SPAT W_{fast}	0.98 [0.96,1.00]
Diff. SPAT ΔW	0.94 [0.88,0.98]
Refl. Gain G	0.98 [0.97,0.99]
Slow SPAT W_{slow}	0.96 [0.89,0.99]
Intr. Stiffness K	0.97 [0.87,1.00]
Intr. Damping B	0.99 [0.97,1.00]

The reported ICCs represent a best-case scenario for optimal experimental conditions, as only short 20-60 s breaks were included between repetitions and participants were not taken out of the instrumented setup between repetitions.

Most clinical and instrumented assessments quantifying the same resistance contribution showed a positive correlation as expected, see Table 6.3. For overall resistance, the MAS was not correlated with the SPAT W_{fast} (r = 0.05). For the reflexive resistance, the Tardieu Scale showed a moderate positive correlation with the instrumented measures ΔW and G (r = 0.60/0.57), whereas both instrumented measures showed a strong correlation (r = 0.86). For the intrinsic resistance, the SPAT W_{slow} showed a strong correlation with both PC technique outcomes of stiffness K (r = 0.74) and damping B (r = 0.71).

Most clinical and instrumented assessments quantifying a different resistance contribution were not correlated as expected, see Table 6.3. For the overall resistance, MAS was not correlated with intrinsic/reflexive measures (r = [-0.19,-0.01]), whereas the SPAT W_{fast} did show strong correlation with the PC reflexive gain G and intrinsic damping B. For the reflexive resistance, the Tardieu Scale was not or weakly correlated with non-reflexive measures (r = [-0.09,0.38]). The reflexive gain G showed strong correlation with SPAT W_{fast} and the SPAT ΔW showed strong correlation with PC intrinsic damping G. For the intrinsic resistance, only PC technique intrinsic damping B showed strong correlations as reported above.

6.4 Discussion

This paper studied the intrinsic and reflexive ankle joint resistance within participants treated with BoNT-A injections to reduce spasticity. We hypothesized that both reflexive and overall joint resistance would decrease 6 weeks after BoNT-A injection, while returning close to baseline value after 12 weeks. Three fundamentally different joint resistance assessments were used: 1) clinical tests (MAS, Tardieu Scale); 2) instrumented SPAT measured over the full ROM with elementary processing; and 3) data-driven PC system identification measured over a limited ROM with model-based processing. Individually, the hypothesized BoNT-A effect (reduction at week 6, return to baseline week 12) was observed in the MAS (5 participants), W_{fast} SPAT (2 participants), Tardieu Scale (2

participants), ΔW SPAT (1 participant) and G (4 participants). On a group-level, our hypothesis was only confirmed for the MAS, a measure of overall joint resistance, which showed a significant reduced resistance at week 6. Regarding validity, all instrumented outcome measures showed a strong correlation when quantifying the same resistance contribution.

6.4.1 Longitudinal Evaluation of BoNT-A Injections

On a group-level, only the MAS showed the hypothesized effect of reduced joint resistance at week 6 with a return close to baseline at week 12. Our MAS results are in line with larger clinical trials evaluating BoNT-A effects with the MAS [6–8]. The MAS should be interpreted with care as the scale is subjective and a non-blinded rater scored the participants [14, 42]. Contrary to the MAS, all instrumented measures showed a more heterogeneous response and did not capture a significant reduction on a group-level 6 weeks after injection. Previous studies using instrumented measures to investigate BoNT-A effects over the full ROM also reported heterogeneity between participants [23–26]. For these instrumented assessment studies, mixed results were reported 4-6 weeks after injection. The studies executed with a device assessing the wrist (Neuroflexor) and estimating resistance components using a biomechanical wrist model with low complexity did report a reduced reflexive response. The study executed with a device assessing the ankle (MOOG manipulator, similar to our study) and estimating resistance with a neuromechanical ankle model with higher complexity did not report a reduction. Therefore, differences in the reported results may be influenced by participant heterogeneity, the experimental setup, the assessed joint and the model used for resistance estimation.

The heterogeneous response among the study population complicated group-level evaluation of the BoNT-A effect. For example, the PC technique showed a reflex reduction in 6 of 9 participants at week 6. The 3 participants without reflex reduction had the lowest reflexive response at baseline. Therefore, these 3 participants had little potential to further reduce the reflexive response and also limited a potential group effect. These 3 participants also had a relatively limited dorsiflexion ROM at baseline and 2 of these 3 participants showed an improved dorsiflexion ROM at week 6. As such, BoNT-A injections may result in better outcomes within people with high reflexive activity and/or clonus than people with only high resistance to passive joint motion. Interpretation of the population heterogeneity was also convoluted by different outcomes for the instrumented measures. A reflex reduction was observed in 5 participants for the SPAT and 6 participants for the PC technique, yet only 3 participants showed a reduction in both outcome measures. As the reflexive response depends on joint angle and ROM, the full and limited ROM used during assessments could potentially explain these differences [35, 43]. Both methods simplified this complex dependency through averaging over the full ROM (SPAT) or assessing a limited ROM (PC). As a result, neither method controlled for variations in the reflexive response due to observed changes in ROM and potential underlying changes in e.g. muscle slack length. Quantitative analysis of the measured individual effects is desired to increase understanding of the heterogeneous response.

Quantitative analysis of individual effects would require a larger participant group and insight into the minimal detectable difference (MDD), which have currently not

been reported yet. To illustrate such an analysis, the PC technique showed a reflex reduction larger than a best-case scenario MDD (6.9 Nm·s/rad) for 3 of 9 participants at week 6. Only best-case scenario MDDs could be computed as experimental conditions were optimal regarding repeatability. Clinically relevant MDDs would require a test-retest reliability design with longer breaks between repetitions, measurements on separated days and removing participants from the measurement device between repetitions [18, 27, 44]. The best-case results did indeed show that both instrumented SPAT and PC technique had excellent ICC between r = [0.94,0.99], whereas typically reported values are between r = [0.85,0.95] for similar instrumented measures [18, 27, 44–46]. Overall, the BoNT-A effect on the reflexive contributions remains ambiguous.

6.4.2 Linear Associations of Joint Resistance Measures

In absence of a gold standard, the validity of the instrumented measures was shown through linear association between the methodologies [5, 27, 28]. As expected, most measures quantifying the same resistance contribution (e.g. ΔW and G) showed moderate to strong correlations. Strong correlations were observed between the instrumented measures, whereas a similar study found moderate similarity between two instrumented measures [28]. However, Andringa *et al.* [28] compared methodologies using a different experimental setup (Neuroflexor and Wristalyzer) and different data processing approaches (low complexity biomechanical and higher complexity neuromechanical model) [17, 47]. In our study, the results were obtained using the same device, which may explain part of the relatively strong correlations observed.

Only between the MAS and SPAT (W_{fast}), both measures of overall joint resistance, no correlation was observed. While both measures compute an overall resistance effect, the characteristics of the applied perturbation differed between the slow velocity (MAS) and fast velocity (SPAT, W_{fast}). Changing perturbation characteristics could affect the relative magnitude of the intrinsic and reflexive contributions within the measured overall response, as both contributions contain velocity- and acceleration-dependent components [10, 48, 49]. Therefore, the lack of association between MAS and fast velocity SPAT could potentially be explained by the different perturbation profiles used.

Besides, a general lack of correlation was observed across joint resistance measures quantifying a different resistance contributions, although unexpected correlations were observed between a couple of outcome measures. The reflexive measures of the instrumented SPAT (ΔW) did show a strong correlation with the intrinsic damping (viscous) contribution of the PC technique (B). Note, the reflexive instrumented SPAT measure was computed as the difference in work between a fast and slow passive movement. Thus, ΔW was considered fully velocity-dependent, which can be attributed to either a reflexive or viscous intrinsic contribution [10]. This could explain the observed commonality with intrinsic damping of the PC technique. The commonality of the reflexive SPAT measures with an intrinsic outcome measure illustrated that the separation of joint resistance contributions could be improved. On the one hand, additional information from an extended experimental dataset might improve the ability to disentangle joint resistance. On the other hand, detailed model-based processing, such as neuromechanical models or data-driven processing, could improve the ability to disentangle joint resistance [10, 23–26]. Andringa *et al.* [28] did show that despite the use of these

type of neuromechanical models, weak correlations between reflexive and intrinsic contribution may remain. Overall, at group-level the quantified intrinsic and reflexive resistance outcome measures matched well, supporting the validity towards clinical application.

6.4.3 Study Limitations and Clinical Application

First, the clinical evaluations in this study were all performed by a non-blinded, trained physiotherapist. Therefore, knowledge of the hypotheses of this study combined with information about the specific session (week 0, 6 or 12) could have biased the MAS and Tardieu Scale scores. Second, spasticity is a complex symptom, which can manifest itself differently within a the passive experimental environment compared with an active or functional environment [4]. Therefore, BoNT-A effects as experienced in daily life and functional tasks may not necessarily be captured in the clinical and instrumented assessments used. In addition, the full complexity of spasticity is difficult to capture within the limited number of participants included in the study. Third, a low reflexive resistance magnitude at baseline before BoNT-A injection was observed in 3 participants, which limited their potential to show a reflex reduction. Scientifically, future studies evaluating longitudinal BoNT-A effects could avoid this limitation by determining a threshold magnitude, e.g. based on MDD, for inclusion of participants in the data analysis. Clinically, these 3 participants illustrate the relevance of adding instrumented measures to enable differentiation between patients with similar MAS values in support of clinical decision making. Fourth, the instrumented evaluations were limited due to natural variations in the ROM shown by multiple participants across sessions. Small variations in ROM were exacerbated in our protocol, because the adjustable hardware endstops restricting manipulator movement for safety could only be adjusted per 10°. For both instrumented measures, variability in the ROM likely translated to additional variability in outcome measures across sessions, as joint resistance depends on joint angle and ROM [35, 43]. Due to simplification in both instrumented measures, the added variability of the ROM could not be controlled for, which reduced the ability to detect BoNT-A effects.

Despite these limitations and heterogeneous results, clinical studies of instrumented measures disentangling joint resistance contributions remain important. First, our results again confirm that the MAS, on which many clinical evaluations of BoNT-A effects are based, does not correlate well with instrumented measures specifically aimed at quantifying the reflexive joint resistance or spasticity. Second, further research into the diagnostic properties of the instrumented measures is of interest to potentially support clinical decision making. For example, previous studies showed that the PC technique could discriminate spastic participants from controls and paretic from non-paretic joints [29, 31]. Towards clinical application, additional investigation into diagnostic properties like the reliability (MDD) and normative data are desired to enable clinical decision making based on the quantified joint resistance contributions. In addition, investigating the relation between instrumented measures and functional outcomes is important given the lack of a gold standard to evaluated the instrumented measures against.

6.5 Conclusions

Our group-level hypothesis of a reduced joint resistance 6 weeks after injection with a return close to baseline at week 12 was only observed in the MAS (overall joint resistance). This observed reduction could not be attributed to an unambiguous group-level reduction of the reflexive or intrinsic resistance as no instrumented measures confirmed the hypothesis. Several individuals did show the hypothesized BoNT-A effect in the reflexive or intrinsic contributions. A moderate to strong correlation between all reflexive measures and a strong correlation between the intrinsic measures supported the validity of the used instrumented measures. Ultimately, objective and reliable joint resistance quantification would improve clinical decision making in prescription of BoNT-A and unravel the effect of BoNT-A injections on spasticity.

References

[1] E. C. Davis and M. P. Barnes, "Botulinum Toxin and Spasticity," *Journal of Neurology Neurosurgery and Psychiatry*, 69(2), pp. 143–147, 2000. doi: 10.1136/jnnp.69.2.143.

[2] A. Brashear and K. Lambeth, "Spasticity," *Current Treatment Options in Neurology*, 11(3), pp. 153–161, 2009. doi: 10.1007/s11940-009-0018-4.

[3] E. Chang, N. Ghosh, D. Yanni, S. Lee, *et al.*, "A Review of Spasticity Treatments: Pharmacological and Interventional Approaches," *Critical Reviews in Physical and Rehabilitation Medicine*, 25(1-2), pp. 11–22, 2013. doi: 10.1615/CritRevPhysRehabilMed.2013007945.

[4] V. Dietz and T. Sinkjær, "Spastic Movement Disorder: Impaired Reflex Function and Altered Muscle Mechanics," *Lancet Neurology*, 6(8), pp. 725–733, 2007. doi: 10.1016/S1474-4422(07)70193-X.

[5] J. C. van den Noort, L. Bar-On, E. Aertbeliën, M. Bonikowski, *et al.*, "European Consensus on the Concepts and Measurement of the Pathophysiological Neuromuscular Responses to Passive Muscle Stretch," *European Journal of Neurology*, 24(7), pp. 981–991, 2017. doi: 10.1111/ene.13322.

[6] L. Shaw, H. Rodgers, C. Price, F. van Wijck, *et al.*, "BoTULS. A Multicentre Randomised Controlled Trial to Evaluate the Clinical Effectiveness and Cost-effectiveness of Treating Upper Limb Spasticity due to Stroke with Botulinum Toxin Type A," *Health Technology Assessment*, 14(26), 2010. doi: 10.3310/hta14260.

[7] J. A. Baker and G. Pereira, "The Efficacy of Botulinum Toxin A for Spasticity and Pain in Adults. A Systematic Review and Meta-Analysis using the Grades of Recommendation, Assessment, Development and Evaluation Approach," *Clinical Rehabilitation*, 27(12), pp. 1084–1096, 2013. doi: 10.1177/0269215513491274.

[8] J.-M. Gracies, A. Brashear, R. Jech, P. McAllister, *et al.*, "Safety and Efficacy of AbobotulinumtoxinA for Hemiparesis in Adults with Upper Limb Spasticity after Stroke or Traumatic Brain Injury: A Double-Blind Randomised Controlled Trial," *The Lancet Neurology*, 14(10), pp. 992–1001, 2015. doi: 10.1016/S1474-4422(15)00216-1.

[9] R. W. Bohannon and M. B. Smith, "Interrater Reliability of a Modified Ashworth Scale of Muscle Spasticity," *Physical Therapy*, 67(2), pp. 206–207, 1987. doi: 10.1093/ptj/67.2.206.

[10] R. E. Kearney, R. B. Stein, and L. Parameswaran, "Identification of Intrinsic and Reflex Contributions to Human Ankle Stiffness Dynamics," *IEEE Transactions on Biomedical Engineering*, 44(6), pp. 493–504, 1997. doi: 10.1109/10.581944.

[11] J. F. M. Fleuren, G. E. Voerman, C. V. Erren-Wolters, G. J. Snoek, *et al.*, "Stop using the Ashworth Scale for the assessment of Spasticity," *Journal of Neurology, Neurosurgery and Psychiatry*, 81, pp. 46–52, 2010. doi: 10.1136/jnnp.2009.177071.

[12] R. T. Katz and W. Z. Rymer, "Spastic Hypertonia: Mechanisms and Measurement," *Archives of Physical Medicine and Rehabilitation*, 70(2), pp. 144–155, 1989.

[13] J. A. Burne, V. L. Carleton, and N. J. O'Dwyer, "The Spasticity Paradox: Movement Disorder or Disorder of Resting Limbs?" *Journal of Neurology, Neurosurgery and Psychiatry*, 76(1), pp. 47–54, 2005. doi: 10.1136/jnnp.2003.034785.

[14] A. D. Pandyan, G. R. Johnson, C. I. M. Price, R. H. Curless, *et al.*, "A Review of the Properties and Limitations of the Ashworth and Modified Ashworth Scales as Measures of Spasticity," *Clinical Rehabilitation*, 13(5), pp. 373–383, 1999. doi: 10.1191/026921599677595404.

[15] F. C. T. van der Helm, A. C. Schouten, E. de Vlugt, and G. G. Brouwn, "Identification of Intrinsic and Reflexive Components of Human Arm Dynamics during Postural Control," *Journal of Neuroscience Methods*, 119(1), pp. 1–14, 2002. doi: 10.1016/S0165-0270(02)00147-4.

[16] E. de Vlugt, J. H. de Groot, K. E. Schenkeveld, J. H. Arendzen, *et al.*, "The Relation between Neuromechanical Parameters and Ashworth Score in Stroke Patients," *Journal of Neuroengineering and Rehabilitation*, 7:35, 2010. doi: 10.1186/1743-0003-7-35.

[17] P. G. Lindberg, J. Gäverth, M. Islam, A. Fagergren, *et al.*, "Validation of a New Biomechanical Model to Measure Muscle Tone in Spastic Muscles," *Neurorehabilitation and Neural Repair*, 25(7), pp. 617–625, 2011. doi: 10.1177/1545968311403494.

[18] L. H. Sloot, M. M. van der Krogt, K. L. de Gooijer-van de Groep, S. van Eesbeek, *et al.*, "The Validity and Reliability of Modelled Neural and Tissue Properties of the Ankle Muscles in Children with Cerebral Palsy," *Gait and Posture*, 42(1), pp. 7–15, 2015. doi: 10.1016/j.gaitpost.2015.04.006.

[19] R. Wang, P. A. Herman, Ö. Ekeberg, J. Gäverth, *et al.*, "Neural and non-neural related properties in the spastic wrist flexors: An optimization study," *Medical Engineering and Physics*, 47, pp. 198–209, 2017. doi: 10.1016/j.medengphy.2017.06.023.

[20] G. E. Voerman, J. H. Burridge, R. A. Hitchcock, and H. J. Hermens, "Clinometric Properties of a Clinical Spasticity Measurement Tool," *Disability and Rehabilitation*, 29(24), pp. 1870–1880, 2007. doi: 10.1080/09638280601143752.

[21] L. Bar-On, E. Aertbeliën, H. Wambacq, D. Severijns, *et al.*, "A Clinical Measurement to Quantify Spasticity in Children with Cerebral Palsy by Integration of Multidimensional Signals," *Gait and Posture*, 38(1), pp. 141–147, 2013. doi: 10.1016/j.gaitpost.2012.11.003.

[22] L. H. Sloot, L. Bar-On, M. M. van der Krogt, E. Aertbeliën, *et al.*, "Motorized versus Manual Instrumented Spasticity Assessment in Children with Cerebral Palsy," *Developmental Medicine and Child Neurology*, 59(2), pp. 145–151, 2017. doi: 10.1111/dmcn.13194.

[23] J. Gäverth, A.-C. Eliasson, K. Kullander, J. Borg, *et al.*, "Sensitivity of the NeuroFlexor Method to Measure Change in Spasticity after Treatment with Botulinum Toxin A in Wrist and Finger Muscles," *Journal of Rehabilitation Medicine*, 46(7), pp. 629–634, 2014. doi: 10.2340/16501977-1824.

[24] R. Wang, J. Gäverth, and P. A. Herman, "Changes in the Neural and Non-Neural Related Properties of the Spastic Wrist Flexors after Treatment with Botulinum Toxin A in Post-Stroke Subjects: An Optimization Study," *Frontiers in Bioengineering and Biotechnology*, 6:73, 2018. doi: 10.3389/fbioe.2018.00073.

[25] K. L. de Gooijer-van de Groep, C. G. M. Meskers, E. de Vlugt, J. H. Arendzen, *et al.*, "Estimating the Effects of Botulinum Toxin A Therapy Post-Stroke. Evidence for Reduction of Background Muscle Activation," in *Identification of Neural and Non-Neural Contributors to Joint Stiffness in Upper Motor Neuron Disease*, Leiden, Netherlands: Leiden University Medical Center (LUMC), 2019, ch. 6, pp. 119–136.

[26] A. Andringa, E. van Wegen, I. van de Port, L. Guit, *et al.*, "The Effect of Botulinum Toxin-A on Neural and Non-neural Components of Wrist Hyper-Resistance in Adults with Stroke or Cerebral Palsy," *PM&R: The Journal of Injury, Function and Rehabilitation*, 14, pp. 486–495, 2022. doi: 10.1002/pmrj.12602.

[27] A. Andringa, E. van Wegen, I. van de Port, and G. Kwakkel, "Measurement Properties of the NeuroFlexor Device for Quantifying Neural and Non-neural Components of Wrist Hyper-Resistance in Chronic Stroke," *Frontiers in Neurology*, 10:730, 2019. doi: 10.3389/fneur.2019.00730.

[28] A. Andringa, C. G. M. Meskers, I. van de Port, S. Zandvliet, *et al.*, "Quantifying Neural and Non-neural Componenets of Wrist Hyper-resistance after Stroke: Comparing Two Instrumented Assessment Methods," *Medical Engineering & Physics*, 98, pp. 57–64, 2021. doi: 10.1016/j.medengphy.2021.10.009.

[29] M. M. Mirbagheri, H. Barbeau, M. Ladouceur, and R. E. Kearney, "Intrinsic and Reflex Stiffness in Normal and Spastic, Spinal Cord Injured Subjects," *Experimental Brain Research*, 141(4), pp. 446–459, 2001. doi: 10.1007/s00221-001-0901-z.

[30] A. C. Schouten, E. de Vlugt, J. J. van Hilten, and F. C. T. van der Helm, "Quantifying Proprioceptive Reflexes during Position Control of the Human Arm," *IEEE Transactions on Biomedical Engineering*, 55(1), pp. 311–321, 2008. doi: 10.1109/TBME.2007.899298.

[31] M. M. Mirbagheri, L. Alibiglou, M. Thajchayapong, and W. Z. Rymer, "Muscle and Reflex Changes with Varying Joint Angle in Hemiparetic Stroke," *Journal of NeuroEngineering and Rehabilitation*, 5:6, 2008. doi: 10.1186/1743-0003-5-6.

[32] M. M. Mirbagheri, M. Ladouceur, H. Barbeau, and R. E. Kearney, "The Effects of Long Term FES-Assisted Walking on Intrinsic and Reflex Dynamic Stiffness in Spinal Cord Injured Patients," *IEEE Transactions on Neural Systems and Rehabilitation Engineering*, 10(4), pp. 280–289, 2002. doi: 10.1109/TNSRE.2002.806838.

[33] M. M. Mirbagheri, D. Chen, and W. Z. Rymer, "Quantification of the Effects of an Alpha-2 Adrenergic Agonist on Reflex Properties in Spinal Cord Injury using a System Identification Technique," *Journal of NeuroEngineering and Rehabilitation*, 7:29, 2010. doi: 10.1186/1743-0003-7-29.

[34] M. M. Mirbagheri, M. W. Kindig, and X. Niu, "Effects of Robotic-Locomotor Training on Stretch Reflex Function and Muscular Properties in Individuals with Spinal Cord Injury," *Clinical Neurophysiology*, 126(5), pp. 997–1006, 2015. doi: 10.1016/j.clinph.2014.09.010.

[35] M. M. Mirbagheri, H. Barbeau, and R. E. Kearney, "Intrinsic and Reflex Contributions to Human Ankle Stiffness: Variation with Activation Level and Position," *Experimental Brain Research*, 135(4), pp. 423–436, 2000. doi: 10.1007/s002210000534.

[36] J.-M. Gracies, J. E. Marosszeky, R. Renton, J. Sandanam, *et al.*, "Short-Term Effects of Dynamic Lycra Splints on Upper Limb in Hemiplegic Patients," *Archives of Physical Medicine and Rehabilitation*, 81(12), pp. 1547–1555, 2000. doi: 10.1053/apmr.2000.16346.

[37] R. C. van 't Veld, A. C. Schouten, H. van der Kooij, and E. H. F. van Asseldonk, "Neurophysiological Validation of Simultaneous Intrinsic and Reflexive Joint Impedance Estimates," *Journal of NeuroEngineering and Rehabilitation*, 18:36, 2021. doi: 10.1186/s12984-021-00809-3.

[38] D. Ludvig and R. E. Kearney, "Real-time Estimation of Intrinsic and Reflex Stiffness," *IEEE Transactions on Biomedical Engineering*, 54(10), pp. 1875–1884, 2007. doi: 10.1109/TBME.2007.894737.

[39] D. T. Westwick and R. E. Kearney, "Identification of Linear Systems," in *Identification of Nonlinear Physiological Systems*, Hoboken, NJ, USA: John Wiley & Sons, Inc., 2003, ch. 5, pp. 103–123. doi: 10.1002/0471722960.ch5.

[40] T. K. Koo and M. Y. Li, "A Guideline of Selecting and Reporting Intraclass Correlation Coefficients for Reliability Research," *Journal of Chiropractic Medicine*, 15(2), pp. 155–163, 2016. doi: 10.1016/j.jcm.2016.02.012.

[41] J. Carpenter and J. Bithell, "Bootstrap Confidence Intervals: When, Which, What? A Practical Guide for Medical Statisticians," *Statistics in Medicine*, 19(9), pp. 1141–1164, 2000. doi: 10.1002/(SICI)1097-0258(20000515)19:9<1141::AID-SIM479>3.0.CO;2-F.

[42] T. Platz, C. Eickhof, G. Nuyens, and P. Vuadens, "Clinical Scales for the Assessment of Spasticity Associated Phenomena, and Function: A Systematic Review of the Literature," *Disability and Rehabilitation*, 27(1-2), pp. 7–18, 2005. doi: 10.1080/09638280400014634.

[43] J. F. Fleuren, M. J. Nederhand, and H. J. Hermens, "Influence of Posture and Muscle Length on Stretch Reflex Activity in Poststroke Patients with Spasticity," *Archives of Physical Medicine and Rehabilitation*, 87(7), pp. 981–988, 2006. doi: 10.1016/j.apmr.2006.03.018.

[44] L. Bar-On, K. Desloovere, G. Molenaers, J. Harlaar, *et al.*, "Identification of the Neural Component of Torque during Manually-applied Spasticity Assessments in Children with Cerebral Palsy," 40(3), pp. 346–351, 2014. doi: 10.1016/j.gaitpost.2014.04.207.

[45] M. M. Mirbagheri, R. E. Kearney, and H. Barbeau, "Quantitative, Objective Measurement of Ankle Dynamic Stiffness: Intrasubject Reliability and Intersubject Variability," in *18th Annual International Conference of the IEEE Engineering in Medicine and Biology Society*, Amsterdam, Netherlands: IEEE, 1996, pp. 585–586. doi: 10.1109/IEMBS.1996.651876.

[46] J. Gäverth, M. Sandgren, P. G. Lindberg, H. Forssberg, *et al.*, "Test-Retest and Inter-Rater Reliability of a Method to Measure Wrist and Finger Spasticity," *Journal of Rehabilitation Medicine*, 45(7), pp. 630–636, 2013. doi: 10.2340/16501977-1160.

[47] K. L. de Gooijer-van de Groep, E. de Vlugt, H. J. van der Krogt, Á. Helgadóttir, *et al.*, "Estimation of Tissue Stiffness, Reflex Activity, Optimal Muscle Length and Slack Length in Stroke Patients using an Electromyography Driven Antagonistic Wrist Model," *Clinical Biomechanics*, 35, pp. 93–101, 2016. doi: 10.1016/j.clinbiomech.2016.03.012.

[48] J. M. Finley, Y. Y. Dhaher, and E. J. Perreault, "Acceleration Dependence and Task-specific Modulation of Short- and Medium-Latency Reflexes in the Ankle Extensors," *Physiological Reports*, 1(3):e00051, 2013. doi: 10.1002/phy2.51.

[49] R. C. van 't Veld, E. H. F. van Asseldonk, H. van der Kooij, and A. C. Schouten, "Disentangling Acceleration-, Velocity-, and Duration-Dependency of the Short- and Medium-Latency Stretch Reflexes in the Ankle Plantarflexors," *Journal of Neurophysiology*, 126(4), pp. 1015–1029, 2021. doi: 10.1152/jn.00704.2020.

Chapter 7

General Discussion

7.1 Introduction

This thesis developed and evaluated a non-invasive integrated spasticity assessment and treatment for a stationary posture. The parallel-cascade (PC) system identification technique, which disentangles overall joint resistance in an intrinsic and reflexive contribution, was selected as analysis methodology. Spasticity, which affects reflexive resistance, is often observed concurrent with other symptoms as hypertonia, contractures and fibrosis, which affect intrinsic resistance. Therefore, the ability to disentangle joint resistance components is essential for spasticity assessment. An offline, time-invariant PC algorithm modified from Kearney *et al.* [1] was used for post-trial evaluation of ankle joint resistance in a neuromechanical and clinical setting. An online, adaptive PC algorithm modified from [2] was used for live estimation during measurements to enable biofeedback on intrinsic and reflexive impedance.

First, neurophysiological validity of the PC technique was investigated as the technique substantially differs from clinical practice. To assess spasticity, clinicians manually apply passive joint movements over the full range of motion (ROM) and score the perceived resistance on a subjective, ordinal scale [3, 4]. In contrast, the PC technique uses perturbations over a limited ROM, which only elicit a short-latency (M1) stretch reflex due to the short perturbation duration (Chapter 2). As a result, the PC technique only captures the monosynaptic stretch reflex pathway and mainly the initial burst response of the muscle spindle. Our studies showed the potential of the PC technique to disentangle intrinsic and reflexive joint resistance through a successful neurophysiological validation of both intrinsic and reflexive pathways (Chapter 4). In addition, the adapted PC algorithms showed good responsiveness, accuracy and reliability in simulation study for both able-bodied participants and people with spasticity (Chapter 3).

Second, feasibility of PC technique-based biofeedback using an operant conditioning protocol was explored to achieve a long-term sustained reflex reduction. Feasibility of the operant conditioning protocol using EMG-based biofeedback was first replicated with a within-session reflex reduction after 4 to 6 conditioning sessions (Chapter 5). However, an operant conditioning protocol providing feedback on reflexive joint resistance estimated with the online PC algorithm did not achieve a reflex reduction. For these long-lasting biofeedback training protocols, we did show feasibility of feedback gamification to improve participant motivation without affecting intervention effectiveness.

Third, the effect of botulinum toxin-A (BoNT-A) injections on ankle joint resistance for patients with spasticity was investigated using the PC technique. We hypothesized

that BoNT-A would reduce the overall joint resistance and its reflexive contribution. On a group-level, only the clinical modified Ashworth Scale (MAS), a measure of overall joint resistance, showed the hypothesized reduction due to BoNT-A injections (Chapter 6). Using the PC technique, this overall reduction could not be attributed to an unambiguous reduction of the reflexive or intrinsic resistance contribution. Still, validity of the PC technique was supported through strong group-level association with instrumented spasticity test (SPAT) outcomes when quantifying the same resistance contribution (i.e. intrinsic or reflexive). These results emphasize the importance of research into methods capable of unravelling joint resistance components instead of using the MAS which evaluates overall joint resistance and muscle tone for spasticity assessment.

7.2 Stretch Reflex Dependency on Perturbation Profile

The stretch reflex and spasticity have been reported to depend on several factors, including: task [5], predictability [6], background muscle activation [7], posture [8, 9] and perturbation profile [10–12]. Regarding perturbation profiles, muscle spindles and the stretch reflex have long been defined as position- and velocity-dependent in both neurophysiological and clinical research [13, 14]. However, stretch reflex dependence on acceleration, force and force derivative has recently been observed [12, 15, 16]. Our results confirmed that the stretch reflex depends on acceleration, velocity and duration (Chapter 2). Overall, neurophysiological and clinical studies on the stretch reflex and spasticity all need to control for these dependencies to avoid confounding effects in study results and interpretation.

The complexity of the stretch reflex arc with many dependent factors impedes our current scientific understanding of the reflex arc. First, discovery of new dependencies can reveal potential confounding effects in previous study results and interpretation. For example, the observed dependency on duration and acceleration uncovered a potential confounding effect on previously reported position and velocity dependencies, as these reports unknowingly did not account for perturbation duration and acceleration [10, 11, 17–21]. Second, interpretation and comparison of quantified reflexive outcome measures across different experiments and devices should always be performed with all stretch reflex dependencies in mind. For example, the reported reflexive gains from the PC technique nonlinearly depend on the exact perturbation duration, velocity and acceleration applied. Thus, stretch reflex and spasticity outcomes are sensitive to perturbation profile design, hardware limitations during experimental execution and precision of the experimental measurements. Consequently, comparing reflexive gain magnitudes between our results and other PC technique studies [1, 2, 8, 22], which reported different perturbation velocities and accelerations, is difficult. Proper comparison between studies would require interpolation/extrapolation of the the nonlinear velocity and acceleration effects. For future motorized reflex and spasticity studies, standardization of study protocol, perturbation design and documentation is recommended to benefit from the precision and objectivity provided by motorized assessment.

Isolated studies do not require standardization of the stretch reflex dependencies to generated valid results and conclusion provided that the reflex dependencies are controlled for. Regarding perturbation dependencies, systematic evaluation controlling for interdependence of the acceleration, velocity and duration across applied perturba-

tions does allow to investigate these dependencies (Chapter 2). Furthermore, while the PC technique simplifies the reflexive pathway to only depend on (half-wave rectified) perturbation velocity, physiological understanding gained from the PC technique is still valid. Use of the PC technique is justified as reflexes are consistently elicited using the same dorsiflexion perturbation profile and experimental device. Thus, by design the acceleration, velocity or duration of each perturbation did not vary within studies. In general, many experimental procedures and reported results for the reflexive pathway are still valid and relevant as stretch reflex dependencies were controlled for.

7.3 Technical Development of Model-based Spasticity Assessment

Key element for development of model-based assessment techniques is that methods should only estimate dynamics and parameters for which the experimental datasets contains enough information. As discussed in Section 1.2, model-based techniques use various sources of information to obtain parameter estimates: experimental measurements (data), a priori physiological knowledge and assumptions [23]. As a result, depending on the goal of the study and specific assessment technique used, a certain amount of experimental data is required to reliably achieve the study goal. For example, a data-driven system identification technique might require a richer experimental dataset than a physics-based neuromechanical model using a priori knowledge and assumptions. Still, examples from all manual instrumented, physics-based neuromechanical models and data-driven system identification techniques have reported a lack of experimental data to reliably estimate model feature and parameters [1, 24–26]. Prior evaluation of the designed model-based techniques in a simulation study can be used to evaluate the minimum amount of data required for reliable parameter estimation.

In general, model-based assessment techniques for the stretch reflex and spasticity could benefit from complementing experimental investigations with simulation studies. Simulation studies can be used to verify isolated theoretical concepts, perturbation profile design and data processing steps used by model-based techniques. For example, our results showed that the inversion of an acausal impulse response function (IRF) as used within the offline PC technique [1, 8] resulted in increase estimation bias and variability (Chapter 3). As this decrease in algorithm performance was already observed in an idealized simulation study, the performance decrease is likely to translate to actual experimental studies. Similarly, simulation studies could be used to optimize perturbation profile design to match the desired scientific aim based on known stretch reflex dependencies, see Section 7.2. Verification of isolated elements of model-based techniques and experimental design is important to avoid reduced responsiveness, accuracy and reliability of the outcome measures in experimental studies.

Simulation studies can also be used to evaluate sensitivity of model-based techniques to expected experimental conditions. Experimental datasets may contain various factors deviating from the ideal conditions, such as measurement noise and voluntary torque contributions deviating from the instructed task. Note, factors like measurement noise do not only increase variability on model-based estimation, but can also influence estimation responsiveness and accuracy, as seen for the PC technique [27]. Previously, many model-based techniques would perform such validation steps during experimental studies using measures like variance accounted for (VAF). However, our simulation

results showed that differences between a VAF of 99.8% and 100.0% could translate to an parameter estimation bias of 5% (Chapter 3). Therefore, reduced responsiveness, accuracy and reliability might have been unnoticed in previous research, because VAF outcomes as low as 90% have been considered good/sufficient [8, 25]. Prior evaluation of sensitivities in simulation can help understand algorithm sensitivities and promote adequate solutions to mitigate identified sensitivities before experimental application. Moreover, knowledge on sensitivities within an idealized simulation environment can support interpretation of sensitivities observed within experimental datasets.

Besides the models and algorithms involved with reflex and spasticity studies, suitable experimental equipment is essential to obtain valid scientific and clinical results. Most instrumented studies on reflexes and spasticity use equipment to perturb the investigated joint and elicit a stretch reflex. Research on the stretch reflex requires fast perturbations given the short time window in which the reflex can be causally influenced (Chapter 2). Fast perturbations are especially required when investigating the monosynaptic pathway and approaches measuring over the full ROM, like the instrumented SPAT, place less stringent requirements on the perturbation profile. Using fast perturbations to elicit reflexes translates to a relatively high-frequency content within the perturbation signals. This desired high-frequency content places several requirements on the experimental setup in order to properly apply the perturbation to the human joint. First, the bandwidth of the robotic actuator and control system should exceed the bandwidth of the applied perturbation. Second, precise measurement systems are desired to collect information on the execution of the applied perturbation. Third, the eigenfrequency of the structure translating the perturbation between the actuator and human joint should exceed the bandwidth of the applied perturbation as well. Failure to obtain such a structural eigenfrequency will result in undesired oscillations, which in reflex studies can unintentionally elicit stretch reflexes. For example, undesired oscillations during 2° plantarflexion perturbations were large enough to actually elicit a stretch reflex in the calf muscles (Appendix A). So, apparently the calf muscles were stretch during plantarflexion perturbations, when shortening of the calf muscles is expected. In short, stretch reflex studies will require actuators with sufficient bandwidth, precise measurements and adequate structural eigenfrequency achieved using a lightweight and stiff construction.

7.4 Spasticity Assessment using Disentangled Joint Resistance

7.4.1 Assessment using System Identification Techniques

The current state-of-the-art for spasticity assessment using data-driven system identification techniques is based on experimental data with time-invariant or slow time-varying characteristics measured over a limited ROM. The neurophysiological validity of the PC system identification technique was shown through linear association with EMG measures (Chapter 4) and the instrumented SPAT measure (Chapter 6). Note, validity for slow time-varying conditions was only shown when averaging over 1 min data segments, as linear association with EMG measures substantially dropped for processing of 6 s long data segments (Chapter 5). The current state-of-the-art lacks system identification technique able to reliably disentangle intrinsic and reflexive resistance contribution in

fast (≤6 s) time-varying conditions.

Applicability of state-of-the-art system identification techniques for spasticity assessment is limited, because controlling for stretch reflex dependencies in a longitudinal clinical setting is challenging. As listed in Section 7.2, the stretch reflex and spasticity have been reported to depend on task, background muscle activation, posture and perturbation characteristics. While motorized assessments can inherently control perturbation characteristics across sessions, factors like posture, task and muscle activity can show longitudinal variation in patient populations. For example in Chapter 6, multiple participants with spasticity showed variation of the ROM across sessions. Similarly, several reflex studies recommended use of an acclimatization session to improve parameter reliability has been recommended (Chapter 5) [28, 29]. Therefore, a clinimetric study evaluating the sensitivity of system identification technique to natural variations in uncontrolled parameters is required. This sensitivity study can confirm validity of the longitudinal application of system identification techniques or show potential issues to be solved and investigated.

7.4.2 Concurrent and Integrated Development of Instrumented Spasticity Assessment Techniques

Concurrent development of fundamentally different techniques as well as cross-fertilization between methodologies and communities is essential towards clinical implementation of an instrumented spasticity assessment technique. Currently, a gold standard is missing as reference during development of instrumented techniques disentangling joint resistance contributions. In absence of a gold standard, future clinimetric studies would benefit from concurrent evaluation of fundamentally different methodologies within the same population to confirm validity of the used methodologies. Spasticity assessment using manual instrumented, motorized instrumented, physics-based modelling or data-driven modelling methods fundamentally differ as various sources of information and assumptions are used. Still, all methods have the same goal, i.e. the quantification of spasticity. For instance, instrumented assessments can be used to investigate the influence of subjectivity and variability introduced through manual assessment. Physics-based nonlinear neuromechanical models can be used to investigate the sensitivity of the data-driven linearized PC technique to longitudinal, nonlinear influences. Vice versa, data-driven system identification techniques can be used to validate the a priori knowledge and assumptions used in neuromechanical models.

A recent study by Andringa *et al.* [30] provides a well-defined set of pre-determined hypotheses to analyze multiple methodologies estimating intrinsic and reflexive joint resistance. First, a moderate-strong positive correlation is expected between the estimated intrinsic resistances and between the estimated reflexive resistances. Second, no or weak correlations are expected between the intrinsic resistance of a method and the reflexive resistance of the method itself and of the alternative method. Third, within a population a similar ranking of participant intrinsic and reflexive resistance is expected for both methodologies. Fourth, a similar association between clinical characteristics and the estimated joint resistance contributions is expected. For example, the amount of correlation of the estimated intrinsic resistance with the MAS is expected similar for both methodologies. Likewise, the amount of correlation of the intrinsic resistance of both methodologies with the passive joint ROM is also expected similar. Compliance

with these hypotheses provides support that both methodologies measure the desired phenomenon, whereas rejection of a hypothesis can provide insight into potential limitations of the compared methodologies.

Besides concurrent development of different techniques, solutions for integrated spasticity assessment and treatment could be found in the unification of different methodologies [23]. First, unification of joint resistance and spasticity concepts on a theoretical level is required to avoid misunderstanding and incorrect interpretation across communities. For example, within the system identification community the term *intrinsic* resistance refers to the combined resistance from tissue-related non-neural origin and tonic neural origin (this thesis). Contrarily, within the biomechanics community the term *intrinsic* is often used to refer to the material properties of musculoskeletal structures, thus only the tissue-related non-neural origin. Similarly, the term spasticity has had various definitions [13, 31, 32], mainly varying between terms referring to the aetiology at spinal level or clinical expression at joint level. Noort *et al.* [32] proposed to only use spasticity specifically linked to an exaggerated stretch reflex, i.e. stretch hyperreflexia (this thesis). Second, unification of methodologies may result in novel approaches, which can combine the complementary advantages of fundamentally different methodologies. For example, Cop *et al.* [23] provided an approach for reliable multi-level understanding of joint resistance through unification of physics-based neuromechanical and data-driven system identification model-based estimation of joint resistance. The proposed methodology would rely on decomposing joint stiffness estimates obtained using system identification into underlying muscle and tendon contributions through neuromechanical modelling.

The proposed standardization of protocols, concurrent development of methodologies as well as unification and cross-fertilization between communities cannot be achieved without findability, accessibility, interoperability, and reusability (FAIR) of published research. For example, the simulation study of Chapter 2 was enabled through open-access availability of the Blum *et al.* [33] detailed biophysical muscle spindle and muscle-tendon unit model. Thus, FAIR research enables the quick use and implementation of published research, especially from other scientific communities. Similarly, concurrent development and evaluation of methodologies within a clinical environment will require FAIR research to enable quick and correct use of fundamentally different methodologies from other communities. In terms of standardization, FAIR research enables direct use of experimental protocols and one-on-one comparison of research data to provide insight in potential differences. As such, open-access publication of all code and data used in each chapter of this thesis is meant to improve both the techniques utilized as well as instrumented spasticity assessments in general.

7.4.3 Future Outlook on Instrumented Spasticity Assessment

A societal goal for reflex and spasticity research is to advance pathophysiological understanding of spasticity and improve clinical decision making. The core challenge, as explored in this thesis, is the need to isolate and quantify the reflexive response without influence of other symptoms like hypertonia, contractures and fibrosis. The current clinical approach using the MAS scale will not provide sufficient insight, as the MAS is a measure of overall joint resistance [34–36]. Based on the MAS score descriptions, a

reduction in MAS might best be coupled to a reduction in muscle tone than spasticity [3]. Therefore, research into novel instrumented methodologies remains relevant for spasticity assessment.

Widespread clinical use of instrumented spasticity assessment still requires proof of diagnostic accuracy and added value for clinical care [37]. For instance, a clinimetric evaluation of the PC technique is lacking despite several clinical studies in small groups of patients [8, 22, 38–40]. As a result, information on the responsiveness, reliability and minimal detectable difference (MDD) of system identification in a clinical setting is missing, especially on an individual level. The lack of a gold standard and the complexity of the reflexive pathway with all dependencies complicate the process of obtaining this clinical information. Eventually, clinically relevant changes in people with spasticity should exceed the MDD of the proposed instrumented assessment methodology to show the diagnostic potential in support of clinical decision making and therapy success prediction.

Added value for clinical care using an instrumented spasticity assessment will require a cost-effective methodology with proven clinical benefit over existing methods. As spasticity can manifest itself differently between passive or clinical setting compared with an active or functional environment, inclusion of functional outcomes is important in future research [41]. For instance for the PC technique, additional research is required whether only exciting the monosynaptic stretch reflex is sufficient to assess spasticity and its functional effects. Besides, the search for a cost-effectiveness methodology adds another dimension to the trade-off between advantages and disadvantages of all methods. For example, a detailed, physics-based neuromechanical modelling approach might require relatively long data collection to reliably estimate the detailed model. Yet, the desired perturbations for these models do not necessarily require a powerful (i.e. expensive) robotic manipulator. Contrarily, the PC technique as used in this thesis could obtain a sufficient amount of data within a few minute, if only a limited ROM is analyzed. Yet, the desired perturbations for the PC technique require a powerful robotic manipulator to unravel intrinsic and reflexive joint resistance.

7.5 Spasticity Treatment using Operant Conditioning

Spasticity treatment using an operant conditioning-based training protocol has previously shown promising results, as functional improvements were reported [42]. Functional improvements were quantified as a 59% increase in gait speed and improved step-cycle symmetry. In addition, participants self-reported on aspects like faster walking, walking greater distance and easier stepping due to the operant conditioning training. This non-invasive spasticity treatment protocol currently uses H-reflex stimulation to electrically elicit a stretch reflex equivalent to mechanical perturbations. Ideally, non-invasive spasticity treatment be developed without need for H-reflex stimulation, given that two of our eleven participants opted out of the training due to discomfort caused by H-reflex stimulation. Moreover, the time-intensiveness and slow improvement rates remain an open challenge for the conditioning protocol. Although our results did show feasibility of using gamification within operant conditioning protocols to increase motivation during these time-intensive protocols (Chapter 5).

As an alternative for H-reflex stimulation, a motorized operant conditioning ap-

proach remains promising [29]. Successful conditioning within a clinical setting, including translation of the training to functional improvements, has yet to be shown for motorized operant conditioning. To fully remove the need for H-reflex stimulation, torque-based data processing or an alternative EMG normalization would be required. EMG-based protocols currently require the use of H-reflex stimulation to check correct placement of EMG electrodes across-sessions. Biofeedback based on the online PC algorithm did not result in a feasible operant conditioning protocol (Chapter 5). Recent developments on the reliable estimation of time-varying joint resistance using system identification might provide new online estimation algorithms to investigate within the operant conditioning paradigm [23, 43]. Similarly, implicit EMG-driven biofeedback during treadmill walking has also shown promising results in a single session [44]. Ultimately, functional improvements due to prescription of such treatment compared to a control group are essential towards clinical implementation.

7.6 Evaluation of Stretch Reflex and Spasticity in Functional Tasks

To bridge the gap between spasticity assessment and treatment in a stationary posture and functional measures, functional evaluation of the stretch reflex and spasticity in a laboratory/clinical setting is of interest. Successful spasticity assessment and treatment methodologies should eventually show their benefit within functional outcome measures. Moreover, incorporating functional tasks into spasticity treatment could potentially be used to enable faster improvement. For example, execution of the H-reflex operant conditioning protocol during gait instead of in stance substantially improved training effectiveness [45]. However, the current state-of-the-art as discussed in this thesis are all executed in a stationary posture. Bridging the gap between a stationary posture and functional measures for spasticity research is challenging, because spasticity can manifest itself differently within a passive or clinical setting compared with an active or functional environment [41]. For instance, the potential difference in spasticity expression might explain why 3 participants receiving BoNT-A injections for spasticity reduction showed little to no reflexive response in our stationary instrumented tests (Chapter 6). For some people with spasticity, stationary methods will remain relevant as several people lack voluntary muscle control to perform a functional evaluation. For people with (residual) voluntary muscle control, evaluation of the stretch reflex and spasticity during functional tasks, e.g. treadmill walking [44, 46, 47], could provide an intermediate step to translate and extend our neuro- and pathophysiological understanding.

The number of available methods to assess the stretch reflex in functional tasks is currently limited, especially methods disentangling intrinsic and reflexive resistance. First, elicitation of the stretch reflex during a functional task poses additional challenges with respect to experiments with stationary posture. To retain relevance of the functional tasks, the experimental equipment should have negligible effect on execution of functional task outside of the applied perturbations. Moreover, functional tasks like treadmill walking have a natural variability, especially in people with neurological impairments, creating a challenge to consistently time perturbations within the gait cycle. Various methods and devices are currently available that could potentially be used for reflex elicitation. Electrical stimulation can be used to elicit the H-reflex during

gait [45]. Treadmill perturbations can be used to evoke stretch reflexes during the stance phase [46, 47]. A robotic perturbator recessed into a walkway can elicit ankle rotations during the stance phase [48, 49]. A transparent lower limb perturbator can apply force perturbations during gait, currently only shown during the swing phase [50]. Note, the robotic perturbators have currently not been used yet to specifically investigate stretch reflexes, instead focusing on the overall resistance response.

Second, reflex quantification during a functional task, especially regarding disentangling intrinsic and reflexive resistance, is challenging with respect to experiments with stationary posture. As discussed before, stretch reflexes and joint resistance depend on various factors, such as muscle activation and posture (joint angle and velocity). These dependencies imply that the stretch reflex response and joint resistance naturally varying during functional tasks. For example, initial reports on joint resistance during walking do report on time-varying modulation of ankle joint resistance [48, 49, 51]. Furthermore, a history-dependence of joint resistance is likely, given that reported joint resistance during movement was lower than resistance in stationary posture for equal muscle activation and posture [52]. Current state-of-the-art has provided first estimates of time-varying joint resistance using system identification during functional tasks for overall joint resistance only [23, 43]. Therefore, novel model-based methods still have to be developed and investigated to provide reliable estimates of intrinsic and reflexive joint resistance during functional tasks.

7.7 Conclusion

This thesis developed and evaluated a non-invasive integrated spasticity assessment and treatment for a stationary posture using the PC system identification technique. Our results showed the neurophysiological validity of the PC technique to assess intrinsic and reflexive joint resistance contributions over slow time-varying or time-invariant data segments. Towards spasticity assessment and treatment open challenges remain to obtain a reliable longitudinal quantification of spasticity and a cost-effective non-invasive spasticity treatment. Ultimately, a cost-effective approach with proven functional benefits for patients with spasticity has to be developed to improve overall quality of life. Based on our results, scientific and clinical development and evaluation would benefit from several recommendations to achieve this goal. First, standardization of study protocol, perturbation design and documentation is recommended to benefit from the precision and objectivity provided by motorized assessment. Second, stretch reflex studies, especially those investigating the monosynaptic pathway, require actuators with sufficient bandwidth, precise measurements and adequate structural eigenfrequency to obtain valid results. Third, concurrent development of fundamentally different techniques as well as cross-fertilization between methodologies and communities is essential in absence of a gold standard. Fourth, the proposed standardization of protocols, concurrent development of methodologies as well as unification and cross-fertilization between communities cannot be achieved without FAIR published research.

References

[1] R. E. Kearney, R. B. Stein, and L. Parameswaran, "Identification of Intrinsic and Reflex Contributions to Human Ankle Stiffness Dynamics," *IEEE Transactions on Biomedical Engineering*, 44(6), pp. 493–504, 1997. doi: 10.1109/10.581944.

[2] D. Ludvig and R. E. Kearney, "Real-time Estimation of Intrinsic and Reflex Stiffness," *IEEE Transactions on Biomedical Engineering*, 54(10), pp. 1875–1884, 2007. doi: 10.1109/TBME.2007.894737.

[3] R. W. Bohannon and M. B. Smith, "Interrater Reliability of a Modified Ashworth Scale of Muscle Spasticity," *Physical Therapy*, 67(2), pp. 206–207, 1987. doi: 10.1093/ptj/67.2.206.

[4] J.-M. Gracies, J. E. Marosszeky, R. Renton, J. Sandanam, *et al.*, "Short-Term Effects of Dynamic Lycra Splints on Upper Limb in Hemiplegic Patients," *Archives of Physical Medicine and Rehabilitation*, 81(12), pp. 1547–1555, 2000. doi: 10.1053/apmr.2000.16346.

[5] J. A. Pruszynski and S. H. Scott, "Optimal Feedback Control and the Long-Latency Stretch Response," *Experimental Brain Research*, 218(3), pp. 341–359, 2012. doi: 10.1007/s00221-012-3041-8.

[6] C. J. Forgaard, I. M. Franks, D. Maslovat, and R. Chua, "Perturbation Predictability Can Influence the Long-Latency Stretch Response," *PLoS ONE*, 11(10):e0163854, 2016. doi: 10.1371/journal.pone.0163854.

[7] P. B. C. Matthews, "Observations on the Automatic Compensation of Reflex Gain on Varying the Pre-Existing Level of Motor Discharge in Man," *The Journal of Physiology*, 374(1), pp. 73–90, 1986. doi: 10.1113/jphysiol.1986.sp016066.

[8] M. M. Mirbagheri, H. Barbeau, and R. E. Kearney, "Intrinsic and Reflex Contributions to Human Ankle Stiffness: Variation with Activation Level and Position," *Experimental Brain Research*, 135(4), pp. 423–436, 2000. doi: 10.1007/s002210000534.

[9] J. F. Fleuren, M. J. Nederhand, and H. J. Hermens, "Influence of Posture and Muscle Length on Stretch Reflex Activity in Poststroke Patients with Spasticity," *Archives of Physical Medicine and Rehabilitation*, 87(7), pp. 981–988, 2006. doi: 10.1016/j.apmr.2006.03.018.

[10] G. N. Lewis, E. J. Perreault, and C. D. MacKinnon, "The Influence of Perturbation Duration and Velocity on the Long-Latency Response to Stretch in the Biceps Muscle," *Experimental Brain Research*, 163(3), pp. 361–369, 2005. doi: 10.1007/s00221-004-2182-9.

[11] J. Schuurmans, E. de Vlugt, A. C. Schouten, C. G. M. Meskers, *et al.*, "The Monosynaptic Ia Afferent Pathway Can Largely Explain the Stretch Duration Effect of the Long Latency M2 Response," *Experimental Brain Research*, 193(4), pp. 491–500, 2009. doi: 10.1007/s00221-008-1647-7.

[12] J. M. Finley, Y. Y. Dhaher, and E. J. Perreault, "Acceleration Dependence and Task-specific Modulation of Short- and Medium-Latency Reflexes in the Ankle Extensors," *Physiological Reports*, 1(3):e00051, 2013. doi: 10.1002/phy2.51.

[13] J. W. Lance, "Symposium Synopsis," in *Spasticity: Disordered Motor Control*, R. G. Feldman, R. R. Young, and W. P. Koella, Eds., Chicago, IL, USA: Year Book Medical Publishers, 1980, pp. 485–495.

[14] E. Burdet, D. W. Franklin, and T. E. Milner, *Human Robotics: Neuromechanics and Motor Control*, 1st. Cambridge, MA, USA: MIT Press, 2013.

[15] K. P. Blum, B. L. D'Incamps, D. Zytnicki, and L. H. Ting, "Force Encoding in Muscle Spindles during Stretch of Passive Muscle," *PLoS Computational Biology*, 13(9):e1005767, 2017. doi: 10.1371/journal.pcbi.1005767.

[16] A. Falisse, L. Bar-On, K. Desloovere, I. Jonkers, *et al.*, "A Spasticity Model based on Feedback from Muscle Force Explains Muscle Activity during Passive Stretches and Gait in Children with Cerebral Palsy," *PLoS ONE*, 13(12):e0208811, 2018. doi: 10.1371/journal.pone.0208811.

[17] G. L. Gottlieb and G. C. Agarwal, "Response to Sudden Torques About Ankle in Man: Myotatic Reflex," *Journal of Neurophysiology*, 42(1), pp. 91–106, 1979. doi: 10.1152/jn.1979.42.1.91.

[18] R. G. Lee and W. G. Tatton, "Long Latency Reflexes to Imposed Displacements of the Human Wrist: Dependence on Duration of Movement," *Experimental Brain Research*, 45(1), pp. 207–216, 1982. doi: 10.1007/BF00235780.

[19] A. F. Thilmann, M. Schwarz, R. Töpper, S. J. Fellows, *et al.*, "Different Mechanisms Underlie the Long-Latency Stretch Reflex Response of Active Human Muscle at Different Joints," *Journal of Physiology*, 444(1), pp. 631–643, 1991. doi: 10.1113/jphysiol.1991.sp018898.

[20] M. J. Grey, B. Larsen, and T. Sinkjær, "A Task Dependent Change in the Medium Latency Component of the Soleus Stretch Reflex," *Experimental Brain Research*, 145(3), pp. 316–322, 2002. doi: 10.1007/s00221-002-1109-6.

[21] N. Kawashima, K. Nakazawa, S. I. Yamamoto, D. Nozaki, *et al.*, "Stretch Reflex Excitability of the Anti-Gravity Ankle Extensor Muscle in Elderly Humans," *Acta Physiologica Scandinavica*, 180(1), pp. 99–105, 2004. doi: 10.1046/j.0001-6772.2003.01230.x.

[22] M. M. Mirbagheri, H. Barbeau, M. Ladouceur, and R. E. Kearney, "Intrinsic and Reflex Stiffness in Normal and Spastic, Spinal Cord Injured Subjects," *Experimental Brain Research*, 141(4), pp. 446–459, 2001. doi: 10.1007/s00221-001-0901-z.

[23] C. P. Cop, G. Cavallo, R. C. van 't Veld, B. F. J. M. Koopman, *et al.*, "Unifying System Identification and Biomechanical Formulations for the Estimation of Muscle, Tendon, and Joint Stiffness during Human Movement," *Progress in Biomedical Engineering*, 3(3), 2021. doi: 10.1088/2516-1091/ac12c4.

[24] L. Bar-On, K. Desloovere, G. Molenaers, J. Harlaar, *et al.*, "Identification of the Neural Component of Torque during Manually-applied Spasticity Assessments in Children with Cerebral Palsy," 40(3), pp. 346–351, 2014. doi: 10.1016/j.gaitpost.2014.04.207.

[25] L. H. Sloot, M. M. van der Krogt, K. L. de Gooijer-van de Groep, S. van Eesbeek, *et al.*, "The Validity and Reliability of Modelled Neural and Tissue Properties of the Ankle Muscles in Children with Cerebral Palsy," *Gait and Posture*, 42(1), pp. 7–15, 2015. doi: 10.1016/j.gaitpost.2015.04.006.

[26] J. H. Pasma, D. Engelhart, A. B. Maier, R. G. K. M. Aarts, *et al.*, "Reliability of system identification techniques to assess standing balance in healthy elderly," *PLoS One*, 11(3):e0151012, 2016. doi: 10.1371/journal.pone.0151012.

[27] D. T. Westwick and R. E. Kearney, "Identification of Linear Systems," in *Identification of Nonlinear Physiological Systems*, Hoboken, NJ, USA: John Wiley & Sons, Inc., 2003, ch. 5, pp. 103–123. doi: 10.1002/0471722960.ch5.

[28] A. K. Thompson, X. Y. Chen, and J. R. Wolpaw, "Acquisition of a Simple Motor Skill: Task-Dependent Adaptation Plus Long-Term Change in the Human Soleus H-Reflex," *Journal of Neuroscience*, 29(18), pp. 5784–5792, 2009. doi: 10.1523/JNEUROSCI.4326-08.2009.

[29] N. Mrachacz-Kersting, U. G. Kersting, P. de Brito Silva, Y. Makihara, *et al.*, "Acquisition of a Simple Motor Skill: Task-dependent Adaptation and Long-term Changes in the Human Soleus Stretch Reflex," *Journal of Neurophysiology*, 122(1), pp. 435–446, 2019. doi: 10.1152/jn.00211.2019.

[30] A. Andringa, C. G. M. Meskers, I. van de Port, S. Zandvliet, *et al.*, "Quantifying Neural and Non-neural Componenets of Wrist Hyper-resistance after Stroke: Comparing Two Instrumented Assessment Methods," *Medical Engineering & Physics*, 98, pp. 57–64, 2021. doi: 10.1016/j.medengphy.2021.10.009.

[31] A. D. Pandyan, M. Gregoric, M. P. Barnes, D. Wood, *et al.*, "Spasticity: Clinical Perceptions, Neurological Realities and Meaningful Measurement," *Disability and Rehabilitation*, 27(1-2), pp. 2–6, 2005. doi: 10.1080/09638280400014576.

[32] J. C. van den Noort, L. Bar-On, E. Aertbeliën, M. Bonikowski, *et al.*, "European Consensus on the Concepts and Measurement of the Pathophysiological Neuromuscular Responses to Passive Muscle Stretch," *European Journal of Neurology*, 24(7), pp. 981–991, 2017. doi: 10.1111/ene.13322.

[33] K. P. Blum, K. S. Campbell, B. C. Horslen, P. Nardelli, *et al.*, "Diverse and Complex Muscle Spindle Afferent Firing Properties Emerge from Multiscale Muscle Mechanics," *eLife*, 9:e55177, 2020. doi: 10.7554/ELIFE.55177.

[34] L. Alibiglou, W. Z. Rymer, R. L. Harvey, and M. M. Mirbagheri, "The Relation between Ashworth Scores and Neuromechanical Measurements of Spasticity Following Stroke," *Journal of NeuroEngineering and Rehabilitation*, 5:18, 2008. doi: 10.1186/1743-0003-5-18.

[35] K. L. de Gooijer-van de Groep, E. de Vlugt, J. H. de Groot, H. C. M. van der Heijden-Maessen, *et al.*, "Differentiation between Non-Neural and Neural Contributors to Ankle Joint Stiffness in Cerebral Palsy," *Journal of NeuroEngineering and Rehabilitation*, 10:81, 2013. doi: 10.1186/1743-0003-10-81.

[36] A. Andringa, E. van Wegen, I. van de Port, L. Guit, *et al.*, "The Effect of Botulinum Toxin-A on Neural and Non-neural Components of Wrist Hyper-Resistance in Adults with Stroke or Cerebral Palsy," *PM&R: The Journal of Injury, Function and Rehabilitation*, 14, pp. 486–495, 2022. doi: 10.1002/pmrj.12602.

[37] L. L. van der Velden, M. A. C. de Koff, G. M. Ribbers, and R. W. Selles, "The Diagnostic Levels of Evidence of Instrumented Devices for Measuring Viscoelastic Joint Properties and Spasticity; A Systematic Review," *Journal of NeuroEngineering and Rehabilitation*, 19:16, 2022. doi: 10.1186/s12984-022-00996-7.

[38] M. M. Mirbagheri, M. Ladouceur, H. Barbeau, and R. E. Kearney, "The Effects of Long Term FES-Assisted Walking on Intrinsic and Reflex Dynamic Stiffness in Spinal Cord Injured Patients," *IEEE Transactions on Neural Systems and Rehabilitation Engineering*, 10(4), pp. 280–289, 2002. doi: 10.1109/TNSRE.2002.806838.

[39] M. M. Mirbagheri, L. Alibiglou, M. Thajchayapong, and W. Z. Rymer, "Muscle and Reflex Changes with Varying Joint Angle in Hemiparetic Stroke," *Journal of NeuroEngineering and Rehabilitation*, 5:6, 2008. doi: 10.1186/1743-0003-5-6.

[40] M. M. Mirbagheri, D. Chen, and W. Z. Rymer, "Quantification of the Effects of an Alpha-2 Adrenergic Agonist on Reflex Properties in Spinal Cord Injury using a System Identification Technique," *Journal of NeuroEngineering and Rehabilitation*, 7:29, 2010. doi: 10.1186/1743-0003-7-29.

[41] V. Dietz and T. Sinkjær, "Spastic Movement Disorder: Impaired Reflex Function and Altered Muscle Mechanics," *Lancet Neurology*, 6(8), pp. 725–733, 2007. doi: 10.1016/S1474-4422(07)70193-X.

[42] A. K. Thompson, F. R. Pomerantz, and J. R. Wolpaw, "Operant Conditioning of a Spinal Reflex Can Improve Locomotion after Spinal Cord Injury in Humans," *Journal of Neuroscience*, 33(6), pp. 2365–2375, 2013. doi: 10.1523/JNEUROSCI.3968-12.2013.

[43] M. van de Ruit, W. Mugge, G. Cavallo, J. Lataire, *et al.*, "Quantitative Comparison of Time-varying System Identification Methods to Describe Human Join Impedance," *Annual Reviews in Control*, 52, pp. 91–107, 2021. doi: 10.1016/j.arcontrol.2021.10.010.

[44] E. Flux, L. Bar-On, A. I. Buizer, J. Harlaar, *et al.*, "Implicit EMG-driven Gaming to Alter Calf Muscle Activation during Gait in Children with Cerebral Palsy," *Gait & Posture*, 90(1), pp. 61–62, 2021. doi: 10.1016/j.gaitpost.2021.09.031.

[45] A. K. Thompson and J. R. Wolpaw, "H-Reflex Conditioning during Locomotion in People with Spinal Cord Injury," *Journal of Physiology*, 599(9), pp. 2453–2469, 2019. doi: 10.1113/JP278173.

[46] L. H. Sloot, J. C. van den Noort, M. M. van der Krogt, S. M. Bruijn, *et al.*, "Can Treadmill Perturbations Evoke Stretch Reflexes in the Calf Muscles," *PLoS ONE*, 10(12):e0144815, 2015. doi: 10.1371/journal.pone.0144815.

[47] E. Flux, M. M. van der Krogt, J. Harlaar, A. I. Buizer, *et al.*, "Functional Assessment of Stretch Hyperreflexia in Children with Cerebral Palsy using Treadmill Perturbations," *Journal of NeuroEngineering and Rehabilitation*, 18:151, 2021. doi: 10.1186/s12984-021-00940-1.

[48] E. J. Rouse, L. J. Hargrove, E. J. Perreault, and T. A. Kuiken, "Estimation of Human Ankle Impedance during the Stance Phase of Walking," *IEEE Transactions on Neural Systems and Rehabilitation Engineering*, 22(4), pp. 870–878, 2014. doi: 10.1109/TNSRE.2014.2307256.

[49] A. L. Shorter, J. K. Richardson, S. B. Finucane, V. Joshi, *et al.*, "Characterization and Clinical Implications of Ankle Impednace during Walking in Chronic Stroke," 11:16726, 2021. doi: 10.1038/s41598-021-95737-6.

[50] R. C. van 't Veld, S. S. Fricke, A. Vallinas Prieto, A. Q. L. Keemink, *et al.*, "A Transparent Lower Limb Perturbator to Investigate Joint Impedance during Gait," in *Converging Clinical and Engineering Research on Neurorehabilitation IV*, Springer International Publishing, 2022, pp. 525–529. doi: 10.1007/978-3-030-70316-5_84.

[51] H. Lee and N. Hogan, "Time-Varying Ankle Mechanical Impedance during Human Locomotion," *IEEE Transactions on Neural Systems and Rehabilitation Engineering*, 23(5), pp. 755–764, 2015. doi: 10.1109/TNSRE.2014.2346927.

[52] D. Ludvig, M. Plocharski, P. Plocharski, and E. J. Perreault, "Mechanisms Contributing to Reduced Knee Stiffness during Movement," *Experimental Brain Research*, 235(10), pp. 2959–2970, 2017. doi: 10.1007/s00221-017-5032-2.

Appendix A

Achilles Ankle Perturbator: Footplate and Perturbation Design

The goal of this appendix is to briefly discuss the hardware and software solutions implemented to successfully execute experimental data collection with the Achilles ankle perturbator device, used in Chapters 2, 4, 5 and 6. The Achilles used a one degree of freedom manipulator (Moog, Nieuw-Vennep, the Netherlands) to apply position perturbations around the ankle joint to elicit stretch reflexes and gather input for the joint impedance estimation algorithms. Before experimental data collection, the footplate, i.e. the connection between actuator and human foot, and stretch perturbation were redesigned, see Fig. A.1. The redesigns were required, as the original footplate unexpectedly elicited stretch reflexes in the calf after both perturbation towards plantar-, and dorsiflexion, see Fig. A.2.

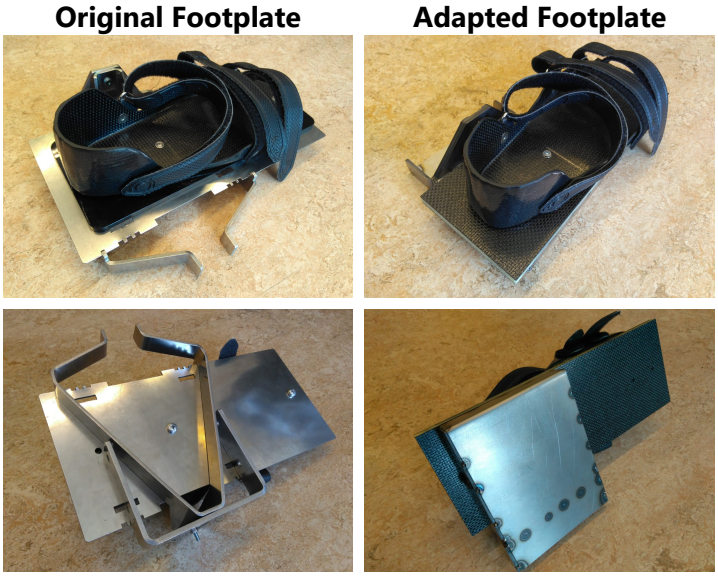

Figure A.1: Redesign of the Achilles ankle perturbator footplate. Overview of both the original *(left)* and adapted *(right)* footplates. The adapted design aimed to reduce weight and increase stiffness around the sagittal plane by introducing a carbon-foam sandwich plate and closed-box support structure. The carbon shoe from the original footplate was reused within the adapted design.

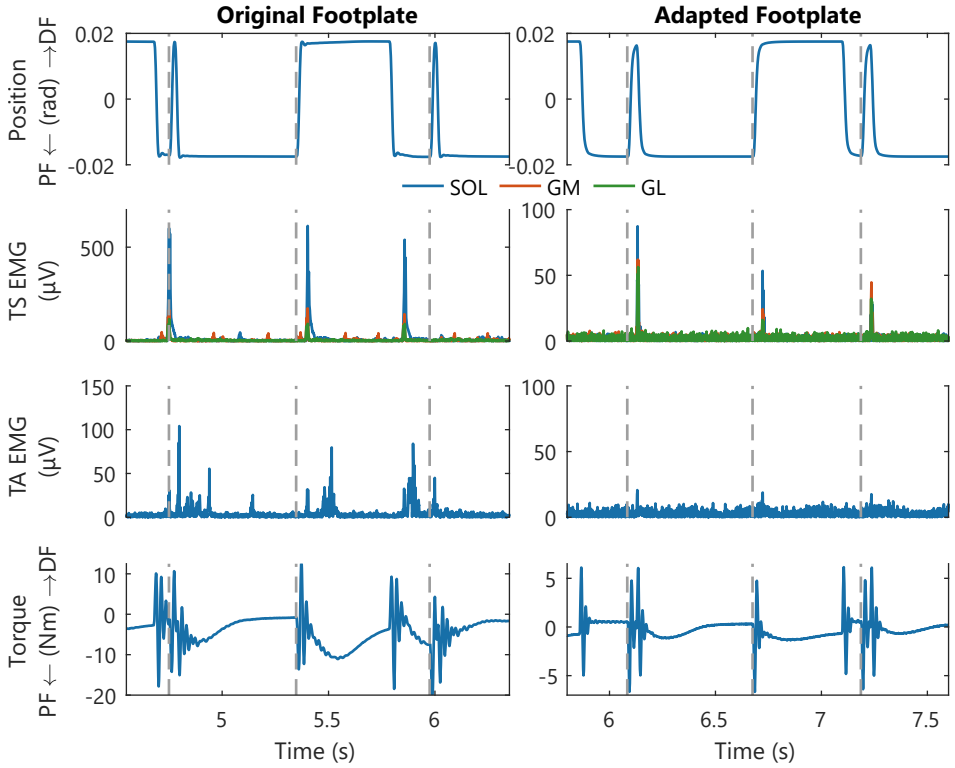

Figure A.2: Time series of measured signals for both Achilles perturbator footplates. Three consecutive dorsiflexion perturbations with perturbation onset *(grey-dashed vertical lines)* are shown. The response to the position perturbations are shown for the high-pass filtered, rectified EMG of Triceps Surae (TS) and TA as well as measured ankle joint torque.

The experimental time series recorded with the original footplate and perturbation design did not consistently elicit a stretch reflex after every dorsiflexion perturbation, see Fig. A.2. Rather, plantarflexion perturbations, which should shorten the calf muscles, sometimes did elicit a stretch reflex as observed in both the electromyography (EMG) and torque response. Subsequently, dorsiflexion perturbations following shortly after plantarflexion perturbations, did not elicit a stretch reflex response for either EMG or torque due to a neural refractory period, see Fig. A.2. We hypothesized that oscillations within the footplate, observed in both the position and torque response, might have elicited these calf muscle reflexes after plantarflexion perturbations. Especially, as motion capture data (Visualeyez II, Phoenix Technologies, Burnaby, Canada) showed that a 0.0007 rad (2% of 0.035 rad amplitude) oscillation amplitude observed at the encoder could result in oscillations of 0.021 rad (61% of 0.035 rad) at the foot.

To reduce oscillatory behavior of the footplate, we first redesigned the footplate to increase the structural eigenfrequencies by reducing weight and increased stiffness in the sagittal plane. A carbon-foam sandwich plate was used to replace steel elements to reduce weight and a closed-box support structure was designed to substantially

increase torsional stiffness, see Fig. A.1. Second, we redesigned the perturbation signal to lower power in the frequency ranges close to and above the structural eigenfrequency. The perturbation was rate-limited and low-pass filtered (2nd-order, 30 Hz, critically-damped), which showed a 63% reduction in oscillation amplitude at the foot in the motion capture data. The combination of both adapted footplate and perturbation signal, avoided any reflex elicitation due to plantarflexion perturbations. Consequently, the experimental data collected with redesigned setup consistently showed a stretch reflex after every dorsiflexion perturbation, see Fig. A.2.

Appendix B

Supplementary Material Chapter 2

Table B.1: Linear mixed model results for Gastrocnemius Medialis M1 stretch reflex response with perturbation parameter predictors. Model parameters are expressed as $\%EMG_{mean}$ per fixed effect unit (± SE). Unconditional main effects were tested using a type-II ANOVA F-test with Kenward-Roger correction for DOF.

Fixed Effect	**Model Param.**	**Statistical Parameters**	
Acceleration	0.65 ± 0.041	$F_{(1,23.8)} = 246$	$p < 0.001$
Velocity	-0.19 ± 1.5	$F_{(1,468)} = 0.0163$	$p = 0.90$
Duration	-0.030 ± 0.062	$F_{(1,9.89)} = 0.370$	$p = 0.64$
Random Effect	**Standard Deviation or Correlation**		
Subject Acceleration	0.073		
Subject Duration	0.12		
Model Fit: R^2-Marginal: 0.42; R^2-Conditional: 0.44; $N = 490$			

Table B.2: Linear mixed model results for Gastrocnemius Lateralis M1 stretch reflex response with perturbation parameter predictors. Model parameters are expressed as $\%EMG_{mean}$ per fixed effect unit (± SE). Unconditional main effects were tested using a type-II ANOVA F-test with Kenward-Roger correction for DOF.

Fixed Effect	**Model Param.**	**Statistical Parameters**	
Acceleration	0.72 ± 0.035	$F_{(1,24.1)} = 412$	$p < 0.001$
Velocity	-1.7 ± 1.6	$F_{(1,9.59)} = 1.17$	$p = 0.31$
Duration	-0.10 ± 0.046	$F_{(1,10.0)} = 5.09$	$p = 0.05$
Random Effect	**Standard Deviation or Correlation**		
Subject Acceleration	0.062		
Subject Velocity	3.0		
Subject Duration	0.063		
Model Fit: R^2-Marginal: 0.56; R^2-Conditional: 0.57; $N = 490$			

Table B.3: Linear mixed model results for Gastrocnemius Medialis M2 stretch reflex response with perturbation parameter predictors. Model parameters are expressed as $\%EMG_{mean}$ per fixed effect unit (± SE). Conditional main effects were tested using a Wald t-test with Kenward-Roger correction for DOF and a Bonferroni correction, applied to the p-value, for multiple comparison per fixed effect. Interactions were tested using a type-II ANOVA F-test with Kenward-Roger correction for DOF.

Fixed Effect	**Condition**	**Model Param.**	**Statistical Parameters**	
Acceleration	35 ms, 2.0 r/s	0.29 ± 0.16	$t(359)$ = 1.78	$p = 0.59$
	35 ms, 2.5 r/s	-0.043 ± 0.17	$t(384)$ = -0.249	$p = 1$
	55 ms, 2.0 r/s	0.051 ± 0.13	$t(270)$ = 0.389	$p = 1$
	55 ms, 2.5 r/s	-0.28 ± 0.11	$t(163)$ = -2.67	$p = 0.07$
	55 ms, 3.0 r/s	-0.61 ± 0.12	$t(246)$ = -4.90	$p < 0.001$
	75 ms, 2.0 r/s	-0.15 ± 0.14	$t(301)$ = -1.05	$p = 1$
	75 ms, 2.5 r/s	-0.48 ± 0.12	$t(228)$ = -3.97	$p < 0.001$
	75 ms, 3.0 r/s	-0.81 ± 0.14	$t(307)$ = -5.71	$p < 0.001$
Velocity	140 r/s^2, 35 ms	18 ± 14	$t(24.1)$ = 1.33	$p = 1$
	140 r/s^2, 55 ms	58 ± 11	$t(12.4)$ = 5.09	$p = 0.001$
	140 r/s^2, 75 ms	70 ± 12	$t(13.8)$ = 5.98	$p < 0.001$
	175 r/s^2, 35 ms	-5.1 ± 13	$t(18.1)$ = -0.408	$p = 1$
	175 r/s^2, 55 ms	35 ± 12	$t(12.6)$ = 3.05	$p = 0.06$
	175 r/s^2, 75 ms	47 ± 12	$t(13.7)$ = 4.02	$p = 0.008$
Short (≤55 ms) Duration	140 r/s^2, 2.0 r/s	3.5 ± 0.39	$t(61.7)$ = 9.11	$p < 0.001$
	140 r/s^2, 2.5 r/s	4.5 ± 0.41	$t(79.3)$ = 10.9	$p < 0.001$
	140 r/s^2, 3.0 r/s	5.5 ± 0.56	$t(199)$ = 9.90	$p < 0.001$
	175 r/s^2, 2.0 r/s	3.1 ± 0.32	$t(31.4)$ = 9.62	$p < 0.001$
	175 r/s^2, 2.5 r/s	4.1 ± 0.30	$t(24.7)$ = 13.5	$p < 0.001$
	175 r/s^2, 3.0 r/s	5.1 ± 0.45	$t(101)$ = 11.5	$p < 0.001$
Long (>55ms) Duration	140 r/s^2, 2.0 r/s	-0.15 ± 0.30	$t(155)$ = -0.495	$p = 1$
	140 r/s^2, 2.5 r/s	0.15 ± 0.24	$t(74.0)$ = 0.625	$p = 1$
	140 r/s^2, 3.0 r/s	0.45 ± 0.31	$t(165)$ = 1.46	$p = 0.88$
	175 r/s^2, 2.0 r/s	-0.49 ± 0.30	$t(146)$ = -1.67	$p = 0.59$
	175 r/s^2, 2.5 r/s	-0.19 ± 0.24	$t(68.3)$ = -0.818	$p = 1$
	175 r/s^2, 3.0 r/s	0.11 ± 0.31	$t(161)$ = 0.351	$p = 1$
Acceleration by Velocity		-0.66 ± 0.15	$F_{(1,448)} = 20.6$	$p < 0.001$
Acceleration by Short-Duration		-0.012 ± 0.011	$F_{(1,448)} = 1.15$	$p = 0.28$
Velocity by Short-Duration		2.0 ± 0.49	$F_{(1,448)} = 17.1$	$p < 0.001$
Acceleration by Long-Duration		-0.0098 ± 0.009	$F_{(1,448)} = 1.25$	$p = 0.26$
Velocity by Long-Duration		0.60 ± 0.38	$F_{(1,448)} = 2.55$	$p = 0.11$
Random Effect		**Standard Deviation or Correlation**		
Subject Acceleration		0.084		
Subject Velocity		33		
Subject Short-Duration		0.63		
Subject Long-Duration		0.30		
Subject Short-Dur. by Long-Dur.		0.97		
Model Fit: R^2-Marginal: 0.67; R^2-Conditional: 0.78; $N = 490$				

Table B.4: Linear mixed model results for Gastrocnemius Lateralis M2 stretch reflex response with perturbation parameter predictors. Model parameters are expressed as $\%EMG_{mean}$ per fixed effect unit (± SE). Conditional main effects were tested using a Wald t-test with Kenward-Roger correction for DOF and a Bonferroni correction, applied to the p-value, for multiple comparison per fixed effect. Interactions were tested using a type-II ANOVA F-test with Kenward-Roger correction for DOF.

Fixed Effect	**Condition**	**Model Param.**	**Statistical Parameters**	
Acceleration	35 ms, 2.0 r/s	0.45 ± 0.18	$t(256)$ = 2.48	p = 0.11
	35 ms, 2.5 r/s	0.097 ± 0.19	$t(293)$ = 0.500	p = 1
	55 ms, 2.0 r/s	0.13 ± 0.15	$t(158)$ = 0.892	p = 1
	55 ms, 2.5 r/s	-0.22 ± 0.12	$t(82.8)$ = -1.80	p = 0.60
	55 ms, 3.0 r/s	-0.56 ± 0.14	$t(139)$ = -4.01	p < 0.001
	75 ms, 2.0 r/s	-0.091 ± 0.16	$t(187)$ = -0.583	p = 1
	75 ms, 2.5 r/s	-0.44 ± 0.14	$t(125)$ = -3.23	p = 0.013
	75 ms, 3.0 r/s	-0.79 ± 0.16	$t(193)$ = -4.96	p < 0.001
Velocity	140 r/s^2, 35 ms	4.9 ± 14	$t(26.8)$ = 0.344	p = 1
	140 r/s^2, 55 ms	59 ± 12	$t(12.9)$ = 5.02	p = 0.001
	140 r/s^2, 75 ms	77 ± 12	$t(14.5)$ = 6.35	p < 0.001
	175 r/s^2, 35 ms	-20 ± 13	$t(19.7)$ = -1.48	p = 0.92
	175 r/s^2, 55 ms	35 ± 12	$t(13.2)$ = 2.94	p = 0.07
	175 r/s^2, 75 ms	53 ± 12	$t(14.4)$ = 4.35	p = 0.004
Short (≤55 ms) Duration	140 r/s^2, 2.0 r/s	3.7 ± 0.48	$t(34.3)$ = 7.88	p < 0.001
	140 r/s^2, 2.5 r/s	5.1 ± 0.50	$t(42.5)$ = 10.2	p < 0.001
	140 r/s^2, 3.0 r/s	6.5 ± 0.65	$t(106)$ = 9.96	p < 0.001
	175 r/s^2, 2.0 r/s	3.2 ± 0.41	$t(20.1)$ = 7.71	p < 0.001
	175 r/s^2, 2.5 r/s	4.6 ± 0.40	$t(16.9)$ = 11.5	p < 0.001
	175 r/s^2, 3.0 r/s	5.9 ± 0.53	$t(52.9)$ = 11.1	p < 0.001
Long (>55ms) Duration	140 r/s^2, 2.0 r/s	-0.30 ± 0.34	$t(114)$ = -0.871	p = 1
	140 r/s^2, 2.5 r/s	0.15 ± 0.28	$t(54.5)$ = 0.545	p = 1
	140 r/s^2, 3.0 r/s	0.60 ± 0.35	$t(122)$ = 1.72	p = 0.53
	175 r/s^2, 2.0 r/s	-0.69 ± 0.33	$t(107)$ = -2.06	p = 0.25
	175 r/s^2, 2.5 r/s	-0.24 ± 0.27	$t(50.5)$ = -0.890	p = 1
	175 r/s^2, 3.0 r/s	0.21 ± 0.35	$t(119)$ = 0.597	p = 1
Acceleration by Velocity		-0.70 ± 0.16	$F_{(1,446)}$ = 19.1	p < 0.001
Acceleration by Short-Duration		-0.016 ± 0.012	$F_{(1,446)}$ = 1.69	p = 0.19
Velocity by Short-Duration		2.7 ± 0.53	$F_{(1,446)}$ = 26.2	p< 0.001
Acceleration by Long-Duration		-0.011 ± 0.010	$F_{(1,446)}$ = 1.35	p = 0.25
Velocity by Long-Duration		0.89 ± 0.41	$F_{(1,446)}$ = 4.68	p = 0.03
Random Effect		**Standard Deviation or Correlation**		
Subject Acceleration		0.15		
Subject Velocity		33		
Subject Short-Duration		0.97		
Subject Long-Duration		0.41		
Model Fit: R^2-Marginal: 0.64; R^2-Conditional: 0.77; N = 490				

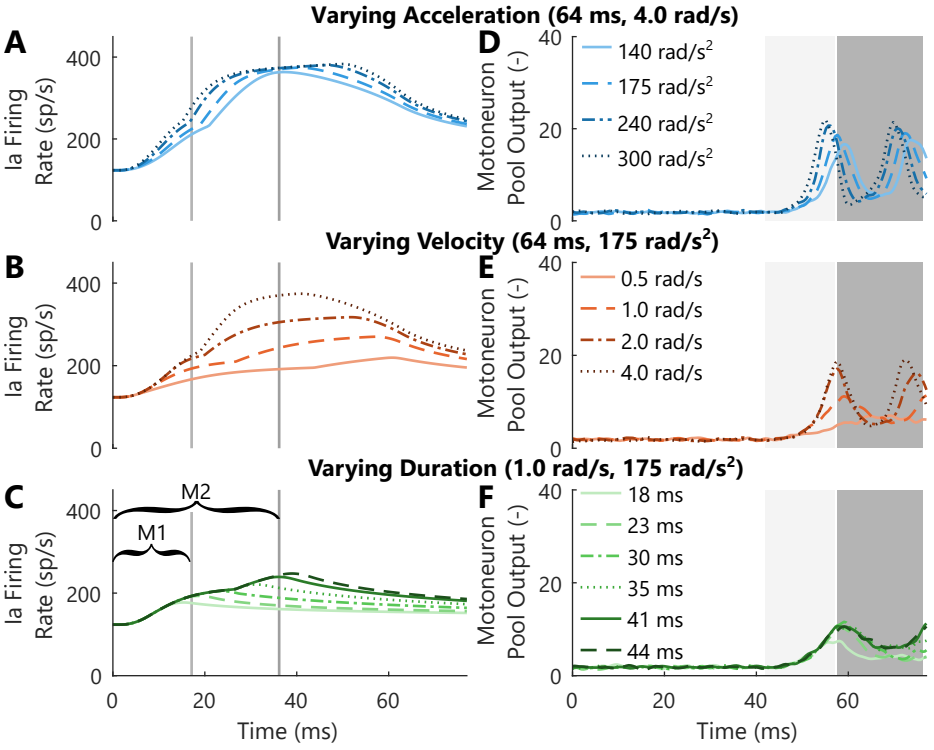

Figure B.1: Simulated stretch reflex responses, as in Fig. 2.5 from manuscript, using the Mileusnic et al. [26] instead of Blum et al. [19] muscle spindle model, as implanted in Schuurmans et al. [15]. The Ia firing rate output *(A-C)* was scaled (gain of 2) to match response magnitude between both Mileusnic and Blum models. The alpha drive motoneuron input was adapted (34 sp/s) to achieve an equal approximate background activity of 10 sp/s *(D-F)*. The visualized M1 and M2 windows *(D-F)* were retained at 42-57 ms and 57.5-76 ms, as in manuscript, thus the Ia firing rate *(A-C)* can only causally influence M1 and M2 between 0-17 and 0-36 ms. With the Mileusnic model, both Ia firing rate *(A-C)* and motoneuron pool output *(D-F)* were influenced by changes in acceleration, velocity and duration, as with the Blum model (Fig. 2.5). Still, substantial differences in the timing were observed between the Mileusnic and Blum models. The Mileusnic model Ia firing rate *(A-C)* clearly showed the lack of an initial burst response, as most Ia firing activity only influenced the M2 bracket (17-36 ms) or even later (>36 ms). Consequently, the motoneuron output *(D-F)*, compared with the Blum model, showed a substantially reduced and delayed response for M1 and M2, as well as a reduced amount of firing and refractory period synchronization. Moreover, both Ia firing rate *(B)* and motoneuron output *(E)* increased with velocity up to 4.0 rad/s, whereas the Blum model showed a plateau in the motoneuron output (Fig. 2.5E) velocity-dependency at 2.0 rad/s. Besides, the influence of increased stretch acceleration and velocity on Ia firing rate *(A and B)* was sustained well after the M2 bracket, whereas in the Blum model steady-state firing rates were reached concurrently for varying velocities (Fig. 2.5B) or even earlier with increasing acceleration (Fig. 2.5A). As result, the second motoneuron output burst *(D)* increased with acceleration up to 300 rad/s^2, whereas the Blum model showed a nonlinear acceleration dependence (Fig. 2.5D) with max. magnitude for the 175 rad/s^2 condition.

Appendix C

Supplementary Material Chapter 5

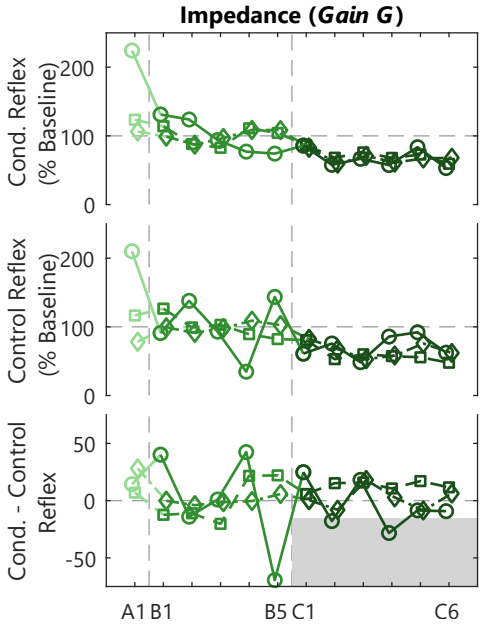

Figure C.1: Reflexive impedance gain G results and within-session effect. Individual participant traces of the average conditioned reflex (mean Blocks 1-3) and control reflex (Block 0) per session for acclimatization (A1), baseline (B1-5) and conditioning (C1-6) sessions. The within-session effect is derived from the difference between the conditioned and control reflex within a session. The Impedance group received feedback on the depicted reflexive impedance gain G. A -15% within-session effect in session C4-6 was defined as success criteria to determine feasibility of the biofeedback method for each participant, see (*grey*) shaded target area. Each icon (circle, square, diamond) per group is linked to an individual participant and consistently used across figures.

Appendix D

Supplementary Material Chapter 6

Table D.1: Best-case minimal detectable difference (MDD) ***(N = 54/78)*** MDDs for the instrumented assessment outcomes based on the ICC values in Table 6.4. The MDD present a best-case scenario as the repeatability was tested under most optimal circumstances.

Outcome Measure	**MDD**
Diff. SPAT ΔW (Nm/kg)	0.026
Slow SPAT W_{slow} (Nm/kg)	0.013
Fast SPAT W_{fast} (Nm/kg)	0.021
Refl. Gain G (Nm·s/rad)	6.9
Intr. Stiffness K (Nm/rad)	10
Intr. Damping B(Nm·s/rad)	0.094

Dankwoord

Veel mensen zijn betrokken geweest bij het schrijven van dit proefschrift. Gelukkig maar, want alle inhoudelijke discussies en samenwerkingen en daarnaast de gezelligheid, sport en ontspanning zijn belangrijk geweest om dit proefschrift voor elkaar te krijgen.

Allereerst wil ik graag mijn (co-)promotoren bedanken. Edwin, Alfred en Herman hartelijk bedankt voor de wekelijkse begeleiding en discussies. Fijn om zo'n breed begeleidend team te hebben met ieder zijn eigen expertises. Edwin, bedankt voor het aanstekelijke enthousiasme voor het onderzoek (en het voetbalteam) en ook voor de ruimte die er was om alle inhoudelijke en minder inhoudelijk zorgen te kunnen bespreken. Alfred, bedankt voor alle praktische hulp, ik heb erg veel geleerd van en baat gehad bij de uren samen achter MATLAB scripts en met de Achilles/BAP in het lab. Herman, bedankt voor de onnoemlijke hoeveelheid ideeën om de kwaliteit en diepgang van het onderzoek te verbeteren.

Buiten de UT begeleiding zijn ook alle deelnemers binnen het NeuroCIMT programma en specifiek het Reflexioning project belangrijk geweest voor de inhoud van dit boekje. Persoonlijk heb ik het enorm gewaardeerd dat deze samenwerkingsverbanden er vanaf het begin van mijn promotie waren. Eline, bedankt voor onze samenwerking, de vele leerzame discussie vanuit onze andere achtergronden en de interessante werktripjes naar Baiona, Aalborg en Chicago. Hopelijk kunnen we nog iets moois publiceren van de data uit Amsterdam. Wieneke, bedankt voor jouw hulp bij en inzicht in het uitvoeren van de klinische experimenten. Marjolein, Noël en Marije, bedankt voor de samenwerking bij het schrijven van de artikelen, in het bijzonder de uitvoering van de Botox-studie van hoofdstuk 6, een mooi voorbeeld waar samenwerking binnen een gebruikerscommissie toe kan leiden!

I would also like to thank all the other collaborations during my period as PhD candidate. Within our own UT-BE department, Pablo, Alejandro, Guillaume, Massimo, Bart, thanks for all the interesting discussions and insights on the unification of system identification and neuromusculoskeletal modelling. Simone, Ander and Arvid, thanks for the collaboration on system identification during walking to add a nice dynamic counterpart to all the static work on the Achilles. Thanks to the people of VUB ELEC for an amazing summer school month in Brussels and in particular Gaia Cavallo and John Lataire for the collaboration on unifying system identification and neuromusculoskeletal modelling. Finally, I would like to thank Natalie Mrachacz-Kersting for the opportunity to visit her lab and Aiko Thompson for all her insights and organizing the operant conditioning special interest group. Your support was vital to fully understand the operant conditioning protocol and to successfully execute the operant conditioning studies at the University of Twente.

Ik wil ook graag het secretariaat en de technici van onze groep hartelijk bedanken voor alle hulp. Lianne, Jeanine, Yolanda, fijn dat er zo'n betrouwbaar en gezellig secretariaat is bij deze groep. Het is fijn dat je altijd bij jullie binnen kan lopen (ook voor een goed gesprek!) en ik had alle door jullie georganiseerde, gezellige borrels niet willen

missen. Wouter, Gerrit, Michiel, Martijn, Quint, Gijs, Nikolai, Victor, bedankt voor alle technische hulp en, in het bijzonder, het uitvoeren van een bulk aan werk om de Achilles experiment klaar te maken. Zowel ik als de proefpersonen hebben de Achilles ervaren als een fijn en betrouwbaar apparaat en dit was zonder jullie hulp niet gelukt.

Om niet te vergeten zijn natuurlijk ook alle proefpersonen die hebben deelgenomen aan de experimenten. Zonder proefpersonen kan dit onderzoek niet gedaan worden, bedankt voor jullie geduld, tijd, enthousiasme en feedback. In het bijzonder hierbij de mensen die het aandurfden om deel te nemen aan de longitudinale experimenten met meerdere sessies, soms tot wel 13 sessies binnen één maand!

All colleagues from the Biomechanical Engineering department have been incredibly important during my PhD and stay in Enschede. I want to thank you all for the great and happy memories to look back upon thinking about my time in Enschede. All the gaming nights, both regular boardgames and D&D (special thanks to Kyrian for all the work), were amazing and a nice way to relax after work. The BW-BSS futsal team was a great way to blow of some steam during lunch breaks, so thank you all for letting me be your captain (to compensate for my on-field performance...). Special thanks to Bob for organizing it for such a long time and for Donatella to have this tradition continue within our group in the future. Special thanks to all my officemates: Simone, Guillaume, Cristina, René and Huawei. Our office was an amazing environment to work at and I missed it dearly during the last covid-years of my thesis, not in the least due to the severe lack of muffins. Simone, thanks for all the good conversations, nice collaboration on system identification, great futsal matches, giving tutorials together and for being my paranymph. Guillaume, thanks for all the good laughs, explanations about the greatness of the south of France, collaboration on system identification and neuromusculoskeltal modelling, letting me explain you some statistics and for being my paranymph.

Next to all the colleagues, I would also like to thank all students who I met during my PhD. I very much enjoyed giving the lectures and tutorials about system identification each year. Special thanks to the students who I supervised during their BSc or MSc thesis: Karlijn, Jasmijn, Alejandro, Margreeth, Andrei, Alessio, Roelien, Jeanine and Lars. Your work always provided interesting discussions and valuable outcomes in support of various chapters in this thesis. Also a special thanks to the student assistants who helped during data collection of Chapter 5. Jasmijn, Laurette, Roelien en Ingrid, thanks for the enthusiastic and accurate execution of all those experimental sessions!

In alle jaren promoveren heeft het leven buiten Enschede ook niet stilgestaan. Ik wil daarbij dan ook alle familie en vrienden bedanken voor de gezelligheid, feestjes, vakanties en boottochtjes. Fijn ook dat jullie af en toe Enschede wisten te vinden voor een borrel of voetbalwedstrijd, ook al voelde dat voor sommige Randstedelingen qua afstand als het einde van de wereld. In het bijzonder ook dank aan mijn ouders, die door hun steun, interesse en inzet zowel voor als tijdens mijn promotietraject, dit alles hebben mogelijk gemaakt. Pa, daarnaast ook bedankt voor de vele, vele tripjes Enschede om samen mijn appartement tot zo'n fijne woning te maken.

Aryanne, jouw steun en samenzijn zijn van onbeschrijfelijke waarde voor mij. Bedankt dat je mijn keuze voor dit traject hebt ondersteunt, ondanks alles wat die keuze ook voor jou betekende. Ik kijk enorm uit naar alle komende jaren samen en als gezinnetje met Corine!

Ronald van 't Veld

Biografie

Ronald van 't Veld werd geboren op 6 juni 1994 te Rijnsburg. Hij studeerde Lucht- en Ruimtevaarttechniek aan de TU Delft met als MSc profiel "Control & Simulation". Als onderdeel van een uitwisselingsprogramma studeerde hij een semester aan de University of Kansas met een focus op vliegtuigontwerp en -dynamica. Voor zijn afstudeerscriptie evalueerde hij een modelgebaseerde regeltechniek (INDI) in een simulatieomgeving ter voorbereiding van een eerste vliegtest met de PH-LAB Cessna Citation II. Direct na het afronden van zijn studie (cum laude) is hij in december 2016 begonnen als promovendus bij de vakgroep Biomedische werktuigbouwkunde van de Universiteit Twente. Tijdens zijn promotieonderzoek werd hij begeleid door prof. dr. ir. Herman van der Kooij, dr. Edwin van Asseldonk en dr. ir. Alfred Schouten met dit proefschrift als resultaat. Het promotieonderzoek was onderdeel van het NWO Reflexioning project, een samenwerking tussen de Universiteit Twente, het Amsterdam UMC, Vrije Universiteit Amsterdam, de Sint Maartenskliniek en industriële partners Motek Medical en TMSi. Naast zijn promotieonderzoek was hij actief betrokken als docent bij het MSc vak "Identification of Human Physiological Systems" en de begeleiding van 6 MSc en 3 BSc studenten tijdens hun afstudeerscriptie.

Scientific Contributions

Journal Publications

[1] **R. C. van 't Veld**, A. C. Schouten, H. van der Kooij, and E. H. F. van Asseldonk, "Neurophysiological Validation of Simultaneous Intrinsic and Reflexive Joint Impedance Estimates," *Journal of NeuroEngineering and Rehabilitation*, 18:36, 2021. doi: 10.1186/s12984-021-00809-3.

[2] C. P. Cop, G. Cavallo, **R. C. van 't Veld**, B. F. J. M. Koopman, *et al.*, "Unifying System Identification and Biomechanical Formulations for the Estimation of Muscle, Tendon, and Joint Stiffness during Human Movement," *Progress in Biomedical Engineering*, 3(3), 2021. doi: 10.1088/2516-1091/ac12c4.

[3] **R. C. van 't Veld**, E. H. F. van Asseldonk, H. van der Kooij, and A. C. Schouten, "Disentangling Acceleration-, Velocity-, and Duration-Dependency of the Short- and Medium-Latency Stretch Reflexes in the Ankle Plantarflexors," *Journal of Neurophysiology*, 126(4), pp. 1015–1029, 2021. doi: 10.1152/jn.00704.2020.

[4] **R. C. van 't Veld**, E. Flux, A. C. Schouten, M. M. van der Krogt, *et al.*, "Reducing the Soleus Stretch Reflex With Conditioning: Exploring Game- and Impedance-Based Biofeedback," *Frontiers in Rehabilitation Sciences*, 2:742030, 2021. doi: 10.3389/fresc.2021.742030.

[5] H. van der Kooij, S. S. Fricke, **R. C. van 't Veld**, A. Vallinas Prieto, *et al.*, "Identification of Hip and Knee Joint Impedance During the Swing Phase of Walking," *IEEE Transactions on Neural Systems and Rehabilitation Engineering*, 2022. doi: 10.1109/TNSRE.2022.3172497.

Conference Contributions

[1] **R. C. van 't Veld**, E. van Kampen, and Q. P. Chu, "Stability and Robustness Analysis and Improvements for Incremental Nonlinear Dynamic Inversion Control," in *AIAA Guidance, Navigation, and Control Conference*, Kissimmee, FL, USA: AIAA, 2018. doi: 10.2514/6.2018-1127.

[2] **R. C. van 't Veld**, A. C. Schouten, H. van der Kooij, and E. H. F. van Asseldonk, "Validation of Online Intrinsic and Reflexive Joint Impedance Estimates using Correlation with EMG Measurements," in *7th International Conference on Biomedical Robotics and Biomechatronics*, Enschede, Netherlands: IEEE, 2018, pp. 13–18. doi: 10.1109/BIOROB.2018.8488123.

[3] A. Moya Esteban, **R. C. van 't Veld**, C. P. Cop, G. Durandau, *et al.*, "Estimation of Time-Varying Ankle Joint Stiffness Under Dynamic Conditions via System Identification Techniques," in *41st Annual International Conference of the IEEE Engineering in Medicine and Biology Society*, Berlin, Germany: IEEE, 2019, pp. 2119–2122. doi: 10.1109/EMBC.2019.8856423.

[4] C. P. Cop, G. Durandau, A. Moya Esteban, **R. C. van 't Veld**, *et al.*, "Model-based Estimation of Ankle Joint Stiffness During Dynamic Tasks. A Validation-based Approach," in *41st Annual International Conference of the IEEE Engineering in Medicine and Biology Society*, Berlin, Germany: IEEE, 2019, pp. 4104–4107. doi: 10.1109/EMBC.2019.8857391.

[5] E. Flux, **R. C. van 't Veld**, E. H. F. van Asseldonk, J. Harlaar, *et al.*, "Validation of an Online Reflex Activity Measure for Use in Feedback Training and Clinical Decision Making," *Gait & Posture*, 73(Suppl. 1), pp. 608–609, 2019. doi: 10.1016/j.gaitpost.2019.07.167.

[6] E. Flux, **R. C. van 't Veld**, M. M. van der Krogt, and E. H. F. van Asseldonk, "Biofeedback-driven Gaming to Reduce Muscle Stretch Reflexes," *Gait & Posture*, 81(Suppl. 1), pp. 99–100, 2020. doi: 10.1016/j.gaitpost.2020.07.083.

[7] **R. C. van 't Veld**, S. S. Fricke, A. Vallinas Prieto, A. Q. L. Keemink, *et al.*, "A Transparent Lower Limb Perturbator to Investigate Joint Impedance during Gait," in *Converging Clinical and Engineering Research on Neurorehabilitation IV*, Springer International Publishing, 2022, pp. 525–529. doi: 10.1007/978-3-030-70316-5_84.

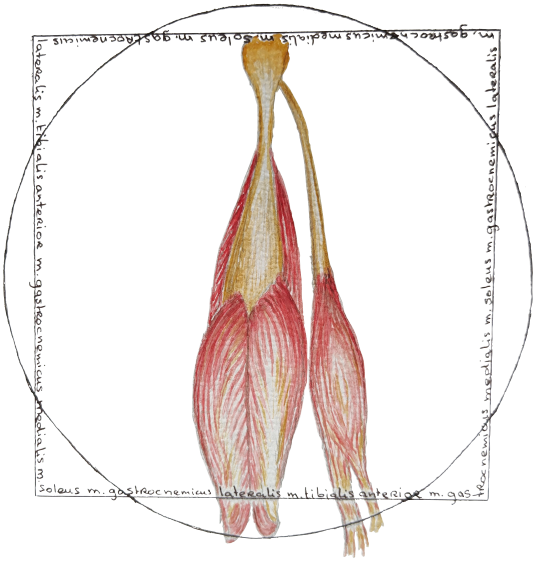
m. gastrocnemicus medialis m. soleus m. gastrocnemius lateralis
lateralis m. tibialis anterior m. gastrocnemicus medialis m
soleus m. gastrocnemius lateralis m. tibialis anterior m. gas
m. gastrocnemicus medialis m. soleus m. gastrocnemius lateralis

Stellingen

behorend bij het proefschrift:

Integrated Spasticity Assessment and Treatment using Disentangled Joint Resistance

door Ronald van 't Veld

1. De stap naar klinische implementatie van een nieuw meetinstrument voor spasticiteit wordt bemoeilijkt door het ontbreken van functioneel klinische eisen tijdens de initiële technische ontwikkeling.
2. De combinatie van het wetenschappelijke systeem (bijv. publicatiedruk) en de individuele uitvoering van complexe taken (bijv. data-analyse) verschaft te weinig verdedigingslagen tegen fouten in publicaties *(Gatenkaasmodel)*.
3. De term "reflexieve stijfheid" zorgt voor een slappe definitie als basis voor de wetenschap en zou niet gebruikt moeten worden.
4. Actief beleid voor het behoud van kennis en ervaring omtrent datasets en onderzoeksapparatuur verbetert de efficiëntie en correctheid van wetenschap.
5. Wetenschappelijk onderzoek naar de beoordeling van spasticiteit is gebaat bij een grotere focus op klinische evaluatie van bestaande technieken en minder op gedetailleerde technische doorontwikkeling.
6. Promovendi die doceren aan de universiteit zouden zelf standaard les moeten krijgen over didactische vaardigheden om de kwaliteit van universitair onderwijs te verbeteren.
7. Een multidisciplinaire aanpak moet een elementair onderdeel zijn van de ontwikkeling van een nieuw meetinstrument voor spasticiteit gezien het gebrek aan een gouden standaard.
8. Pas beginnen met FAIR principes tijdens publicatie is niet fair; uitvoeren van FAIR onderzoek is alleen succesvol als dit direct vanaf de start gebeurt.

Deze stellingen worden opponeerbaar en verdedigbaar geacht en zijn als zodanig goedgekeurd door promotor prof. dr. ir. H. van der Kooij en co-promotoren dr. E. H. F. van Asseldonk en dr. ir. A. C. Schouten.

Propositions

accompanying the dissertation:

Integrated Spasticity Assessment and Treatment using Disentangled Joint Resistance

by Ronald van 't Veld

1. The step towards clinical implementation of a new spasticity assessment device is impeded by the lack of functional clinical requirements during initial technical development.
2. The combination of the scientific system (e.g. publication pressure) and the individual execution of complex tasks (e.g. data analysis) provides too few safety barriers against errors in publications *(Swiss cheese model)*.
3. The term "reflexive stiffness" provides a weak definition as basis for science and should not be used.
4. Active policies to retain knowledge and experience concerning datasets and research devices improves efficiency and correctness of science.
5. Scientific research on spasticity assessment would benefit from a greater focus on clinical evaluation of existing technologies and less on detailed technical developments.
6. PhD candidates who teach at universities should themselves by default follow courses on didactic skills to improve the quality of university education.
7. A multidisciplinary approach should be an elementary part of the development of a new spasticity assessment device given the lack of a gold standard.
8. Only starting with FAIR principles during publication is not fair; execution of FAIR research is only successful if execution happens right from the start.

The propositions are considered to be opposable and defendable and have been approved as such by the promotor prof. dr. ir. H. van der Kooij and co-promotors dr. E. H. F. van Asseldonk en dr. ir. A. C. Schouten.